INTEGRATED SENSITIVITY ANALYSIS, CALIBRATION, AND UNCERTAINTY PROPAGATION ANALYSIS APPROACHES FOR SUPPORTING HYDROLOGICAL MODELING

by

©Hongjing Wu

A thesis submitted to the School of Graduate Studies
in partial fulfillment of the requirements for the
Degree of Doctor of Philosophy

Faculty of Engineering and Applied Science
Memorial University of Newfoundland
May, 2016

St. John's **Newfoundland and Labrador**

ABSTRACT

The successful performance of a hydrological model is usually challenged by the quality of the sensitivity analysis, calibration and uncertainty analysis carried out in the modeling exercise and subsequent simulation results. This is especially important under changing climatic conditions where there are more uncertainties associated with climate models and downscaling processes that increase the complexities of the hydrological modeling system. In response to these challenges and to improve the performance of the hydrological models under changing climatic conditions, this research proposed five new methods for supporting hydrological modeling.

First, a design of experiment aided sensitivity analysis and parameterization (DOE-SAP) method was proposed to investigate the significant parameters and provide more reliable sensitivity analysis for improving parameterization during hydrological modeling. The better calibration results along with the advanced sensitivity analysis for significant parameters and their interactions were achieved in the case study.

Second, a comprehensive uncertainty evaluation scheme was developed to evaluate three uncertainty analysis methods, the sequential uncertainty fitting version 2 (SUFI-2), generalized likelihood uncertainty estimation (GLUE) and Parameter solution (ParaSol) methods. The results showed that the SUFI-2 performed better than the other two methods based on calibration and uncertainty analysis results. The proposed evaluation scheme demonstrated that it is capable of selecting the most suitable uncertainty method for case studies.

Third, a novel sequential multi-criteria based calibration and uncertainty analysis (SMC-CUA) method was proposed to improve the efficiency of calibration

and uncertainty analysis and control the phenomenon of equifinality. The results showed that the SMC-CUA method was able to provide better uncertainty analysis results with high computational efficiency compared to the SUFI-2 and GLUE methods and control parameter uncertainty and the equifinality effect without sacrificing simulation performance.

Fourth, an innovative response based statistical evaluation method (RESEM) was proposed for estimating the uncertainty propagated effects and providing long-term prediction for hydrological responses under changing climatic conditions. By using RESEM, the uncertainty propagated from statistical downscaling to hydrological modeling can be evaluated.

Fifth, an integrated simulation-based evaluation system for uncertainty propagation analysis (ISES-UPA) was proposed for investigating the effects and contributions of different uncertainty components to the total propagated uncertainty from statistical downscaling. Using ISES-UPA, the uncertainty from statistical downscaling, uncertainty from hydrological modeling, and the total uncertainty from two uncertainty sources can be compared and quantified.

The feasibility of all the methods has been tested using hypothetical and real-world case studies. The proposed methods can also be integrated as a hydrological modeling system to better support hydrological studies under changing climatic conditions. The results from the proposed integrated hydrological modeling system can be used as scientific references for decision makers to reduce the potential risk of damages caused by extreme events for long-term water resource management and planning.

ACKNOWLEDGEMENT

First and foremost, I would like to express my sincere thanks to Dr. Bing Chen as well as Dr. Kenneth Snelgrove and Dr. Leonard M. Lye for their excellent supervision and guidance during my research. Without their support this thesis would not have been possible. I am also very grateful to Dr. Baiyu Zhang for her additional guidance and help.

I also gratefully acknowledge the Faculty of Engineering and Applied Science, Memorial University of Newfoundland (MUN), the Natural Sciences and Engineering Research Council of Canada (NSERC), the Canada Foundation for Innovation (CFI), and Toronto-Dominion (TD) Bank Canada for financial support. An expression of thanks is also extended to the United Nations Development Programme (UNDP) for project support.

Additional gratitude is given to my colleagues Dr. Pu Li, Dr. Liang Jing, Jisi Zheng, Xiao Zheng, Zelin Li, Bo Liu, Weiyun Lin, and Dr. Yinchen Ma for their friendship and assistance in the course of my research programme. Special thanks are given to my friend Pu Gao for providing assistance to me in developing the Java code for the proposed uncertainty analysis method in downscaling studies.

Finally, I would like to express my special appreciation to my parents and my aunt's family for their love and continued support. The deepest thanks are expressed to my girlfriend Jinghua Guo for her endless help, encouragement and patience.

RESEARCH CONTRIBUTIONS

1) A statistical design of experiment method, the DOE-SAP method, was developed for hydrological modeling. The DOE-SAP method can construct DOE models for representing the relationship between the model parameters and responses (surface runoff, sediment, etc.). This method can efficiently investigate the sensitivity of different parameters and provide the effect of each main parameter and the interactions between different parameters on the responses, which cannot be offered by traditional sensitivity analysis methods. Through the DOE-SAP method, better sensitivity analysis and parameterization can be achieved for hydrological modeling. The method can be applied to different types of simulation models thus showing the flexibility and advantages of the DOE-SAP method. This method has been applied to sub-surface remediation system simulation and achieved reasonable results (Li *et al.*, 2015a, 2015b).

2) Using a new comprehensive uncertainty evaluation scheme for uncertainty analysis methods in hydrological modeling which includes the R-factor, P-factor, ratio of P-factor and R-factor, computation efficiency, and performance of best estimates (NSE and R^2), three uncertainty analysis methods (SUFI-2, GLUE, and ParaSol) were compared and discussed using a real case study. According to the evaluation results from two real-world case studies, the SUFI-2 method shows the advantages over other two methods. From the proposed evaluation scheme, the uncertainty analysis method which can provide the best hydrological simulation and the more reliable uncertainty analysis results will

be identified for supporting hydrological studies and water resource management. Moreover, the developed comprehensive evaluation scheme can be applied to other hydrological modeling studies, and provide a scientific solution for selecting the most suitable uncertainty analysis method for case studies under different situations.

3) A novel sequential multi-criteria based calibration and uncertainty analysis (SMC-CUA) method was proposed for hydrological studies and was tested using a hypothetical and a real case study. Comparing with other uncertainty analysis methods, the SMC-CUA method can apply advanced sampling methods to parameter sampling with multiple simulation iterations. The advanced sampling method can efficiently search the high probability density region of parameters and dramatically improve computational efficiency of the SMC-CUA method. The application of multiple criteria could screen the refined behavioral parameter sets among the behavioral parameter sets, leading to better calibration and more accurate predictions and controlling the phenomenon of equifinality during hydrological modeling. After each iteration, the parameter ranges are always centered on the best simulation results and narrowed down from the original ranges thus reducing the parameter uncertainty after each iteration. The reduced parameter uncertainty is quite important and useful when conducting uncertainty analysis for propagation effects in climate change studies. Due to the high efficiency, better calibration for simulation predictions, and parameter uncertainty reduction, the proposed method could be used for high dimensional and complex hydrological models

to support better calibration and uncertainty analysis of hydrological studies, especially under climatic changing conditions.

4) A response based statistical evaluation method (RESEM) for evaluating the uncertainty associated with a single downscaling method and the uncertainty propagation effects on hydrological responses was developed. The proposed method can effectively evaluate the propagation effect of uncertainties from statistical downscaling to hydrological modeling using 95PPU of the hydrological responses. A successful demonstration of the method was made through a real case study. By using RESEM, the uncertainty propagated from statistical downscaling can be evaluated and controlled, and the future prediction of hydrological responses can be presented in the hydrograph with uncertainty information (95PPU) under pre-defined GCM scenarios. The developed RESEM for quantifying the propagation uncertainty can also be applied to other hydrological models showing its generality.

5) An integrated simulation-based evaluation system for uncertainty propagation analysis (ISES-UPA) was proposed for evaluating the uncertainty propagation effect from the statistical downscaling and hydrological modeling. Limited studies have focused on breaking down the total uncertainty into different uncertainty components. However, the ISES-UPA method provided a successful attempt to investigate the effects and contributions of different uncertainty components to the total uncertainty of hydrological modeling under changing climatic conditions. By using ISES-UPA, the uncertainty from statistical downscaling, uncertainty from hydrological modeling, and the total

uncertainty from two uncertainty sources can be compared and quantified. When applying future climate scenarios to make important decisions on water resource management under changing climatic conditions, the total propagated uncertainty information could provide more confidence to decision makers for reducing the potential risk of damages caused by extreme events.

6) This research also proposed an integrated system for hydrological modeling under changing climatic conditions. This includes the combined use of DOE-SAP, SMC-CUA, and ISES-UPA methods developed in the different chapters. By using the integrated system, better calibration results of hydrological modeling can be achieved and more reliable results for quantifying uncertainty propagation effects from statistical downscaling to hydrological modeling can be conducted.

TABLE OF CONTENT

LIST OF TABLES

LIST OF FIGURES

LIST OF SYMBOLS AND ABBREVIATIONS

ALPHA_BNK	Baseflow alpha factor for bank storage (days)
ALPHA_BF	Baseflow alpha factor (days)
AMJ	April, May, and June
ANOVA	Analysis of variance
ARS	Agricultural Research Service
ASA	Aggregate Simulation Areas
AVSWAT	ArcView SWAT
b'	New range after next iteration
BaRE	Bayesian recursive estimation
BATEA	Bayesian total error analysis
$b_{j,lower}$,	Lower bound of the parameter range
$b_{j,min}$,	Minimum value of the parameter range
$b_{j,max}$	Maximum value of the parameter range
$b_{j,upper}$	Upper bound of the parameter range
BMA	Bayesian model averaging
CCD	Central composite design
CH_K	Effective hydraulic conductivity in main channel alluvium (mm/hr)
CN	Curve number
CN_2	Initial SCS runoff curve number for moisture condition II
DEM	Digital elevation model
DOE	Design of experiment

DOE-SAP	DOE-aided sensitivity analysis and parameterization
DREAM	Differential evolution adaptive Metropolis method
Dv	Runoff volumes
E_a	Amount of evapotranspiration on day *i* (mm H_2O)
ESCO	Soil evaporation compensation factor
FAST	Fourier Amplitude Sensitivity Test
GCM	Global climate model
GGES	Greenhouse gas emission scenarios
GIS	Geographic information system
GLUE	Generalized likelihood uncertainty estimation
GW_DELAY:	The delay time (days)
GWQMN	Threshold depth of water in the shallow aquifer required for return flow to occur (mm H_2O)
GW_REVAP	Groundwater "revap" coefficient
HadCM3	Hadley Centre Coupled Model 3
HEC-HMS	Hydrologic Engineering Center - Hydrologic Modeling System
HPD	High probability density
HRUs	Hydrologic Response Units
HSPF	Hydrologic Simulation Program-FORTRAN
H3A2a	Hadley Centre Coupled Model 3 for A2 scenario
IPCC	Intergovernmental Panel on Climate Change
ISES-UPA	Integrated simulation-based evaluation system for uncertainty propagation analysis

IWHR	Institute of Water Resources and Hydropower Research
JAS	July, August, September
JFM	January, February, March
k	Number of observed data points
LHS	Latin Hypercube sampling
$L(\theta_i)$	Generalized likelihood
MCMC	Markov chain Monte Carlo
MC	Monte Carlo
MUSLE	Modified Universal Soil Loss Equation
n	Total number of values within the period of analysis
NCEP	National Center for Environmental Prediction
ncepmslpas	Mean sea level pressure
ncepp__fas	Surface airflow strength
ncepp__uas	Surface zonal velocity
ncepp__vas	Surface meridional velocity
ncepp__zas	Surface vorticity
ncepp_thas	Surface wind direction
ncepp_zhas	Surface divergence
ncepp5_fas	500 hPa airflow strength
ncepp5_uas	500 hPa zonal velocity
ncepp5_vas	500 hPa meridional velocity
ncepp5_zas	500 hPa vorticity
ncepp5thas	500 hPa wind direction

ncepp5zhas	500 hPa divergence
ncepp8_fas	850 hPa airflow strength
ncepp8_uas	850 hPa zonal velocity
ncepp8_vas	850 hPa meridional velocity
ncepp8_zas	850 hPa vorticity
ncepp8thas	850 hPa wind direction
ncepp8zhas	850 hPa divergence
ncepp500as	500 hPa geopotential height
ncepp850as	850 hPa geopotential height
ncepr500as	Relative humidity at 500 hPa
ncepr850as	Relative humidity at 850 hPa
nceprhumas	Near surface relative humidity
ncepshumas	Surface specific humidity
nceptempas	Mean temperature at 2m
NDVI	Normalized Difference Vegetation index
NSE	Nash-Sutcliffe coefficient
n_p	Number of peak flow during the study period
nq_{in}	Number of the observed data bracketed by the 95PPU
OFAT	One-factor-at-a-time
OND	October, November, December
ParaSol	Parameter solution
p_{min}	Minimum number of complexes required in population
Q_{gw}	Amount of return flow on day i (mm H_2O)

$Q_{o,i}$	Observed and simulated values on day *i* (m^3/s)
Q_{surf}	Amount of surface runoff on day *i* (mm H_2O)
$Q_{s,i}$	Simulated values on day *i* (m^3/s)
$\overline{Q}_o$	Average values of the observed surface runoff (m^3/s)
$\overline{Q}_i$	Average values of the simulated surface runoff (m^3/s)
R	Correlation coefficient
R^2	coefficient of determination
RCMs	Regional climate models
RCHRG_DP	Deep aquifer percolation fraction
R_{day}	Amount of precipitation on day *i*
RESEM	Response based statistical evaluation method
RSM	Response surface method
r_CN_2	the ratio changes of soil conservation service curve number
S	Retention parameter (mm H_2O).
SCE-UA	Shuffled complex evolution
SCS	Soil Conservation Service
SDSM	Statistical Downscaling Model
SLURP	Semi-distributed Land Use-based Runoff Process
SMC-CUA	Sequential multi-criteria based calibration and uncertainty analysis
SUFI-2	Sequential uncertainty fitting version 2
SOL_AWC	Available water capacity of the soil layer (mm H_2O/mm soil)
SRES	Special Report on Emissions Scenarios
SWAT	Soil and water assessment tool

SWAT-CUP	SWAT Calibration and Uncertainty Programs
SW_t	Final soil water content (mm H_2O)
SW_o	Initial soil water content (mm H_2O)
SWMM	Storm Water Management Model
SFTMP	Snowfall temperature (°C)
TOPAZ	TOpographic PArameteriZation
$t_{o,j}$	Observed time for accessing the peak flow (hour)
$t_{s,j}$	Simulated time for accessing peak flow (hour)
USACE	U.S. Army Corps of Engineers
USDA	United States Department of Agriculture
USDA-ARS	United States Department of Agriculture–Agricultural Research Service
w_{seep}	Amount of water entering the vadose zone from soil prolife on day i (mm H_2O)
95PPU	95% prediction uncertainty
σ_x	Standard deviation of the observed variable x

CHAPTER 1.

INTRODUCTION

1.1 Background

Hydrological models are simplified, conceptual, mathematical representatives of hydrologic processes to simulate water balance and water cycle (Moradkhani and Sorooshian, 2008; Ghoraba, 2015). It also can help people to understand the hydrological processes and make hydrological prediction for different purposes. A large number of hydrological models have been developed and applied to a variety of areas such as flood control, water resources management, water quality control, land planning, and climate change studies. Among the different hydrological models, the distributed hydrological models have advantages in accounting for spatial variability of watersheds, but their applications were usually constrained due to the need for high-resolution distributed variables and inputs, and high demand in computational capability (Refsgaard, 1997; Carpenter and Georgakakos, 2006; Van Griensven *et al.*, 2006; Blasone *et al.*, 2008a). In recent years, the accelerating development of computer technology have dramatically changed the situation and made distributed hydrological models more popular in supporting hydrological studies and watershed management.

To obtain behavioral hydrological simulation results, sensitivity analysis and calibration are important tools. Sensitivity analysis is important to support hydrological modeling which involves a variety of characteristics for which some input values cannot be accurately measured and clearly defined (Scott *et al.*, 2003; Gooseff *et al.*, 2005; Foglia *et al.*, 2009; Zhan *et al.*, 2013; Song *et al.*, 2015). By using sensitivity analysis results, calibration can be more easily to be conducted, because insignificant parameters can be eliminated and optimal regions within factor space can be examined for subsequent calibration study. Most traditional sensitivity analysis methods are time consuming and unable to investigate the

interactions between parameters, leading to the difficulties of efficient and accurate calibration and affecting the simulation performance.

On the other hand, due to the complexity of the hydrological system and the lack of information, uncertainty inherently exists and challenges the implementation of hydrological models. The simulation performance always suffers from the different sources of uncertainty (such as input, parameter and structure of models). The potential improvement in hydrological prediction for distributed models requires a great number of high resolution inputs and parameters, leading to more uncertainties involved in modeling processes. Although the model's inherent uncertainties cannot be easily reduced by uncertainty analysis during hydrological modeling, it still can help determine the level of risk for water resource planning and management and provide a better decision support (Iskra and Droste, 2008). Comparing with the model structure uncertainty, the parameter uncertainty in hydrological modeling is easier to control and reduce through proper uncertainty analysis. A great number of methods have been developed for quantifying the parameter uncertainty (Benke *et al.*, 2008; Gong *et al.*, 2011; Shen *et al.*, 2012; Ficklin and Barnhart, 2014). The interests in how to effectively and accurately provide uncertainty analysis for hydrological models is growing, especially for studying climate change impacts on the water system (Xue *et al.*, 2014).

Warming of climate system is now evident from observations of increased global atmospheric and ocean temperatures, widespread melting of snow and ice, and rising global average sea level. General Circulation Models (GCMs) are mathematical models to describe and simulate general circulation of atmosphere and ocean. Currently, most GCMs consistently predict an increasing trend in frequency and magnitudes of extreme climate event and variability in precipitation (IPCC, 2014). The Intergovernmental Panel on Climate

Change (IPCC) has stated that there is a high confidence that the current climate changes have apparently affected the physical, biological and hydrological system (Chen *et al.*, 2011). According to IPCC's report, observational evidence from all continents and most of oceans indicate that a great number of natural systems are being affected by global climate changes, especially the temperature increases and extreme events. The terrestrial water resource will be significantly influenced by climate change condition in the future and cause many severe problems (Srikanthan and McMahon, 2001; Xu and Singh, 2004). Due to the changes in the hydrological cycle, climate change can affect many aspects of water resources, including drinking water supplies, flood and drought, irrigation, and hydropower production, etc (Hassan *et al.*, 2013). As one of the most important aspects, understanding global warming effects on hydrologic cycle is an essential and challenging study nowadays. Therefore, there is a need to predict and quantify the impacts of climate change, especially the impacts on water resource management.

For water resource management purposes, especially for future prediction and long-term planning, hydrological models are frequently used to simulate the hydrological impacts under changing climatic conditions by using GCM data as input data (Minville *et al.*, 2008b; Chen *et al.*, 2011; Wu and Chen, 2014b). However, the mismatch of spatial resolution between GCMs outputs and the data requirement for hydrological models is a major obstacle to most of hydrological studies (Xu, 1999; Wilby and Dawson, 2007; Dibike *et al.*, 2008; Sennikovs and Bethers, 2009). Therefore, downscaling methods have been developed to process the coarse data into data with high resolution for the use of hydrological studies. Downscaling methods are important for assessment of potential climate change impacts arising from the future increases of greenhouse gas concentration when conducting

hydrological studies (Wilby and Dawson, 2007; Chen *et al.*, 2013). However, downscaling methods could also involve additional uncertainty into the hydrological modeling system. Therefore, quantification of added uncertainty from downscaling is quite important as well.

1.2 Statement of problems

Sensitivity analysis, also referred to as error analysis or quantification of error contribution, is a type of study to obtain all the information flowing in or out of a model (Arbia *et al.*, 1998; Heuvelink, 1998; Saltelli *et al.*, 2000). Sensitivity analysis is quite crucial to support hydrologic modeling, because some parameters cannot be easily measured or clearly defined but have significant contributions to the final responses (Cryer and Havens, 1999). Traditionally, sensitivity analysis is conducted by using the one-factor-at-a-time (OFAT) method for hydrological models (Song *et al.*, 2015). This method only adjusts one parameter at a time, which sacrifices some information due to the lack of consideration of the interactions between the parameters (Montgomery, 2008). However, the interactions between different parameters cannot be ignored and will significantly affect the results of sensitivity analysis for most cases. Moreover, for some high dimensional structure and complex hydrological models, the traditional sensitivity analysis method requires a lot of computational resources and may not be able to achieve a good estimation for optimized parameter sets. Therefore, more advanced and scientific sensitivity analysis with consideration of interactions between parameters should be recommended for hydrological studies. It can improve the calibration process and lead to a better performance of hydrological simulation.

Uncertainty normally refers to the lack of knowledge or incomplete information about specific factors, parameters, model structure, input, output, or measurement errors. Therefore, hydrological models always suffer from a number of uncertainties, especially uncertainties in predictions during calibration process. Generally, for hydrological modeling, uncertainties arise from measurement errors associated with system input, from model structural problems due to assumptions and simplification, and from approximation in determining parameters (Blasone *et al.*, 2008b; Yang *et al.*, 2008). Among these three sources, parameter uncertainty is inevitable but relatively easy to control through an appropriate calibration (especially for some conceptual or empirical parameters). The direct measurement of parameters is usually labor-/time-consuming and costly, leading to quantitative or qualitative limitations in observed data and introducing uncertainties into the modeling system. Furthermore, the interactions and correlations between parameters can also cause uncertainties. For example, different parameter sets might result in similar prediction results. This non-uniqueness (known as the phenomenon of equifinality) is an inherent property of inverse modeling (Beven and Binley, 1992; Abbaspour et al., 2007; Abbaspour, 2011). Any inappropriate modification or adjustment of key parameters may further increase the level of uncertainty and cause negative consequences. In some cases, underestimation of uncertainty may cause unexpected losses and overestimation of uncertainty may lead to resources waste (Shen *et al.*, 2012). Moreover, simplification and assumption of model structure and other imperfect knowledge on current stage of hydrological modeling also make uncertainty inevitable. Therefore, uncertainty analysis is necessary and critical to ensure the success of hydrological modeling (Beven and Binley, 1992; Vrugt *et al.*, 2003; Yang *et al.*, 2007a; Yang *et al.*, 2007b).

The terms "persistent" and "irreducible" have been used to describe the uncertainty associated with the climate change, and the uncertainty extensively exists at the global and regional scale for different complex systems (Ficklin, 2010; Li *et al.*, 2013; Chen *et al.*, 2014). The climate change information required for many hydrological studies is much finer than that provided by global or regional climate models. The downscaling methods have been constructed to meet the data requirement of hydrological models, and used to assess potential climate change impacts arising from future increases of greenhouse gas concentration (Wilby *et al.*, 2002). Generally, the major uncertainty in climate change studies comes from the selection of different GCMs, and the outputs of different GCMs and scenarios will lead to considerable differences in the downscaled results (Rowell, 2006; Kay *et al.*, 2009; Prudhomme and Davies, 2009; Ahmed *et al.*, 2013). On the other hand, the stochastic characteristics of downscaling methods lead to different future climate ensembles of data sets even using a single GCM output, indicating that the downscaling methods will involve additional uncertainty in climate projections. Although GCMs are considered to be the largest uncertainty in climate change studies, the uncertainty related to downscaling also needs to be taken into account for a better estimation and understanding of the impacts of climate change. However, the greatest interests have been given to the uncertainty that arise from GCMs, and the uncertainty during downscaling has been given much less attention (Graham *et al.*, 2007a; Chen *et al.*, 2011). In the meantime, uncertainty propagation effect is very important to be evaluated in hydrological studies if climate change effects have been considered. However, limited attempts have been made to quantify the uncertainty from downscaling on hydrological studies, and few studies integrated systematic probabilistic methods to quantify the propagation uncertainties.

1.3 Research Objectives

To conduct scientific and high performance hydrological studies under changing climatic conditions, three processes during modeling can be improved, including: 1) sensitivity analysis and calibration can improve the simulation performance; 2) uncertainty analysis plays an important role in quantifying the uncertainties in hydrological modeling for understanding the impacts of uncertainty, and 3) statistical downscaling can provide more credible and meaningful prediction results using GCMs. The specific objectives of this thesis mainly include:

- to develop a DOE-aided sensitivity analysis and parameterization (DOE-SAP) method for improving parameterization for hydrological modeling;
- to conduct hydrological modeling studies and using a developed comprehensive uncertainty evaluation scheme to compare three different uncertainty analysis methods through two real case studies;
- to develop a novel sequential multi-criteria based calibration and uncertainty analysis (SMC-CUA) for efficient parameter calibration and uncertainty analysis for hydrological modeling;
- to propose an innovative response based statistical evaluation method (RESEM) for quantifying and evaluating uncertainties from statistical downscaling to hydrological modeling;
- to establish an integrated simulation-based evaluation system for uncertainty propagation analysis (ISES-UPA) to quantify the uncertainty propagation effects

and contributions of different uncertainty sources in hydrological modeling under climate change conditions.

These developed methods were applied to real-world case studies to demonstrate their feasibility on improving the accuracy of hydrological simulation and quantifying the uncertainties from different sources in downscaling studies. The developed methods (mainly including the DOE-SAP, SMC-CUA, and ISES-UPA) can be integrated as a hydrological modeling system for hydrological studies under changing climatic conditions. If the proposed system is successfully applied to case studies, the prediction results for hydrological responses along with uncertainty analysis results can be used as the scientific references with high confidence for supporting long-term water resource management and planning.

1.4 Structure of the thesis

Chapter 2 mainly focuses on the comprehensive reviews of watershed modeling, two hydrological models used for the case studies in the thesis, climate change and downscaling methods, sensitivity analysis and uncertainty analysis.

Chapter 3 introduces an advanced sensitivity analysis and parameterization method for hydrological modeling by using the statistical design of experiment. The proposed method has been applied to a hydrological study in the Deer River watershed near Churchill, Manitoba, Canada, to the test its feasibility. Using the proposed approach, the contribution of each parameter and how they interact with one another were evaluated.

Chapter 4 provides the comparison study for three uncertainty analysis methods under same modeling framework, including the sequential uncertainty fitting algorithm

(SUFI-2), the generalized likelihood uncertainty estimation (GLUE) method, and the parameter solution (ParaSol) method. The uncertainty analysis methods were applied to two real-case studies. A comprehensive evaluation scheme was proposed for comparison, such as R-factor, P-factor, the ratio of P-factor and R-factor, computational efficiency, and performance of best calibrated results (NSE and R^2), and advantages and disadvantages were discussed in this chapter.

Chapter 5 presents a novel calibration and uncertainty analysis method for hydrological modeling studies. By using advanced sampling methods for parameter sampling, along with implementation of multiple iterations with parameter range evolution in each iteration and behavioral parameter sets screening using multiple criteria, the proposed method can achieve more efficient calibration and more balanced and reliable uncertainty analysis. The feasibility and flexibility of the proposed method were tested using a hypothetical case and a real case study.

Chapter 6 proposes a method to quantify the propagation effects of uncertainties from statistical downscaling to hydrological modeling. A real case study was conducted to demonstrate the feasibility and performance of the developed method. Statistical downscaling model (SDSM) was applied to downscale the H3A2a (A2 emission scenario in Hadley Centre Coupled Model 3) outputs, and the downscaled results were subsequently used as inputs to a distributed hydrological model — the soil and water assessment tool (SWAT). The uncertainty associated with the statistical downscaling was evaluated.

Chapter 7 provides a framework to evaluate the contributions of different uncertainty sources from statistical downscaling and hydrological modeling to the total propagated uncertainty. The proposed method was validated through a real-world case study.

The uncertainty from statistical downscaling, uncertainty from hydrological modeling, and the total enlarged uncertainty from two uncertainty sources were compared and quantified through the proposed method.

Chapter 8 summarizes the thesis and provides recommendations for the future research.

CHAPTER 2.

LITERATURE REVIEW

2.1 Hydrological modeling

Hydrology is one of the earth sciences. It is a multidisciplinary subject which studies the occurrence, circulation, storage, the chemical and physical properties, and distribution of surface and ground water on the earth (Bedient *et al.*, 2012). The major areas of hydrology include the physical, chemical, and biological reactions of water in the natural and artificial environment. Moreover, the study of hydrology also includes some topics from traditional fluid mechanics, hydrodynamics, and water resources engineering (Maidment, 1993). The modern hydrologic problems also include considerations of water quality and contaminant transport. Hydrological modeling focuses on modeling of all the hydrologic processes at watershed scale and determines the hydrologic responses by integrating all those hydrologic processes (Singh and Frevert, 2003).

The early efforts were made by Harvard University, Stanford University and U.S. Army Corps of Engineers (USACE) during the 1960s, and the researchers used early versions of digital computers to simulate watershed behavior. The first available major watershed hydrological model is the Stanford Watershed Model (Crawford and Linsley, 1966), and this model later had been combined into the Hydrologic Simulation Program-FORTRAN (HSPF) (Johanson and Davis, 1980). After these early attempts, many modeling approaches were developed and applied during the 1970s for floodplain hydrology, agricultural drainage, urban storm water, reservoir design and river basin management. With the development of hardware and software since the 1970s, there are larger and more extensive hydrologic data-monitoring efforts made for the development and application of a number of models in hydrology. Those models incorporate various mathematical equations to describe hydrological transport processes and storages to calculate the water balances in

space and time. With the advance of high performance computational power and more available historical observed data, water resource researchers and hydrologists are able to improved scale, resolution and accuracy of hydrological simulation, and application of hydrological models becomes more extensive in different areas (Daniel *et al.*, 2011; Bedient *et al.*, 2012; Oubeidillah *et al.*, 2014). Nowadays, a large number of hydrological models have been developed and applied in variety of areas such as flood control, water resources management, water quality control, land planning, and climate change studies (Golmohammadi *et al.*, 2014).

2.1.1 **Hydrological models**

According to a wide range of characteristics, hydrologic simulation models can be classified into various categories. The primary features for distinguishing the hydrological modeling approaches include the nature of the algorithms applied (including empirical, conceptual, or physically-based), whether a stochastic or deterministic approach applied to the input or parameter specification, whether the spatial representation and model's processes is lumped or distributed (Georgakakos and Carpenter, 2003; Liu and Weller, 2008; Daniel *et al.*, 2011). Actually, these models can be far more complicated and combine more functions.

Based on model’s processes, most of hydrological simulation models can be classified as lumped or distributed models. The main characteristic of lumped models is viewing the basin as a single spatial unit where the watershed parameters and variables are averaged over this unit, and the model will not take the spatial variability of the basin into account (Daniel *et al.*, 2011). On the other hand, the distributed model will account for the spatial variability of the basin with all variables being fully represented in the model

(Refsgaard, 1997; Carpenter and Georgakakos, 2006). Practically, most models can be viewed as semi-distributed models: some processes such as rainfall and runoff variables are distributed; however, many other watershed characteristics and processes in basin are lumped (Singh, 1995). For simulation or forecasting of a streamflow hydrograph, many simple lumped models will be good enough and sufficient to be applied. However, for scientific research it may require to use a more detailed, physically-based, fully-distributed model to achieve the goal (Kite, 1997). The advantages of distributed models include the potential for better runoff simulation performance at the basin outlet and providing runoff simulation at interior points (outlets of each sub-basin). Due to these advantages, distributed models are usually applied as the foundation of other environmental models, such as the models for water quality, sediment transport, plant growth, wetland restoration, irrigation improvement, etc (Moreda *et al.*, 2006). However, the high requirements of data resolution and quality of distributed variables and inputs make the applications of distributed models constrained and challenged previously until development of computer technology in recent years.

Due to the increase of spatial data and availability and computational improvement, more distributed hydrological models were applied to hydrological studies (Daniel *et al.*, 2011; Golmohammadi *et al.*, 2014). Some examples of distributed models are MIKE SHE (Abbott *et al.*, 1986a, 1986b), SWAT (Arnold *et al.*, 1995), SLURP (Kite, 1975), SWMM V5.0 (Rossman, 2010), HSPF (Johanson and Davis, 1980), WATFLOOD (Kouwen, 1998), amongst others. **Table 2.1** shows the brief description of some distributed hydrological models.

Table 2.1 Brief descriptions of some distributed hydrological models.

Name	Description
MIKE-SHE (Abbott *et al.*, 1986b, 1986a)	MIKE-SHE (Système Hydrologique Européen) is a physically-based and spatially distributed hydrological model which has been widely used in Europe. Besides the basic function of simulating the water cycle from rainfall to channel discharge, adaptive modular enables MIKE-SHE to handle solute transport, particle tracking as well as geochemical reactions.
SWAT (Arnold *et al.*, 1995)	SWAT (Soil and Water Assessment Tool) is a physically-based continuous distributed model that operates on a daily time step in an ungauged watershed developed by the USDA (United States Department of Agriculture). It can predict the impacts of management practices on hydrology, sediment, and water quality in large complex watersheds using the hydrologic response units (HRUs) as the basic computational units.
SLURP (Kite, 1975)	SLURP (Semi-distributed Land Use-based Runoff Process) is a distributed conceptual model. SLURP was developed for simulating and predicting hydrological features at macroscale basins using the Aggregate Simulation Areas (ASA) as the basic computational units.
SWMM (Rossman, 2010)	SWMM (Storm Water Management Model) is a comprehensive mathematical model and designed for modelling the quantity and quality of urban water cycle. The watershed is delineated into sub-catchments based on the variety of hydrological attributes. Flow routing is computed by a combination of the continuity equation and Manning's equation.
HSPF (Johanson and Davis, 1980)	HSPF (Hydrological Simulation Program – Fortran) was completed by the USGS and U.S. EPA as a successor of the SWM (Stanford Watershed Model). HSPF is designed to assess and predict the land use scenario, reservoir operations, and even pollutants transportation because it has embedded water quality modules besides general hydrological processes.
WATFLOOD (Kouwen, 1998)	WATFLOOD is a mesoscale, distributed, partially physically-based hydrological modeling system, developed by University of Waterloo. WATFLOOD can be described as an integrated set of computer-based programs to forecast flood flows or do simulations for watersheds with response times ranging from one hour to several weeks using grouped response units (GRUs) as the basic computational units.

In this thesis research, due to the watershed size, data and model availability, two distributed hydrological models have been selected applied to different real case studies,

including the SLURP and SWAT model. An introduction of two models has been provided in next sections.

2.1.2 **SLURP**

The SLURP (Semi-distributed Land Use-based Runoff Process) model (Kite, 1975) was developed for simulating and predicting hydrological features at macroscale basins, under the concept of dividing the whole catchment into multiple Aggregate Simulation Areas (ASA) and using distributed parameters and data. The major objective in using the ASA is to model hydrologically-consistent subareas of the watershed. According to Kite's definition, SLURP is a distributed conceptual model and can fit somewhere between the lumped basin models and fully distributed physically-based models at the other. The SLURP model is able to simulate the behavior of a watershed at many points and in many variables, but can avoid the data and computation-hungry excesses of the fully distributed models (Kite, 1997). SLURP is applicable for simulating the hydrological cycle from precipitation to runoff and other related effects such as reservoirs, dam, regulators, water extractions and irrigation schemes. This model can be used for predicting the impacts of changes in water management within a basin or identify the impact of various external factors such as climate change or land cover degradation. The data source of this model may be obtained from locally-available climate data or public-domain data sets available on internet. Topographical and meteorological data such as land cover mapping, vegetation indices (for leaf area index and for evapotranspiration calculation), cloud cover, snow extent and snow water equivalent may be collected from satellite images. The SLURP model applies a vertical water balance to each of its units and land cover using four nonlinear reservoirs, including one for the snowpack, one for canopy, one for a fast response storage and one for a slow response store

(Kite, 1998). Through different processes built in SLURP, the model can route the precipitation and generate the hydrological responses (e.g., runoff). Runoff from each landcover is first routed to the nearest stream channel and routed down towards to the outlet of the ASA. The user can choose to simply accumulate the runoff from each ASA or chose Muskingum Channel Routing or Muskingum-Cunge routing. By conducting these procedures, runoff is accumulated from each landcover within each ASA, and the combined runoff is converted to streamflow and routed between each ASA (Jain *et al.*, 1998).

The TOpographic PArameteriZation (TOPAZ) model can be used to compute all the physiographic input data needed for SLURP. TOPAZ can make use of digital elevation data to define the basin, sub-basins and the stream framework. SLURPAZ, an interface which is usually built in TOPAZ, can be applied to format the output data from TOPAZ and land cover data to produce the formal format for a SLURP command file. In addition, SLURPAZ also can form a weights file used to compute ASA-average meteorological data from station data (Kite, 1997). Through this process, SLURP can simulate furrow or sprinkler irrigation by using both surface and groundwater, and water extraction for urban or industrial use from river or groundwater. SLURP can provide maps of basin-wide crop transpiration, soil evaporation and net runoff for use in performance evaluations irrigation schemes or to investigate water availability (Kite, 1998).

SLURP has been applied in various hydrological studies. Barr *et al.* (1997) used the SLURP model to simulate the global water cycle and assessed the impact of varying climate condition and water resources. Jain *et al.* (1998) conducted the hydrological modeling for simulating runoff at the Bhakhra Dam outlet of the Satluj watershed, demonstrating the SLURP model is capable for the applications in India using available meteorological data,

topographic and satellite imagery. Thorne and Woo (2006) applied the SLURP model to simulate mountainous basins which include complex landscape and land cover and compared results with available measured data. Armstrong and Martz (2008) developed a methodology for determining the impact of varying levels of land cover data on the hydrological response using the SLURP model. St. Laurent and Valeo (2007) listed several deficiencies of SLURP through simulating two large water sheds in northern Manitoba. All these studies have demonstrated that the SLURP model is a useful hydrological tool for simulating the hydrological responses in different types of watersheds. However, the parameters which must be estimated directly for different land class (such as Manning's n, infiltration rate, hydraulic conductivity, etc.) need to be carefully calibrated in the SLURP model to achieve quality simulation results, because the model is distributed and land class parameters are applied to large areas (Kite, 1997; Jain *et al.*, 1998). The SLURP model was previously applied to a case study in the Deer River watershed of Canada, and the auto-calibration process built-in SLURP was conducted by our colleagues (Jing and Chen, 2011b). In this research, an advanced sensitivity analysis and calibration method is proposed, and the method was applied to this case study to test whether better calibration results can be achieved. Therefore, the SLURP model was selected as one of the hydrological models in this thesis research.

2.1.3 **SWAT**

SWAT (Soil and Water Assessment Tool) was developed by the United States Department of Agriculture (USDA) Agricultural Research Service (ARS) and designed to predict the impacts of management practices on hydrology, sediment, and water quality in large complex watersheds with various soils, land use and management conditions over long

periods of time (Arnold *et al.*, 1995). As a physically-based continuous distributed model, SWAT operates on a daily time step in an ungauged watershed. SWAT is able to simulate a number of different physical processes in a watershed. Initially, a watershed needs to be partitioned into many sub-watersheds or sub-basins for modeling purpose in SWAT, because the sub-areas within a watershed are dominated by different land uses or because the soils are dissimilar enough in properties to impact hydrology of areas. By dividing a watershed into many sub-basins, the users can easily reference different areas of the watershed to one another spatially. Watershed delineation in the SWAT model is generated from a given digital elevation model (DEM) into a number of sub-basins. Input information for each sub-basin can be classified into different categories, including climate, Hydrologic Response Units (HRUs), ponds/wetlands, groundwater, and the main channel/reach draining the sub-basin (Neitsch *et al.*, 2011). Within each sub-basin, the HRUs, which consist of similar land use and soil type combinations, are the basic modeling units. Physical characteristics, such as slope, reach dimensions, and meteorological data are considered for each sub-basin. The watershed delineation module of ArcView SWAT (AVSWAT) is based on the elementary raster functions provided within ArcView and its spatial analyst extension (Di Luzio *et al.*, 2004). The meteorological data from the station nearest to the centroid of each sub-basin are used in SWAT (Abbaspour *et al.*, 2007), and in each HRU of the sub-basin, the processes such as canopy interception of precipitation, partitioning of precipitation, snowmelt water, and irrigation water between surface runoff and infiltration, evapotranspiration, infiltration, surface runoff, percolation, underground flow, sediment erosion, and crop growth are simulated (Gassman *et al.*, 2007). The nutrient and sediment fluxes from each HRU are accumulated and routed to the main outlet of each sub-basin. Discharge and sediment fluxes

are routed within the stream network from one sub-basin to another, and finally to the outlet of the watershed. Channel routing is calculated using either the variable storage routing method or the Muskingum river routing method (Arnold *et al.*, 1995; Xue *et al.*, 2014).

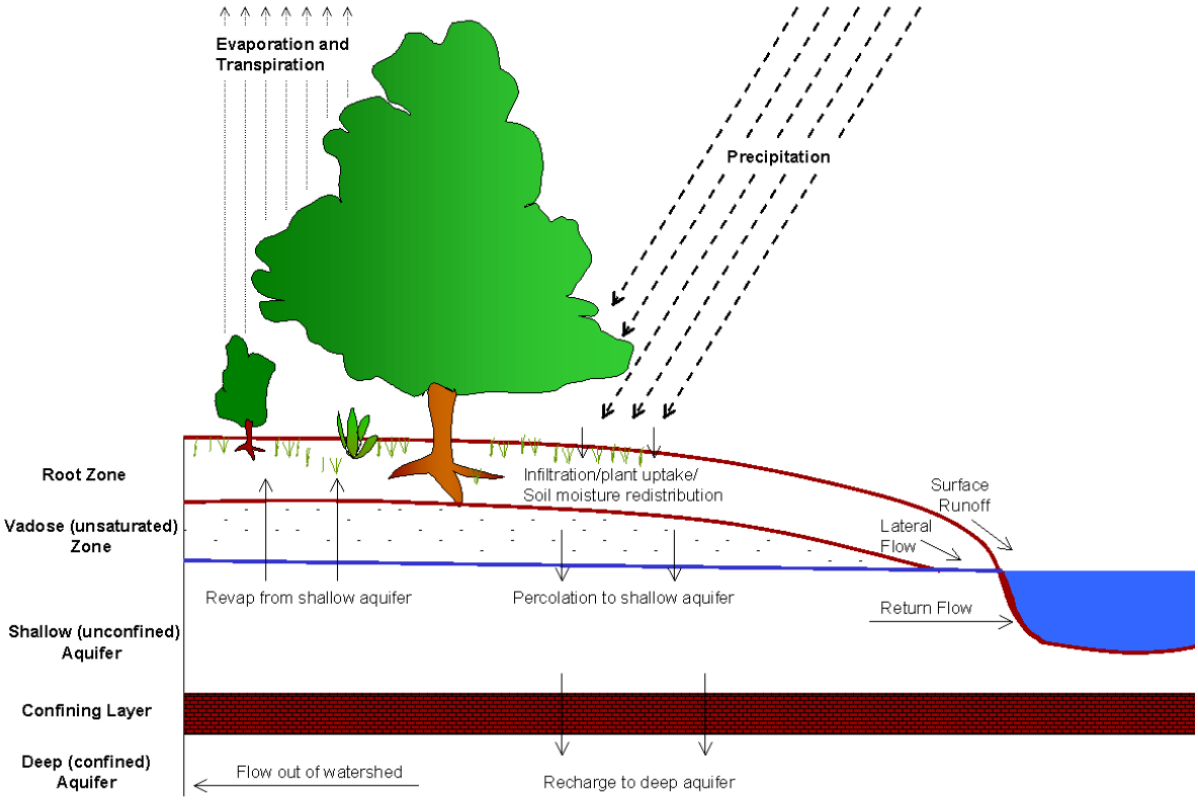

Figure 2.1 Schematic of the hydrological cycle for watersheds (Neitsch *et al.*, 2011)

Water balance is the key and driving force for different hydrologic processes occur in the watershed using SWAT. To accurately predict the movement of water, sediments, pesticides or nutrients, the hydrological cycle simulated using SWAT should conform the observations in watersheds. In SWAT, hydrological simulation can be grouped into two major divisions: the land phase of the hydrological cycle is the first division shown in **Figure**

2.1, and it controls the amount of water, sediment, pesticide and nutrient loadings to the main channel from each sub-basin; the second division is the water routing phase of the hydrological cycle, defined as the movement of water, sediment, nutrients and organic chemicals through the channel network of the watershed to the outlet (Neitsch *et al.*, 2011). Within these two divisions, many water cycle processes, such as precipitation, surface runoff, infiltration, evaporation, plant uptake, lateral flow, and percolation to lower soil levels (Abbaspour *et al.*, 2007), need to be accurately modeled to get good performance from hydrological simulation. Otherwise, it will affect downstream simulations, such as the simulation of sediment yield, nutrient and pesticide loadings. In other words, to get a reliable simulation performance, water balance simulation is very important and the basis of SWAT modeling process. The water balance equation applied in the SWAT model is shown below:

$$SW_t = SW_0 + \sum_{i=1}^{t}\left(R_{day} - Q_{surf} - E_a - w_{seep} - Q_{gw}\right)_i \qquad 2.1$$

where t is the time in days, SW_t and SW_o are the final and initial soil water content respectively (mm H_2O), R_{day} is amount of precipitation on day i (mm H_2O), Q_{surf} is the amount of surface runoff on day i (mm H_2O), E_a is the amount of evapotranspiration on day i (mm H_2O), w_{seep} is the amount of water entering the vadose zone from soil prolife on day i (mm H_2O), and Q_{gw} is the amount of return flow on day i (mm H_2O) (Neitsch *et al.*, 2011; Ghoraba, 2015).

The Soil Conservation Service (SCS) curve number method has been widely used to predict the amount of runoff produced from a given rainfall event, and the equation is shown below (Arnold *et al.*, 1998):

$$Q_{surf} = \frac{(R_{day} - 0.2S)^2}{(R_{day} + 0.8S)} \quad 2.2$$

where Q_{surf} is the daily surface runoff (mm H_2O), R_{day} is amount of precipitation for the day (mm H_2O), and S is the retention parameter (mm H_2O).

The retention parameter (S) varies spatially due to the changes in soils, landuse, and slope or varies temporally due to the changes in water content in soil layers. The retention parameter can be describe as follows (Neitsch *et al.*, 2011):

$$S = 25.4\left(\frac{1000}{CN} - 10\right) \quad 2.3$$

where CN is the curve number for the day.

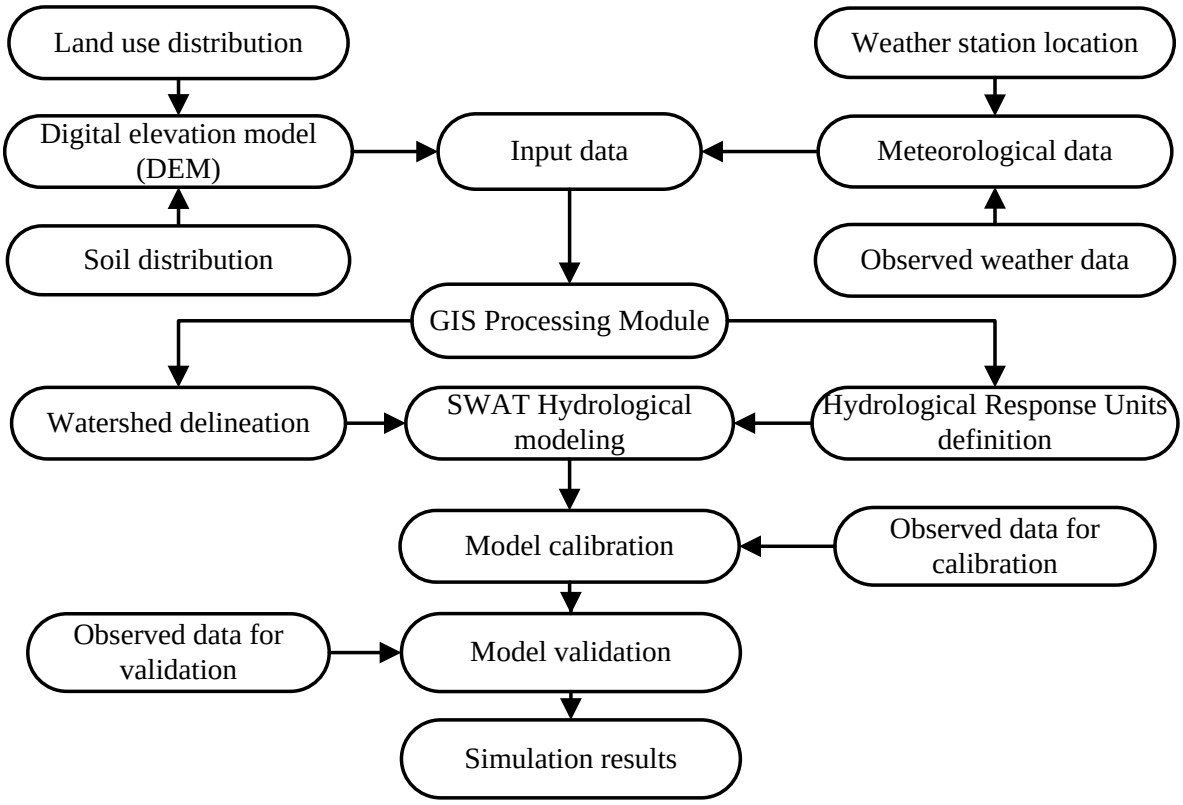

Figure 2.2 The general framework of the SWAT model

For application of the SWAT model, several procedures can be followed for successfully achieving good modeling results. In the first step, the spatial data (DEM, information of soil and land use) are required in the preprocessing phase and fed into the SWAT model through ArcSWAT (SWAT built in the ArcGIS interface). The spatial information can be made use by the Geographic information system (GIS) Processing module built in ArcSWAT to delineate the watershed and generate the HRUs and sub-watersheds (Wu and Chen, 2014a; Ghoraba, 2015). The digital water channel network can be manually burned in ArcSWAT, the water channel network generated by using DEM can be auto adjusted to the real water channels. When the observed climate, precipitation and runoff data are prepared, the hydrological modeling using SWAT can be conducted. After proper

calibration and validation, the simulation results can be used as the guide for water resource management for the study area. The general framework of the SWAT model is shown in **Figure 2.2**.

In previous studies, the SWAT model has been applied to many real world case studies and this has proved to be a successful model of runoff and water quality simulation for many areas. This indicates its feasibility and flexibility to model different regions and environmental conditions. Abbaspour *et al.* (2007) used SWAT to simulate all related hydrological processes affecting quantity, sediment and nutrient loading in the pre-alpine/alpine Thur watershed in Switzerland. Yang *et al.* (2008) applied SWAT to the Chaohe Basin in China for discharge simulation and uncertainty analysis; Rostamian *et al.* (2008) estimated the runoff and sediment in two mountainous basin in Iran using the SWAT model and reasonably good results were obtained.

Generally, comparing with other hydrological models, the SWAT model has some advantages:

- SWAT is a physically-based continuous distributed model;
- is suitable for ungaged basins;
- is a free source and open code software, and can be easier to edited for future studies;
- has a lot of modules developed by other users to improve adaptively of the original SWAT
- can simulate the sediment and nutrients in water, and has the potential to link to hydrodynamic model for simulation of pollutant transport

Since the SLURP model was selected for a case study in this research for the first technical chapter (**Chapter 3**), comparison of the SLURP and SWAT model is provided in **Table 2.2**. In the other four chapters, two real case studies were conducted in this research, including the hydrological modeling for Wenjing River watershed and for the Huolin River watershed. According to the data availability and ungaged properties of the study area, the SWAT model is considered to be able to perform reasonably good simulation for surface runoff for the two case studies. Therefore, the SWAT model was selected.

Table 2.2 The comparison of two hydrological models:

Model	SLURP	SWAT
Model type	Distributed, conceptual model	physically-based, continuous, distributed model
Adaptation of scale	Macroscale (greater than 10^4 km^2)	River basin or watershed scale (10^2 - 10^5 km^2)
Basic computational units	Aggregate Simulation Areas (ASA)	Hydrologic response units (HRUs)
Function	Simulating and predicting hydrological features at macroscale basins	Predict the impact of land management practices on water, sediment, and agricultural chemical yields in large watersheds.

Source: (Liebscher, 1993; Arnold *et al.*, 1998; Gassman *et al.*, 2007; Jing and Chen, 2011a; Neitsch *et al.*, 2011; Ghoraba, 2015)

2.2 Climate change and downscaling methods

2.2.1 **Climate Change**

It is widely accepted that global warming is occurring and is causing a series of changes to the environment, such as a rise in sea level, destabilization of local climate, forest fires, Arctic ice shrinkage, glacier retreat and disappearance. The growth of population and modern industries are the major contributors to increases in greenhouse gas emissions, which is considered to be the main reason for causing climate change (Hasselmann *et al.*, 2003). The Intergovernmental Panel on Climate Change (IPCC) claimed that there is strong evidence to support the conclusion that climate change has considerable impacts on different aspects in water basins and regions (Chen *et al.*, 2011; IPCC, 2014). Due to the changes in the hydrological cycle, climate change can affect many aspects of water resources, including drinking water supplies, flood and drought, irrigation, and hydropower production, etc (Hassan *et al.*, 2013). Therefore, there is a need to predict and quantify the impacts of climate change, especially the impacts on water resource management. However, climate change is a very complicated problem involving different conditions and interactions among ocean, atmosphere, and land surface. In order to use mathematical descriptions to simulate large-scale physical process, general circulation models (GCMs) were developed. These models are considered to be able to provide credible predictions and projections of climate changes into the next 100 years (Jiang *et al.*, 2007; Mpelasoka and Chiew, 2009).

GCMs are mathematical models used to describe and simulate general circulation of atmosphere and ocean based on the Navier-Stokes equations, and many different GCMs have been created in the past two decades to investigate the global warming effects due to the

increasing greenhouse gas concentration in atmosphere (Sennikovs and Bethers, 2009). Most GCMs consistently predict an increasing trend in frequency and magnitude of extreme climate event and variability in precipitation (IPCC, 2007). Terrestrial water resource will be significantly influenced by climate change in the future and cause many severe problems (Srikanthan and McMahon, 2001; Xu and Singh, 2004). For prediction purposes, hydrological models are frequently used to simulate the hydrological impacts (especially water balance) of climate change by using GCM data as input (Salathé, 2003; Diaz-Nieto and Wilby, 2005; Minville *et al.*, 2008a; Chen *et al.*, 2011). However, the resolution of GCMs are too coarse (normally 350km per grid) to be directly applied to hydrological studies at a basin or regional scale. The direct use of the coarse-resolution GCM output for regional hydrological studies has been shown to yield unrealistic hydrological results (Wood *et al.*, 2004; Bae *et al.*, 2011; Hassan *et al.*, 2013). Due to the mismatch of spatial and temporal resolution between GCMs outputs and the data input requirement of hydrological models, application of GCM outputs is a major obstacle to most of hydrological studies under changing climate conditions (Xu, 1999; Wilby and Dawson, 2007; Dibike *et al.*, 2008; Sennikovs and Bethers, 2009; Chadwick *et al.*, 2011; H. Chen *et al.*, 2012; J. Chen *et al.*, 2012). Therefore, it is necessary to develop algorithms to process the coarse data into data with high resolution for use within hydrological models.

2.2.2 **Downscaling methods**

Consequently, downscaling methods have been developed to solve the spatial and temporal resolution mismatch problems to meet the requirement. These play a significant role in assessment of potential climate change impacts arising from future increases of

greenhouse gas concentration (Wilby *et al.*, 2002; Chen *et al.*, 2011). Traditionally, downscaling methods have been classified into two major categories: dynamic downscaling and statistical downscaling. A summary of the advantages and disadvantages of statistical and dynamical downscaling is shown in **Table 2.3**.

Dynamic downscaling methods are based on dynamic formulations using the initial and time-dependent lateral boundary conditions of GCMs to establish regional climate models (RCMs) for the production of finer resolution climate outputs (Caya and Laprise, 1999). However, due to high computational demand and cost, dynamic downscaling methods are available for limited areas and studies (Solman and Nuñez, 1999; Chadwick *et al.*, 2011). Moreover, the outputs of RCMs are still too coarse (e.g., the grid resolution for Canadian GCM is 45km) for most practical applications, such as hydrological studies (Ahmed *et al.*, 2013). Therefore, statistical downscaling methods are developed to overcome these difficulties. Compared with dynamic downscaling methods, statistical downscaling methods (such as multiple linear regression, nonlinear regression, and stochastic weather generator) are normally easier and cost efficient to implement, and can link the state of some variables representing a large spatial scale (GCM/RCM grid scale, the predictors) and the state of other variables representing a smaller scale (small watershed/catchment scale, the predictands) by using more computationally efficient methods (Chen *et al.*, 2011). Therefore, statistical downscaling methods are the most widely used methods in hydrological impact studies under climate change scenarios (Khan *et al.*, 2006b; Ahmed *et al.*, 2013; Tofiq and Guven, 2014).

Table 2.3 The main advantages and disadvantages of statistical and dynamical downscaling. (Wilby and Dawson, 2007; H. Chen *et al.*, 2012; J. Chen *et al.*, 2012)

	Advantages	Disadvantages
Statistical downscaling	Local scale climate information from GCM scale outputs; Cheap, computationally undemanding and readily transferable; Ensembles of climate scenarios permit uncertainty analyses; Applicable to 'exotic' predictands such as air quality and wave heights	Choice of domain size and location affects results; Dependent on the realism of GCM boundary forcing; Requires high quality data for model calibration; Predictor–predictand relationships are often non–stationary and assumptions have to be made; Choice of predictor variables affects results; Choice of empirical transfer scheme affects results; Low–frequency climate variability problematic.
Dynamical downscaling	10–50 km resolution climate information from GCM scale output; Respond in physically consistent ways to different external forcings; Resolve atmospheric processes such as orographic precipitation; Consistency with GCM	Choice of domain size and location affects results; Dependent on the realism of GCM boundary forcing; Requires significant computing resources; Ensembles of climate scenarios seldom produced; Initial boundary conditions affect results; Choice of cloud/ convection scheme affects (precipitation) results; Cannot readily transferred to new regions or domains.

2.2.3 **Statistical downscaling**

Usually, the statistical downscaling methods mainly include: transfer function (Wilby *et al.*, 1998), weather typing (Schoof and Pryor, 2001), and stochastic weather generator (Zhang, 2005; Khan *et al.*, 2006a; Chen *et al.*, 2011). Transfer function approaches establish statistical linear/nonlinear relationships between observed local climatic variables (predictands) and large scale GCM/RCM outputs (predictors). Due to the choice of predictor variables, mathematical transfer functions, or statistical fitting procedures, downscaling schemes could be different. Many algorithms such as linear/nonlinear regression, artificial neural networks, canonical correlation and principal component analyses have all been used to obtain predictor-predictand relationships. Although these approaches are easy to apply, the main drawbacks are: 1) the models usually explain only a fraction of observed climate variability (especially in precipitation series); and 2) the probable lack of stationary relationship between the predictors and predictands (Wilby and Wigley, 1997; Wilby and Dawson, 2007). Weather typing methods usually involve grouping local meteorological variables in relation to different classes of atmospheric circulation (von Storch *et al.*, 1993). Climate change scenarios are established by re-sampling from observed data or by generating synthetic sequences of weather pattern and then re-sampling from observed data. Weather pattern downscaling can be obtained on sensible linkages between climate on the large scale and weather on the regional scale. The main feature of the weather typing method is that local variables can be closely linked to global circulation. However, the reliability of this method highly depends on a stationary relationship between local climate and global climatic circulation (especially precipitation, since there is no strong correlation between daily precipitation and large scale circulation) (Wilby *et al.*, 2002). Stochastic weather

generator methods, which are based on the perturbation of their parameters according to changes projected by large scale climate models, can provide alternative weather sequences compensate for the inadequate length of observed climate records (Zhang, 2005; Qian *et al.*, 2010; Wilks, 2010). Weather generator methods are able to consider the correlation and dependence of the weather variables with each other on the same day as well as over time both at a station (temporal) and between stations (spatial) (Hobson, 2005). These methods have been widely used for agricultural impact assessment and enable the efficient production of large ensembles of scenarios for risk analysis (Wilby and Dawson, 2007). The most important advantage of weather generator methods is their ability to rapidly produce enough climate scenarios for quantifying the impacts of the extreme climate events and for investigating local natural variability (Chen *et al.*, 2011). However, the disadvantage may relate to the low skill at reproducing inter-annual to decadal climate variability (Wilby *et al.*, 2004). The advantages and disadvantages of each downscaling method result in different future climate projection. For example, some downscaling methods cannot capture the extreme climate events which are particular concern in hydrological studies.

Among the many statistical downscaling methods, the Statistical Downscaling Model (SDSM) (Wilby *et al.*, 2002) is another important statistical technique for downscaling large scale climate data. The SDSM model can be best described as a hybrid of the stochastic weather generator and transfer function method. During downscaling with the SDSM model, a multiple regression-based model can be developed between a few selected large scale GCM predictor variables and local scale predictantds (such as precipitation and temperature). The regression equation parameters can be estimated using the efficient dual simplex algorithm. The SDSM is able to construct climate change scenarios for small sites at the

daily time scale using grid resolution GCM output (Wilby and Dawson, 2007). Previous studies show that SDSM performs relatively well in simulating the main characteristics of temperature, however, only a part of the observed climate variability can be explained (especially precipitation) (Dibike and Coulibaly, 2005; Dibike *et al.*, 2008).

The SDSM model can achieve daily weather series by statistical downscaling through seven steps, including (Wilby and Dawson, 2007):

Step 1: quality control and data transformation—few meteorological stations can provide fully accurate and complete data sets, and this step can handle missing and imperfect data;

Step 2: screening of predictor variables—the key problem for all statistical downscaling methods is to find an empirical relationship between gridded predictors and local predictantds. This step is required to assist user to select appropriate downscaling predictors for model calibration;

Step 3: model calibration—construct and calibrate downscaling models based on multiple linear regression equations using a specified predictand and a set of predictor variables;

Step 4: weather generator (using observed predictors)—generates ensembles of synthetic daily weather series by using given observed atmospheric predictor variables and enables the verification of calibrated downscaled models (using independent data) and synthesis artificial time series representative of current climate conditions;

Step 5: statistical analysis—a number of statistics (e.g., mean, maximum, minimum, variance, peaks above/below thresholds, percentiles) could be generated to evaluate both downscaled scenarios and observed climate data;

Step 6: graphical analysis of output—three options for graphical analysis are provided, including frequency analysis, comparative results and time series analysis;

Step 7: scenario generation (using climate model predictors)—final step of SDSM downscaling process and ensembles of synthetic daily weather series can be produced by using daily atmospheric predictor variables from GCMs.

As it is mentioned above, the SWAT model was applied to real case studies in this research. Due to popularity, easy implementation, and daily time scale data requirement from the SWAT model, SDSM is selected in this study. This allows coupling with the developed method to control and quantify the uncertainty propagation effects during downscaling.

2.3 Sensitivity analysis

Sensitivity analysis, also referred to as error analysis (Heuvelink, 1998) or quantification of error contribution (Arbia *et al.*, 1998), is a type of study to obtain all the information flowing in or out of a model (Saltelli *et al.*, 1999; Saltelli *et al.*, 2000). Specifically, sensitivity analysis always refers to one or a series of procedures to determine how much total model uncertainty can be attributed to the uncertainty associated with each individual model factors, including all model parameters, inputs, variables and outputs (Manson, 2003; Song *et al.*, 2015). Sensitivity analysis is paramount in model validation where attempts are made to compare the simulation results to the observed results. This type of analysis is used to indicate the most important parameters (which means the parameters that need to be most accurately measured or controlled), thus it can give the guidance to experimental programs and help modelers to improve the simulation performance.

Sensitivity analysis could provide a method to determine the significant parameters and rank them by their order of importance (Cryer and Havens, 1999).

There are a number of reasons to conduct sensitivity analysis for mathematical models, and Saltelli *et al.* (2000) and Manson (2003) listed some important reasons, including: 1) to determine if a model resembles the system or process for the study; 2) to determine the model factors which most contribute to the variability of model outputs and which may need more information and additional research to improve data quality and the knowledge bases; 3) to determine the parameters which are insignificant and can be eliminated when doing calibration; 4) to determine if and which group of the factors interact with each other; 5) to examine if there is some region of input factors space for which the model variation is a maximum; 6) to examine optimal regions within the factor space for subsequent calibration study. Therefore, sensitivity analysis is necessary and crucial when conducting modeling studies, especially hydrological modeling studies.

Sensitivity analysis can support hydrological modeling which involves a variety of characteristics for which some input values cannot be accurately measured and clearly defined (Scott *et al.*, 2003; Gooseff *et al.*, 2005; Foglia *et al.*, 2009). Traditionally, sensitivity analysis has been classified into two major categories, local sensitivity analysis and global sensitivity analysis. Local sensitivity analysis is primarily carried out through the computation of partial derivatives of model output functions regarding small changes in model input, and it typically involve a concentration on localized impact of a single factor of a model (Saltelli *et al.*, 1999). Global sensitivity analysis is the study how to apportion model input factor uncertainty to the model total output uncertainty in order to determine which input factor contributes most to the overall uncertainty of the model (Song *et al.*, 2015).

There are a number of techniques available for sensitivity analysis, including the first order Taylor local sensitivity method (McCuen, 1974; Beven and Kirkby, 1979; Piper, 1989), the Fourier Amplitude Sensitivity Test (FAST) (Cukier *et al.*, 1973), Nonlinear methods (Sobol's, 1993), Analysis of variance (ANOVA) and other variance-based techniques, bootstrap method (Archer *et al.*, 1997), extended Fast (Saltelli *et al.*, 1999), as well as a series of one-factor-at-a-time (OFAT) approaches (Daniel, 1958). In recent hydrological studies, more global sensitivity analysis methods have been applied to case studies due to their advantages over the local sensitivity analysis methods (Song *et al.*, 2015). Among above methods, the OFAT based method (e.g., the Morris method) is the simplest and most popular technique used in performing sensitivity analysis, and many studies has applied the OFAT based method to hydrological studies (Morris, 1991; Zhan *et al.*, 2013; Baroni and Tarantola, 2014; Song *et al.*, 2015). For instance, Singh and Woolhiser (1976) and Singh (1977) used the OFAT method to evaluate the sensitivity of linear and non-linear rainfall-runoff model structures to systematic errors in rainfall. Paturel *et al.* (1995) made use of OFAT method to examine the effects of systematic and random errors on model inputs to a simplified catchment model (Manson, 2003). Herman *et al.* (2013) demonstrated that the Morris method can more efficient screen the significant parameters than the Sobol's method. King and Perera (2013) applied the Morris method to investigate the importance of input variables for the estimation of yield of urban water supply system. Although many sensitivity analysis have been conducted using the OFAT based method, this method can only adjust one parameter at a time. This sacrifices some information due to the lack of consideration of the interactions between the parameters (Montgomery, 2008). Therefore, with consideration of interactions between model parameters, a new DOE aided sensitivity analysis method has

been developed in this research in **Chapter 3** to provide a more efficient, accurate and reliable sensitivity analysis for supporting a better parameterization.

2.4 Uncertainty analysis

Uncertainty normally refers to lack of knowledge or incomplete information about specific factors, parameters, model structure, input, output, or measurement errors. Uncertainty in model prediction can arise from measurement errors associated with the system input and output, from model structure errors caused by the use of a simplified mathematical model to represent spatially distributed real-world processes, and from problems with parameter estimation (Blasone *et al.*, 2008b). For instance, the environment may appear more complex than abstractions and simplifications imply (e.g., kinetic process in pesticide absorption), or too large and interconnected to observe everything at once (e.g., global weathering of minerals), or too small to observe at practical scales (e.g., soil pore volume in the study field), or too various to capture (e.g., infiltration rates in certain soils) or too hard to get stable and accurate measurements (e.g., hydraulic conductivity), or lack of ability to observe some parameters (e.g., soil matrix over large areas) (Brown and Heuvelink, 2005; Smithson, 2012). Imperfect knowledge makes the uncertainty inevitable on the current stage of hydrological studies (Xue *et al.*, 2014).

2.4.1 **Uncertainties in hydrological modeling**

Hydrological models always suffer from a number of model uncertainties, especially uncertainties in the predictions during calibration process. Quantification of uncertainty during hydrological modeling has attracted much attention in hydrological literature in recent

decades (Li *et al.*, 2010). There are a variety of previous studies that have focused on uncertainty analysis for hydrological modeling (Liu *et al.*, 2002; Kavetski *et al.*, 2006; Gallagher and Doherty, 2007; Shen *et al.*, 2008; Thyer *et al.*, 2009; Poulin *et al.*, 2011; Shen *et al.*, 2012; Wu and Chen, 2014a; Xue *et al.*, 2014). Generally, in hydrological modeling, uncertainties arise from three possible sources: model inputs, model structures, and model parameters.

As one of the most important uncertainty sources, input data always significantly influence final responses of the simulation. Input uncertainty results from bias and errors in the input data (such as rainfall and temperature), and more importantly, the extension of point data to distributed data over large areas in distributed models. It is quite difficult to account for and quantify the input uncertainty (Yang *et al.*, 2008). Normally, hydro-meteorological data are the most important model input data for hydrological modeling, and model outputs are always sensitive to input data, especially rainfall (Abbaspour, 2011). Therefore, rainfall data have a great impact on the hydrological simulation results. The study conducted by Lopes (1996) showed that the inhomogeneity of the rainfall distribution (especially the spatial inhomogeneity) had significant effects on surface flow and sediment. Usually, uncertainties of sediment yield are larger than those of surface flow, and these uncertainties are increased by the inhomogeneity of the spatial rainfall distribution (Hao *et al.*, 2003; Xue *et al.*, 2014). Quantification of input uncertainties is performed to obtain random variables rather than point inputs. For example, the National Weather Service has successfully achieved rainfall forecasts quantitatively in the form of probability forecasting (Seo *et al.*, 2000).

Model structural uncertainties have not been fully studied due to their complexity. The complexity results from model simplifications, assumptions and applications of the model under conditions that are not consistent with the model design (Tripp and Niemann, 2008). Normally, the conceptual model uncertainty (also called model structural uncertainty) could arise from following situations: a) model uncertainties due to simplifications in the conceptual model (e.g., the assumption in universal soil loss equation for estimating sediment loss); b) model uncertainties due to occurrence of some hydrological processes in the watershed but not considered or included in the model (e.g., the "second-storm effect" effecting the mobilization of particulates from soil surface in the SWAT model) (Abbaspour *et al.*, 2007); c) model uncertainties due to the occurrence of hydrological processes are unknown or unaccountable to the modeler even though the corresponding modules are included in the model system (e.g., various forms of reservoirs, water transfer, or irrigation affecting water quality); and d) model uncertainties due to hydrological processes unknown to the modeler and not included in the model system either (e.g., dumping of waste material and chemicals in the rivers or some activities that dramatically change the hydrology or water quality such as constructions of roads, dams, tunnels and bridges) (Abbaspour, 2011).

Uncertainties of model parameters exist because their values were obtained from empirical estimation, such as physical significance, generalized inference, and calibration of observed data may not ensure the reliability and precision of modeling results (Beck, 1987). Because direct measurement of parameters from physical system is time consuming, costly and low efficiency, only limited numbers of measured data are available for most cases. Moreover, some direct measurement will inevitably involve some measurement errors and lead to more uncertainties into system. The interactions between the parameters also will

cause uncertainties. For example, single valued parameter sets will lead to a single output of modeling. However, in an inverse application, an observed output value could be more or less reproduced with many different parameter sets. This non-uniqueness is an inherent property of inverse modeling, and also demonstrate the uncertainties of parameters during the modeling (Beven and Binley, 1992; Duan, 2003; Abbaspour *et al.*, 2007; Abbaspour, 2011). There are still many obvious errors for certain parameters in parameter sets (which can produce reasonable outputs), and need to be removed to reduce the uncertainties. Because of the large number of unknown or immeasurable parameters and errors in the data used for parameter calibration, parameter uncertainty is necessary to be controlled and quantified.

2.4.2 **Uncertainties in climate change and downscaling**

The uncertainties associated with climate change are considered as inevitable, and these uncertainties exist at the global scales (such as climate feedback processes) and the regional scale (such as population growth) (Ficklin, 2010). The uncertainties during the application of downscaling process also arise from the data used and the concept on which the downscaling models are based. Different uncertainties will be involved no matter what downscaling methods are implemented during downscaling.

Generally, GCMs are considered to be the largest source of uncertainty when quantifying the climate change impacts (Chen *et al.*, 2011). Many studies have focused on the uncertainties from GCMs and the application of different downscaling methods (Hamlet and Lettenmaier, 1999; Hobson, 2005; Graham *et al.*, 2007a; Graham *et al.*, 2007b). Ficklin (2010) used a stochastic method with bracketed output from multiple GCMs and emission scenarios to quantify the 95% confidence interval of streamflow and agricultural pollutant

(sediment and nitrate) transport changes under climate change in the Sacramento and San Joaquin watershed by using the SWAT model. Rowell (2006) compared different sources of uncertainties for precipitation and temperature in the United Kingdom and found out that uncertainty from GCMs is the largest. Prudhomme and Davies (2009) pointed out that uncertainties from GCMs are greater than those from downscaling methods and greenhouse gas emission scenarios (GGES). Kay *et al.* (2009) also compared different uncertainty sources of five GCMs, downscaling methods, hydrological model structure and parameters. According to the results, uncertainties from GCMs are still the largest; however, other sources of uncertainty are significant if the GCMs' impacts are not taken into account. Wilby and Harris (2006) used four GCMs, two GGES, two downscaling techniques (SDSM and changing factor), two hydrological model structures and two of hydrological model parameter sets to quality the uncertainty sources by using probabilistic methods. Chen *et al.* (2011) quantified the impacts of climate change on river basin in Quebec, Canada and compared the uncertainties related to six different downscaling methods including dynamic downscaling and statistical downscaling. Due to complexity and unique advantage of different downscaling method, authors suggested that one or more downscaling method should be used to evaluate the uncertainties for any climate change impact studies.

Some attempts have been made to quantify and compare the uncertainty during downscaling to hydrological studies. Mpelasoka and Chiew (2009) compared the impact of three empirical downscaling methods (including constant scaling, daily scaling and daily translation) using a daily rainfall-runoff model driven with future daily rainfall series in Australia. The uncertainty associated with the choice of different empirical downscaling methods was much smaller comparing with that related to GCMs. Chen *et al.* (2011)

compared six downscaling methods to investigate the uncertainty of downscaling methods in quantifying climate change impact on the hydrology of a Canadian River basin. The results indicated the selection of downscaling methods could also lead to large uncertainty up to the level of GCMs and GGESs. Teutschbein *et al.* (2011) assessed the uncertainty by using three statistical downscaling methods (including an analog sorting method, a multi-objective fuzzy-rule-based classification and the statistical downscaling model) to model precipitation from two GCMs, and the monthly mean streamflow and flood peaks in spring and autumn for a meso-scale watershed were simulated. After comparison and analysis, they concluded that the choice of downscaled precipitation time series had a major impact on the streamflow simulation. Chen *et al.* (2013) evaluated the uncertainty of six empirical downscaling methods by quantifying the impact of climate change through the hydrological modeling results from two case studies in the North America. The results indicated that both the empirical downscaling method and RCM simulation leads to great uncertainty on simulated streamflow and the uncertainty associated with the choice of the empirical downscaling method is slightly smaller than that of RCM.

Limited studies assessed the uncertainty related to the choice of downscaling methods, and even fewer studies have focused on estimating the uncertainty based on a single downscaling method and the uncertainty propagation effect on hydrological responses. Moreover, limited literatures reported uncertainty analysis approaches which are specifically developed for quantifying the uncertainty propagated from downscaling to hydrological modeling. In this research, an attempt to quantify and evaluate the uncertainty propagation effect during statistical downscaling to hydrological modeling under a single statistical downscaling framework will be made.

2.4.3 **Uncertainty analysis methods**

There are many uncertainty analysis methods available to investigate uncertainty during hydrological modeling (especially parameter uncertainty), such as Bayesian techniques (Kuczera and Parent, 1998; Thiemann *et al.*, 2001; Kavetski *et al.*, 2002; Vrugt *et al.*, 2003), sequential uncertainty fitting (SUFI-2) (Abbaspour *et al.*, 2004; Abbaspour *et al.*, 2007), generalized likelihood uncertainty estimation (GLUE) (Freer *et al.*, 1996; Zak and Beven, 1999), Markov chain Monte Carlo (MCMC) (Gilks, 2005), Bayesian recursive estimation (BaRE) (Thiemann *et al.*, 2001), Bayesian total error analysis (BATEA) (Ajami *et al.*, 2007; Kuczera *et al.*, 2007), automatic calibration and uncertainty assessment using response surfaces (Mugunthan and Shoemaker, 2006), Parameter solution (ParaSol) (Van Griensven and Meixner, 2006), and the Bayesian model averaging (BMA) (Hoeting *et al.*, 1999; Vrugt and Robinson, 2007). Among these methods, SUFI-2, GLUE and ParaSol are three important and popular techniques for uncertainty analysis. The SUFI-2 method has been widely applied to analyze parameter sensitivity and identify critical sources of uncertainty (Abbaspour *et al.*, 2004; Rostamian *et al.*, 2008; Abbaspour, 2011). The GLUE method is one of the most popular methods to evaluate uncertainties in rainfall-surface flow simulation (Montanari, 2005) and is also applied to uncertainty analysis for hydrological forecasting (Mantovan and Todini, 2006; Stedinger *et al.*, 2008; Li *et al.*, 2010). By using the shuffled complex evolution (SCE-UA) algorithm (Duan *et al.*, 1992), the ParaSol method is expected to efficiently optimize a model and provide parameter uncertainty estimates without being based on assumptions on prior parameter distributions for the sampling strategy (Van Griensven and Meixner, 2007).

2.4.3.1 **Generalized likelihood uncertainty estimation (GLUE)**

The GLUE method (Beven and Binley, 1992), inspired by the Hornberger and Separ method of sensitivity analysis (Hornberger and Spear, 1981), has been developed to represent prediction uncertainty within the context of the Monte Carlo analysis coupled with Bayesian estimation and propagation of uncertainty. Beven and Binley (1992) stated that equivalence of different parameter sets within a system should be expected. For example, in the area of hydrology, there are numerous different mechanisms of hydrological response, such as infiltration excess overland flow, saturation excess overland flow, subsurface storm flow, and throughflow/interflow, and normally these mechanisms are not mutually exclusive: they may occur in different areas of a watershed during a storm or at one area of a watershed in different storm event. In general, any physically based hydrological model should be able to predict storm runoff response based on all above mechanisms or combination of them. When a storm event is predicted by a certain hydrological model, it is possible to have different parameter sets to represent different combinations of above mechanisms. The hydrologists and experts might have reasons to prefer which combination of parameter sets is better than others according to their experiences or observation for a particular event. However, there still may be a number of sets of parameter values are pretty equally likely as the simulators of the system, which is hard to determine (Beven and Binley, 1992; Montanari, 2005; Pappenberger *et al.*, 2005; Vrugt *et al.*, 2009). Due to above reasons, the GLUE method calls for a rejection of the concept of a unique global optimum parameter set, and looks for different parameter sets which can produce fit model predictions with similarly good performance. This concept, defined as "equifinality", can be directly addressed by the evaluation of different sets of parameters within the GLUE method (Blasone *et al.*, 2008b).

Because of the suitability for parallel implementation on distributed computer systems, flexibility and relative ease of implementation and use, and the ability to handle different error structures and models without major modifications to the method itself, the GLUE method has been used in a wide variety of applications (Blasone *et al.*, 2008b; Yang *et al.*, 2008; Shrestha *et al.*, 2009). Since it was introduced in 1992, the GLUE framework has been applied to uncertainty assessments in environmental modeling, including rainfall-runoff modeling (Beven and Binley, 1992), soil erosion modeling (Brazier *et al.*, 2001), groundwater modeling and well capture zone delineation (Feyen *et al.*, 2001), flood inundation (Aronica *et al.*, 2002), distributed hydrological modeling (McMichael *et al.*, 2006), and ground radar-rainfall estimation (Tadesse and Anagnostou, 2005). Particularly in hydrological applications, the GLUE method becomes one of the most popular methods for analyzing parameter uncertainty in hydrological modeling and has been widely used over past two decades to analyze and estimate the predictive uncertainty (Freer *et al.*, 1996; Beven and Freer, 2001; Montanari, 2005; Shrestha *et al.*, 2009).

Despite the popularity of the GLUE method on environmental modeling, there are some theoretical and practical concerns which have been pointed out and discussed in the literature (Kuczera and Parent, 1998; Ballio and Guadagnini, 2004; Montanari, 2005; Mantovan and Todini, 2006; Blasone *et al.*, 2008b; Stedinger *et al.*, 2008). For example, the most important drawback is that GLUE derived parameter distribution and uncertainty bounds are entirely subjective and have no clear statistical meaning to support (Blasone *et al.*, 2008b). Mantovan and Todini (2006) claimed that the GLUE method is inconsistent with the formal Bayesian inference processes leading to some overestimation of uncertainty for both the parameter and the predictive uncertainty estimation. Kuczera and Parent (1998) pointed

out that there is a practical problem with the GLUE method, which is if a model has a large number of parameters the sample size for the respective parameter distributions would be quite large to achieve a reliable estimation of model uncertainties and requires extensive computational resources. Normally, the GLUE method applies a rather simplistic Monte Carlo (MC) sampling scheme to sample from the prior parameter distributions in order to find a well-distributed set of behavioral models and their associated predictive simulation uncertainty. For relative simple and low-dimensional sampling problem, the MC approach is adequate and easy to apply. However, when facing relative high-dimensional and complex estimation problems this approach is hard to find stable and consistent estimates of the set of behavioral models (Blasone *et al.*, 2008b; Shrestha *et al.*, 2009). Moreover, although the MC based GLUE for uncertainty analysis of hydrological models is very flexible, conceptually simple and straightforward, it becomes impractical in real time applications when there is a limited time to perform the uncertainty analysis due to the large number of model runs required. In addition, the traditional MC based simulation also lacks well-established convergence criteria to terminate the simulation at a desired level of accuracy, and the subjective information will be involved and cause more uncertainties (Ballio and Guadagnini, 2004).

To compensate for some drawbacks of the GLUE methods, some attempts have been made by using Latin Hypercube sampling (LHS) method, Markov Chain Monte Carlo (MCMC) methods, delayed rejection adaptive Metropolis method, and differential evolution adaptive Metropolis method (DREAM) to improve sampling efficiency and the feasibility of the GLUE method (Makowski *et al.*, 2002; Pappenberger *et al.*, 2005; Haario *et al.*, 2006; McMichael *et al.*, 2006; Mugunthan and Shoemaker, 2006; Vrugt *et al.*, 2008). In these

above Metropolis algorithm based uncertainty analysis methods, the comparison of the statistics of multiple sample chains in parallel could provide a formal solution to estimate the required model runs to achieve convergence and obtain stable statistics of the model parameters and output (Shrestha *et al.*, 2009). In this study, a modified calibration and uncertainty method was developed to overcome some drawbacks of the original GLUE method which has been provided in **Chapter 5**.

2.4.3.2 **Sequential uncertainty fitting version 2 (SUFI-2):**

The SUFI-2 method is based on a Bayesian framework, and it determines uncertainties through the sequential and fitting process in which iteration and unknown parameter estimates are achieved before the final estimates. In this method, parameter uncertainties accounts for various possible sources, such as uncertainty in model input, model structure, model parameters, and observed data. A required stopping rule is a critical value of an objective function. For most studies, the Nash-Sutcliffe coefficient (NSE) was defined as the objective function. An indicator P-factor, which is defined as the ratio of the number of the observed data falling with their respective prediction intervals to the total number of observed data, can be used to evaluate the capability of the prediction intervals to capture the observed data. P-factor is the percentage of measured data bracketed by the 95% prediction uncertainty (95PPU) calculated at the 2.5% and 97.5% levels of the cumulative distribution of the output variables. Another measure quantifying the strength of uncertainty analysis is called the R-factor, which is equal to the average thickness of 95PPU band divided by the standard deviation of the observed data (Abbaspour *et al.*, 2007). If prediction bounds are large enough to include most of observed data, it means that parameter variability

alone can compensate for other sources of error, and thus it can account for the total output uncertainty (Bastola *et al.,* 2011). However, the larger uncertainty is not the desired results people looking for. The relatively small uncertainty interval which covers most of observed data is the expected result as the good uncertainty analysis.

The concept behind the uncertainty analysis of the SUFI-2 method is graphically shown in **Figure 2.3**. The **Figure 2.3(a)** illustrates that a single parameter value produces a single model response, while **Figure 2.3(b)** shows the propagation of the parameter uncertainty leads to the 95PPU of the model response (the shaded region). From **Figure 2.3(c)**, it clearly depicted that due to the increase of parameter uncertainty the 95PPU becomes wider which means the output uncertainty also increases (not necessarily linearly). In **Figure 2.3(d)**, the red line represents the observed response. **Figure 2.3(d)** also indicates that the observed response is totally outside of 95PPU, which means there are mistakes of modeling settings or structure errors of the model and new model settings should be used or other suitable hydrological models can be applied. The SUFI-2 method begin with assuming a large parameter uncertainty (physically meaningful range) to make the measured data fall into the 95PPU, and decrease the uncertainty in several steps while monitoring the P-factor and R-factor. The previous parameter ranges will be updated by calculating the sensitivity matrix and equivalent of Hessian matrix, followed by calculating the covariance matrix, 95% confidence intervals of the parameters, and correlation matrix. Through this process, parameters are updated with new ranges which are always smaller than the previous ranges and centered around the best simulation (Abbaspour *et al.*, 2004; Abbaspour *et al.*, 2007; Abbaspour, 2015).

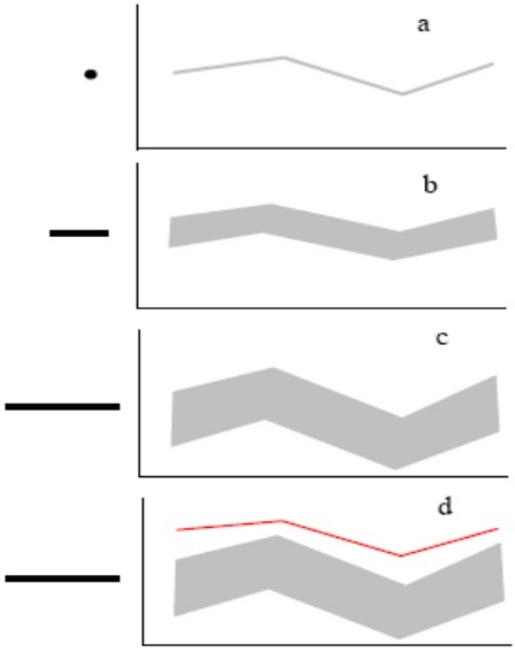

Figure 2.3 The illustration of the relationship between parameter uncertainty and prediction uncertainty
(Abbaspour, 2015)

The purpose of the SUFI-2 method is to search for bracketing most of the measured data with smallest possible uncertainty band, which means good results should have a relative large P-factor with relative smaller R-factor. These two measures can be used to evaluate the performance of uncertainty analysis. Theoretically, the value for P-factor ranges from 0 and 100%, and R-factor ranges between 0 and infinity. A P-factor of 1 and R-factor of 0 is a simulation that exactly matches the measured data. Certainly, a large P-factor can be achieved at the expense of a larger R-factor. Therefore, a balance between these two measures has to be made. When acceptable P-factor and R-factor are obtained, the reduced parameter uncertainty ranges are the desired parameter ranges (Abbaspour, 2011).

2.4.3.3 **Parameter solution (ParaSol)**

The ParaSol method (Van Griensven and Meixner, 2006) is a method that performs optimization and uncertainty analysis for complex models (such as distributed hydrological models and water quality models). The ParaSol method aggregates objective functions into a global optimization criterion, minimizes these objective functions or a global optimization criterion by using SCE-UA, and performs uncertainty analysis with a choice between two statistical concepts.

The SCE-UA method is a global search method to minimize a single objective function by using competitive complex evolution (CCE) algorithm to update/evolve each complex (Duan *et al.*, 1994). This method is mainly based on four important concept, including: 1) combination of deterministic and probabilistic approaches; 2) systematic evolution of a complex of points spanning the parameter space towards to global optimum; 3) CCE algorithm; and 4) complex shuffling method (Nelder and Mead, 1965; Duan *et al.*, 1994; Abbaspour, 2011).

Many studies has proved that SCE-UA is a robust, flexible and efficient algorithm for model calibration and optimization, and the method has been widely used in watershed model calibration and other areas of hydrology including soil erosions, subsurface hydrology, remote sensing, and land surface modeling (Manetsch, 1990; Wang, 1991; Sorooshian *et al.*, 1993; Duan *et al.*, 1994; Duan, 2003). A robust global optimization method needs to possess properties, including: 1) global convergence for multiple regions of attractions; 2) the ability to avoid being trapped by small pits and bumps on the response surface; 3) robustness for differing parameter sensitivities and interdependence; 4) ability to handle high-parameter dimensionality; and 5) non-reliance on the availability of an explicit expression for an

objective function. Comparing other methods for calibrating watershed, SCE-UA has its own advantages to sampling for posterior distribution, such as: 1) combination of deterministic and probabilistic methods; 2) the ability for systematic evolution within a complex spanning the parameter space towards to the global optimum; 3) competitive evolution; and 4) complex shuffling. Due to the synthesis of above elements, the SCE-UA has been proofed efficient and robust (Manetsch, 1990; Wang, 1991; Duan *et al.*, 1992; Duan *et al.*, 1994).

Normally, the first step, SCE-UA selects an initial population by random sampling throughout the feasible parameters space for n parameters to be optimized and computes the criterion value at each point. The next step is to rank the points according to criterion values, and partition the population into several complexes (communities) which contain 2n+1 points. Each complex is then evolved by using CCE algorithm to share information between complexes. The last step is to check the convergence and reduction in the number of complexes. If criteria are fully satisfied, the optimization can be stopped.

Some of examples of successful applications of the ParaSol method can be found in literatures. The ParaSol method has been successfully tested by a simple bucket model and applied to a case study of the Honey Creek, OH, USA (Van Griensven and Meixner, 2007). Yang *et al.* (2008) conducted uncertainty analysis using the ParaSol method for hydrological modeling using the SWAT model, and the results were used to compare with results from other methods. Setegn *et al.* (2010) applied the ParaSol method to uncertainty analysis in the Lake Tana Basion, Ethiopia. Wu *et al.* (2013) and Wu and Chen (2014a) successfully applied the ParaSol method as uncertainty analysis method, and reasonably good results have been achieved.

2.5 Summary

This research is trying to develop different methods to support and improve the performance of hydrological simulation under changing climatic conditions, and the developed methods include an advanced sensitivity analysis and calibration method, a novel calibration and uncertainty analysis method, and a new method for statistically evaluating the uncertainty propagation effect during statistical downscaling. In order to achieve these goals, comprehensive review has been conducted to support each developed method.

In this literature chapter, hydrological modeling, climate change and downscaling methods, sensitivity analysis, and uncertainty analysis were reviewed. As the importance of uncertainty analysis in this thesis research, more efforts were paid to uncertainty analysis. Different sources of uncertainty were first discussed, including input uncertainty, model structure uncertainty, and parameter uncertainty were reviewed and discussed; and then three important and popular uncertainty analysis methods for hydrological modeling were reviewed; at last, uncertainty during downscaling studies was discussed. The comprehensive review in this chapter provides the scientific references for advantages and disadvantages of current available methods, and the proposed methods are trying to fill the gap or overcome some drawbacks of current methods. The detailed proposed methods and case studies are provided in following chapters.

CHAPTER 3.

A DOE-AIDED SENSITIVITY ANALYSIS AND PARAMETERIZATION (DOE-SAP) METHOD FOR HYDROLOGICAL MODELING

The contents in the chapter are based on the following publications:

1. **Wu, H.J**., Lye, L. and Chen, B. (2012). A design of experiment aided sensitivity analysis and parameterization for hydrological modeling. *Canadian Journal of Civil Engineering*, 39, 460-472.
   Role: I developed the model, conducted case studies and drafted manuscript. Dr. Leonard M. Lye is my PhD supervisory committee member and provided advice in developing the method and manuscript drafting. Dr. Bing Chen is my PhD supervisor and provided advice in manuscript drafting.

2. **Wu, H.J.**, Lye, L., and Chen, B. (2010). Sensitivity Analysis of the Input Parameters of the SLURP Hydrological Model Using Design of Experiment (DOE) Methodology. CSCE 2010 General Conference proceeding, Winnipeg, Manitoba, CA, GC-059.
   Role: I developed the model, conducted case studies and drafted manuscript. Dr. Leonard M. Lye is my PhD supervisory committee member and provided advice in developing the method and manuscript drafting. Dr. Bing Chen is my PhD supervisor and provided advice in manuscript drafting.

3.1 Background

Sensitivity analysis is important to support hydrologic modeling which involves a variety of characteristics for which some input values cannot be accurately measured and clearly defined (Scott *et al.*, 2003; Gooseff *et al.*, 2005; Foglia *et al.*, 2009). Traditionally, sensitivity analysis is conducted by using the one-factor-at-a-time (OFAT) method. This method can only adjust one parameter at a time, which sacrifices some information due to the lack of consideration of the interactions between the parameters (Czitrom, 1999; Montgomery, 2008; Zhang *et al.*, 2009). To address this issue, this study integrates the use of design of experiment (DOE) methodology particularly fractional factorial design and central composite design (CCD) with a hydrological model to improve the modeling performance by examining interactions of the key parameters and further optimizing the parameterization process. The Semi-distributed Land Use-based Runoff Process (SLURP) hydrological model (Kite, 1975) will be employed to simulate the targeted wetland system in the Deer River watershed, near Churchill, Manitoba.

The objectives of this study are 1) to apply statistical DOE method to understand and quantify the contributions of key parameters and their interactions in the hydrological model; 2) to conduct a DOE aided sensitivity analysis for the key parameters; and 3) to optimize the parameter sets to support the calibration of the key input parameters to improve simulation performance. The DOE-aided method was proposed and successfully applied to a hydrological model (the SLURP model) and improved the performance of simulation results for the Deer River watershed.

3.2 Methodology

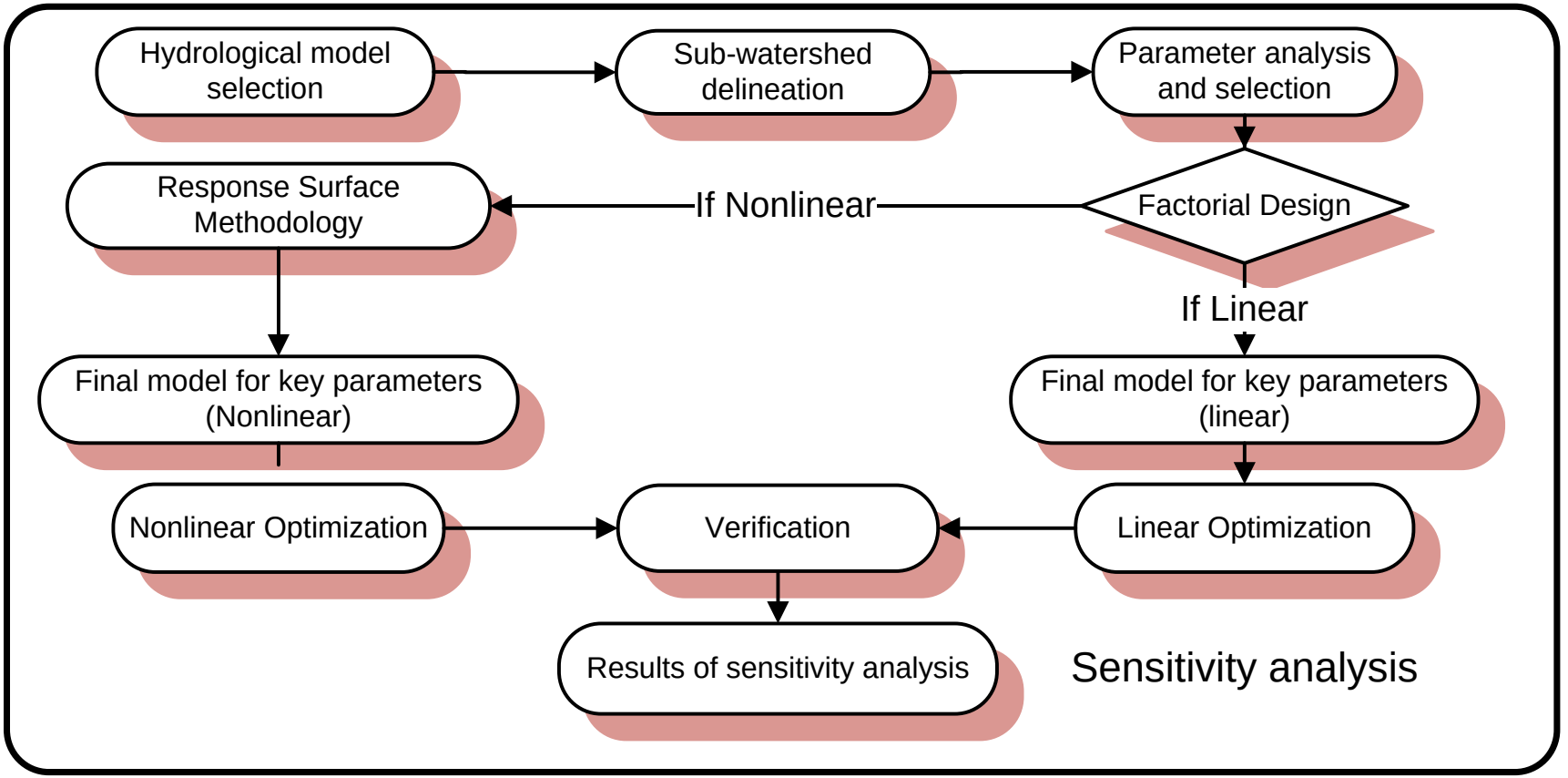

Figure 3.1 The Proposed DOE-aided sensitivity analysis and parameterization method

3.2.1 **Framework of the DOE-aided sensitivity analysis and parameterization method**

Figure 3.1 shows the framework of the proposed DOE-aided sensitivity analysis and parameterization (DOE-SAP) method. The method makes use of statistical DOE method to build a model to represent the relationship between the parameters and hydrologic responses. Depending on the features of the established DOE model, the final predicted parameter sets can be achieved through linear optimization or nonlinear optimization procedures. The major steps are briefly described as follows:

3.2.2 **Hydrological modeling**

Hydrological models are described as simplified, conceptual representations of a part of the hydrologic cycle, and mainly used for understanding hydrological processes and for hydrologic prediction (Singh, 1995). Among them, the SLURP hydrological model is a widely recognized simulation tool, which was developed for simulating and predicting hydrological features at macroscale basins. It adopted the concept of dividing the whole catchment into multiple aggregate simulation areas (ASA) and could utilize some distributed parameters and data (Kite, 1997). Su *et al.* (2000) used the SLURP model to simulate the water level variations over a 28-year period for a prairie wetland in Saskatchewan and obtained good results. In this study, the SLURP model was selected to simulate the runoff and provide a better understanding of the water balance of the Deer River watershed in the Hudson Bay lowlands.

3.2.3 **Parameter analysis**

After choosing the model, the second step to determine which parameters should be taken into account for further sensitivity analysis and optimization. For most hydrological

models, the most important input parameters or parameters with significant effects on the runoff will be considered. The effects of the parameters usually are shown in the model's manual where the developer has conducted traditional sensitivity analysis. For the SLURP model, there are a total of 31 parameters, which can be derived from measurement, estimation or calibration. Among the 31 parameters, ten parameters are considered relatively more important than others, and the level of contribution of each parameter to the final runoff has been shown in the model user's manual. If all 31 parameters were selected for parameter analysis, the number of experimental runs would become very large and time-consuming. In this study, these ten important parameters were selected to test the sensitivity on the goodness of fit of the observed and simulated runoff through the proposed DOE-aided sensitivity analysis method.

3.2.4 **Linear parameterization**

Factorial design and response surface method (RSM) are two of the major approaches in DOE methodology (Bajsic and Kunsek, 2003; Karimi *et al.*, 2010). Factorial design is commonly used to determine the influence of different factors in a system or procedure. Basically, factorial design is satisfactory to estimate linear response surface with a very low number of experimental runs (Plesu *et al.*, 2009; Simate *et al.*, 2009). If the linear DOE model can adequately represent the relationship between the parameters and response and capture the optimal value of the response, the factorial design will be the most efficient method for optimization. Linear optimization could be applied for the linear DOE model, which was obtained by factorial design, to predict the optimal value of the linear DOE model.

3.2.5 **Nonlinear parameterization**

If the DOE model obtained from selected parameters and the response is linear, factorial design can adequately generate the final response model (which only contains key parameters); however, if the DOE model is nonlinear, RSMs can be used after screening out the key factors from factorial design. As a collection of mathematical and statistical techniques, RSM is commonly applied in practice to investigate and optimize nonlinear responses (Li *et al.*, 2008). RSMs could reduce the number of experiments needed to evaluate the multiple parameters and their interactions in order to optimize the response that is influenced by various parameters (Kwak, 2005; Aslan, 2007). Central composite design (CCD) is a popular RSM technique that can be used to investigate the curvature of the nonlinear response surface and find its maximum or minimum response (Khawas *et al.*, 2011). CCD gives almost as much information as a three-level factorial design but far more efficient, and has been demonstrated to be sufficient to describe the majority of responses in curved surface (Kannan *et al.*, 2004; Karimi *et al.*, 2010). CCD was selected for the second-round experiment in this study. Once the CCD response model fit the response surface well and accurately captured the center points, nonlinear optimization could be applied to find the best combination of different parameters to achieve the optimal value.

3.2.6 **Response selection**

An important response should be selected before the DOE model can be established. This response should be able to demonstrate the performance of the simulation of the hydrological model. In this study, Nash-Sutcliffe coefficient (NSE, which was calculated by using observed runoff and response of simulation from the SLURP model) was used to evaluate the performance of simulation. Due to the nonlinearity of the DOE model obtained

from the input parameters and NSE, by using the factorial design (minimum run resolution V design) and CCD, the relationship between the input parameters and NSE was investigated.

3.2.7 **Optimization**

After the factorial design and RSM were conducted, the final response model with key parameters should be able to adequately represent the relationship between key input parameters and response. To improve the simulation efficiency, linear/nonlinear optimization can be applied to optimize the results of the response model. By making use of the results, the combination of the values of each parameter which can achieve the optimized value can be calculated. In this case, because the NSE was selected as the response in factorial design and CCD, the highest NSE value means the best performance. To maximize the NSE value, nonlinear optimization was used to calculate the largest value of NSE from the final response model, and to obtain the corresponding values for each factors in the final response model.

3.2.8 **Verification**

The results obtained from optimization of the response surface were verified using the original hydrological model with parameters suggested by the factorial design and RSM model. In this study, a new combination of each key parameter was used as new input values for the SLURP model to verify feasibility of the CCD response model. By using a new combination of the values of each parameter, the optimized responses predicted by the CCD response model will be compared with the results obtained from the SLURP model. The results demonstrated that the CCD response model had an ability to represent the relationship between key input parameters and NSE calculated by using observed runoff and response of simulation from the SLURP model.

3.2.9 **Sensitivity analysis**

The coefficient of each key factor in the final model generated by the RSM methods can show the magnitudes of their effects on the final response. From the results, a sensitivity analysis on key parameters in the hydrological model can be conducted. The greater absolute value of coefficient, the more sensitive the factor. In this study, through previous verification, the CCD response model was tested to determine that it was capable of modeling the relationship between input parameters and calculated NSE in the SLURP model. Therefore, the value of coefficient for each key parameter in the final response model can be used to show the relative contributions of the factors on the response.

3.3 Case study

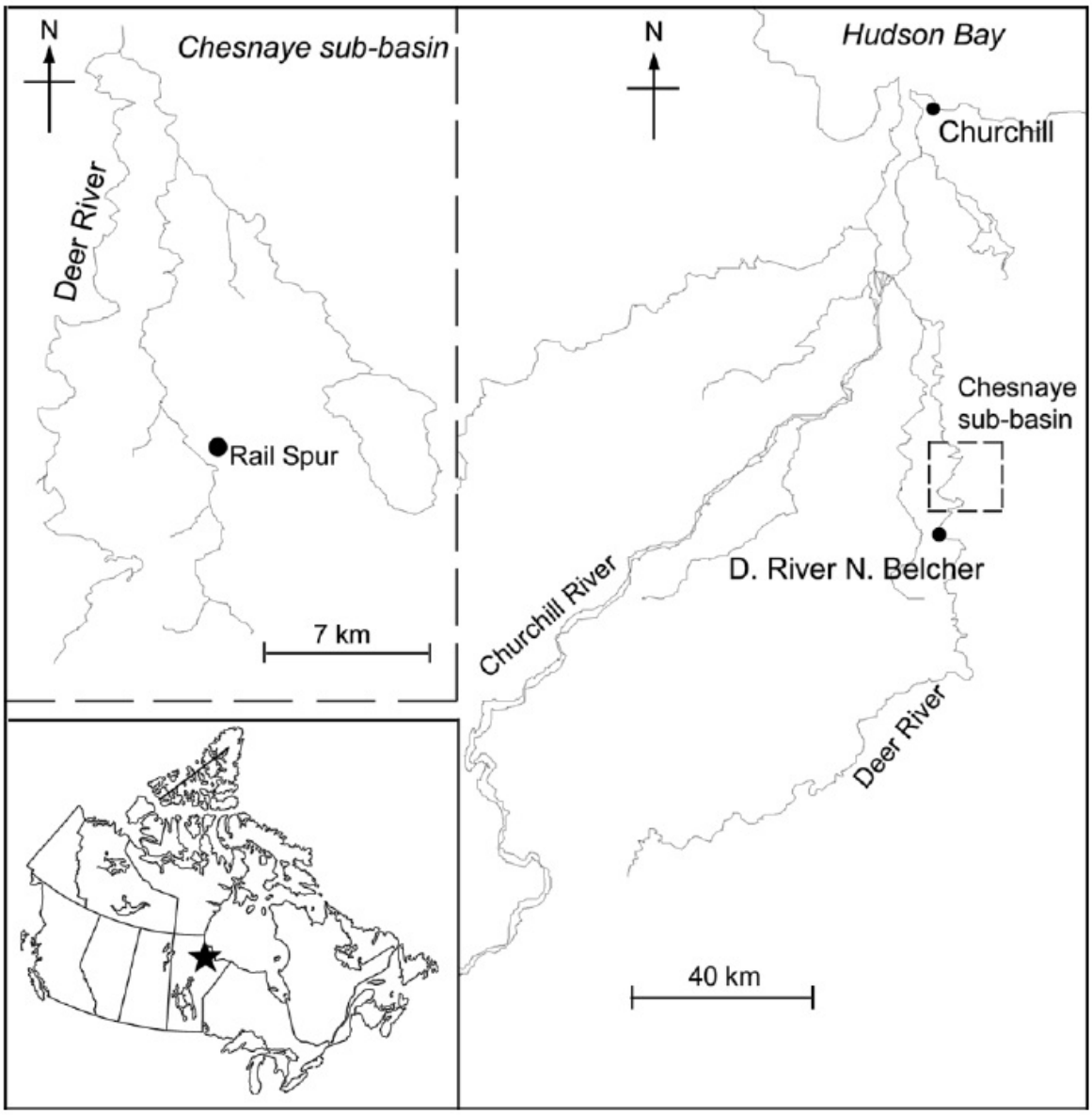

Figure 3.2 The Map of the Deer River Watershed

The study area is located in the Deer River watershed near Churchill, Manitoba. This watershed represents a typical sub-arctic wetland system which is a part of the Hudson Bay lowlands (**Figure 3.2**). To understand the water balance in this watershed, extensive field investigations were carried out in the past four years, through which the hydrological and meteorological data have been collected. In Jing and Chen (2011a) study, TOpographic PArameteriZation (TOPAZ) was used to delineate the watershed into aggregated simulation

areas (ASAs) for supporting the SLURP model to simulate the runoff in the watershed. The NSE and deviation of runoff volumes (Dv) for twenty-eight years runoff data were used to evaluate the performance of the SLURP model (Jing and Chen, 2011a).

The ten important parameters which can be optimized by the automatic calibration process that is built in the SLURP model, include "Initial contents of snow storage", "Initial contents of slow storage", "Maximum infiltration rate", "Manning roughness coefficient", "Retention constant of fast storage", "Maximum capacity for fast storage", "Retention constant for slow storage", "Maximum capacity for slow storage", "Precipitation factor", and "Rain/snow division temperature". The SLURP model can make use of meteorological data and daily historic surface runoff to optimize those parameters in order to achieve the best fit between the observed and simulated results. The values for the ten parameters were calibrated using ten years of daily runoff data (1978-1987), and the model was also validated by using the next ten years (1988-1997) of daily runoff data. The results showed that the SLURP model could adequately represent the water balance in this subarctic wetland system (Jing, 2009). To further improve the performance of the SLURP model, those parameters were selected to examine the main effects and their potential interactions.

Model evaluation statistics such as NSE and D_v were recommended by ASCE Task Committee (1993) as well as the commonly used statistical indicator, correlation coefficient (R), were extensively used to evaluate hydrological model in previous studies (Verma *et al.*, 2010). NSE is commonly used to test the goodness of fit of hydrological models. For a perfect fit, the NSE is equal to 1. Therefore, the closer NSE is to 1, the better the model. The D_v known as the percentage bias is one of the simplest goodness-fit criterion. For an ideal model, the value of D_v should be 0. The correlation coefficient (R) reflects the degree of

colinearity between the observed data and predicted data. According to the definition, a perfect model could give a correlation coefficient equal to 1. These three indicators were selected to evaluate the performance of the optimization of the model. The NSE, Dv and R can be determined by using the following equations (Nash and Sutcliffe, 1970; Kite, 1997; MacLean, 2005; Verma *et al.*, 2010):

$$NSE = 1 - \frac{\sum_{i=1}^{n}\left(Q_{s,i} - Q_{o,i}\right)^2}{\sum_{i=1}^{n}\left(Q_{o,i} - \overline{Q_o}\right)^2} \tag{3.1}$$

$$D_v(\%) = \left(\frac{\sum_{i=1}^{n}\left(Q_{s,i} - Q_{o,i}\right)}{\sum_{i=1}^{n} Q_{o,i}}\right) * 100 \tag{3.2}$$

$$R = \frac{\frac{1}{n} * \sum_{i=1}^{n}\left(Q_{o,i} - \overline{Q_o}\right) * \left(Q_{s,i} - \overline{Q_o}\right)}{\sqrt{\left(\frac{n * \sum_{i=1}^{n} {Q_{o,i}}^2 - \left(\sum_{i=1}^{n} Q_{o,i}\right)^2}{n * (n-1)}\right)} * \sqrt{\left(\frac{n * \sum_{i=1}^{n} {Q_{s,i}}^2 - \left(\sum_{i=1}^{n} Q_{s,i}\right)^2}{n * (n-1)}\right)}} \tag{3.3}$$

Where $Q_{o,i}$ and $Q_{s,i}$ are the observed and simulated values on day i, respectively; $\overline{Q}_o$ and $\overline{Q}_i$ are the average values of the observed and simulated surface runoff (m^3/s), respectively; and n is the total number of values within the period of analysis.

To obtain the best performance of the SLURP model, (Jing, 2009) used the automatic calibration module built in the SLURP model to obtain the optimized values for the ten

parameters. From the result of calibration, the average NSE, Dv and R value were 0.461, 0.150 and 0.684 for the period of 1978-1987, respectively. For the next ten years (1988-1997), the average values of NSE, Dv and R were equal to 0.513, 0.170, and 0.722, respectively.

Using the Normalized Difference Vegetation index (NDVI) method, the whole watershed can be classified into six types of land cover in the Deer River watershed, which are water cover, impervious cover, marsh cover, shrub cover, coniferous cover, and deciduous cover. Typically, each parameter has different values for those six types of land cover after calibration and validation. Because the target of this study is to determine the sensitivity of those ten input parameters and their interaction via statistical DOE methodology and conduct the calibration. The most important parameters among these ten parameters have to be screened, and the curvature of the final response model needs to be determined. The combination of parameters that was provided by automatic calibration to achieve the best fit can be further improved by using the DOE results. The factorial design was firstly applied to preliminary estimate the effects of different parameters, and then RSM was used to build a DOE model to represent the relationship between significant parameters and the response. The DOE model descriptions and settings are shown in next section.

3.4 Results and discussion

3.4.1 **Minimum runs of design resolution V**

To screen for the most important parameters, a minimum run resolution V factorial design for ten factors was first conducted. According to the definition, a design of resolution V has no main effects or two factor interactions aliased with any other main effect or two-

factor interaction, but two-factor interactions are aliased with three-factor interactions (Deng and Tang, 1999; Xu, 2009). Normally, three-factor interactions can be ignored. As it is mentioned above, these ten important input parameters were viewed as factors in the experiment. The factor A to K signify the parameter "Initial Contents of snow storage", "Initial Contents of slow storage", "Maximum infiltration rate", "Manning roughness", "Retention constant for fast storage", "Maximum capacity for fast storage", "Retention constant for slow storage", "Maximum capacity for slow storage", "Precipitation factor", and "Rain/snow division temperature", respectively. Each parameter has six values for the corresponding types of land cover. Therefore, there are a total of 12 values (6 upper bound and 6 lower bound values) for one parameter (factor), as shown in **Table 3.1**. Because the DOE method can investigate the optimal factor space (which can lead to the optimized objective function results), the parameter ranges were set relatively large for the DOE model. In the first round of factor screening, the values for the upper and lower bounds of each parameter were 130% and 70% of the automatic optimized values, respectively. Once the nonlinearity in the model was determined, a narrower range would be used for the next phase of experimentation using CCD.

Table 3.1 Factors and their upper and lower bound values

Factor (Parameter)	Lower bound value			Upper bound value		
A: Initial Contents of snow storage (mm)	7.00E-01	7.00E-01	7.00E-01	1.30E+00	1.30E+00	1.30E+00
	7.00E-01	7.00E-01	7.00E-01	1.30E+00	1.30E+00	1.30E+00
B: Initial Contents of slow storage (%)	6.84E+00	6.04E+00	2.97E+00	1.27E+01	1.12E+01	5.51E+00
	4.79E+00	4.13E+00	4.34E+00	8.89E+00	7.67E+00	8.07E+00
C: Maximum infiltration rate (mm/day)	7.06E+01	9.97E+01	7.48E+01	1.31E+02	1.85E+02	1.39E+02
	1.03E+02	7.83E+01	7.40E+01	1.92E+02	1.46E+02	1.38E+02
D: Manning roughness (n)	1.40E-02	5.60E-02	7.00E-03	2.60E-02	1.04E-01	1.30E-02
	4.90E-02	1.40E-02	2.10E-02	9.10E-02	2.60E-02	3.90E-02
E: Retention constant for fast storage (day)	2.59E+01	3.68E+01	3.81E+00	4.81E+01	6.84E+01	7.09E+00
	5.24E+00	4.40E+01	2.83E+01	9.72E+00	8.18E+01	5.27E+01
F: Maximum capacity for fast storage (mm)	6.67E+01	9.37E+01	3.72E+02	1.24E+02	1.74E+02	6.90E+02
	4.09E+02	2.62E+02	4.88E+02	7.59E+02	4.86E+02	9.06E+02
G: Retention constant for slow storage (day)	9.15E+01	1.20E+02	4.80E+02	1.70E+02	2.22E+02	8.92E+02
	5.22E+02	4.99E+02	5.23E+02	9.70E+02	9.27E+02	9.71E+02
H: Maximum capacity for slow storage(mm)	2.37E+02	1.82E+02	2.53E+02	4.41E+02	3.39E+02	4.71E+02
	7.20E+01	4.35E+01	4.43E+01	1.34E+02	8.09E+01	8.22E+01
J: Precipitation factor	7.00E-01	7.00E-01	7.00E-01	1.30E+00	1.30E+00	1.30E+00
	7.00E-01	7.00E-01	7.00E-01	1.30E+00	1.30E+00	1.30E+00
K:Rain/snow division temperature ℃	-3.71E-02	-7.34E-01	-1.29E+00	-2.00E-02	-3.96E-01	-6.94E-01
	-1.21E+00	-7.93E-01	-4.11E-01	-6.50E-01	-4.27E-01	-2.21E-01

Note: Each parameter has 6 lower and upper bound values for corresponding 6 types of land cover.

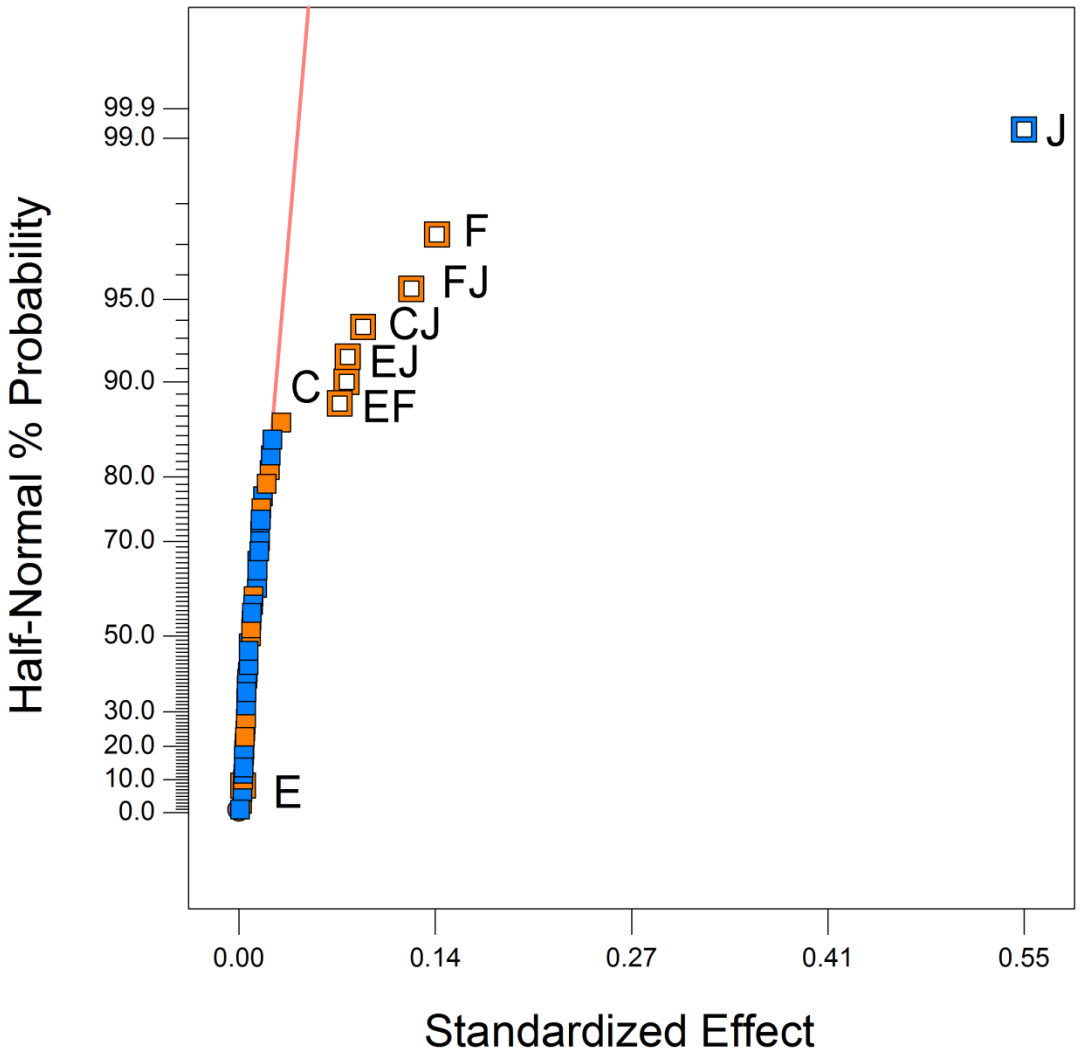

Figure 3.3 The Half-Normal Plot

In this study, Design Expert 7.1® was used to analyze the effects of different parameters (factors). The Half-Normal plot is shown in **Figure 3.3**. Viewed from **Figure 3.3**, factors C, F, J, CJ, EF, EJ, and FJ stood out as significant to the model. Factor E on its own was not significant. However, the interactions of EF and EJ were significant. Hence for the hierarchical reasons, this factor was included for further analysis. The analysis of variance (ANOVA) is shown in **Table 3.2**.

Table 3.2 The ANOVA of Minimum runs of design resolution V

Source	Sum of Squares	df	Mean Square	F Value	p-value Prob>F	
Model	5.02	8	0.63	209.9	<0.0001	significant
C-Maximum infiltration rate	0.076	1	0.076	25.4	<0.0001	
E-Retention constant for fast store	1.14E-04	1	1.14E-04	0.038	0.8457	
F-Maximum capacity for fast store	0.26	1	0.26	85.78	<0.0001	
J-Precipitation factor	4.02	1	4.02	1347	<0.0001	
CJ	0.1	1	0.1	33.75	<0.0001	
EF	0.066	1	0.066	22.21	<0.0001	
EJ	0.077	1	0.077	25.92	<0.0001	
FJ	0.19	1	0.19	65.01	<0.0001	
Curvature	0.14	1	0.14	47.67	<0.0001	significant
Residual	0.14	47	2.99E-03			
Cor Total	5.3	56				
Std. Dev.	0.055	R-Squared	0.9728			
Mean	0.086	Adj R-Squared	0.9681			
C.V. %	63.22	Pred R-Squared	N/A			
PRESS	N/A	Adeq Precision	37.75			

As can be seen, factors C, F, J, CJ, EF, EJ and FJ are significant model terms because the p-value of these factors are smaller than 0.05 (other main parameters and interactions are insignificant and removed due to the higher p-value). There is significant curvature measured by the difference between the average of center points and the average of the factorial points in the design space. There are four main diagnostic plots to check the assumptions of ANOVA. These are: "normal plot of residuals", "residuals vs. predicted", "Residuals vs. Run", and "Predicted vs. Actual", which have been shown below:

(a)

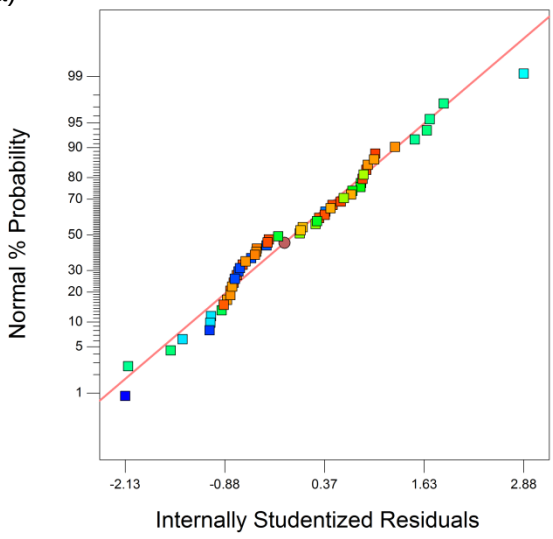

(b)

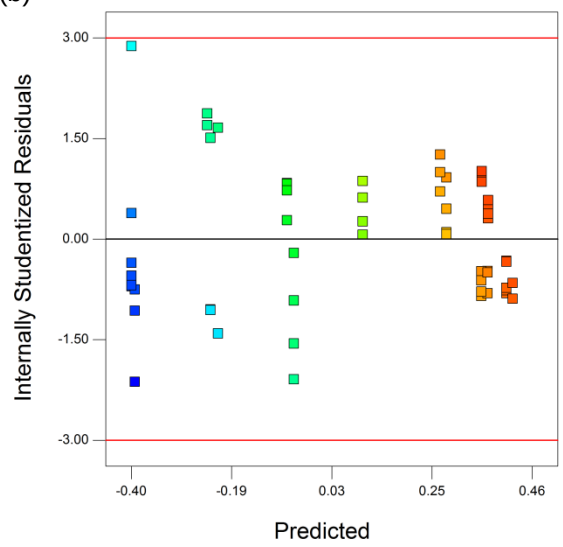

(c)

(d)

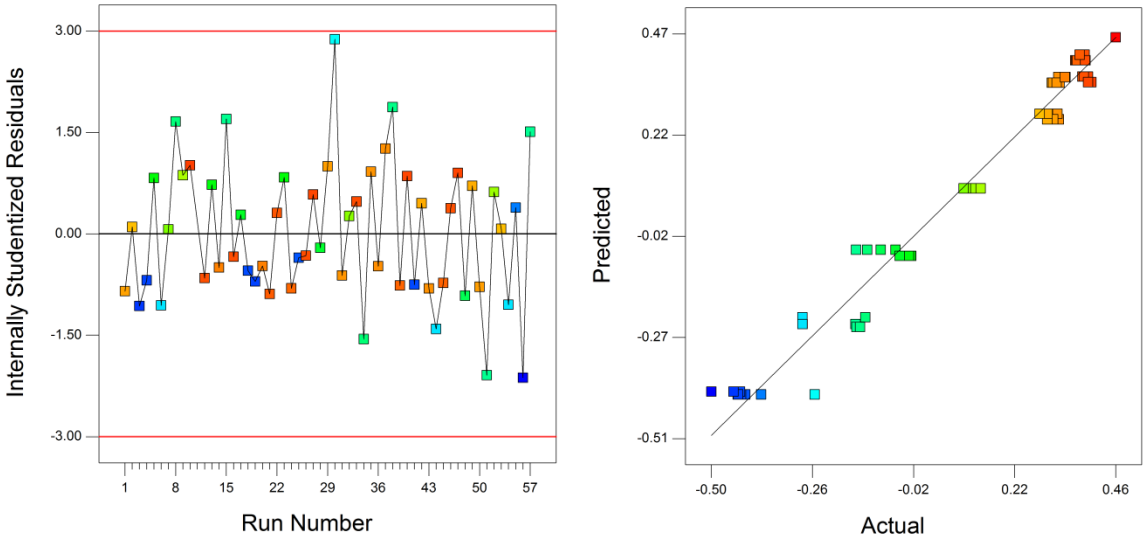

Figure 3.4 Diagnostic plots for assumption of ANOVA: (a) normal plot of residuals, (b) residuals vs. predicted, (c) residuals vs. run, and (d) predicted vs. actual.

From **Figure 3.4(a)**, all the residuals are close to the straight line indicating that a normal distribution of residuals assumption is satisfied. **Figure 3.4(b)** shows that the residuals were scattered randomly within the upper and lower bounds and do not accumulate in any area fulfilling the assumption of homoscedasticity. **Figure 3.4(c)** shows all the residual points when plotted against run order are spread within upper and lower bounds and shows no patterns. This plot indicates the independence assumption is satisfied. In **Figure 3.4(d)**, all the points are close to the straight line, which indicates the "predicted versus actual" plot is very good and the model fits well. Therefore, all the diagnostic plots indicated all the required assumptions of ANOVA were met.

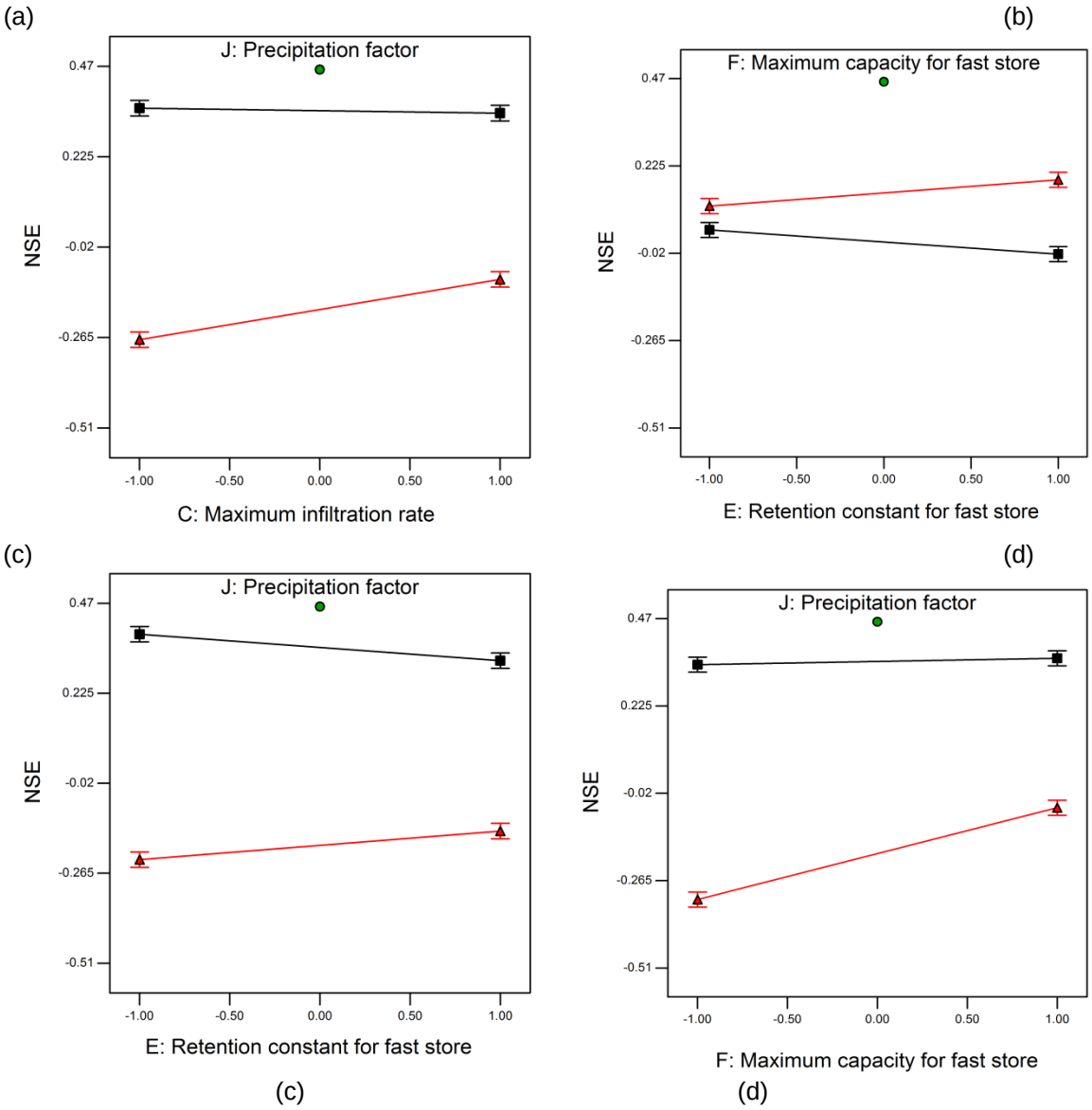

Figure 3.5 Interaction model graphs

Figure 3.5 shows the four two-factor interactions graph. The lines with triangle marks are the factors (showed in top of each graph) at high levels, and the lines with square marks are their low levels. The "-1.00" to "1.00" in X axis of each graph shows the low level to high level of factors (showed in bottom of each graph). **Figure 3.5(a)** shows the interaction between "Maximum infiltration rate" and "Precipitation factor". This interaction

revealed that: at low level of "Precipitation factor", the NSE would decrease slightly when "Maximum infiltration rate" changed from low level to high level; at a high level of "Precipitation factor", the NSE increased much more with "Maximum infiltration rate" changing from low level to high level. In addition, at low level of "Precipitation factor" the NSE was always higher than the NSE at high level. Similarly, **Figure 3.5(b)** shows that: at low level of "Maximum capacity for fast storage", the NSE would decrease when "Retention constant for fast storage" changes from low level to high level; at a high level of "Maximum capacity for fast storage", the NSE increased with "Retention constant for fast storage" changing from low level to high level. At high level of "Maximum capacity for fast storage" the NSE was always higher than the NSE at low level of "Maximum capacity for fast storage". However, at high level of "Retention constant for fast storage" the NSE increased much more than the NSE increased at low level of "Retention constant for fast storage". **Figure 3.5(c)** shows the interaction of "Retention constant for fast storage" and "Precipitation factor", which is similar to the interaction effects of "Maximum infiltration rate" and "Precipitation factor". **Figure 3.5(d)** shows the interaction of "Maximum capacity for fast storage" and "Precipitation factor". This interaction shows that: at low level of "Precipitation factor", the NSE would increase slightly when "Maximum capacity for fast storage" changes from low level to high level; at a high level of "Precipitation factor", the NSE increased significantly with "Maximum capacity for fast storage" changing from low level to high level. It also shows that at low level of "Precipitation factor" the NSE was always high. From another point of view, at both low and high levels of "Maximum capacity for fast storage", the NSE was decreasing when "Precipitation factor" changes from low level

to high level. As shown in all the four interaction graphs, due to the curvature of the model the center point could not be modeled accurately by using the current model.

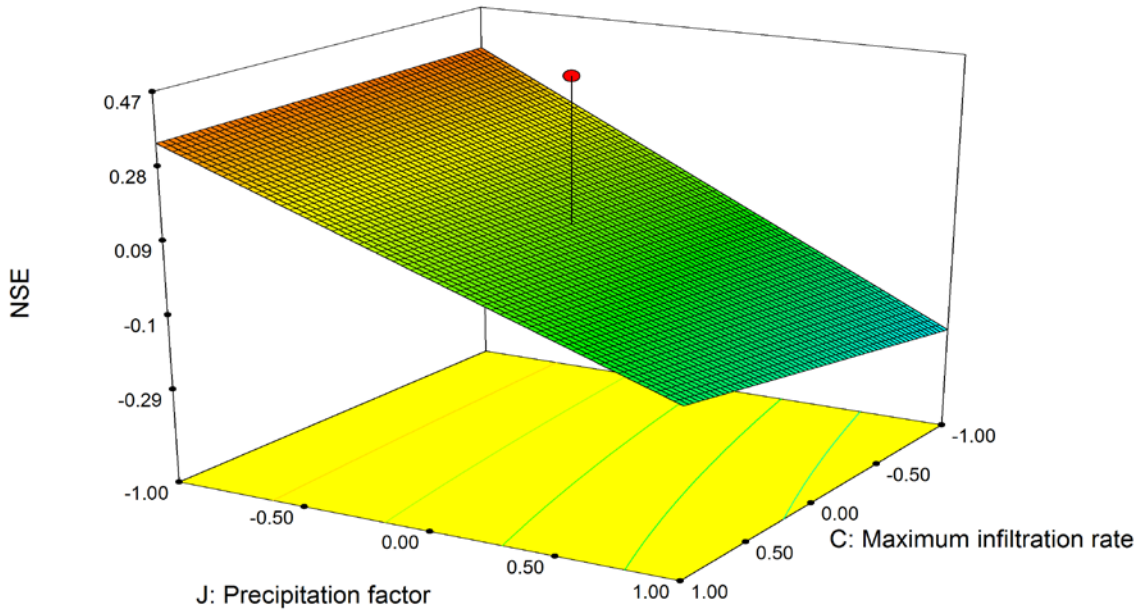

Figure 3.6 Three dimensional surface graph of interaction between factor "Precipitation factor" and "Maximum infiltration rate".

Figure 3.6 shows the 3D surface model graph of the interaction of "Precipitation factor" and "Maximum infiltration rate". The response surface of the factorial design is the flat surface. Therefore, the NSE value of centre point (red dot) is much higher than the NSE point in the predicted surface of factorial design shown in **Figure 3.6**. Because the response surface of factorial design cannot represent the nonlinearity of the relationship between significant parameters and the response, it is necessary to design the second experiment to model the nonlinear effect. Furthermore, to save the number of experimental runs, the six insignificant factors can be removed from the first round of experiment.

3.4.2 **Central composite design (CCD)**

If all 10 parameters were used for CCD response model, the number of experiment runs would become quite large, and it would cost more time and lower the efficiency of the experiment. Therefore, after the parameters screening process from the first round, insignificant factors can be deleted before proceeding to the second round. The most important factors in the first-round experiment are "Maximum infiltration rate", "Retention constant for fast storage", "Maximum capacity for fast storage", and "Precipitation factor". These four parameters were selected for the second-round experiment. To model the curvature of the response model generated by parameters and NSE values, the second-round experiment was conducted using the central composite design (CCD) method. To obtain a more accurate model, it is necessary to narrow down the ranges of factors. According to the trendline for connecting the lower bound point, the center point and the upper bound point in the 3D response surface model graphs (**Figure 3.6**), the most likely point to get the maximum NSE should be located in the range of 70% and 110% of the automatic optimized values. The new lower and high bound values of those parameters for CCD response model are shown in **Table 3.3**.

After the four factors and their lower bound values and upper bound values were decided, the experiment based on the CCD was conducted to estimate the effects of these parameters and try to predict the possible maximum NSE. In the second-round of simulation, the original automatic optimized values were used for the remaining six parameters. Validation is necessary to check the accuracy of this CCD response model, and the results are discussed in the later section. The ANOVA of the four-factor CCD response model is shown in **Table 3.4** below.

Table 3.3 Refined factors and the values of upper and lower bounds

Factor (parameter)	Lower bound value			Upper bound value		
C: Maximum infiltration rate (mm/day)	7.06E+01	9.97E+01	7.48E+01	1.11E+02	1.57E+02	1.18E+02
	1.03E+02	7.83E+01	7.40E+01	1.63E+02	1.23E+02	1.16E+02
E: Retention constant for fast storage (day)	2.59E+01	3.68E+01	3.81E+00	4.07E+01	5.79E+01	5.99E+00
	5.24E+00	4.40E+01	2.83E+01	8.23E+00	6.92E+01	4.45E+01
F: Maximum capacity for fast storage (mm)	6.67E+01	9.37E+01	3.72E+02	1.05E+02	1.47E+02	5.84E+02
	4.09E+02	2.62E+02	4.88E+02	6.42E+02	4.11E+02	7.67E+02
J: Precipitation factor	7.00E-01	7.00E-01	7.00E-01	1.10E+00	1.10E+00	1.10E+00
	7.00E-01	7.00E-01	7.00E-01	1.10E+00	1.10E+00	1.10E+00

Table 3.4 ANOVA of four-factor central composite design

Source	Sum of Squares	df	Mean Square	F Value	p-value Prob>F	
Model	0.08	6	0.013	23.75	< 0.0001	significant
E-Retention constant for fast store	2.14E-05	1	2.14E-05	0.038	0.8472	
F-Maximum capacity for fast store	5.39E-03	1	5.39E-03	9.63	0.0061	
J-Precipitation factor	3.84E-03	1	3.84E-03	6.86	0.0174	
EJ	7.21E-03	1	7.21E-03	12.88	0.0021	
FJ	2.33E-03	1	2.33E-03	4.16	0.0563	
J^2	0.061	1	0.061	108.91	< 0.0001	
Residual	0.01	18	5.60E-04			
Cor Total	0.09	24				
Std. Dev.	0.024	R-Squared	0.8878			
Mean	0.38	Adj R-Squared	0.8505			
C.V. %	6.3	Pred R-Squared	0.7882			
PRESS	0.019	Adeq Precision	15.289			

The results indicated that factors F, J, EJ and J^2 were the significant model terms. Because the P-value of FJ was 0.0563 and was very close to 0.05, this interaction was also considered in the final model in order to provide a more accurate prediction. Obviously, the factor J, "Precipitation factor", was involved in several significant terms in the model, which means this factor had multiple contributions to the final response. For example, even though decreasing the value of "Precipitation factor" might increase the NSE, it was not easy to determine whether the parameter "Precipitation factor" has a negative impact or positive impact on the final results, since the increase may be caused by the interactions which involve this factor. The assumptions of the ANOVA were checked and the model was found satisfactory. **Figure 3.7(a)** and **(b)** show the 3-D surface plot of the two interaction terms. They indicated that the second-round CCD response model could more accurately capture the curvature of the NSE response, and predict the possible maximum NSE, in comparison with the first-round (**Figure 3.6**).

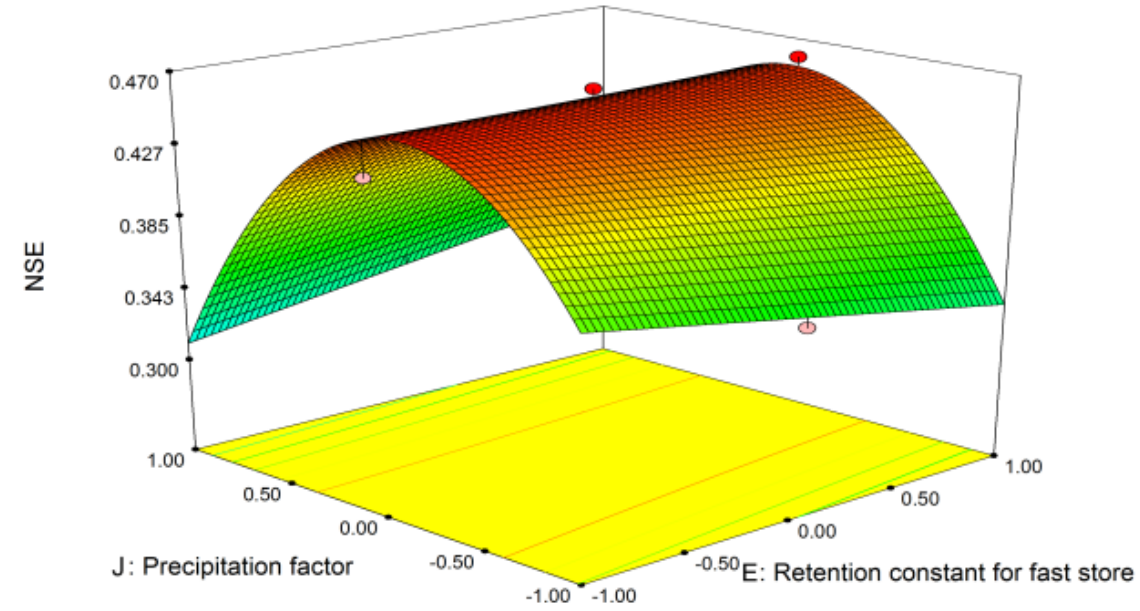

(a)

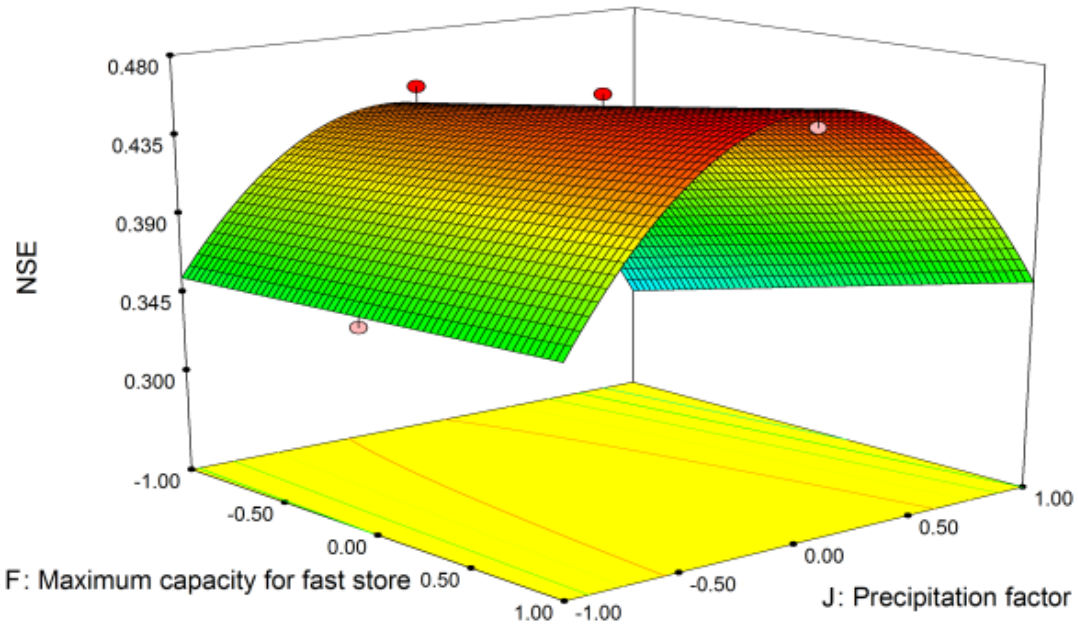

(b)

Figure 3.7 3D surface model graphs by using CCD

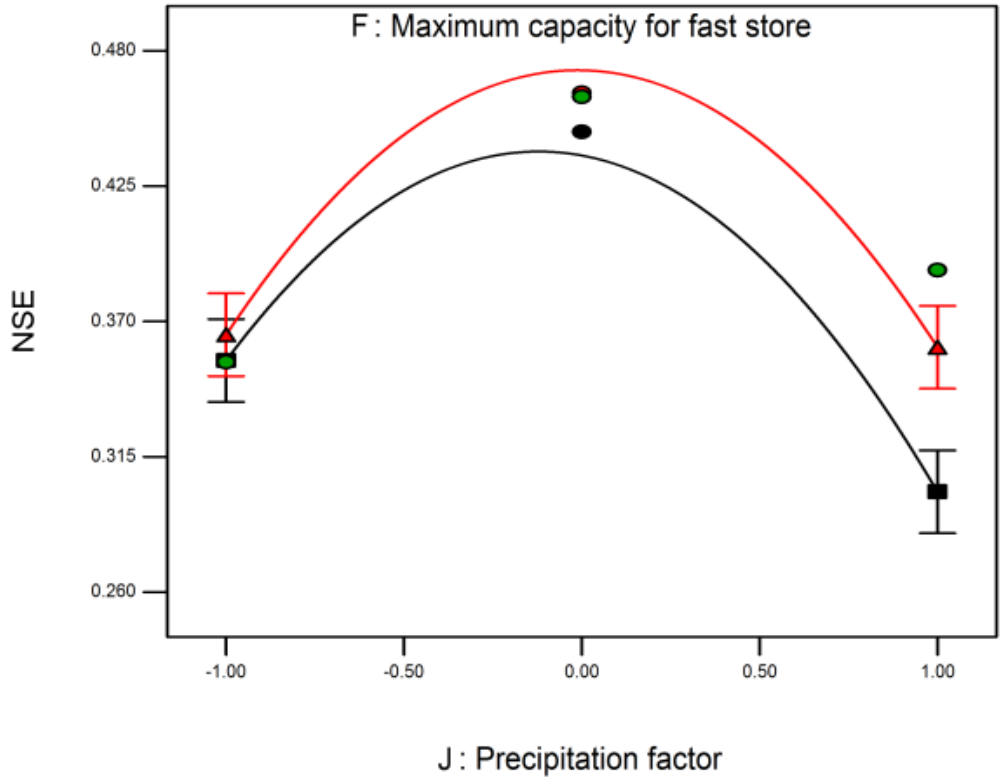

(a)

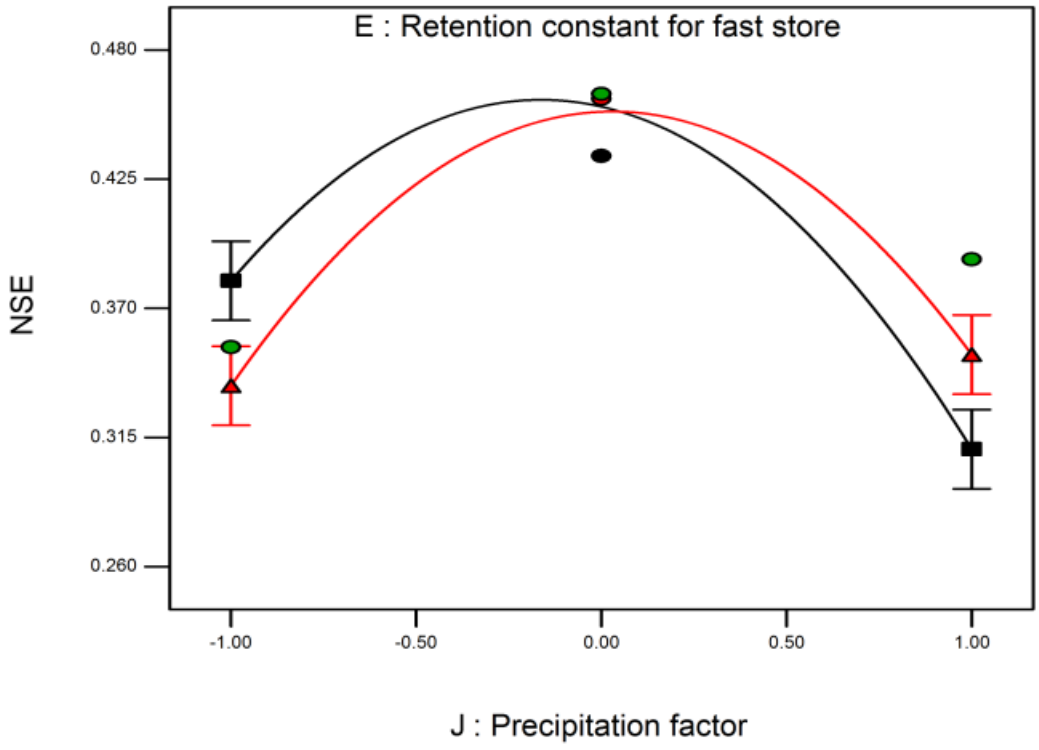

(b)

Figure 3.8 The interaction graph of "Maximum capacity for fast store" and "Precipitation factor" (a) and "Retention constant for fast store" and "Precipitation factor" (b)

Figure 3.8(a) shows the interaction graph of "Maximum capacity for fast store" and "Precipitation factor". The lines with triangle and square marks denote the upper and lower bounds of "Maximum capacity for fast store", respectively. In order to obtain a higher NSE value, the maximum value for "Maximum capacity for fast store" was preferred. **Figure 3.8(b)** shows the interaction graph of "Retention constant for fast store" and "Precipitation factor", which revealed that in order to get the highest NSE the minimum value of "Retention constant for fast store" should be selected and the value of "Precipitation factor" should be close to but smaller than the centre point. Once the information was collected from DOE methodology, point prediction could be conducted to check the accuracy of this CCD response model.

The regression equation for the NSE using the selected factors in coded factors is given by:

$$\begin{aligned} \text{NSE} &= 0.45474 - 1.09022 \times 10^{-3} * E + 0.017311 * F - 0.014608 * J \\ &+ 0.021230 * E * J + 0.012071 * F * J - 0.11 * J^2 \end{aligned} \tag{3.4}$$

The highest NSE was 0.474 by taking the maximum value of "Maximum capacity for fast store", the minimum value of "Retention constant for fast store" and coefficient "-0.11" for "Precipitation factor". The optimized results were further verified by using Lingo® through nonlinear optimization for equation 3.4. To validate the predicted maximum NSE, these values combined with other parameters that took their original values, were set as the new input data of the SLURP model. After that, the new simulation was conducted by the SLURP model, and the new results showed that the NSE for the new setting was 0.476, which was close to NSE value of 0.474 as predicted by the CCD response model and was

also greater than the original NSE value of 0.461 (Jing and Chen, 2011b) by using automatic optimized parameters. The simulated data were also used to calculate the D_v and R, and both of them improved from 0.150 to -0.025, and from 0.684 to 0.690 respectively. The NSE for the next ten year from 1988-1997 was also calculated to test the performance of the prediction. Correspondingly, the NSE, D_v and R value for the simulation during the period of 1988-1997 were 0.524, -0.033, and 0.728 respectively, better than their original values (NSE = 0.513, D_v = 0.170, and R = 0.722) (Jing and Chen, 2011b). It demonstrated that it was possible to effectively predict a reasonable combination of each parameter in the SLURP model to obtain a better performance of simulation by using the proposed method. Although the improvement is not quite significant, the main purpose of this study is to test the feasibility of the proposed method. Moreover, the original results are obtained through automatic calibration and considered to be the optimized simulation. Therefore, the small improvement still can show the advantage of the proposed method.

In this case, the second-round CCD response model could adequately represent the relationship between key input parameters and NSE calculated by using observed runoff and response of simulation from the SLURP model. The coefficient list and the final equation obtained from the ANOVA of the CCD response model are very useful to investigate the contribution of different factors and can help researchers conduct and control the experiment in a better way. The coefficient list is shown in **Table 3.5** as follow.

Table 3.5 Coefficient list of the significant terms in CCD

Factor	Coefficient	df	Standard Error	95% CI Low	95% CI High	VIF
Intercept	0.455	1.000	0.009	0.437	0.473	
E-Retention constant for fast store	-0.001	1.000	0.005	-0.012	0.010	1.000
F-Maximum capacity for fast store	0.017	1.000	0.005	0.006	0.028	1.000
J-Precipitation factor	-0.015	1.000	0.005	-0.026	-0.003	1.000
EJ	0.021	1.000	0.006	0.009	0.033	1.000
FJ	0.012	1.000	0.006	0.000	0.024	1.000
J^2	-0.110	1.000	0.010	-0.131	-0.089	1.000

Table 3.5 shows the estimated coefficient for each significant factor, which came from the regression analysis. Because the low level and high level were set as "-1" and "1" for each factor in the design, the coefficients for those factors were comparable. The positive coefficient means the factor has the positive effects to the response. In this case, the positive effect indicates when the value of that particular factor is increasing, the NSE would increase. As it was shown in **Table 3.5**, the main factor (F) "Maximum capacity for fast store" (0.017), interaction (EJ) of "Retention constant for fast storage" and "Precipitation factor" (0.021), and interaction (FJ) of "Maximum capacity for fast store" and "Precipitation factor" (0.012) have positive effects to the NSE. On the other hand, the main factor (J) "Precipitation factor" (-0.015) and quadratic factor term (J^2) of "Precipitation factor" (-0.11) showed the negative effects to NSE (in this study, since both main factor term and quadratic factor term of "Precipitation factor" are significant to the model, it implies that the precipitation effect is not linear.). Therefore, according to these coefficients, it indicated: the interaction (EJ) of "Retention constant for fast storage" and "Precipitation factor" (0.021) had greatest positive impact on the final response and the quadratic factor term (J^2) of "Precipitation factor" (-0.11) had greatest negative effect. From this coefficient list, it also clearly showed that the

parameter (J) "Precipitation factor" was not only involved in factor terms with negative effect, but in factor terms with positive effect. In this case, when it came to the contribution of the parameter (J) "Precipitation factor", a more accurate picture of this particular factor was provided by using the DOE aided method. Simply adjusting the main factor to optimize the response is not the most efficient way, and may miss the optimum desired response. Therefore, in order to efficiently obtain the optimized response, the sensitivity of a factor should be evaluated by taking the main effect of that factor and the interactions with other factors into account.

3.5 Summary

In this study, a new integrated sensitivity analysis method was developed by incorporating statistical DOE methodology, linear or nonlinear optimization, and verification process to improve the performance of hydrological modeling. To test the developed method, a case study in the Deer River watershed was conducted. The original values of the parameters were provided by automatic calibration that is built in the SLURP model to obtain the best fit between the observed and simulated data, so the original NSE value is the "optimal value" suggested by the SLURP model. However, the proposed methods could still successfully improve the "optimal value" of NSE and investigate the effects of each parameters and their interactions at the same time which cannot be derived from the SLURP model.

When the ten important parameters were selected, a minimum run resolution V fractional factorial design was applied to screen out the more important ones among them. Through the first round of the experiment significant four out of ten parameters were

selected as the four main factors for the CCD in the second round. The final model could be optimized by using the nonlinear optimization, and the greatest value for NSE was obtained. The new combination of each key parameters was used as a new parameter set for the SLURP model to verify the feasibility of the CCD response model. The results show that the maximum final response predicted by CCD was quite close to the results obtained from the SLURP model and larger than the original calibrated results. The sensitivity analysis conducted also showed that the interaction between "retention constant for fast storage" and "precipitation factor" and the main factor of "maximum capacity for fast store" had the greatest positive effects on the NSE. On the contrary, the quadratic factor term and the main factor of "precipitation factor" showed the greatest negative impact on NSE. The "precipitation factor" was involved in several interaction effects with other factors, which cannot be determined using traditional sensitivity analysis, the one-factor-at a-time (OFAT) method. The study demonstrated the advantages of the DOE aided sensitivity analysis which can efficiently investigate the interactions between parameters and their contributions to simulation responses for supporting better calibration.

CHAPTER 4.
EVALUATING UNCERTAINTY ESTIMATES IN DISTRIBUTED HYDROLOGICAL MODELING BY GLUE, SUFI-2, AND PARASOL METHODS

The contents in the chapter are based on the following publications:

1. **Wu, H.J.**, and Chen, B. (2015). Evaluating uncertainty estimates in distributed hydrological modeling for the Wenjing River watershed in China by GLUE, SUFI-2, and ParaSol methods. *Ecological Engineering*, 79, 110-121, 10.1016/j.ecoleng.2014.05.014/
   Role: I developed the model, conducted case studies and drafted manuscript. Dr. Bing Chen is my PhD supervisor and provided advice in method development and manuscript drafting.

2. Xue, C., Chen, B., and **Wu, H.J.** (2014). Parameter uncertainty analysis of Surface flow and Sediment Yield in the Huolin Basin in China. *Journal of Hydrologic Engineering*, 19(6), 1224-1236, 10.1061/(ASCE)HE.1943-5584.0000909.
   Role: I drafted manuscript, conducted results analysis and discussion. Chen Xue provide the original data of the case study. Dr. Bing Chen is my PhD supervisor and provided advice in method development and manuscript drafting.

3. **Wu, H.J.**, Chen, B., and Li, P. (2013). Comparison of Sequential Uncertainty Fitting Algorithm (SUFI-2) and Parameter Solution (ParaSol) Method for Analyzing Uncertainties in Distributed Hydrological Modeling – A Case Study. CSCE 2013 General Conference proceeding, Montreal, Quebec, CA, Gen-309.
   Role: I developed the model, conducted case studies and drafted manuscript. Dr. Bing Chen is my PhD supervisor and provided advice in method development and manuscript drafting. Dr. Pu Li is the presenter for the conference.

4. **Wu, H.J.,** and Chen, B. (2014). Hydrological Modeling and Uncertainty Analysis for the up reach of the Wenjing Watershed, Sichuan, China. Poster presented at 2014 13th IWA Specialized Conference on Watershed and River Basin Management, San Francisco, USA.
   Role: I developed the model, conducted case studies and drafted poster. Dr. Bing Chen is my PhD supervisor and provided advice in method development and poster drafting.

4.1 Background

Due to the complexity of the hydrological system and the lack of information, uncertainty inherently exists and challenges the implementation of distributed hydrological models. The potential improvement in hydrological prediction for distributed models requires a great number of high resolution inputs and parameters, leading to more uncertainties involved in modeling processes. Generally, uncertainties arise from measurement errors associated with system input, from model structural problems due to assumptions and simplification, and from approximation in determining parameters (Blasone *et al.*, 2008b; Yang *et al.*, 2008). Among these three sources, parameter uncertainty is inevitable but relatively easy to control through an appropriate calibration especially for some conceptual or empirical parameters. There are growing interests in investigating uncertainties associated with hydrological studies and their effects on model performance nowadays (Yang *et al.*, 2007a; Shen *et al.*, 2008; Yang *et al.*, 2008; Jin *et al.*, 2010; Shen *et al.*, 2010). A variety of methods have been developed to characterize, quantify and control the parameter and modeling uncertainties. Among these methods, the sequential uncertainty fitting algorithm (SUFI-2), the generalized likelihood uncertainty estimation (GLUE) method, and the parameter solution (ParaSol) method are three widely used methods for parameter uncertainty analysis in environmental modeling. However, limited studies have been reported on comparing the capability of these three uncertainty analysis methods in capturing the impact of parameter uncertainty within the same modeling framework (Vrugt *et al.*, 2003; Mantovan and Todini, 2006). In order to fill the knowledge gap, this study is to apply these three methods to distributed hydrological modeling systems, quantify the impact of parameter uncertainties, and examine their performance and capability. The uncertainty

analysis methods were applied to two real case studies, including hydrological studies in the upstream of the Wenjing River watershed in Southwest China and in the Huolin River watershed in Northern China. The results can provide a scientific reference for understanding the strength and shortcomings of three uncertainty analysis methods. The uncertainty analysis method with the best performance can be selected to evaluate the impacts of uncertainties and improve the prediction accuracy of hydrological modeling for future studies.

4.2 Methodology

The general framework of three uncertainty analysis methods (SUFI-2, GLUE and ParaSol) is shown in **Figure 4.1**. The detailed introduction of three uncertainty analysis methods and the SWAT model is provided in the following sections.

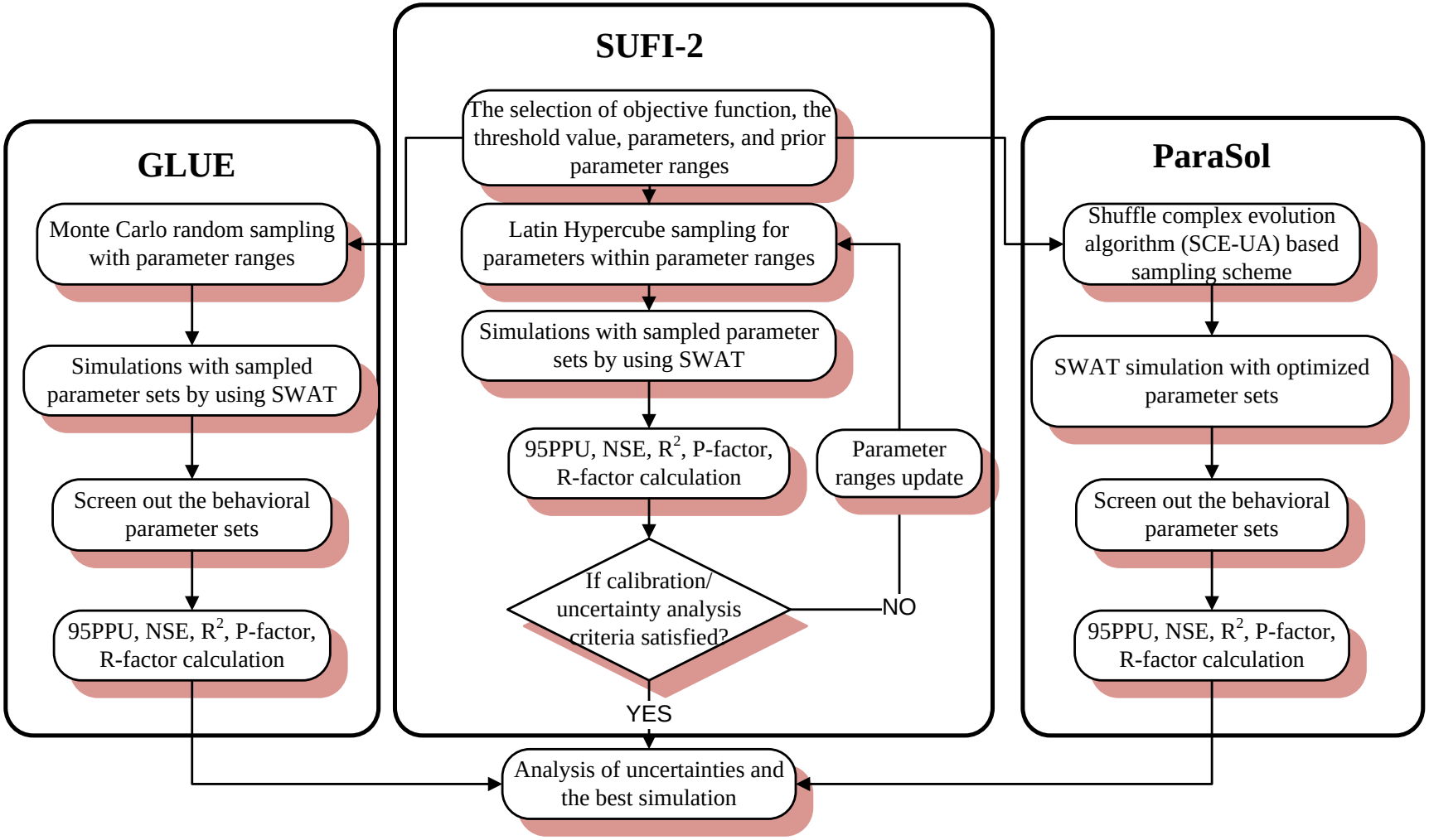

Figure 4.1 The general framework of three uncertainty analysis methods

4.2.1 **SUFI-2**

Based on a Bayesian framework, the SUFI-2 method determines uncertainties through the sequential and fitting process. In SUFI-2, the several iterations for updating the estimates of unknown parameters are required to achieve the final estimates. In this method, parameter uncertainties account for different possible sources, including model input, model structure, parameters, and observed data for calibration and validation purposes. An objective function needs to be defined before uncertainty analysis and assigned with a required stopping rule.

The degree to which all uncertainties considered is quantified by a measure referred to the P-factor. The P-factor is the percentage of observed data bracketed by the 95% prediction uncertainty (95PPU) (which is calculated at the 2.5% and 97.5% levels of the cumulative distribution of the output variables). Another measure quantifying the strength of uncertainty analysis is called the R-factor, which is equal to the average thickness of 95PPU band divided by the standard deviation of the observed data. A P-factor of 1 and R-factor of 0 is a simulation that exactly matches the observed data, which is the ideal case of simulation and cannot be achieved for real cases due to uncertainties from different sources and measurement errors. Certainly, a large P-factor can be achieved at the expense of a larger R-factor. If the R-factor is large, the ranges of parameters are larger than the optimal parameter ranges and more parameter uncertainties will remain. Normally, a value of less than 1 is a desirable result for the R-factor (Abbaspour, 2011). Hence, a balance between these two factors has to be monitored while decreasing parameter uncertainty, and the ratio of P-factor and R-factor can be used to evaluate the strength and goodness of fit of uncertainty analysis.

When acceptable P-factor and R-factor are obtained, the reduced parameter uncertainty ranges are the preferred ones.

The SUFI-2 method assumes a large parameter uncertainty (or physically meaningful range) to ensure the observed data fall into the 95PPU for the first iteration, and decrease the uncertainty in steps while monitoring the P-factor and R-factor for next several iterations. The goal of the SUFI-2 method is to search for bracketing most of the observed data with the smallest possible uncertainty band, which means that good results should have a relatively large P-factor with relatively small R-factor. These two measures can also be used to evaluate the performance of other uncertainty analysis methods. The initial parameter ranges are updated by calculating the sensitivity matrix and equivalent of Hessian matrix, followed by calculating the covariance matrix, 95% confidence intervals of the parameters, and correlation matrix. Parameters are then updated with new ranges which are always centered around the values of the optimal parameter set that leads to the best simulation (using equation 4.4 and 4.5 shown in below). The major procedures of SUFI-2 are shown as follows (Abbaspour *et al.*, 2007; Yang *et al.*, 2008; Abbaspour, 2011; Xue *et al.*, 2014):

Step 1: An objective function and reasonable parameter ranges [$b_{j,min}$, $b_{j,max}$] are pre-defined. There are a number of ways to formulate an objective function, and the Nash-Sutcliffe coefficient (NSE) and coefficient of determination (R^2) are two of the most popular objective functions (Legates and McCabe Jr, 1999). The reasonable parameter ranges are normally obtained from expert knowledge and references. If there are no reliable information for parameter ranges, the ranges should be as large as possible (yet physically meaningful);

Step 2: Latin Hypercube (McKay *et al.*, 1979) sampling is carried out in the hypercube [$b_{j,min}$, $b_{j,max}$] leading to n parameter combinations, where n is the number of required simulation iterations. The sampled parameter sets are used as the parameter inputs of SWAT simulations.

Step 3: The 95PPU is calculated for simulated surface runoff through the objective function. Assessed uncertainty measures are calculated as the percentage P of the observed data bracketed by the 95PPU band, and the average distance $\bar{d}$ between the upper and the lower 95PPU (or the degree of uncertainty) determined from:

$$\bar{d} = \frac{1}{k}\sum_{l=1}^{k}\left(q_U - q_L\right)_l \qquad (4.1)$$

where, l is an iterate, k is the number of observed data points for variable q, and $\bar{d}$ is calculated by the R-factor:

$$R = \frac{\overline{d_x}}{\sigma_x} \qquad (4.2)$$

where, σ_x is the standard deviation of the observed variable x. A value less than 1 is a desirable measure for the R-factor.

The percentage P of observed data bracketed by the 95PPU band is derived by:

$$P = \frac{nq_{in}}{N}\cdot 100\% \qquad (4.3)$$

where, N is the total number of observed values, nq_{in} is the number of the observed data bracketed by the 95PPU. A reasonable combination of different factors needs to be determined for the appropriate parameter ranges for the next iteration. In this study, the

criteria are set as: when $NSE \geq 0.7$ and $R^2 \geq 0.7$， $P \geq 0.5$, and R ≤ 1, the model simulation results are acceptable and the parameter uncertainty ranges are considered as appropriate.

Step 4: Further sampling rounds are required to update parameter ranges (if the criteria are not fulfilled), which are calculated by:

$$b'_{j,\min(new)} = b_{j,lower} - Max\left[\frac{\left(b_{j,lower} - b_{j,\min}\right)}{2}, \frac{\left(b_{j,\max} - b_{j,upper}\right)}{2}\right] \quad (4.4)$$

$$b'_{j,\max(new)} = b_{j,upper} + Max\left[\frac{\left(b_{j,lower} - b_{j,\min}\right)}{2}, \frac{\left(b_{j,\max} - b_{j,upper}\right)}{2}\right] \quad (4.5)$$

where b' is the new range after one more iteration. To be noticed, it is possible to produce inappropriate ranges for some parameters because equations 4.4 and 4.5 can only ensure that the updated parameter ranges are always centered on the best estimates. Therefore, manual adjustment is required to avoid using possibly unreasonable values based on the available practical information of parameters. For example, some parameters cannot be negative values. If the new lower bound values of these parameters are negative, subjective adjustment is always required (Abbaspour, 2011).

4.2.2 **GLUE**

The GLUE method is different from most calibration procedures used in hydrological modeling, in which the global optimum parameter set is sought and any assessment of parameter uncertainty is made with respect to that global optimum. The objective of the GLUE method is to identify a set of behavioral models within the universe of possible parameter combinations. The term "behavioral" is used to signify the models that are

considered to be acceptable on the basis of available data and knowledge. Distributed hydrological models are always involved a great number of parameter interactions and nonlinearities. The parameter interactions and nonlinearities can be implicitly addressed through the GLUE method by the likelihood measure, which summarizes the nonlinear responses of a particular model in fitting the available data (Vázquez *et al.*, 2009). The main output of the GLUE method for assessing uncertainty of modeling is the prediction interval at each time step bounded by the lower prediction limits and higher prediction limits. If prediction bounds are large enough to include most of the observed data, it means that parameter variability alone can compensate for other sources of error, and thus it can account for the total output uncertainty. The major steps of the GLUE method are shown below (Abbaspour, 2011; Bastola *et al.*, 2011):

Step 1: The objective function is defined. NSE is the most popular objective function used in the GLUE method.

Step 2: A "likelihood weight" is derived for each behavioral parameter by:

$$w_i = \frac{L(\theta_i)}{\sum_{k=i}^{N} L(\theta_k)} \tag{4.6}$$

Where N is the number of behavioral parameter sets, and $L(\theta_i)$ is the generalized likelihood measure.

Step 3: Parameter ranges are assigned according to physical meaning and current understanding of parameters, and then Monte Carlo random sampling scheme are applied. Due to missing information, the prior distributions of parameters are assumed as uniform. This is the typical assumption in hydrologic modeling, because usually the prior distribution form of parameters was difficult to determine (Blasone *et al.*, 2008b).

Step 4: Model parameter uncertainty analysis is conducted. The random sampled parameter sets are used as the parameter inputs for the SWAT model, and corresponding output, surface runoff, can be simulated. The dot plots of NSE against aggregate different parameters under the GLUE approach are generated, and parameter uncertainty can be analyzed according to behavioral simulations.

Step 5: Model prediction uncertainty analysis is conducted. The upper and lower bounds of model prediction results are determined for prediction intervals of simulation results. By sorting the likelihood values from small to large within behavioral simulations according to the assumption of threshold, the time series of model prediction uncertainty under the given confidence level could be estimated.

4.2.3 **ParaSol**

In the ParaSol method, the simulations performed by the modified SCE-UA are further used for uncertainty analysis and find solutions near the optimum. After the optimization from SCE-UA, the simulations are divided into behavioral and non-behavioral simulations according to criterion value similar to the GLUE methodology. However, unlike

GLUE, the SCE-UA algorithm is seeking for global minimum of the objective function. The threshold value can be defined by either the χ^2-statistics where the selected simulations correspond to the confidence region (CR) or Bayesian statistics which could point out the high probability density (HPD) region for parameters or the model outputs. Both methods screen out behavioral simulations based on the preset threshold value of objective functions (the good simulations are the simulations with the value of the objective function less than the threshold value).The prediction uncertainty from the ParaSol method is hence generated equally from the good simulations (Van Griensven and Meixner, 2006; Abbaspour, 2015). The major steps of ParaSol are shown below (Duan *et al.*, 1992; Abbaspour, 2011):

Step 1: The modified SCE-UA algorithm is conducted. The procedures of original SCE-UA are shown as follows: 1) The *s* sample points are randomly sampled in the reasonable parameter range, and the likelihood values (criterion value) are computed at each point. Usually, uniform probability distribution can be used to generate the sample if lack of prior information; 2) The *s* points are sorted in ascending order of likelihood values; 3) The *s* points are partitioned into *p* groups (called complexes), and each complex contains *m* points. The complexes are partitioned, so that the first complex contains every $p(k - 1) + 1$ ranked point, the second complex contains every $p(k - 1) + 2$ ranked point and so on, where $k = 1, 2,\ldots, m$; 4) Each complex is evolved according to the competitive complex evolution (CCE) algorithm; 5) The points in the evolved complexes are combined into a single sample population, and the sample population is sort by ascending sequence according to likelihood values; 6) If any of the pre-specified convergence criteria are satisfied, stop; otherwise, continue; 7) The reduction of the number of complexes is then checked -- if the minimum

number of complexes required in population (p_{min}) is less than *p*, remove the lowest ranked complex; set $p = p - 1$ and $s = pm$; return to Step 4; If $p_{min} = p$, go back to Step 4. In order to increase the usefulness of SCE-UA for uncertainty analysis, two adjustment has been made: the randomness of the algorithm has been increased by using random samples to replace the worst results in each loop to improve the coverage of parameter space; when parameter values are outside the defined ranges, a value equal to the minimum/maximum bound is used instead of a random sampled value.

Step 2: After optimization through the application of modified SCE-UA, the simulation are divided into behavioral and non-behavioral simulations based on their values of the objective function.

Step 3: Prediction uncertainty is constructed by equally weighting all behavioral simulations, which is similar the last procedure of the GLUE method.

4.2.4 **SWAT**

According to the digital elevation model (DEM), SWAT can partition watershed into many sub-watersheds or sub-basins for the modeling purpose, because the sub-areas within a watershed are dominated by different land uses or soils and are dissimilar enough in properties to impact hydrology of areas. Runoff volume is calculated by using the Curve Number method (USDA Soil Conservation Service, 1972). Channel routing is calculated using either the variable storage routing method or the Muskingum routing method, and

Modified Universal Soil Loss Equation (MUSLE) is used to estimate the sediment yield at hydrological response units (HRUs) (Arnold *et al.*, 1998).

In this study, since only simulation for surface runoff were conducted and used for uncertainty analysis, SWAT requires specific information about weather, soil properties, topography, vegetation, and land management practices as the main input data (Neitsch *et al.* 2011). Through hydrological simulation for surface runoff, a number of output files are generated in SWAT simulations, including summary input file, summary output file, the HRU output file, the sub-basin output file and the main channel or reach output file (Arnold *et al.* 2013). The surface runoff of all sub-basins and HRUs level output results were applied to three uncertainty analysis methods. By changing the parameter combinations, three uncertainty analysis methods can be applied to achieve the desired results.

4.3 Case study #1: A case study in the Wenjing River watershed

4.3.1 **Study area and data acquisition**

Water scarcity and growing population problems have become severe in China recently. As the main drinking water source for Chengdu (the capital and largest city of Sichuan province), the efficient water resource management for Wenjing River watershed is quite important and urgent. However, to the authors' knowledge, very limited hydrological modeling works have ever been conducted for this area. This study can provide scientific support for local water resource department and good reference for evaluating the performance of three uncertainty analysis methods.

Therefore, the upper reaches of the Wenjing River watershed were selected as the study area, which is located in the city of Chongzhou in Southwest China (shown in **Figure 4.2**). This watershed belongs to the hilly region, and the drainage area is 653 km^2. Fig. 2 also shows the DEM map of the upper reaches of the Wenjing River watershed. The elevation increases from southeast to northwest and the highest point is located in the west with an elevation of 3,846 m. The annual average temperature in the watershed is 15.9 ^oC. The average annual sunshine duration is 1,161.5 hours, and the average annual precipitation is 1,012.4 mm. The annual amount of precipitation is high in summer (588.0 mm) and can be as low as 29.9 mm in winter (IWHR, 2005).

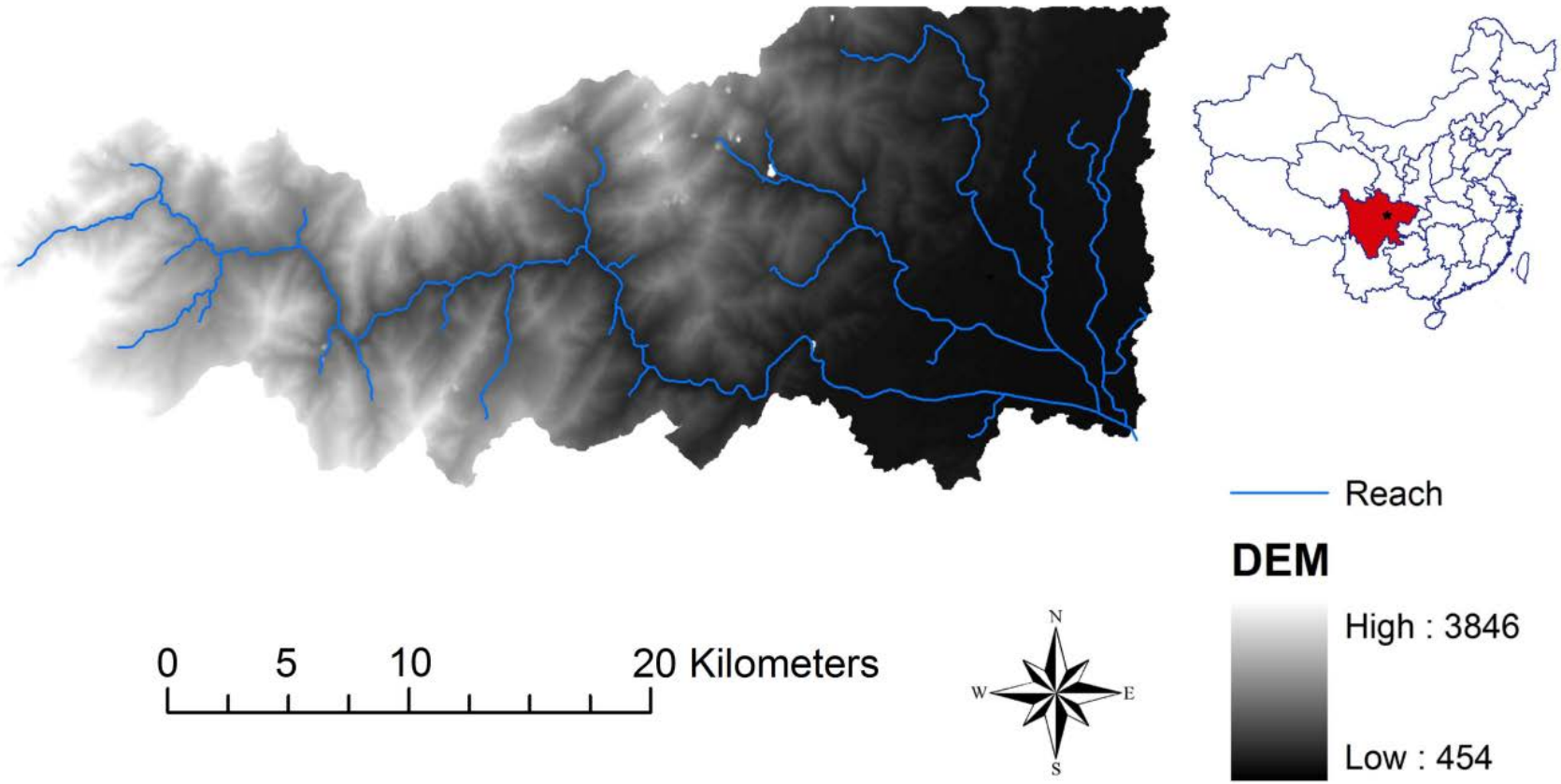

Figure 4.2 The location and DEM map of the upper reaches of the Wenjing River watershed

By using a 30-meter resolution DEM, the whole watershed has been delineated to 61 sub-basins, and the outlet is located at sub-basin No. 61 in the southeast of the watershed (**Figure 4.3**). A digital stream channel map provided by the local water resource department was used to calibrate the water channel generated by DEM. By considering soil, land use and elevation, the watershed was divided into 270 HRUs for hydrological modeling by using SWAT. **Figure 4.4** shows the 10 group of land uses classified in the study area, and the 8 major soil groups are shown in **Figure 4.5**. The meteorological data, including temperature, precipitation, wind speed, solar radiation, relative humidity data, were used to as input for the SWAT model.

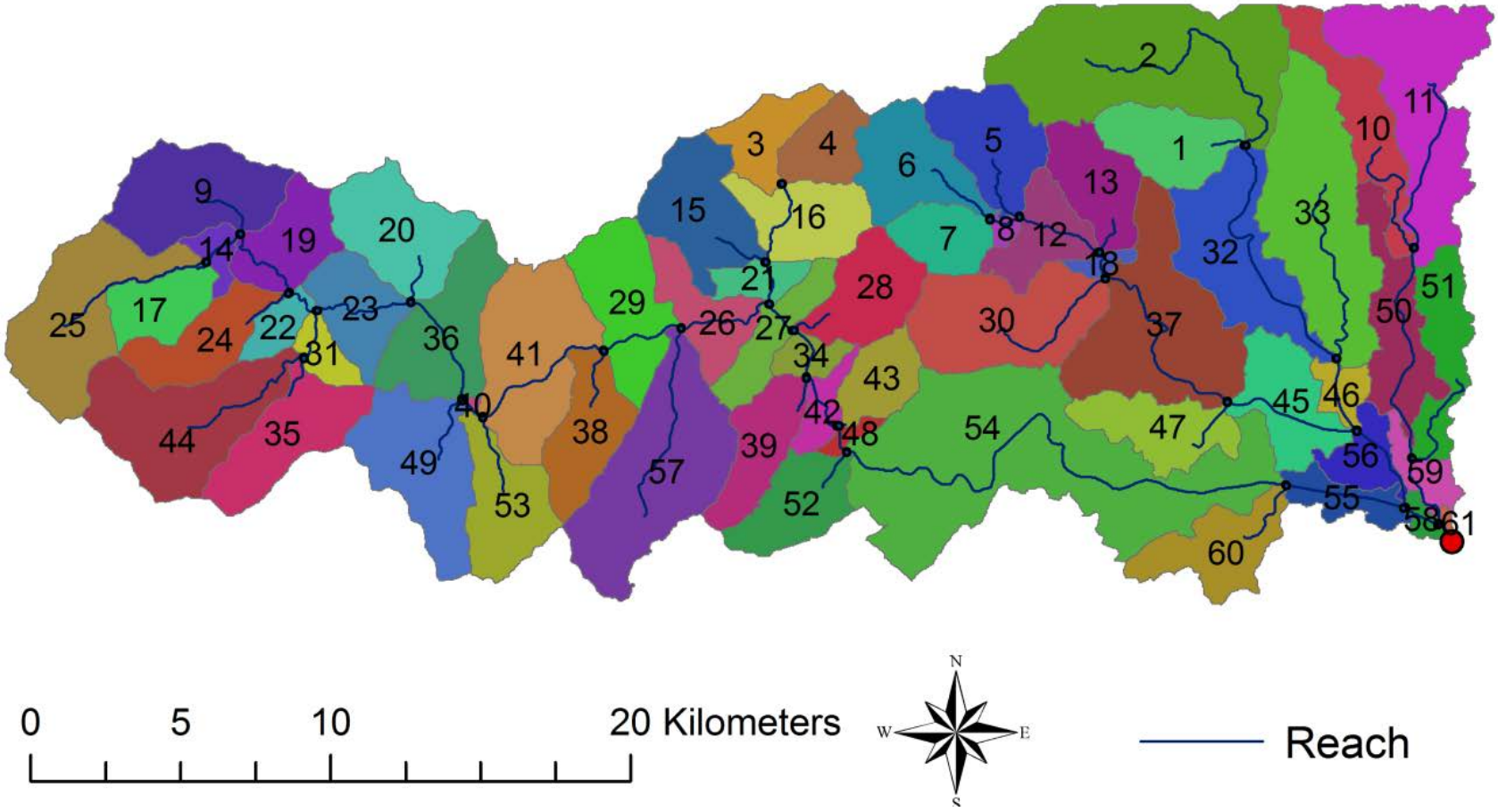

Figure 4.3 Delineation of the Wenjing River watershed and watershed outlet (sub-basin No. 61)

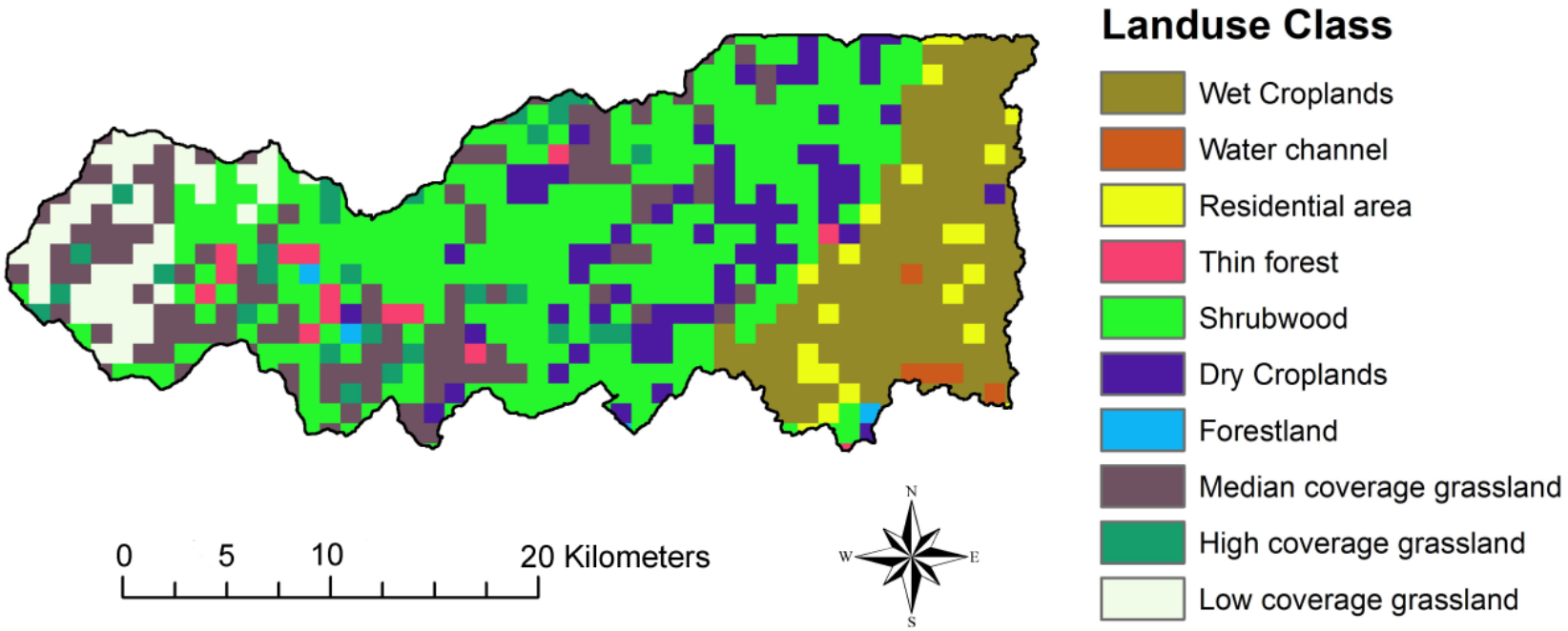

Figure 4.4 Land use classification in the Wenjing River watershed

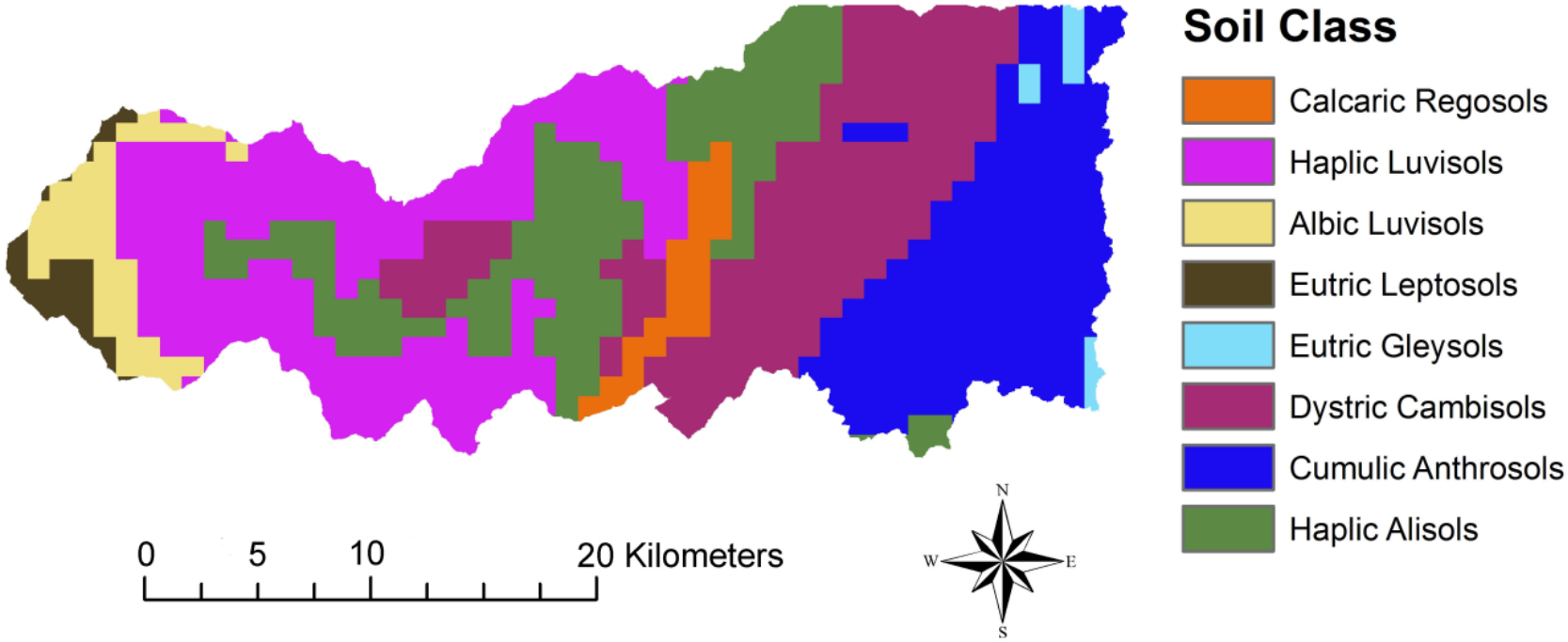

Figure 4.5 Soil classification in the Wenjing River watershed

The observed data were obtained from the Water Authority of Chongzhou including the average monthly runoff data from 1998 to 2002. The three-year data from 1998 to 2000 were used for calibration, and the remaining two years data were used for validation. Of note, as a major tributary of the Wenjing River, the runoff contribution from the Bojiang River cannot be neglected. Due to the lack of observed runoff data of the Bojiang River, the simulated runoff from the study area were assumed to contribute 47.1% of the total runoff in the Wenjing River watershed based on an investigation reported by the China Institute of Water Resources and Hydropower Research (IWHR, 2005).

4.3.2 **Results and discussion**

4.3.2.1 **Modeling results**

The SUFI-2 method was used for calibration, and three iterations with 1000 runs were conducted. The parameter settings can be found in **Table 4.1**. According to the previous assumption, the 47.1% of the recorded runoff data in the Yuantong station was used to compare the simulation results. Due to this assumption, both NSE and R^2 of the best simulation were selected to evaluate the simulation performance to improve the reliability of the analysis in this study. The definition of NSE was given as the equation 3.1 in **Chapter 3**, and the definition R^2 are shown below (Abbaspour, 2011):

$$R^2 = \frac{\left[\sum_{i=1}^{n}(Q_{o,i} - \overline{Q_o})\left(Q_{s,i} - \overline{Q_s}\right)\right]^2}{\sum_{i=1}^{n}(Q_{o,i} - \overline{Q}_o)^2 \sum_{i=1}^{n}(Q_{s,i} - \overline{Q}_s)^2} \quad (4.7)$$

Where Q_o and Q_s represent the observed and simulated surface runoff (m^3/s), respectively; $Q_{o,i}$ and $Q_{s,i}$ are the observed and simulated values on day *i*, respectively; $\overline{Q}_o$ and $\overline{Q}_i$ are the average values of the observed and simulated surface runoff (m^3/s), respectively; and n is the total number of values within the period of analysis.

The simulated and observed results were compared and the associated hydrograph was generated for Years 1998-2000 (**Figure 4.6**) as the calibration period. The remaining two years monthly runoff data (2001-2002) were used for validation, and the hydrograph of the validation results is shown in **Figure 4.7**. The scatter plots of simulated and observed runoff in the calibration and validation period are shown in **Figure 4.8** and **Figure 4.9**, respectively. The NSE and R^2 of the best simulation are 0.77 and 0.80 for the calibration period, and 0.74 and 0.87 for the validation period, respectively, indicating reasonable consistency between the simulated and observed runoff as well as responses to precipitation. After the acceptable simulation was obtained, uncertainly analysis can be further conducted. For the better comparison, P-factor and R-factor were used to compare the performance of different uncertainty analysis methods.

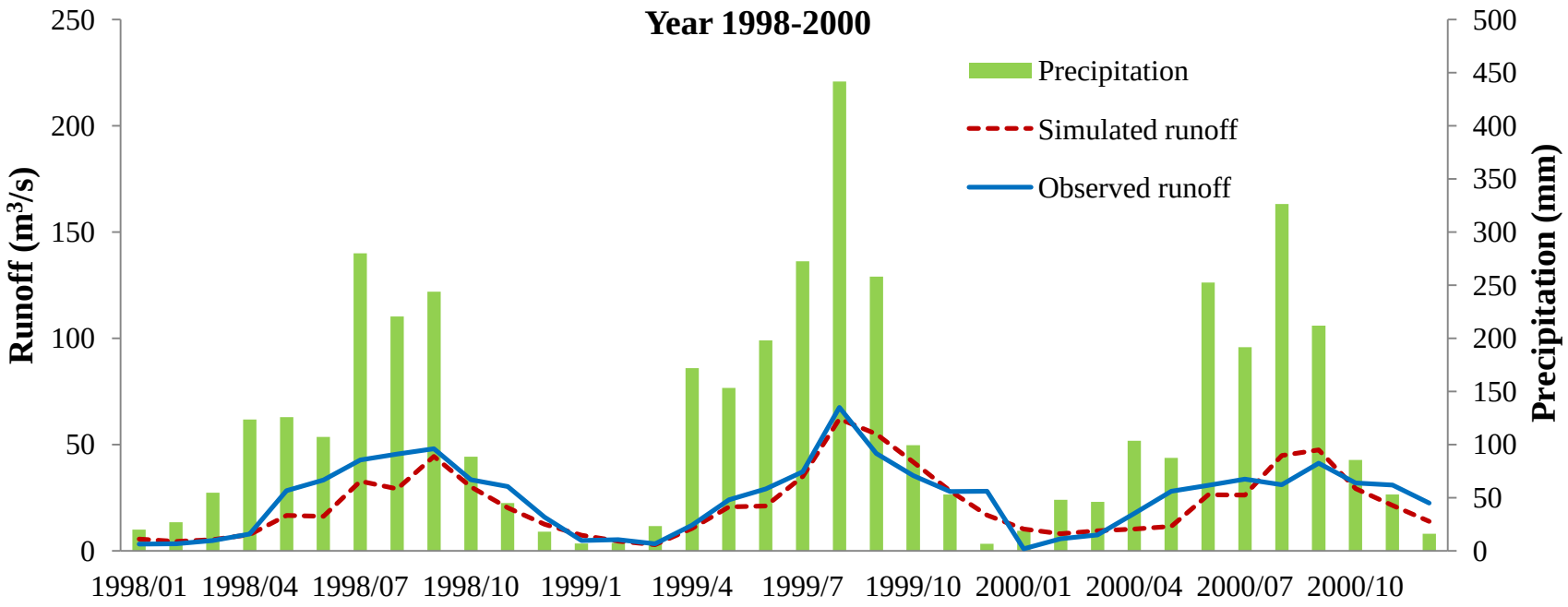

Figure 4.6 The average monthly simulated runoff, and observed runoff and precipitation in the calibration period of 1998-2000

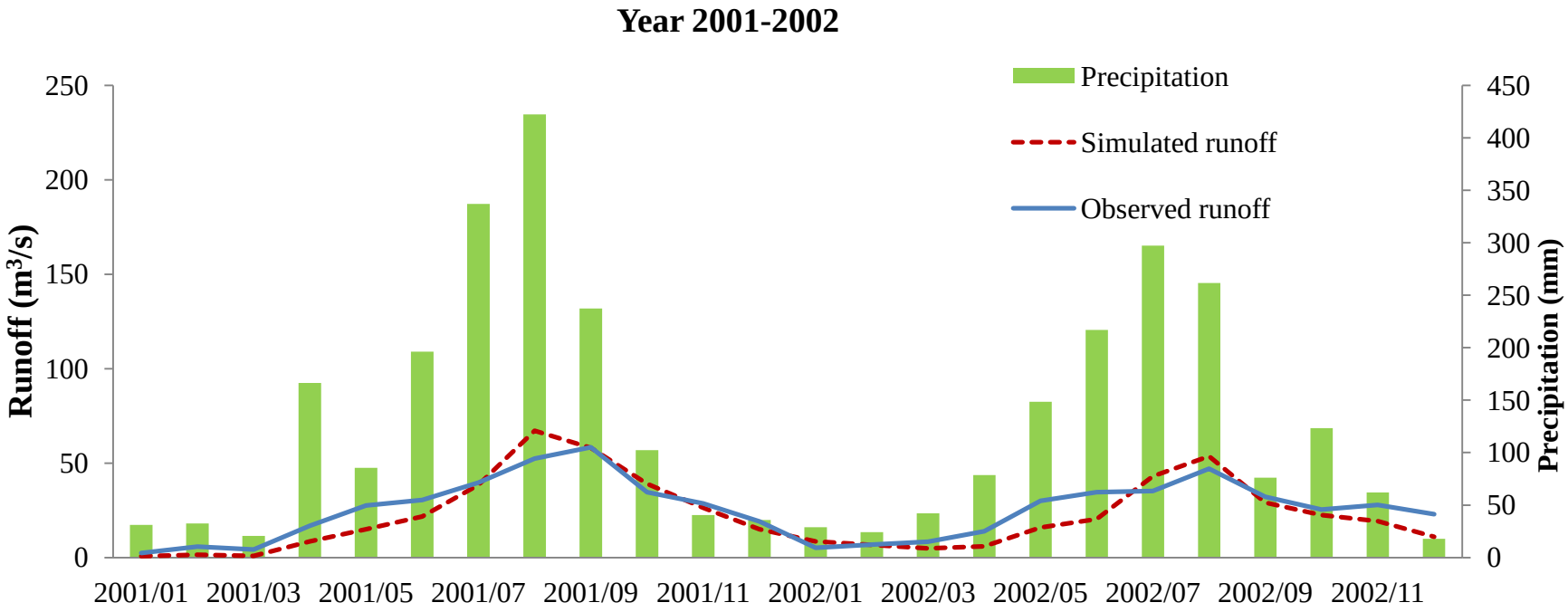

Figure 4.7 The monthly average simulated runoff, and observed runoff, and precipitation in the validation period of 2001 to 2002.

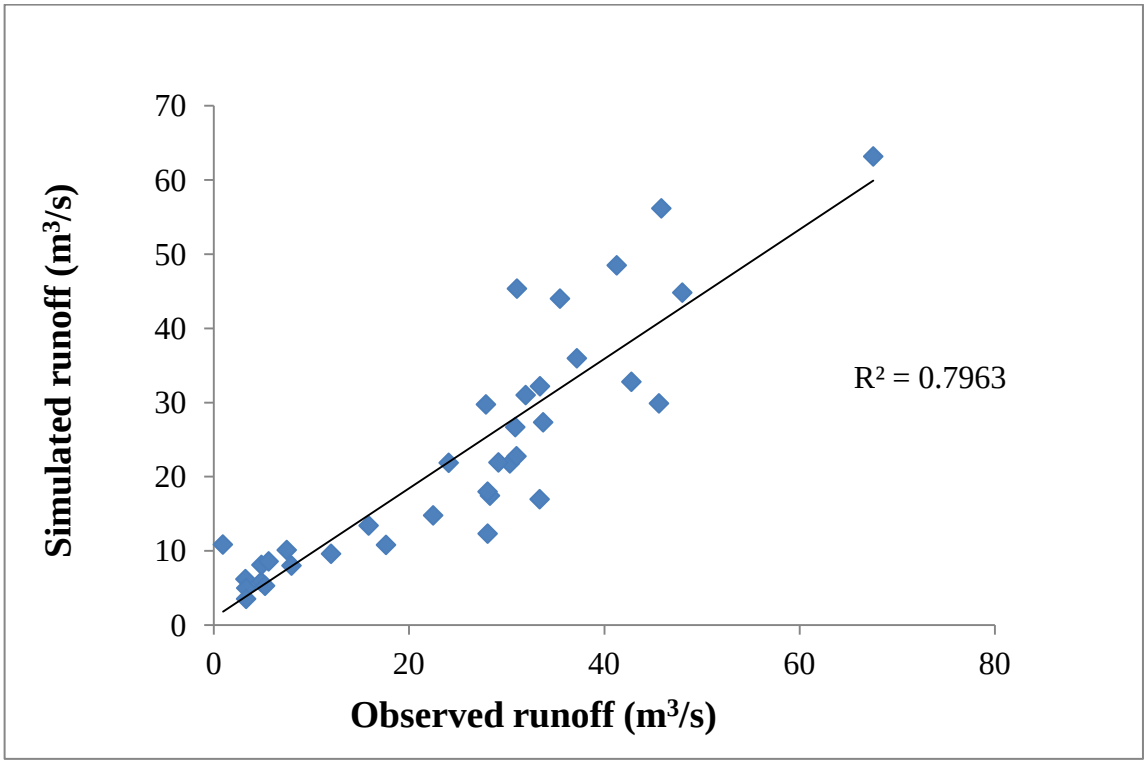

Figure 4.8 The scatter plot of simulated and observed runoff for the calibration period

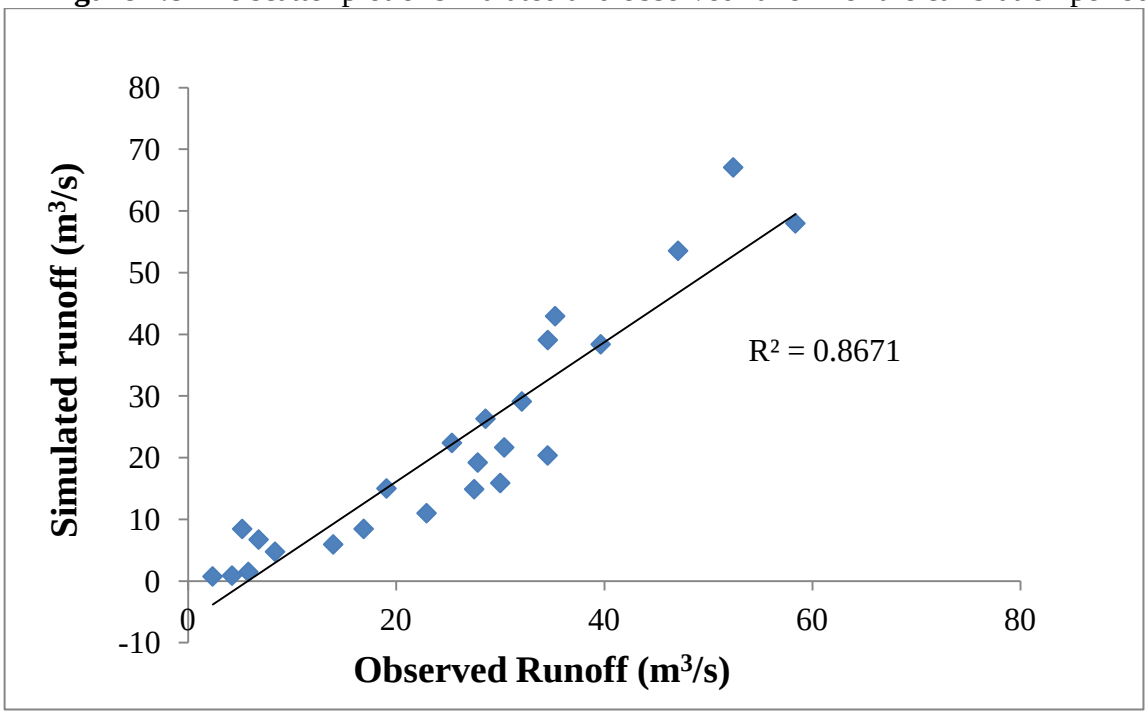

Figure 4.9 The scatter plot of simulated and observed runoff for the validation period

4.3.2.2 **Uncertainty analysis**

SUFI-2

Because the LHS method is a high-efficient sampling method, it can reduce the sampling points within a certain space comparing to the Monte Carlo random sampling method. Usually, the number of simulation for one iteration could be set to 500-1000 (Abbaspour, 2011; Xue *et al.*, 2014). In this study, three iterations with 1,000 model runs per iteration were conducted to estimate the uncertain effect of the calibrated models. Three iterations with 1,000 model runs per iteration were conducted to estimate the uncertain effect of the calibrated models. NSE was selected as the objective function. If NSE $\geq$ 0.4, the simulation results and the parameter uncertainty ranges were acceptable. There are three methods for adjusting parameter values in this study, including replacing the existing parameter value (*v*), adding a given value to the existing parameter value (*a*), and multiplying (1 + a given value) to the existing parameter value (*r*). The results from the last iteration were used for uncertainty analysis. The original parameter ranges were set based on the available information and physical meaning of parameters. Each iteration could provide the best estimation of parameter sets and then suggest new ranges of the parameters for the next iteration based on the evaluation of simulation performance. To be noticed, some suggested ranges were outside the physically meaningful parameter ranges during the iterations, manual adjustments have been made to those parameters to make them not exceed the maximum/minimum absolute range values. The suggested ranges were further adjusted to agree with the physical meaning and the requirements of the SWAT model.

According the calibration manual and other references, 11 parameters have been selected for calibration. The parameter and results from the first, second and third iteration

are shown in **Table 4.1**. The final parameter ranges were utilized as initial inputs for the GLUE and ParaSol methods.

Table 4.1 Parameters ranges and siumlation results for each iteration

Aggregate parameters	change type	parameter ranges 1st iteration	The best estimation	parameter ranges 2nd iteration	The best estimation	Final parameter ranges
CN_2	r	-0.25, 0.3	-0.17	-0.4, 0.1	-0.23	-0.35, -0.1
ALPHA_BF	v	0.4, 1.0	0.83	0.6, 1.0	0.93	0.77, 0.92
GW_DELAY	v	10, 300	122.96	35.0, 215.0	51.83	37.0, 111.0
GWQMN	v	0, 2000	147	0.0, 1100.0	329.45	0.0, 450.0
ESCO	v	0.8, 1	0.95	0.87, 1.0	0.97	0.95, 1.0
CH_K	v	5, 130	52.94	14.0, 92.0	23.87	26.0, 81.0
ALPHA_BNK	v	0, 1.0	0.94	0.45, 1.0	0.62	0.63, 1
SOL_AWC	r	-0.2, 0.4	0.29	-0.1, 0.55	0.10	-0.22, 0.15
SFTMP	v	-5, 5	4.60	-0.2, 9.0	5.52	-0.3, 5.4
GW_REVAP	v	0.02, 0.5	0.11	0.01, 0.3	0.02	0.02, 0.09
RCHRG_DP	v	0, 1	0.01	0, 0.5	0.08	0, 0.16

Note (Winchell et al., 2009):
CN_2: Initial SCS runoff curve number for moisture condition II.
ALPHA_BF: Baseflow alpha factor (days).
GW_DELAY: The delay time, δgw cannot be directly measured.
GWQMN: Threshold depth of water in the shallow aquifer required for return flow to occur (mm H_20).
ESCO: Soil evaporation compensation factor.
CH_K: Effective hydraulic conductivity in main channel alluvium (mm/hr).
ALPHA_BNK: Baseflow alpha factor for bank storage (days).
SOL_AWC: Available water capacity of the soil layer (mm H_2O/mm soil).
SFTMP: Snowfall temperature (°C).
GW_REVAP: Groundwater "revap" coefficient.
RCHRG_DP: Deep aquifer percolation fraction.

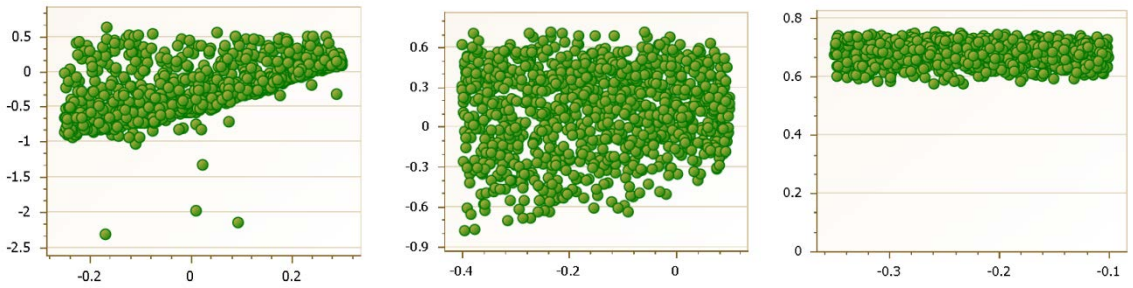

(a) CN_2

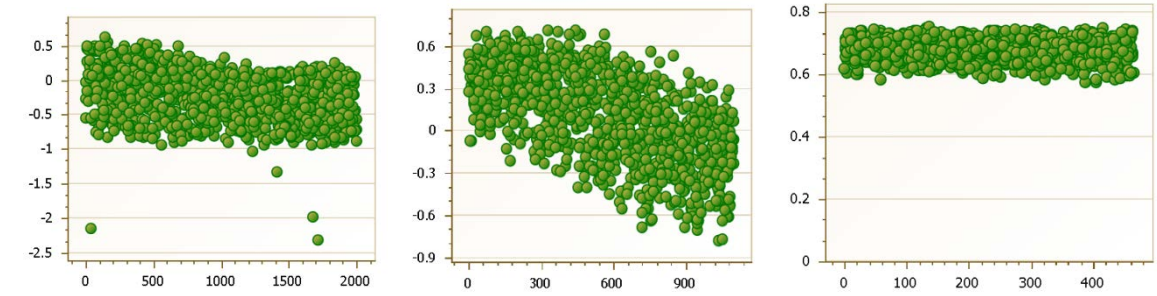

(b) GWQMN.gw

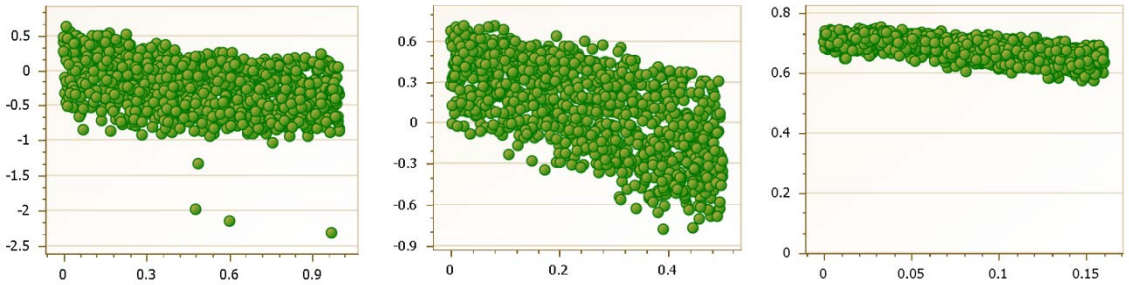

(c) RCHRG_DP.gw

Figure 4.10 Dotplots for NSE against different parameters: (a) CN2, (b) GWQMN.gw, and (c) RCHRG_DP.gw
Note: The Y-axis indicates the NSE values, and the X-axis indicates the value of parameters.

Figure 4.10 shows the dotplots of NSE against three selected parameters in three iterations (with 1,000 runs each). Because other parameters are not quite sensitive to the simulation results (no special trends or patterns for dotplots), the dotplots of three parameters (CN_2, GWQMN.gw, and RCHRG_DP.gw) with special and typical trends for NSE against

parameter ranges were shown in **Figure 4.10(a), (b),** and **(c)** as examples, respectively (the definition of the parameters have been provided in the note of **Table 4.1**. The dense dot area with high NSE values is the desired optimized region for parameters. Moreover, the parameter ranges were updated through three iterations. The parameter ranges were reduced without losing most of the optimized simulation results. From **Figure 4.10**, it is shown that the NSE values were approaching their greater values in the last iteration. The values of NSE of the best simulation for first, second, and third iteration are 0.63, 0.72 and 0.77, and the number of behavioral simulation are 31, 214 and 1000 out of 1,000 in three iterations, respectively, demonstrating the improvement of simulation during three iterations.

In the second iteration, due to certain unreasonable parameter ranges, NSE values of some simulation results are much lower than the threshold value. However, the trends still can be used to guide the direction of optimization. For the parameter CN_2, there is an increasing trend within the range [-0.25, 0.3] for NSE values in the first iteration. Therefore, the parameter ranges were shifted to bigger values based on calculation results of equations 4.4 and 4.5. Because the dots almost spread out in the whole space for the second iteration, the updated parameter range could not be the main reason to generate so many non-behavioral simulations. However, for the parameter GWQMN.gw, when the parameter ranges shifted from [0, 2000] to [0, 1100], many non-behavioral simulations occurred in the range starting from 450 up to 1100. The bigger values of the parameter within the range are, the lower NSE values were obtained. It demonstrates that the parameter in this range can cause more non-behavioral simulations when the parameter values are close to 1100. The dotplot of parameter RCHRG_DP.gw is very similar to that of parameter GWQMN.gw, which can lead to the same conclusion: both dotplots of GWQMN.gw and RCHRG_DP.gw

show that the inappropriate parameter ranges of these two parameters could be the main reasons to obtain a great number of dots below the threshold value in the second iteration. Therefore, the ranges for GWQMN.gw and RCHRG_DP.gw have been adjusted to [0, 450] and [0, 0.16] in the third iteration using equation 4.4 and 4.5, respectively. When ranges of all parameter have been updated and reduced, the NSE values are approaching their optimized values.

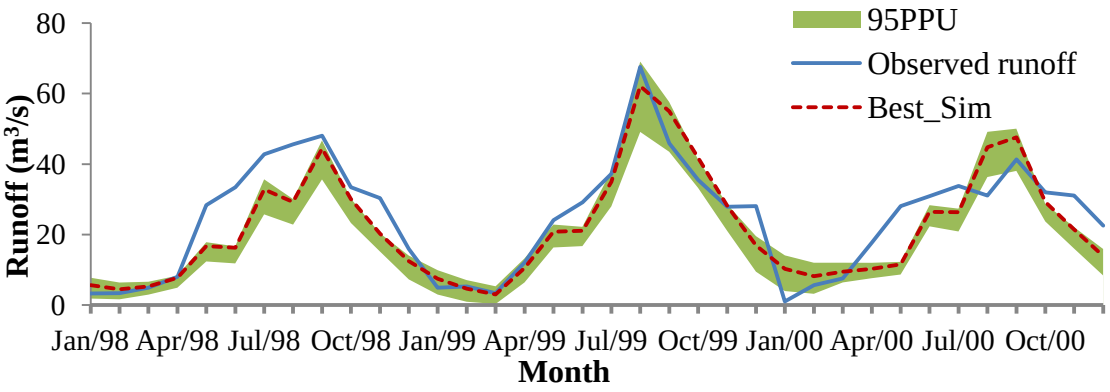

Figure 4.11 The best simulated runoff with 95PPU against observed runoff by using the SUFI-2 method

Figure 4.11 shows the hydrograph of the simulated runoff with 95PPU against the observed runoff by using SUFI-2. The green band region is the 95% prediction interval for the parameter set of the best estimation, and it can cover most of the peak flow periods and dry periods. After 3 iteration, the best estimation parameter sets can achieve NSE = 0.77.

The simulated runoff was compared with the observed runoff. The overall performance of the three-year period in terms of NSE, R^2, P-factor and R-factor are 0.77, 0.80, 0.56 and 0.48, respectively (shown in **Table 4.2**). As shown in **Figure 4.11**, the calibrated model always underestimated the runoff rate in spring and summer (from April to

August). From each figure, the simulated runoff matches with the trend of precipitation better than the observed runoff, especially from April to August. According to the local water resource report, it may be caused by some unknown human activities in the upper reaches of the watershed (irrigation channels or small hydropower dams) (IWHR, 2005). The underestimation of snowmelt also could lead to relatively small amount of runoff during spring and summer each year. Other possible reasons for the mismatch could be the general issues of hydrological modeling, such as limited meteorological data, incomplete soil and landuse database, inaccurate GIS information, etc. Those uncertainties can significantly affect the simulation results, and lead the relatively poor simulation performance as seen in the year of 1998 and 2000.

GLUE

Typically, the GLUE method assumes wide physically meaningful ranges for each parameter to cover more possible behavioral solutions. Therefore, GLUE only requires one iteration with a large number of simulation runs. Because the parameter ranges used for GLUE in this study have been reduced to appropriate ranges after two iterations from SUFI-2, relatively small number of simulation runs (5000) could be used for uncertainty analysis. For a better comparison, the NSE was also selected as the objective function to keep the consistency with SUFI-2. Similarly, due to the application of optimized the parameter ranges, more behavioral parameter sets could be obtained from the reduced parameter ranges. Therefore, the relative higher threshold value of 0.7 was preset to screen the behavioral and non-behavioral parameter sets for GLUE. The 95PPU was obtained at the 2.5% and 97.5% of the accumulative distribution of prediction uncertainty from behavioral parameter sets.

The prediction uncertainty along with the best estimation is shown in **Figure 4.12**, and statistic summary of behavioral simulations is given in **Table 4.2**.

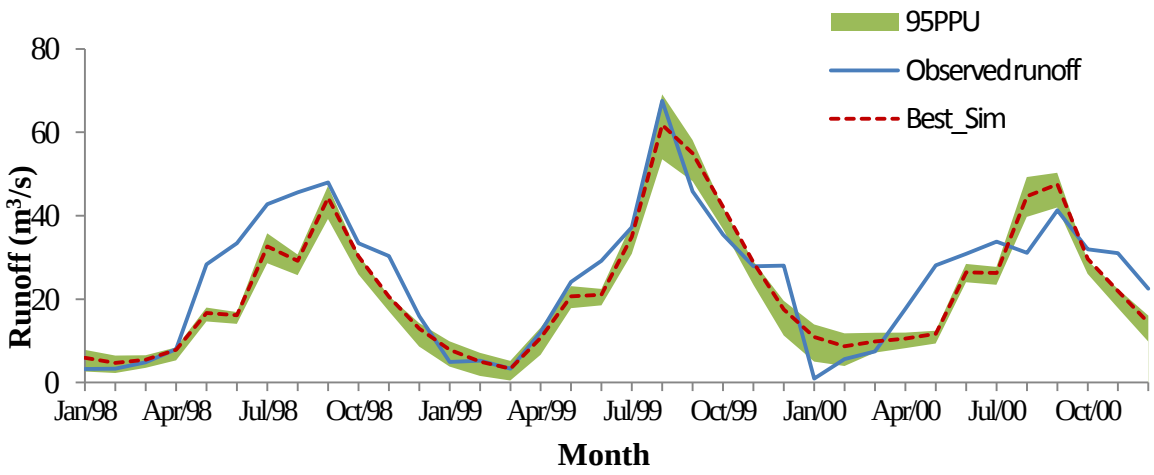

Figure 4.12 The best simulated runoff with 95PPU against observed runoff by using the GLUE method

As it is shown in **Figure 4.12**, the 95PPU region from GLUE is narrower than that of the SUFI-2 method, which is corresponding to the R-factor = 0.37 (smaller than last iteration of the SUFI-2 method with R-factor = 0.48). The P-factor value (0.36) is also smaller than the one from the SUFI-2 method (0.56). The NSE (0.76) and R^2 (0.79) of the best simulation are slightly smaller than the results from the last iteration of the SUFI-2 method (0.77 and 0.80, respectively) as well. The SUFI-2 also has a greater ratio of P-factor and R-factor, demonstrating the SUFI-2 method can achieve better uncertainty analysis results than the GLUE method. Therefore, based on comparison results from the case study, the SUFI-2 method was proved to be able to provide more accurate simulation and more confident uncertainty analysis than the GLUE method in this study.

ParaSol

To compare performance of other the two uncertainty analysis methods, the ParaSol method was conducted last. In this study, 3,000 ParaSol simulation runs were conducted for uncertainty analysis. The initial parameter ranges used in the ParaSol method are the same as those adopted in the GLUE method. After conducting uncertainty analysis using the ParaSol method, the statistics summary of behavioral simulation results was obtained, and the hydrograph of simulated runoff with 95PPU against observed runoff are shown in **Figure 4.13**.

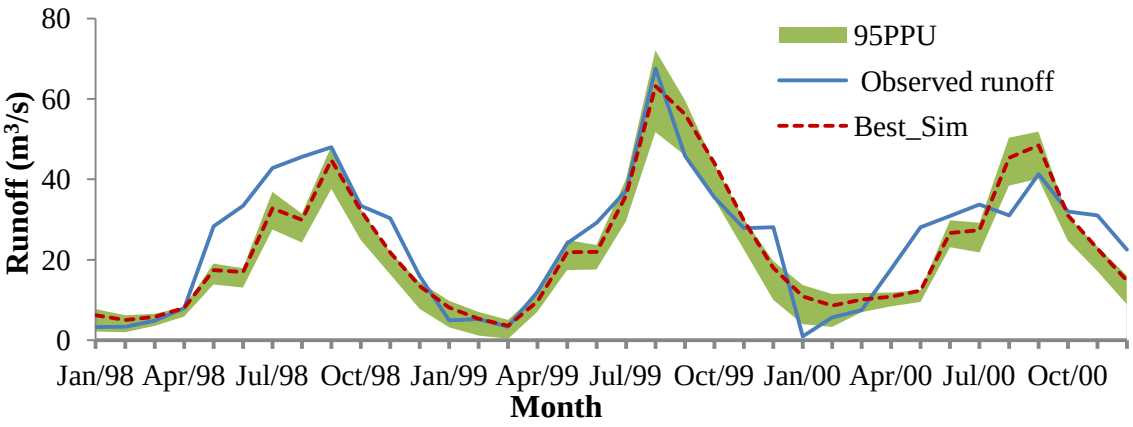

Figure 4.13 The best simulated runoff with 95PPU against observed runoff by using the ParaSol method.

In **Figure 4.13**, it showed that the uncertainty region are similarly wide like the results from the SUFI-2 method, and can cover most of peak flow periods and dry periods as well. According to statistics results, the P-factor and R-factor values were 0.44, 0.47; R^2 and NSE of the best simulation are 0.80 and 0.77, respectively (shown in **Table 4.2**). The best simulation from ParaSol can achieve the same good NSE and R^2, showing the simulation power is as good as SUFI-2. However, the ratio of P-factor and R-factor is the lowest among

the three methods, demonstrating the limited ability for conducting uncertainty analysis. The best simulations of ParaSol provided slightly larger NSE and R^2 values than those of the GLUE method, and showed the similar good results as for the SUFI-2 method. On the other hand, by considering the balance of the uncertainty analysis results, the SUFI-2 method achieved best performance for uncertainty analysis.

4.3.2.3 **Results comparison**

Table 4.2 The statistic summary of the results of three uncertainty analysis methods.

Variable	P-factor	R-factor	R^2	NSE	P/R
Third iteration SUFI-2	0.56	0.48	0.80	0.77	1.17
5,000 times GLUE	0.36	0.37	0.79	0.76	0.97
3,000 times ParaSol	0.44	0.47	0.80	0.77	0.94

Table 4.2 shows the statistic summary of the uncertainty analysis results of three methods. In terms of modeling performance, all the three methods achieved similarly good results. The SUFI-2 method provided the highest NSE (0.77) and R^2 (0.80) from the best simulation among three methods, and generated more balanced prediction uncertainty ranges (R-factor = 0.48) with the best coverage of measurement (P-factor = 0.56) at the same time. The Parasol method resulted in same values of NSE (0.77) and R^2 (0.80) of the best simulation as SUFI-2 and better than the values from GLUE, showing its advantage on accurately capturing the optimized parameter sets. However, the uncertainty analysis results from the ParaSol method barely showed the improvement on P-factor (0.44) and R-factor (0.47) comparing the SUFI-2 method. The NSE (0.76) and R^2 (0.79) of the best simulation

from the GLUE method are a slightly worse than the SUFI-2 and ParaSol methods, and the GLUE method also generated the second best results of uncertainty analysis due to the good ratio of P-factor (0.36) and R-factor (0.37). The uncertainty intervals from GLUE are much smaller than other two methods. This may be caused by the lower number of simulation runs (5,000), because the GLUE method typically need a large number of simulation runs. The subjective threshold value (NSE = 0.7) may also cause the GLUE method with small uncertainty bands, because quite a big portion of parameter sets were screened as the non-behavioral parameter sets. Of note, because the R-factor values applied in the case study were quite small for three uncertainty analysis methods, it led to small bands of the 95PPU and thus compromised the number of observed values within the 95PPU (which can be seen from P-factors). Although the final results turned out to be not good as expected due to different limitations, the ratio of P-factor and R-factor is high enough (greater than 1 for SUFI-2, and closed to 1 for GLUE and ParaSol) for a typical uncertainty analysis (Yang *et al.*, 2008), indicating the acceptable performance of uncertainty analysis in this study. Moreover, as the main purpose of this study is to compare the performance of three uncertainty analysis methods by using a real case study, the performance of these methods can be compared through evaluating the P-factor, R-factor, ratio of P-factor and R-factor, NSE and R^2 of the best simulation from three uncertainty analysis methods.

By considering the computational requirement of each method, the SUFI-2 method achieved the best uncertainty analysis results in 3,000 simulations in total 3 iterations, and the ParaSol method obtained similarly good results by using 3,000 runs. The GLUE method provided the worst uncertainty analysis than other the two methods by using 5,000 simulations. The application of the GLUE method is easier than the other two methods on

the sensitivity analysis and global optimization calculation, because of its conceptual simplicity and relatively simple Monte Carlo sampling method applied. However, because computational efficiency of GLUE is really low, especially for high dimensional and complex models, it needs more computational resources and time for estimating the uncertainty. The SUFI-2 method applies the LHS scheme leading to a high efficiency on calculating optimal results, and this characteristic is very important for computationally demanding models. Due to all parameter sets of SUFI-2 were used for analysis of model parameter uncertainty, the uncertainty ranges normally are greater than the results from GLUE by using same simulation runs. The ParaSol method applied SCE-UA sampling scheme, which also is a high-efficient sampling scheme to localize the global optimum of the parameters ranges. In this study, only 3,000 simulation runs by using ParaSol can achieve better good simulation results comparing the results from the GLUE with simulation 5000 runs.

By comparing the results from three uncertainty analysis methods, it shows that the SUFI-2 method performs better than the other two methods due to the good NSE and R^2 values of the best simulation results and the best ratio of prediction uncertainty ranges and the relative coverage of measurement (1.17). When conducting hydrological simulation for surface runoff, the SUFI-2 method is preferred for this area by using SWAT as the modeling tool. Using the calibrated optimal parameter sets, the local water resource managers and decision makers can obtain more confident prediction intervals for surface runoff according to observed meteorological input data. The potential risk can be identified and predicted with high confidence by using updated parameter settings from SUFI-2 for the protection of local

life and property. Therefore, the SUFI-2 method could provide more reliable and efficient uncertainty analysis than the GLUE and ParaSol method in this study.

4.4 Case study #2: A case study in the Huolin River watershed

4.4.1 Study area and data acquisition

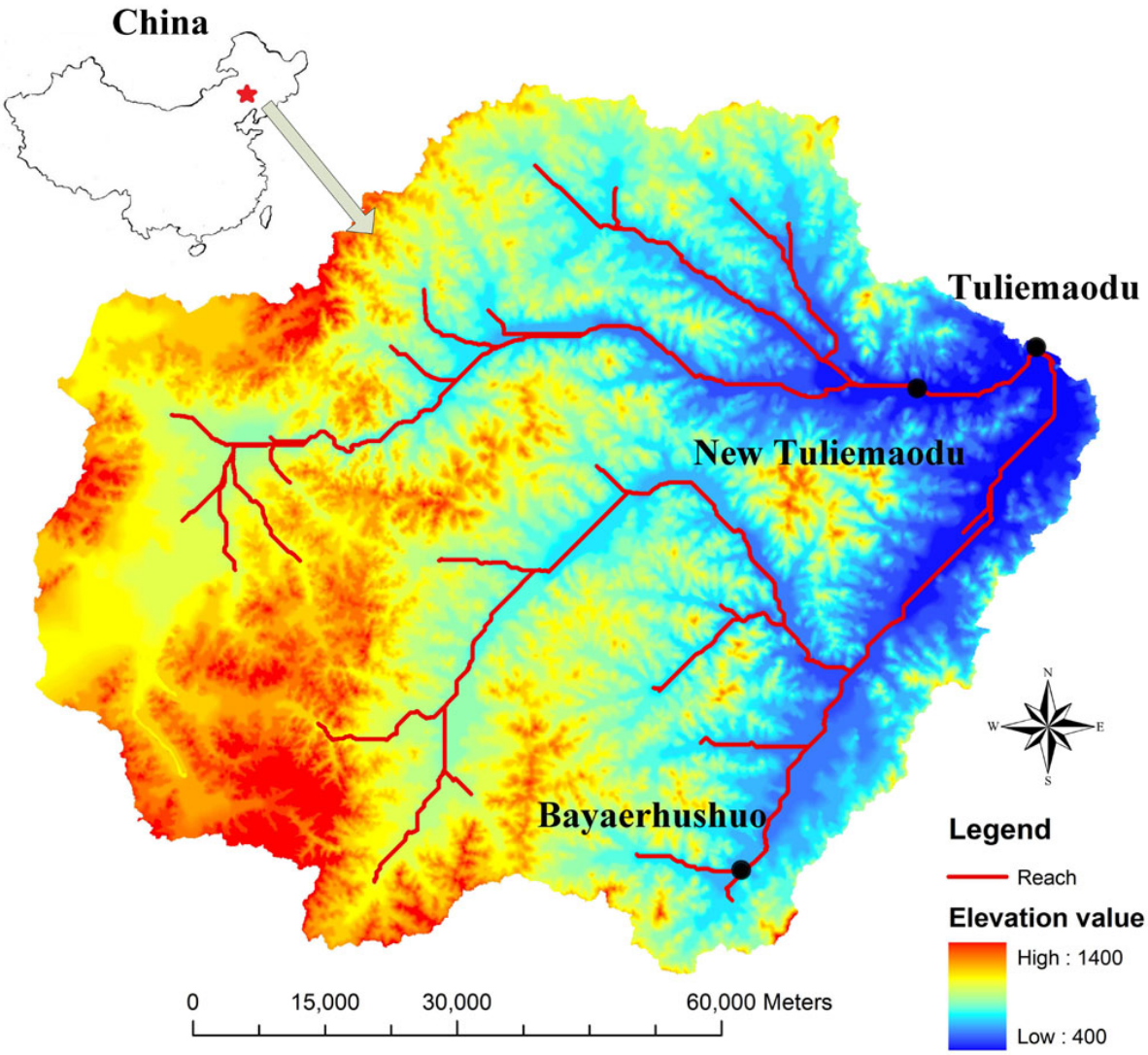

Figure 4.14 Location of study area in the Huolin River watershed

The study area is located in the headwater area of the Huolin River, which is one of the major tributaries of the Nen River in the basin of Songhua River in North China, with an area of 8102 km^2 (**Figure 4.14**). The topography is characterized by a hilly land and the average channel slope is approximately 23°. Average annual accumulated runoff at the Tuliemaodu station (located in the major surface runoff yield area of the Huolin River) is 3.08×10^8 m^3. The study area belongs to a temperate continental and semi-arid climate region, and the average elevation is 1439 m. The average annual maximum, minimum, and mean temperature are 21.4°C, -16.4°C, and 4.5°C to 5.6°C, respectively (Zhang and Chen, 2008**).** The annual accumulative rainfall varies between 350 and 400 mm. The dominated soils are the Chernozem soil, the meadow soil, and the brown loamy soil in the study watershed. The main land uses in the study area are cropland, grassland, and forest.

The Xianghai Nature Reserve, an important international nature wetland reserve, is located in the Huolin River's downstream region**.** Due to climate change, deforestation, water loss, soil erosion, and various human activities, the water scarcity and flooding threats have become severe problems in North China. With the increase of population, more human activities significantly affect the environment and hydrologic conditions in the study basin. The decreasing precipitation and declining groundwater level have caused seasonal water deficiency in the lower reach of the Huolin watershed as well (Bian *et al.*, 2006). In order to conserve the various natural resources, scientific and efficient water resource management for the whole watershed is quite important for the study area. Therefore, hydrological modeling with consideration of uncertainty for surface runoff and sediment is desired for supporting water resource management in the watershed.

In the study area, there are three stations for monitoring daily streamflow, including the Bayaerhushuo station, Tuliemaodu station, and New Tuliemaodu station (shown in **Figure 4.14**). The monthly sediment data are only collected at the Tuliemaodu station. All stations are operated by the Song Liao Conservancy Commission of Ministry of Water Resource of China and the Neimeng University of China (Xue, 2011), which provided the streamflow and sediment datasets used in this study.

In order to conduct successful hydrological modeling, parameter calibration is one of the key steps, especially for parameters which are unable to be directly measured and estimated. Among them, soil property and groundwater parameters are the hardest parameters to estimate. For example, some soil data are hard to access in certain areas, such as the number of soil layers, soil depth, and saturated hydraulic conductivity of different layers. This will cause a high degree of uncertainty when estimating the parameters used for simulating the surface runoff and sediment yield (e.g., CN_2 values). Similarly, some groundwater parameters (e.g., groundwater delay) are hard to obtain, making uncertainties inevitable. Therefore, careful calibration and uncertainty analysis are required in this study to achieve an acceptable simulation results.

The study area was divided into 39 subbasins and 228 HRUs. The SWAT model was calibrated and validated based on the observed surface runoff at Tuliemaodu station. Data from 1989 to 1990 were used as warm-up period of the simulation. The data from 1991 to 1996 were used for calibration, and the data from 1997 to 2000 were used for validation.

4.4.2 **Results and Discussion**

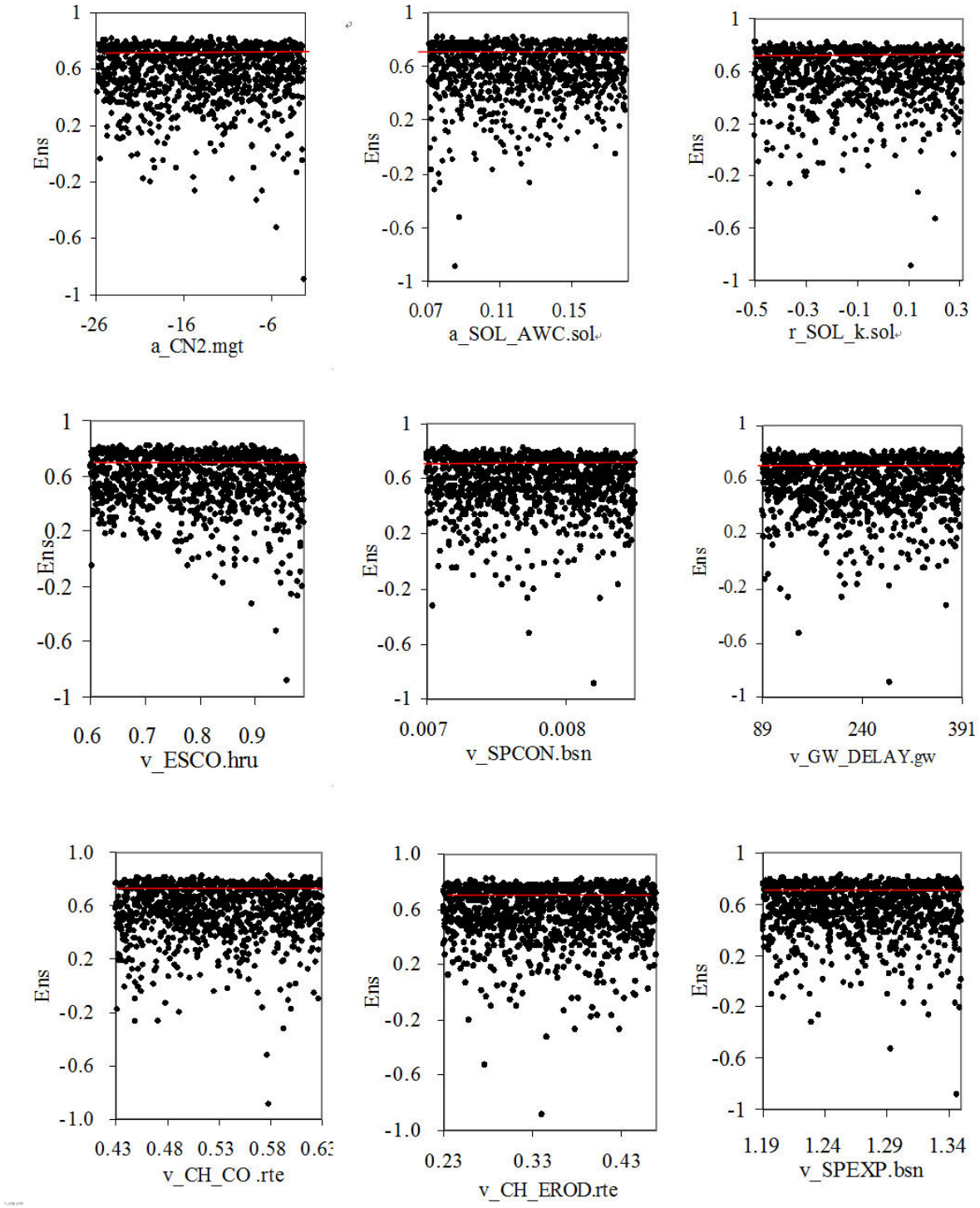

Figure 4.15 Dotplots of NSE against each aggregate parameter in SUFI-2

4.4.2.1 **Uncertainty analysis results using SUFI-2**

In the SUFI-2 method, model calibration and uncertainty analysis were simultaneously conducted. Nine of the most influential parameters were selected. **Table 4.3** shows the parameter descriptions, changing types of each parameter, prior distributions, best-fit estimations, and final parameter uncertainty ranges.

Parameter uncertainty analysis

Three iterations, with 1000 runs in each iteration, were conducted when using the SUFI-2 method. After each iteration, the updated parameter ranges were set as the prior distribution for the next iteration. The results from the third iteration (**Figure 4.15**) show that all parameter sets were taken as "behavioral" results and contributed to the 95PPU iteration. Posterior distributions were assumed to be independent and uniformly distributed in SUFI-2. However, the phenomenon of equifinality obviously occurred in both high NSE range (e.g., 0.81) and low NSE range (e.g.,-0.018). As it is shown in **Table 4.3**, parameter ranges of posterior distributions were narrowed through three iterations.

Model prediction uncertainty analysis

Table 4.4 shows the values of relative measurements coverage (P-factor), the width (R-factor), NSE and R^2 for surface runoff and sediment yield. The values of NSE for surface runoff in the calibration period and validation periods are 0.83 and 0.92, respectively, which are acceptable for model simulation; the R-factor in the validation period is 1.19 which is larger than 0.97 of the calibration period—primarily due to one large observation causing a large standard deviation in the calibration. **Figure 4.16** shows the surface runoff simulation with 95PPU derived by SUFI-2 from the third iteration. According to the results of the P-factor, most of the observations are included in the 95PPU (0.88 during the calibration period

and 0.9 during the validation period). The ratios of P-factor and R-factor for surface runoff are 0.91 and 1.29 for the calibration and validation period, respectively; the ratios of P-factor and R-factor for sediment are 0.69 and 0.6 for the calibration and validation period, respectively. The uncertainty for sediment is relatively larger than runoff, which makes the P/R is lower than runoff. The results also demonstrate that the SWAT model was successfully applied to the study area and reasonable uncertainty analysis results for runoff were achieved by using SUFI-2. **Figure 4.16(a)** indicates that the 95PPU has a good coverage for observations in 1992, 1995 and 1996, while it is somehow slightly overestimated in 1991, 1993 and 1994, especially in the recession period. Uncertainties were calculated in the recession by SWAT, which has been reported by Yang *et al.* (2008).

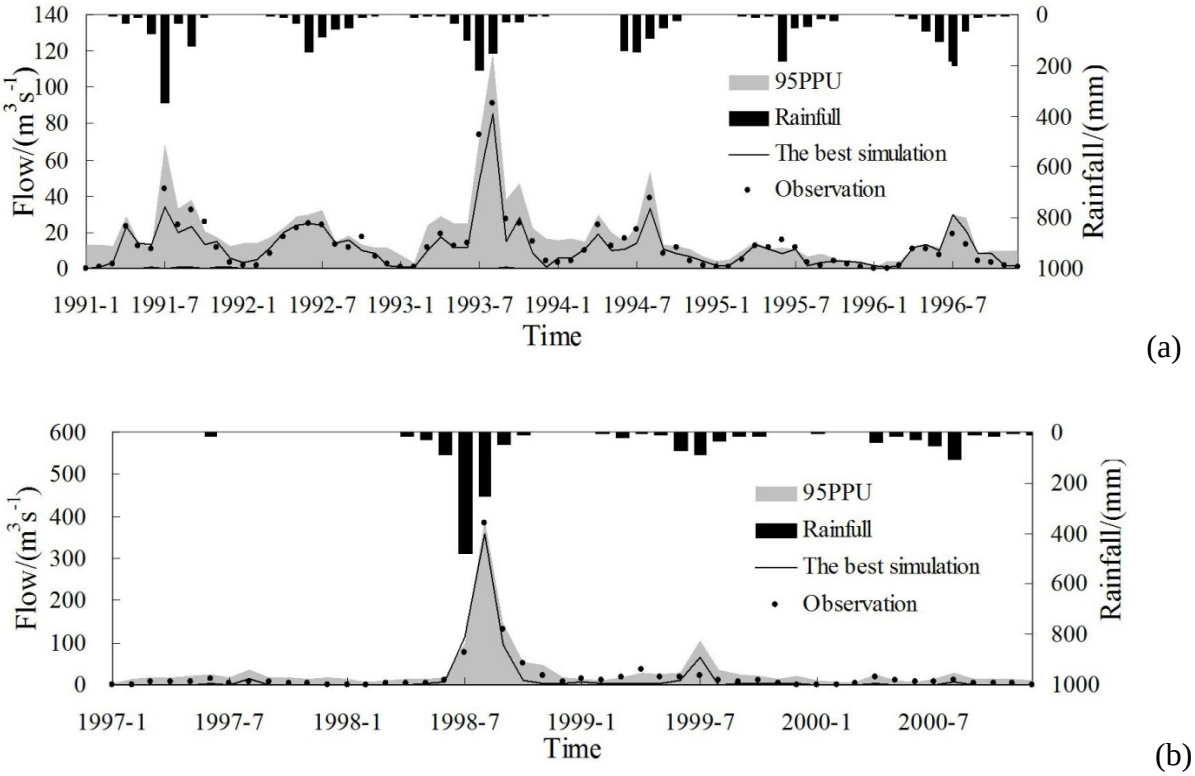

Figure 4.16 Simulated and observed surface runoff for (a) calibration period (1991–1996); (b) validation period (1997–2000) by using SUFI-2

Table 4.3 Model parameters and initial values for SUFI-2

parameters	Description	Change type	Prior distribution of parameters	The best estimation	Final parameter range
CN2	Initial SCS CN II value	a	U(-30,30)	-18.11	(-25.3, -1.87)
ESCO	Soil evaporation compensation factor	v	U(0,1)	0.94	(0.569, 0.959)
SOL_K	Saturated hydraulic conductivity [mm/hr]	r	U(-0.5,0.5)	-0.48	(-0.48, 0.33)
SOL_AWC	Available water capacity [mm H20/mm soil]	a	U(0,0.3)	0.12	(0.07, 0.18)
GW_DELAY	Groundwater delay [days]	v	U(30,400)	101	(90, 319)
SPCON	Linear reentrainment parameter for channel sediment routing	v	U(0.001,0.01)	0.0078	(0.0066,0.0081)
SPEXP	Exponent reentrainment parameter for channel sediment routing	v	U(1.0,1.5)	1.388	(1.29,1.41)
CH_COV	Channel cover factor	v	U(0,0.8)	0.138	(0.12,0.15)
CH_EROD	Channel erodibility factor	v	U(0,0.6)	0.189	(0.13,0.33)

Table 4.4 Simulation results of surface runoff and sediment yield for SUFI-2.

Variable	Period	P-factor	R-factor	NSE	R^2	P/R
Runoff	The calibration period（1991-1996）	0.88	0.97	0.83	0.85	0.91
	The validation period（1997-2000）	0.90	0.70	0.92	0.93	1.29
Sediment	The calibration period（1991-1996）	0.82	1.19	0.64	0.87	0.69
	The validation period（1997-2000）	0.77	1.29	0.77	0.84	0.60

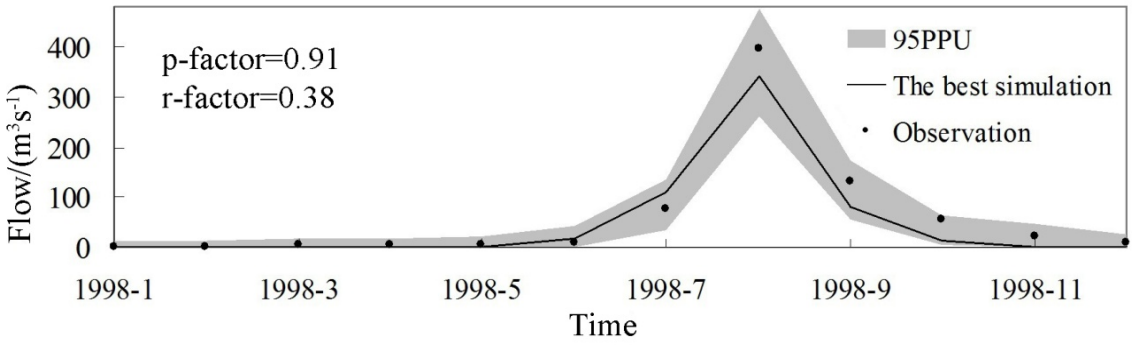

(a)

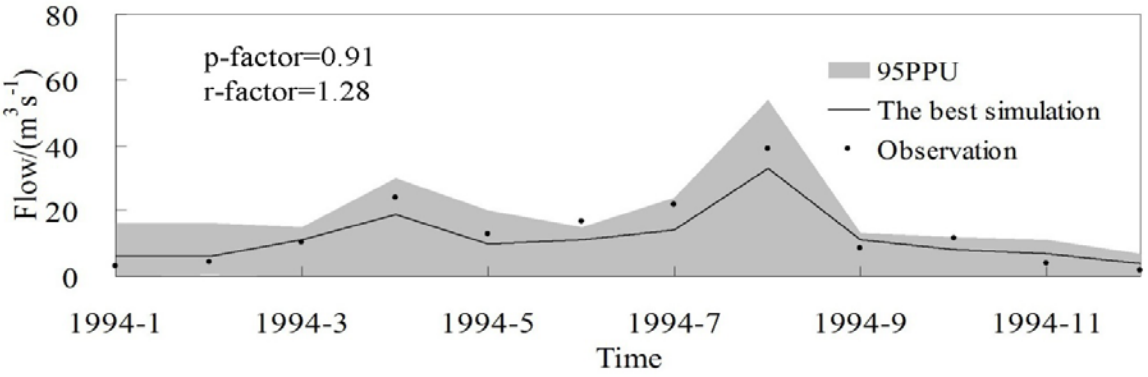

(b)

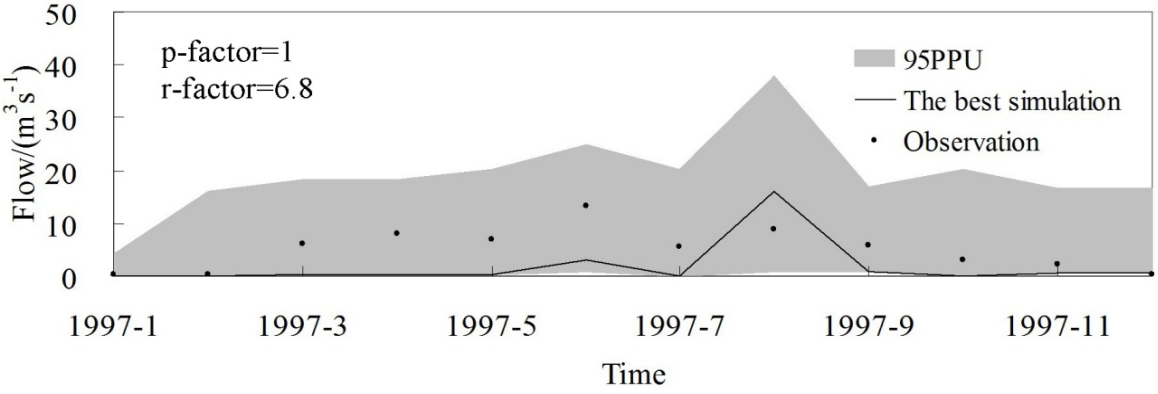

(c)

Figure 4.17 Simulated surface runoff for (a) wet (1998), (b) average (1994), and (c) dry (1997) years

To further understand the hydrologic process, surface runoff in wet (1998), average (1994) and dry (1997) years were analyzed in the validation period (**Figure 4.17**). All P-factors in these years are over 0.9, indicating more than 90% of observed data are bracketed by 95PPU of surface runoff. However, the dry year has larger prediction uncertainties (R-factor=6.8) than the average and wet years which are determined by surface runoff mechanism in SWAT and the characteristics of the study region. The results demonstrate that precipitation in the wet and average years mainly contributes to surface runoff and lateral flow. The retention parameter varies spatially due to changes in soil, land use, management, and slope, as well as temporally due to changes in soil water content (Neitsch *et al.*, 2011). The retention parameter could be estimated and calculated by the physical characteristics of the study area to reduce the subjective influence for surface runoff. Because CN_2 values determine the retention parameter, the satisfactory surface runoff simulation can be obtained from the CN_2 value by using SUFI-2. Through the SUFI-2 method, the uncertainties can be relatively reduced. For dry years, groundwater normally dominated the surface runoff. Because the knowledge of model parameters for simulating underground surface runoff is insufficient, the uncertainty of model parameters in simulated results of dry years was larger than that of wet and average years.

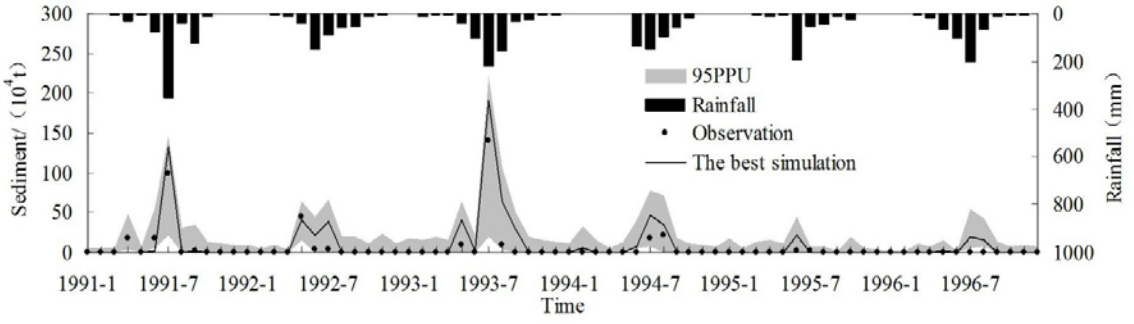

(a)

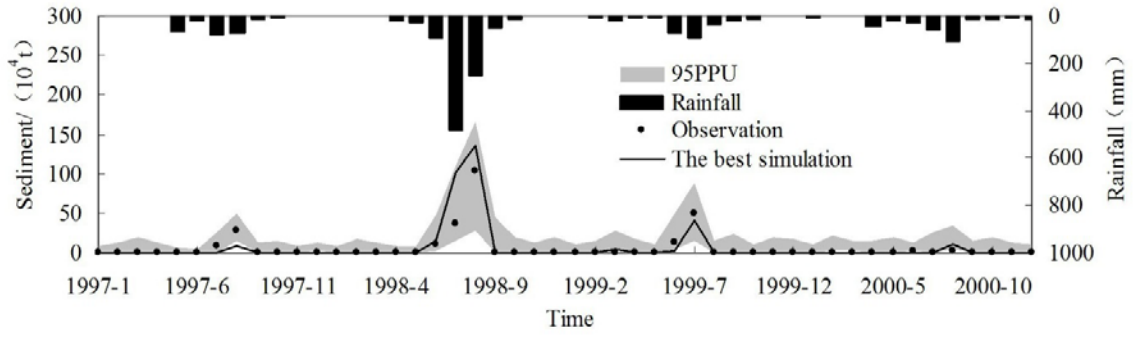

(b)

Figure 4.18 Simulated and observed sediment yield of calibration (1991–1996) (a) and validation (1997–2000) (b) by using SUFI-2

Figure 4.18 shows the simulation results of sediment, and 0.82 and 0.77 of observed data were included in the 95PPU during the calibration period and validation period (shown in **Table 4.4**), respectively. Measurements which were not included in 95PPU were mainly small load points. In other words, most of the data out of the 95PPU band were from the small sediment yield. The R-factor values in both the calibration and validation period for sediment is larger than the R-factor values of discharge, indicating larger uncertainties of sediment yield. Sediment is mainly influenced by precipitation and surface runoff. Precipitation has many uncertainties itself (e.g., spacial and temporal uncertainties), and surface runoff is the driving force to sediment yield and also is the carrier for sediment during movement. Therefore, the sediment yield is inevitably influenced by those

uncertainties. On the other hand, the uncertain sources of sediment also include some specific sensitive parameters which only have significant impacts on sediment (e.g., sediment transport coefficient and Exponent in sediment transport equation etc.). Consequently, arising from precipitation, surface runoff, and specific parameters of sediment, the uncertainties of sediment are relatively larger than surface runoff. In addition, the "second-storm" effect exists for simulating sediment in SWAT. Some literature showed that after a storm there was less sediment to be moved, thus a similar level or stronger second or third storm could actually result in smaller sediment yield (Abbaspour *et al.*, 2007). However, the SWAT model cannot account for this effect, leading to overestimating the sediment yield and causing more uncertainties to the sediment yield simulation.

4.4.2.2 **Uncertainty analysis results using GLUE**

Parameter uncertainty analysis

According to the above discussions, NSE was selected as the objective function, and threshold value was set to 0.7. Parameter combinations with the NSE values higher than the threshold value are considered as "behavioral parameter sets", whereas those below the threshold value are considered as "non-behavioral parameter sets". Based on the Monte Carlo random samples method, 30,000 samples were generated by using uniform distribution according to the analysis results of the minimum and optimum number of simulation runs. **Table 4.5** shows the initial values, the best estimation and the final parameter ranges of GLUE. **Figure 4.19** is the dotplot of behavioral parameter sets against the likelihood function.

Table 4.5 Model parameters and initial values for GLUE

Parameters	Change type	Original parameters ranges	The best estimation	Final parameter range
CN2	a	(-30,30)	-27.918	(-29.96, -2.31)
ESCO	v	(0,1)	0.186	(0.02, 0.29)
SOL_K	r	(-0.5,0.5)	0.098	(-0.33, 0.49)
SOL_AWC	a	(0,0.3)	0.449	(0.02, 0.093)
GW_DELAY	v	(30,400)	308	(30.58, 388.34)
SPCON	v	(0.001,0.01)	0.00905	(0.0012, 0.0093)
SPEXP	v	(1.0,1.5)	1.29	(1.28, 1.48)
CH_COV	v	(0,0.8)	0.508	(0.29, 0.57)
CH_EROD	v	(0,0.6)	0.722	(0.54, 0.73)

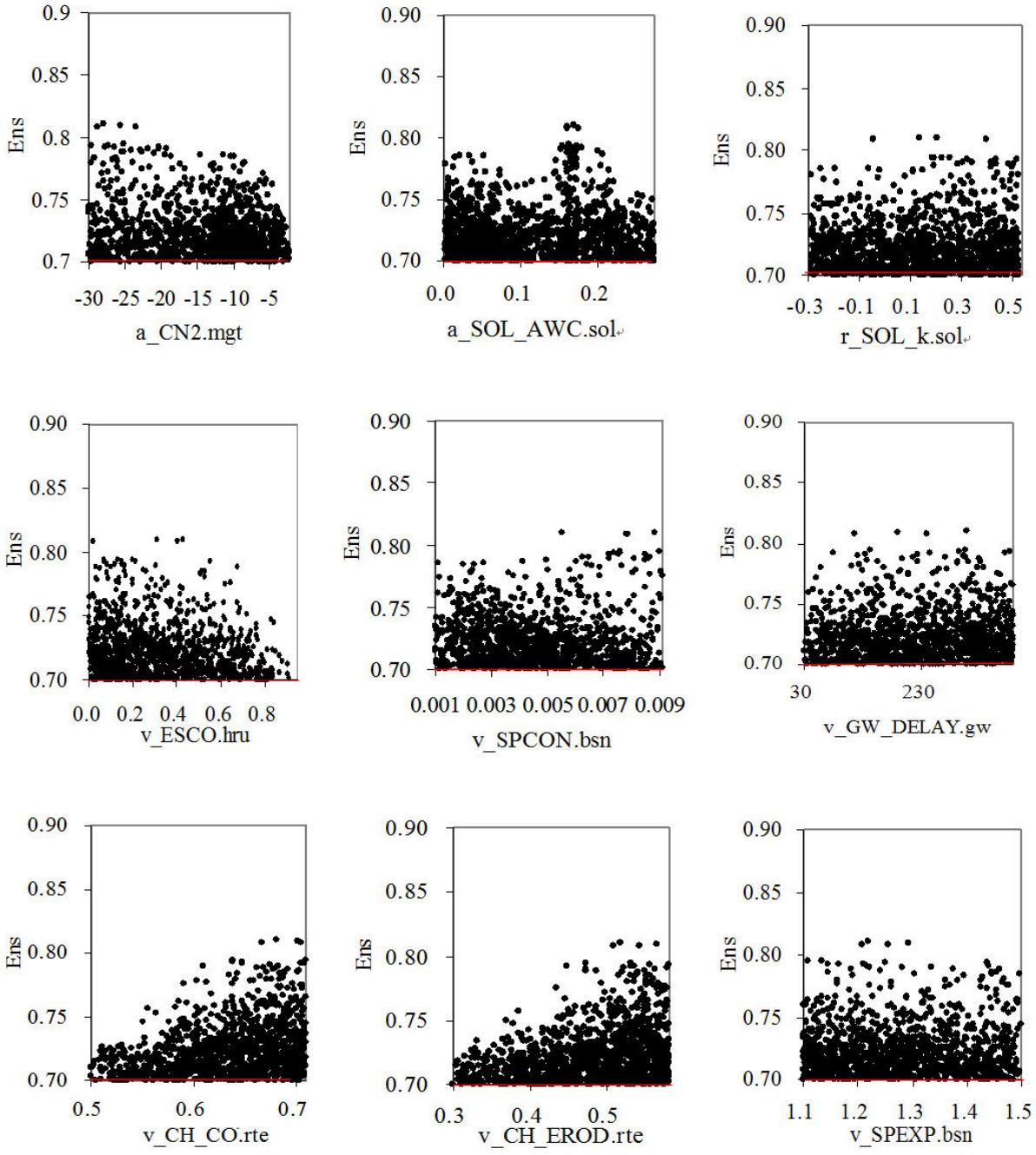

Figure 4.19 Dotplots of NSE against each behavioral parameter sets in GLUE

Figure 4.19 demonstrates that many parameter sets with similarly good values of the NSE can be found within the posterior ranges and the phenomenon of equifinality is very obvious. The posteriors of some parameters have obvious peak areas (eg. CN2, SOL_AWC,

ESCO, CH_CO, CH_EROD), which have significant influence on the results of model simulations.

Model prediction uncertainty analysis

As shown in **Table 4.6**, most of the surface runoff observations are bracketed by the 95PPU (0.83 during the calibration period and 0.9 during the validation period). The 0.79 and 0.76 sediment yield observations are bracketed by the 95PPU during the calibration and validation period, respectively. The NSE values for surface runoff are 0.81 and 0.83 in the calibration and validation periods, respectively; and the NSE values for sediment are lower than those of surface runoff, which are 0.61 and 0.79 for the calibration and validation period. The larger R-factor values for sediment yield in both the calibration (0.95) and validation (0.98) periods indicate larger uncertainties for sediment yield than those for surface runoff (0.83 and 0.71, respectively). The ratios of P-factor and R-factor for runoff are 1 and 1.28 for the calibration and validation period, respectively; the ratios of P-factor and R-factor for sediment are 0.83 and 0.77 for the calibration and validation period. The results also show that the SWAT model was successfully applied to the study area and reasonably good uncertainty analysis results were achieved for runoff and sediment by using the GLUE method.

Table 4.6 Simulation results of surface runoff and sediment yield for GLUE

Variables	Period	P-factor	R-factor	NSE	R^2	P/R
Runoff	The calibration period（1991-1996）	0.83	0.83	0.81	0.81	1
	The validation period（1997-2000）	0.90	0.71	0.83	0.85	1.28
Sediment	The calibration period（1991-1996）	0.79	0.95	0.61	0.84	0.83
	The validation period（1997-2000）	0.76	0.98	0.79	0.86	0.77

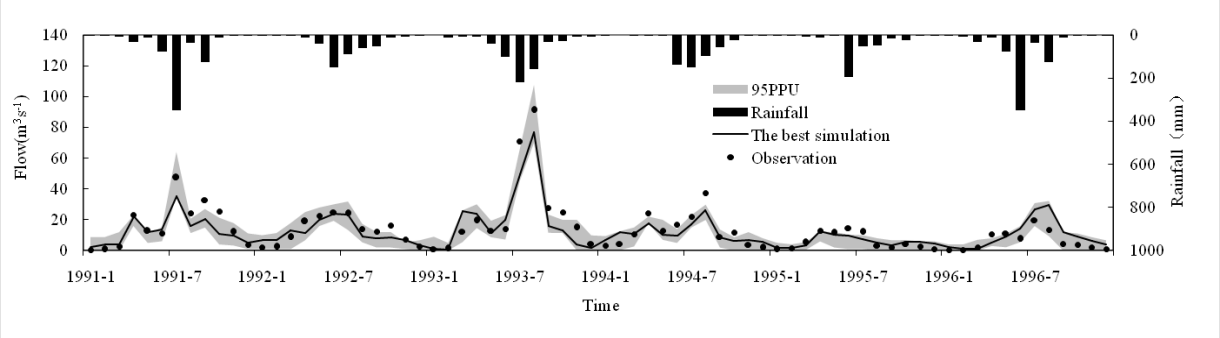

(a)

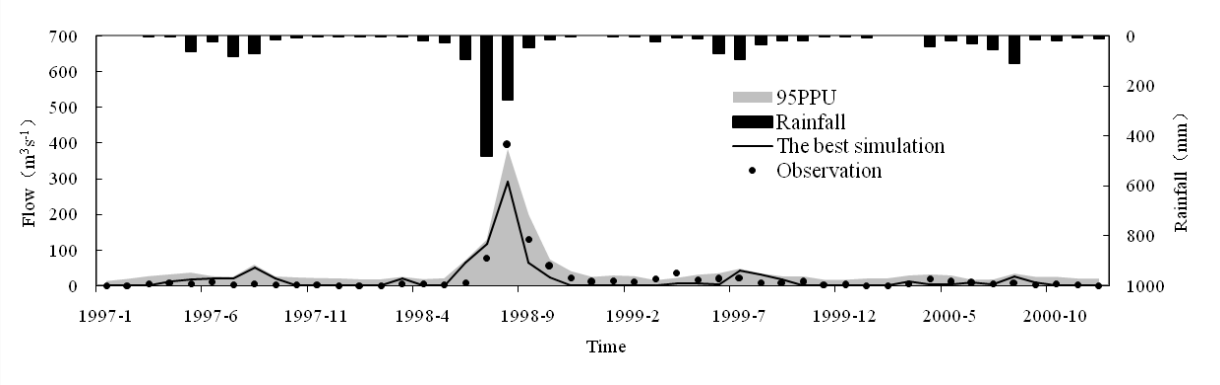

(b)

Figure 4.20 Simulated and observed surface runoff for the calibration period (1991–1996) (a) and validation period (1997–2000) (b) by using GLUE

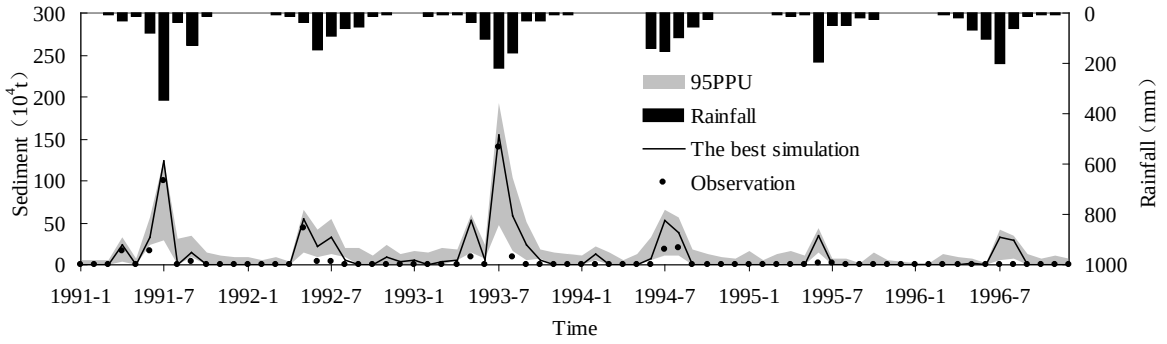

(a)

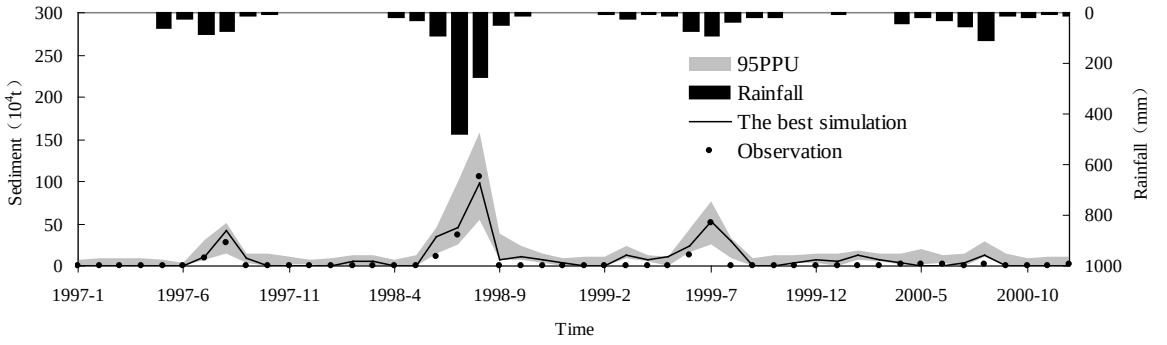

(b)

Figure 4.21 Simulated and observed sediment yield for the calibration period (1991–1996) (a) and validation period (1997–2000) (b) by using GLUE

4.4.2.3 **Results comparisons**

Comparative analysis was conducted in three aspects: parameter uncertainties, the model prediction uncertainties and the computation efficiency of the SUFI-2 and GLUE methods.

Parameter uncertainty

Firstly, **Figure 4.15** and **Figure 4.19** show the parameters' posterior distribution results from the application of the SUFI-2 and GLUE method, respectively. The parameters'

posterior distributions through the SUFI-2 method tend to be uniformly distributed, and optimal parameter values spread in the whole posterior range. However, some poor simulation results are also generated by using the SUFI-2 method. In contrast, some of the parameters were not evenly distributed in the posterior distribution by using the GLUE method, which demonstrates that the GLUE method can provide a more objective distribution for posterior distribution and has its advantages.

Secondly, through a comparison between **Table 4.3** and **Table 4.5**, it is clear shown that the parameter ranges from the GLUE method are wider than those from the SUFI-2 method, which can be attributed to the fact that the GLUE method considers parameter correlations while the SUFI-2 method does not. In the SUFI-2 method, all parameter sets from samples are set as behavioral parameters that contribute to the final uncertainties, leading to extra uncertainties and some poor simulation results. Contrastingly, in the GLUE method, the parameter sets will be viewed as "behavioral parameter sets" when their likelihood values are higher than the threshold value; the likelihood values below the threshold value will be considered as "non-behavioral" parameter sets and removed from further analysis. Only the behavioral parameter sets would contribute to the final uncertainty ranges leading to more reasonable uncertainty ranges by using the GLUE method.

Best simulation performance

As it is shown in **Table 4.4** and **Table 4.6**, for surface runoff, the NSE and R^2 values are 0.83 and 0.85 using the SUFI-2 method in the calibration period, which are greater than those values using the GLUE method (NSE = 0.81 and R^2 = 0.81); the NSE and R^2 values are 0.92 and 0.93 using the SUFI-2 method in the validation period, which are greater than those values for the GLUE (NSE = 0.83 and R^2 = 0.85) method as well. Similarly, for

sediment, the NSE and R^2 values are 0.64 and 0.87 using the SUFI-2 method in the calibration period, which are greater than those values using the GLUE method (NSE = 0.61 and R^2 = 0.84); the NSE and R^2 values are 0.77 and 0.84 using the SUFI-2 method in the validation period, which are slightly smaller than those values for the GLUE (NSE = 0.79 and R^2 = 0.86) method. In general, the results indicate that the SUFI-2 method can provide a better calibration results than GLUE method for surface runoff.

Model prediction uncertainty

As it is shown in **Figure 4.16** and **Figure 4.20**, both the SUFI-2 and GLUE methods show a better coverage in the recession periods of the hydrographs than the peak periods, also have a clear annual variation (e.g., overestimated for 1991, 1993 and 1994 by the SUFI-2 method, and overestimated for 1991 and 1993 by the GLUE method). In these two methods, parameter uncertainties are expressed as the total uncertainty, so that an impact on wet season and dry season would eventually be balanced from a long term point of view.

According to the simulation results shown in **Table 4.4** and **Table 4.6**, the R-factors for surface runoff in calibration and validation periods are 0.97 and 0.70 by using SUFI-2, and greater than the R-factors of 0.83 and 0.71 by using GLUE. The results have also been shown in **Figure 4.16** and **Figure 4.20**, and the prediction uncertainty range from SUFI-2 is wider than that from GLUE. Usually, uncertainties of sediment yield are relatively larger than that of surface runoff due to the complex hydrological system (Hao *et al.*, 2003). For the uncertainty of sediment yield in this study, the R-factors are 1.19 and 1.29 for calibration and validation periods by using SUFI-2, and also are greater than those of 0.95 and 0.98 by using GLUE. This is also in agreement with the hydrograph in **Figure 4.18** and **Figure 4.21**. Therefore, it is easy to determine that the model prediction uncertainties of simulated surface

runoff and sediment yield during calibration and validation periods using SUFI-2 are greater than those using GLUE. The main reason could be concluded that some poor simulation results have great effects on simulation results when using SUFI-2. Due to the removal of the non-behavioral parameter sets, the parameter ranges have been narrowed down, leading to small prediction uncertainty ranges by using GLUE. However, when considering the coverage of observed data, the SUFI-2 (0.91 and 1.29 for the calibration and validation period, respectively) and GLUE method (1 and 1.28 for the calibration and validation period, respectively) achieve very similar values of the ratio of P-factor and R-factor for runoff, demonstrating the ability of both methods to provide similarly good balanced uncertainty analysis results for surface runoff, which agrees with the conclusion from the first case study.

Computational efficiency

The application of the GLUE method is easier than that of the SUFI-2 method in the sensitivity analysis and global optimization calculation. A Latin Hypercube sampling was carried out in the SUFI-2 method and a relatively discrete parameter space was considered. The SUFI-2 method does not have computationally expensive problems. Therefore, only 3,000 simulation runs were conducted in this study. On the other hand, the GLUE method makes use of the Monte Carlo simulation for random sampling. In order to get reasonably good outputs, a certain number of sampling runs are required. In this study, the computation efforts for the GLUE method are 10 times (30,000 runs) of the SUFI-2 method. Therefore, the SUFI-2 method is more efficient for uncertainty analysis, and this practical advantage is quite valuable when handling some high dimensional and complex hydrological models.

4.5 Summary

Two real case studies were conducted in this chapter, including a case in the upstream of the Wenjing River watershed in Southwest China and a case in the Huolin River watershed in North China. The uncertainty analysis results using the SUFI-2, GLUE and ParaSol method were compared for the case study in the Wenjing River watershed, and uncertainty analysis results using the SUFI-2 and GLUE method were compared for the case study in the Huolin River watershed. The uncertainty for surface runoff was considered and evaluated in both cases, and the uncertainty of sediment was also considered in the case of the Huolin River watershed. The advantages and disadvantages of each method have been compared through the comprehensive evaluation scheme. The results were discussed separately in each study, and the key findings can be summarized as follows:

For the case in the Wenjing River watershed, three uncertainty analysis methods, SUFI-2, GLUE, and ParaSol, were studied through a distributed hydrological modeling system (SWAT) in order to examine their performance and capability in quantifying parameter uncertainties. The validation results showed that NSE and R^2 were 0.74 and 0.87 during the verification periods, respectively, demonstrating acceptable simulation performance. In general, by considering both modeling performance and computational efficiency, the results indicated the advantages of using SUFI-2 method in this study, due to its good accuracy for calibration results (NSE and R^2), the best coverage of measurement (P-factor) with reasonably small uncertainty impacts (R-factor), and higher computational efficiency on complex distributed hydrological models. The method could efficiently capture modeling uncertainties and quantify the associated impacts. The study demonstrated it as a capable tool to support distributed hydrological modeling with more reliable and accurate

prediction in watershed management practices. It is desired to undertake extended studies to further examine the capability of these three methods as well as to made similar efforts in studying other uncertainty analysis methods.

For the case in the Huolin River watershed, based on the simulation results of hydrological modeling, the SUFI-2 and GLUE methods were applied to analyze the parameter uncertainties of surface runoff and sediment yield in the study area. Some key conclusion can be derived from this case study: 1) According to the uncertainty analysis results of the surface runoff, the dry years have slightly larger prediction uncertainties than the average and wet years. Because the groundwater dominated the surface runoff in dry years and the knowledge of model parameters for simulating the underground surface runoff is insufficient, it leads to larger uncertainties than the uncertainties of average and wet years (which are dominated by precipitation); 2) A Latin Hypercube sampling (3,000 runs in this study) was carried out when using the SUFI-2 method, and it achieved the smallest number of simulation runs to obtain good prediction uncertainty ranges; 3) The 30,000 simulation runs showed the disadvantage and inefficiency of the global sampling method adopted by the GLUE method. Therefore, the application of GLUE to complex hydrological models will lead to far more computation time, and more energy and resource consumption; 4) Three aspects, including the parameter uncertainties, model prediction uncertainties and computation efficiency, were compared by using the results of uncertainty analysis. The SUFI-2 method is able to apply a small number of simulation runs to achieve reasonable prediction uncertainty ranges. The SUFI-2 method is very important for complex structural and high computationally demanding models, and can greatly improve operation efficiency to obtain better simulation estimates. On the other hand, the GLUE method could provide

small uncertainty ranges for parameters to improve the simulation performance of simple models. For a general model, the implementation of the GLUE method is relatively simple, and the GLUE method can provide the posterior distributions (which are only generated by behavioral parameter sets) for model parameters, and could also more accurately quantify the parameter uncertainties. When considering the ability of uncertainty analysis, both methods showed the similar good uncertainty analysis results for surface runoff. Overall, the SUFI-2 method is able to provide better optimized simulation results with reasonably good uncertainty analysis, which agrees with the conclusions from the first case study.

CHAPTER 5.
A SEQUENTIAL MULTI-CRITERIA BASED CALIBRATION AND UNCERTAINTY ANALYSIS (SMC-CUA) METHOD FOR HYDROLOGICAL MODELING

The contents in the chapter will result in the potential publication:
Wu, H.J. and Chen, B. A novel statistical method for efficient parameter calibration and uncertainty analysis for hydrological modeling. (to be submitted to the Journal of Hydrologic Engineering, ASCE).
Role: I developed the model, conducted case studies and drafted manuscript. Dr. Bing Chen is my PhD supervisor and provided advice in manuscript drafting.

5.1 Background

Uncertainty is an expression of confidence about what people can understand both as individuals and communities, and is subjective. Based on personal experiences, assumptions and knowledge, different people will give different conclusions on how uncertain something is (Cooke, 1991; Brown and Heuvelink, 2006). Imperfect knowledge on current stage makes the uncertainty inevitable, especially in hydrological studies. As many distributed hydrological models are extensively used to support decision making process of watershed management nowadays, it is important and necessary for modelers to conduct a careful calibration and uncertainties analysis. Calibration is always a challenging task because of model input, model structure, parameter, and output uncertainty (Yang *et al.*, 2008).

In this chapter, a novel calibration and uncertainty analysis method, a sequential multi-criteria based calibration and uncertainty analysis (SMC-CUA) method, was proposed for hydrological modeling studies. The feasibility and flexibility of the SMC-CUA method were tested using a hypothetical case and a real case study. In the proposed method, instead of using the Monte Carlo random sampling method for prior distribution sampling of model parameters, the advanced sampling methods, such as Latin Hypercube Sampling (LHS) method or Shuffled complex evolution (SCE-UA), can be used as the sampling method for parameter prior distributions to improve the sampling efficiency. Moreover, new criteria could be involved to screen out the impractical behavioral simulations produced by some behavioral parameter sets and can control the phenomenon of equifinality at the same time.

It is different from the generalized likelihood uncertainty estimation (GLUE) method which accepts all the parameter sets as behavioral parameter sets if the likelihood values are greater than the pre-defined threshold value. To our knowledge limited studies have been

focused on refine the posterior distribution of parameters and results to make the simulation more accurately. The GLUE method normally applies only one likelihood function which should increase monotonically with the similarity in behavior increase (e.g., Nash–Sutcliffe coefficient) (Beven and Binley, 1992). The objective of the GLUE method is to identify a set of behavioral models within the universe of possible parameter combinations. The term "behavioral" is used to signify the models that are considered to be acceptable on the basis of available data and knowledge. Therefore, a threshold value needs to be predefined before screening the behavioral and non-behavioral parameter sets. However, among a number of behavioral parameter sets, some parameter sets can achieve a high value for the likelihood function but are still not reasonable in practice. Because the NSE only evaluates the goodness-of-fit of the overall simulation of runoff, there are some impractical and inaccurate simulation results within behavioral results. For example, it could have a more than 0.8 of NSE value for the overall simulation for runoff, but the simulated peak flow is quite different from observed peak flow or the time for the peak flow in simulation is much different from the time for corresponding peak flow in observation. In this study, a novel calibration and uncertainty analysis method for overcoming some drawbacks of the GLUE method will be developed. Similar to the sequential uncertainty fitting version 2 (SUFI-2) method, multiple iterations were adopted to improve the simulation and uncertainty analysis performance. Moreover, different algorithms for updating the parameter ranges were applied in each iteration, and the proposed method was applied to a hypothetical case and a real case study.

The hydrological modeling study in the upstream of the Wenjing River watershed was selected for calibration and uncertainty analysis using the proposed method as the real case study. The LHS method was used as the advanced sampling method for sampling

parameter points within parameter ranges, and the coefficient of determination (R^2) was used as an additional criterion to screen the refined behavioral simulations. The performance of the proposed method was evaluated, and the calibration and uncertainty analysis results of the proposed method were compared to the SUFI-2 and GLUE method through case studies.

5.2 Methodology

5.2.1 **The SMC-CUA method**

A new calibration and uncertainty analysis method, the SMC-CUA method, for hydrological model was proposed in this study. The framework is shown in **Figure 5.1**. The traditional and widely used likelihood function Nash–Sutcliffe coefficient (NSE) was selected for this study. By making use of advanced sampling methods for prior distributions and new criteria for screening the behavioral parameter sets for posterior distributions, more narrowed and reliable parameter uncertainty ranges could be provided to improve the simulation performance. The detailed procedures of the proposed uncertainty analysis method are provided as follows:

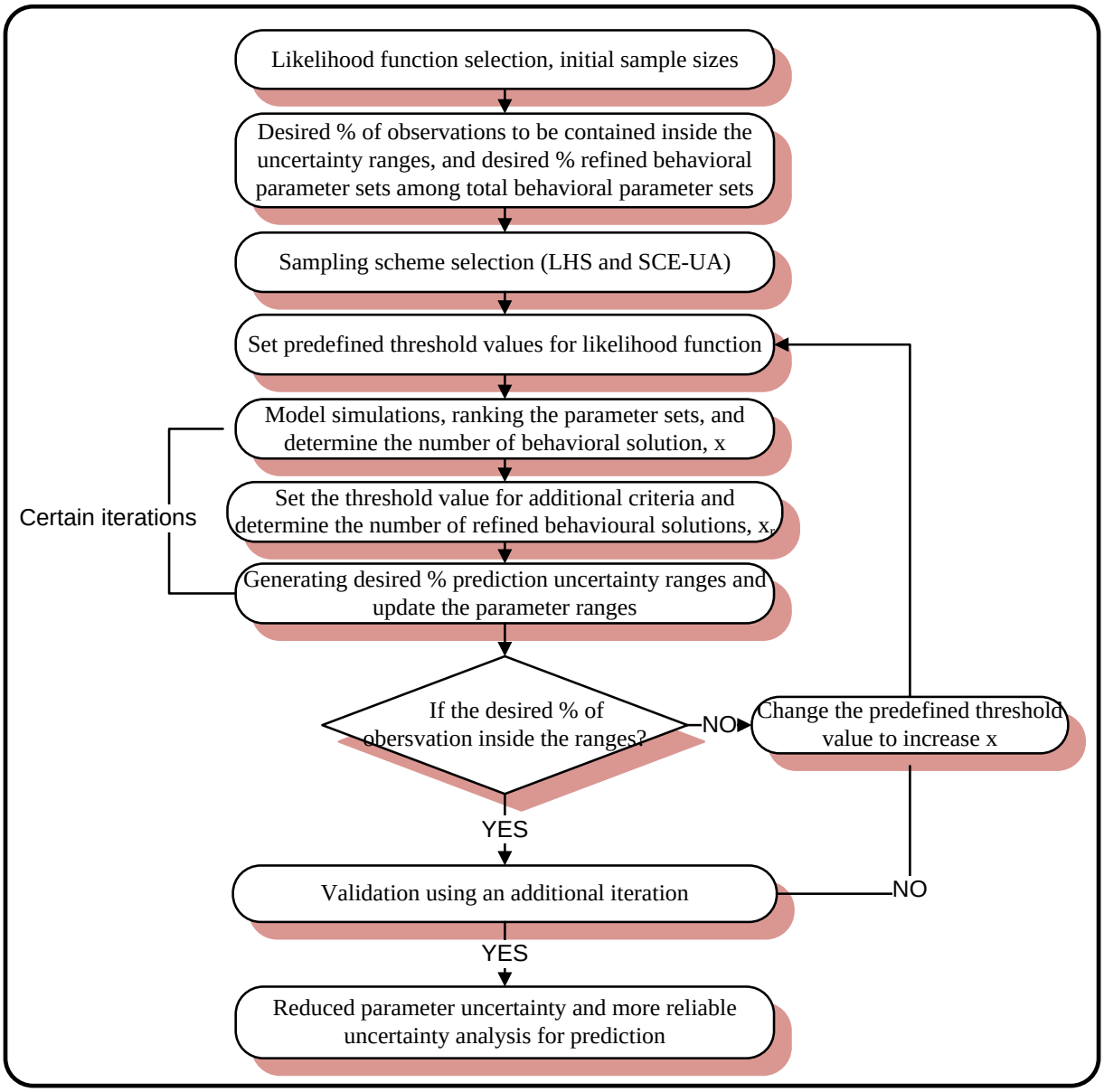

Figure 5.1 The framework of the SMC-CUA method for calibration and uncertainty analysis

Step 1: The likelihood function can be defined. As a popular objective function, NSE can be selected (Freer *et al.*, 1996). The equation of NSE has been provided in **Chapter 3** equation 3.1 (Wu *et al.*, 2012). The likelihood function of NSE selected in this study is same as other uncertainty analysis studies in previous chapters, and it can be used to compare the

performance of different uncertainty analysis methods. The initial sample sizes need to be defined. Due to the application of multiple iterations and high-efficient sampling methods, relatively small numbers of sample size for each iteration can be used.

Step 2: To decide what percentage of observations to be contained inside the uncertainty ranges and what percentage of refined behavioral parameter sets among the total behavioral parameter sets (which can achieve objective function values greater than the predefined threshold value) are desired. If the number of behavioral parameter sets is too small, the parameter ranges suggested for next iteration may not be accurate. Therefore, certain percentage of behavioral parameters has to be ensured for obtaining reasonably good estimation for the next iteration.

Step 3: Parameter ranges can be assigned according to physical meaning and current understanding of parameters. And then, advanced sampling schemes can be applied, which can be the Latin hypercube sampling (LHS) method or the Shuffled complex evolution (SCE-UA) method. Due to missing information, the prior distributions of parameters are usually assumed as uniform distributions. This is the typical assumption in hydrological modeling, because normally the prior distribution form of parameters was difficult to determine (Blasone *et al.*, 2008b).

Step 4: The threshold value of the likelihood function needs to be defined for screening the behavioral parameter sets and non-behavioral parameter sets. If a high value of the objective function threshold is set, normally small number of behavioral parameter sets can be found.

For different iterations, multiple choices of likelihood function values can be applied for better estimating the parameter ranges. For example, for the first iterations, due to the lack of information, relatively low threshold values can be selected.

Step 5: Hydrological simulation can be conducted and likelihood function values of simulations from each parameter sets are calculated. The simulations generated from parameter sets are ranked according to their likelihood values, and the parameter sets with likelihood values lower than the threshold value were removed. The remaining parameter sets are called behavioral parameter sets.

Step 6: Some additional criteria can be provided and used to screen out the "bad" behavioral simulations, even though the NSE values of them are greater than the pre-defined threshold value. If the additional criteria cannot be fulfilled through evaluation, these behavioral parameter sets will be removed and the remaining parameter sets are called "refined behavioral parameter sets". By using the additional criteria, the phenomenon of equifinality can also be controlled during hydrological modeling. For example, the coefficient of determination (R^2) can be used as an additional criterion for screening refined behavioral parameter sets (the equation of R^2 has been provided in Equation 4.7 in **Chapter 4**). Moreover, if new information is added into system (e.g., the new observation has been conducted leading to some updates of parameter ranges for some parameters), some behavioral parameter sets can also be removed since the new constraints have been involved. Eventually, the number of refined behavioral parameter sets will be reduced and determined, and prediction uncertainty will be reduced and quantified correspondingly. Some potential

attempts of additional criteria can be considered as follows (which have not been tested in current study):

$$L_2 = \frac{1}{n_p}\sum_{j=1}^{n_p}\left|\frac{Q_{o,j} - Q_{s,j}}{Q_{o,j}}\right| \qquad (5.1)$$

Where $Q_{o,j}$ is the observed peak flow (m^3/s), $Q_{s,j}$ is the simulated peak flow (m^3/s), n_p is the number of peak flow during the study period. It can be assumed that the difference between observed peak flow and simulated peak flow cannot be more than 30% for a behavioral simulation. Therefore, for parameter sets have L_2 the greater than 30%, these parameter sets will be removed from total behavioral parameter sets. The remaining parameter sets are considered as refined behavioral parameter sets.

$$L_3 = \frac{1}{n_p}\sum_{j=1}^{n_p}\left|t_{o,j} - t_{s,j}\right| \qquad (5.2)$$

Where $t_{o,j}$ is the observed time for accessing the peak flow (hour), $t_{s,j}$ is the simulated time for accessing peak flow (hour). For example, if difference between the time to peak flow in observation and in simulation results cannot be more than 3 hours is assumed, any parameter sets making L_3 greater than 3 hours will be removed to obtain the refined behavioral parameter sets.

Step 7: Model prediction uncertainty analysis can be conducted in this step. The upper and lower bounds of model prediction results can be determined by using prediction intervals of

simulation results for surface runoff. By sorting the likelihood values of simulations from each parameter sets, the time series surface runoff prediction uncertainty under the given confidence level could be estimated. For most studies, 2.5% and 97.5% of the cumulative distribution of surface runoff can be set as the low and high bounds as prediction uncertainty, respectively. Therefore, 95 percent prediction uncertainty (95PPU) of the surface runoff simulation can be obtained through the analysis. For the next iteration, the parameter ranges are updated accordingly by using the parameter ranges for the simulations achieving the 95PPU of surface runoff. Due to the number of refined behavioral parameter sets can always be reduced after each iteration, the corresponding parameter ranges will be reduced. After obtaining the updated parameter ranges, go back to **Step 5** for the new iteration till the desired number of iteration has been done.

Step 8: When 95PPU of surface runoff are obtained, the desired percentage of observation inside the 95PPU can be determined. If the percentage is too low and cannot meet the pre-set value, go back to **Step 4** and change the threshold value of the likelihood function to a lower one or adjust the critical value of other criteria to increase the behavioral parameter sets for getting a reasonable estimation of parameter ranges. If the percentage of observation is reasonably good, the next step can be proceeded.

Step 9: Validation of the proposed method is necessary. After obtaining the parameter ranges from the last iteration of simulations, the new updated parameter ranges will be applied for an additional iteration to check if the reasonable reasons are achieved. If simulation results are acceptable, go to the last step; if not, go back to **Step 4**.

Step 10: The calibrated simulation with uncertainty analysis can be achieved. This proposed method makes use of multiple iterations with advanced sampling methods and screens out the "bad" behavioral parameter sets using additional criteria to efficiently and accurately search the optimal results with consideration of uncertainty. The reduced parameter ranges also lead to smaller parameter uncertainty reflected by 95PPU of the surface runoff, and could provide more confidence for policy makers.

5.2.2 **Two sampling schemes**

5.2.2.1 **Latin hypercube sampling (LHS)**

LHS is a probabilistic procedure and can also be viewed as a compromise method which combines many desired features of random sampling and stratified sampling for producing more stable analysis outcomes than random sampling (Helton and Davis, 2003). Many studies have proved that the LHS is a very efficient way for assessing output uncertainty of models (e.g., most distributed hydrological model) with many parameters (Iman *et al.*, 1980; Melching, 1995; Christiaens and Feyen, 2002). This technique applies a stratified sampling scheme, which allows an efficient description of the output, and the standard LHS method contains three major steps as follow (Janssen *et al.*, 1992):

Step 1: Equiprobable subdivision — in LHS, the probability distribution of each model parameters is subdivided into *T* ranges/intervals with a probability of occurrence equal to *1/T* respectively;

Step 2: Stratified sampling — a single value can be sampled within each range/interval according to the probability distribution (normally the uniform distribution is assumed for parameters);

Step 3: Random pairing — *T* data sets of *p* (*p* is the number of parameters to be sampled) parameters are created.

The LHS method is ensured a more uniform coverage of parameter space and could present a better performance than other methods in estimating the statistics of a population of function with less model simulations (Blasone, 2007). Moreover, the LHS is very easy to be implemented for model parameter sampling. Therefore, by using the LHS method, the high-efficient sampling for uncertainty analysis can be relatively easy to achieve.

5.2.2.2 **Shuffled complex evolution (SCE-UA):**

A robust global search algorithm, SCE-UA algorithm developed by Duan *et al.* (1992), can also be used to sample parameter sets for prior distribution. Originally this method is used to minimize a single objective function and is based on a synthesis of four concepts: 1) combination of deterministic and probabilistic methods; 2) ability for systematic evolution within a complex to lead the parameter space towards to the global optimum; 3) multiple competitive evolutions; and 4) complex shuffling in each community. Because of these features, the SCE-UA method is effective and robust, and also flexible and efficient. The major steps of the SCE-UA method are described below (Duan *et al.*, 1994):

Step 1: Generate sample — sample *s* points randomly in the reasonable parameter range and compute the likelihood value (criterion value) at each point. Normally, the uniform probability distribution can be used to generate the sample if lack of prior information;

Step 2: Rank points — sort the *s* points in ascending order of likelihood value.

Step 3: Partition into complexes — Partition *s* points into *p* groups (called complexes), and each complex contains *m* points. The complexes are partitioned, so that the first complex contains every *p(k-1)+1* ranked point, the second complex contains every *p(k-1)+2* ranked point and so on, where *k=1,2,…,m;*

Step 4: Evolve each complex — evolve each complex according to the competitive complex evolution (CCE) algorithm;

Step 5: Shuffle complexes — combine the points in the evolved complexes into a single sample population, and sort the sample population by ascending sequence according to likelihood values;

Step 6: Check convergence — if any of the pre-specified convergence criteria are satisfied, stop; otherwise, continue;

Step 7: Check the reduction of the number of complexes—if the minimum number of complexes required in population (p_{min}) is less than *p*, remove the lowest ranked complex; set *p=p-1* and *s=pm*; return to Step 4; If $p_{min}=p$, go back to Step 4 (Duan *et al.*, 1992).

By using the SCE-UA method, considerable improvements can be made due to an adaptive sampling method that uses information from past draws to update the search direction. In such way, the SCE-UA method would probably result in a more robust and

efficient parameter and prediction uncertainty estimates comparing traditional random Monte Carlo sampling method.

5.2.3 **Hydrological modeling**

The hydrological modeling was conducted by using the soil and water assessment tool (SWAT), and the simulation results were used for analysis. SWAT is a continuous-time, spatially distributed hydrological model developed by the United States Department of Agriculture–Agricultural Research Service (USDA-ARS) (Arnold *et al.*, 1998) to assist water resource managers in predicting impacts of land management practice on water, sediment and agricultural chemical yields (Neitsch *et al.*, 2011). The SWAT model can make use of watershed information (e.g., weather, soil, topography, vegetation and land management practices) to simulate watershed hydrological processes such as surface and subsurface runoff, water quality, erosion and sedimentation (Muleta and Nicklow, 2005). One of the advantages of the SWAT model is that SWAT can be used for ungaged river basins. Other detailed introductions have been provided in previous chapters. By considering data availability, SWAT has been selected for this case study.

5.3 Case studies

In this chapter, two case studies have been included. One case study is a hypothetical case using the demo data of SWAT Calibration and Uncertainty Programs (SWAT-CUP), and another case study is a real case study using the hydrological simulation results from the upstream of the Wenjing River watershed in Chongzhou, China. The SMC-CUA method was applied to simulation results for both cases to test the feasibility and flexibility. For the

hypothetical case study, the proposed method was simplified by using only two iterations without adding any additional criterion for the comparison of GLUE method; for the real case study, four iterations were conducted to compare the results from SUFI-2 and GLUE method.

5.4 Results and discussion

5.4.1 **Demo data from SWAT-CUP**

In the hypothetical case, as a preliminary test, the simplified SMC-CUA method was applied to data from the demo of SWAT-CUP. The NSE was used as the likelihood function. For a simplified case, the performance improvement of calibration and calibration was tested using two iterations with 1,000 simulations each. The threshold value was set to 0.8 due to the really good match between the simulated and observed surface runoff. At least 35% of observation should be included in 95PPU for each iteration for achieving the acceptable uncertainty analysis results in this study. There are total ten parameters involved in calibration and uncertainty analysis process, which are CN_2 (initial SCS runoff curve number for moisture condition II), ALPHA_BF (baseflow alpha factor), GW_DELAY (delay time), CH_N2 (Manning's "n" value for the main channel), CH_K2 (effective hydraulic conductivity in main channel alluvium), ALPHA_BNK (baseflow alpha factor for bank storage), SOL_AWC(1) (available water capacity of the first soil layer), SOL_K(1) (Saturated hydraulic conductivity for the first soil layer), SOL_BD(1) (Moist bulk density for the first soil layer), and SFTMP (snowfall temperature). The LHS method was used for generating the 2,000 parameter sets from uniform prior distributions of each parameter. After the first iteration, the parameter ranges were adjusted according to the NSE results for the

purpose of testing the performance of multiple iterations. The NSE values verse some parameter for iteration 1 and 2 were shown in Figure 5.2 and Figure 5.3.

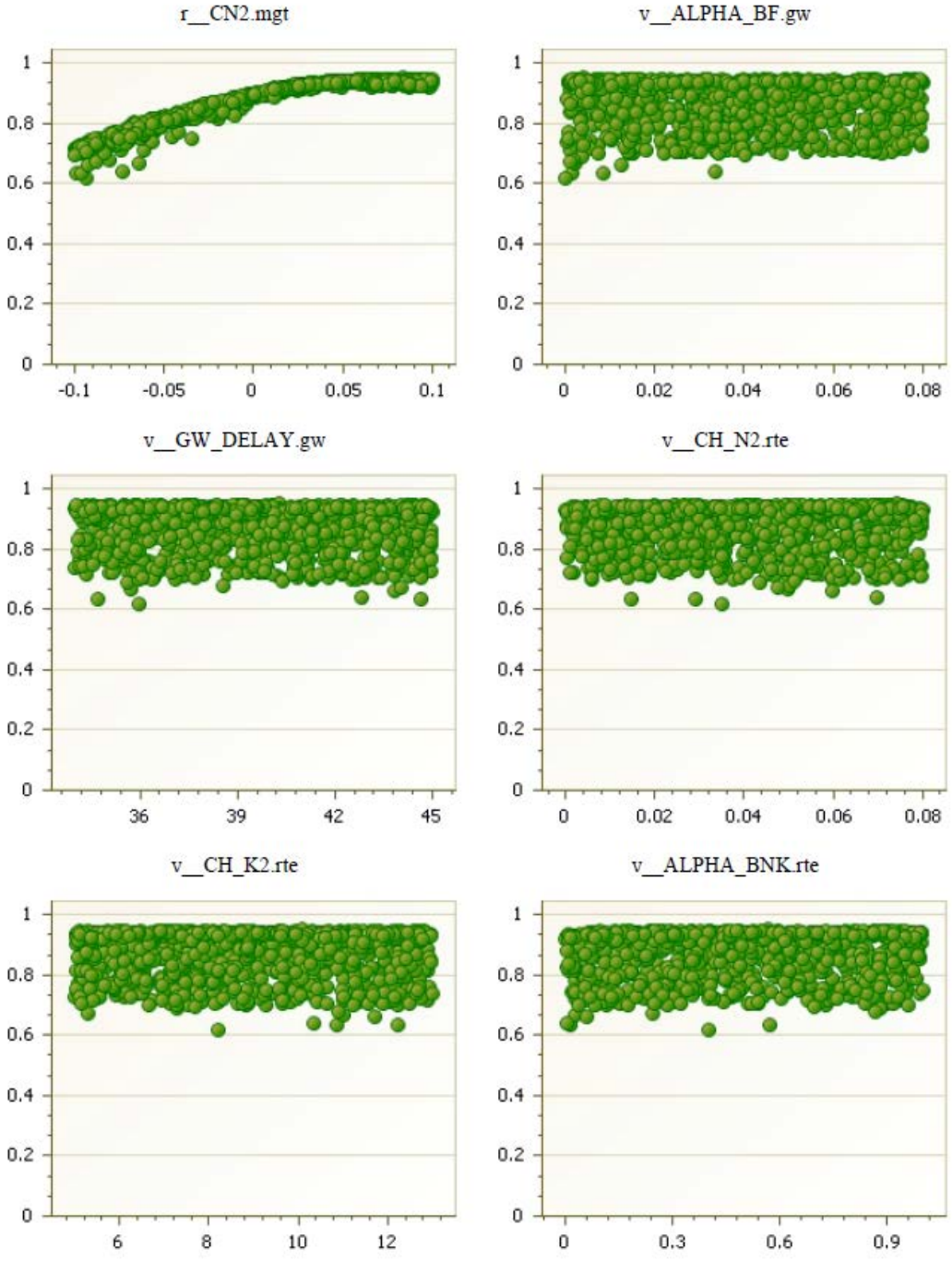

Figure 5.2 The NSE values of samples in the original parameter ranges for different parameters (first iteration)

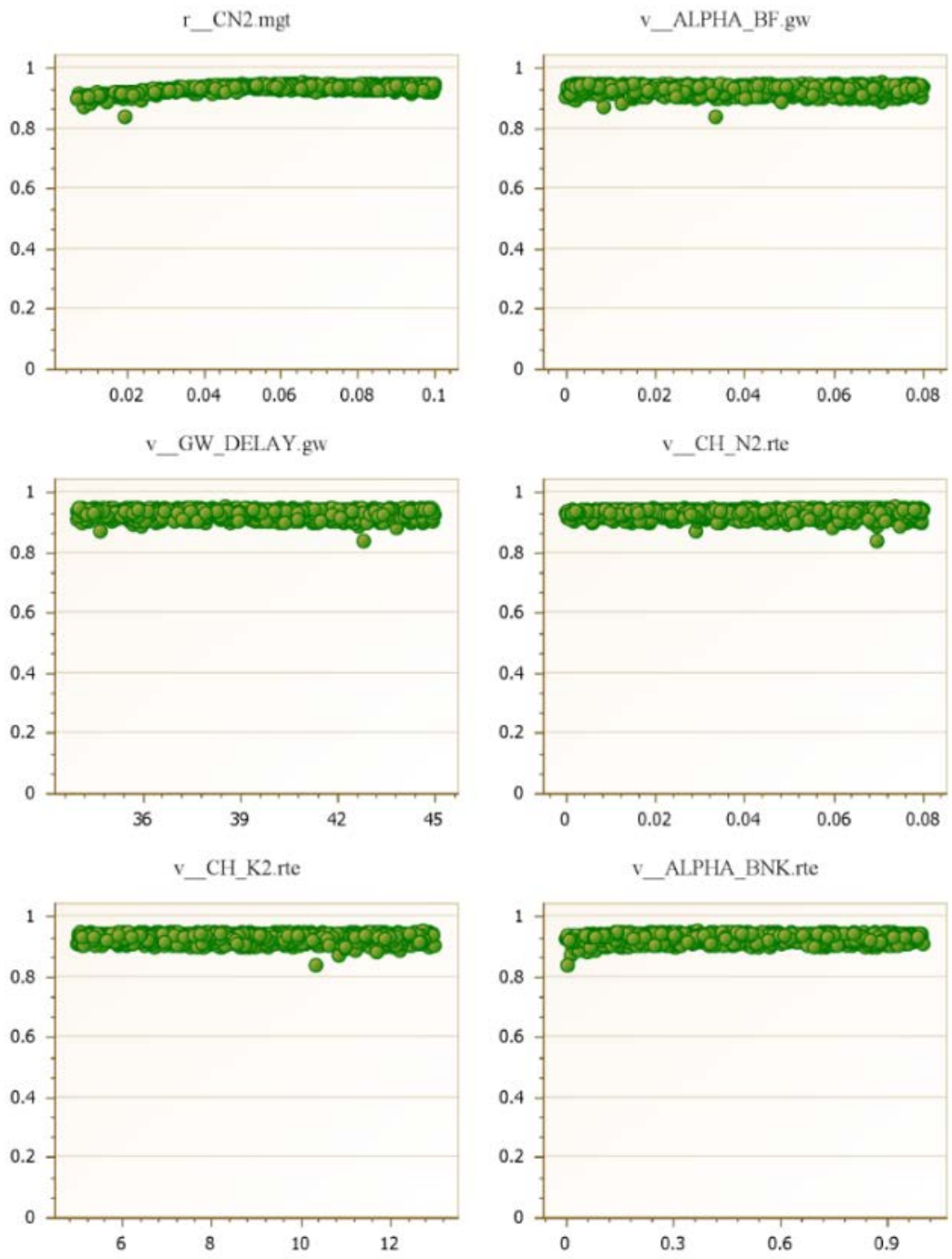

Figure 5.3 The NSE values of samples in the updated parameter ranges for different parameters (second iteration)

The preliminary results using demo data of SWAT-CUP were shown in **Table 5.1**. Through the first iteration, the 95PPU of surface runoff can be obtained and the new parameter ranges can be updated by ranking the behavioral parameter sets, correspondingly. For example, from plot for parameter r_CN_2 (the ratio changes of soil conservation service curve number) in **Figure 5.2**, it is shown that there is an obvious curvature within original pre-defined parameter space and the NSE value increases with the increasing r_CN_2 value. Therefore, the desirable solutions should locate in the region of larger values of r_CN_2 within the pre-defined feasible space. Through evaluation of the value of the objective function, some impractical parameter sets were removed from behavioral parameter sets. By using refined behavioral parameter sets, the 95PPU and parameter ranges were updated. As a simplified case, only parameter CN_2 was adjusted for the second iteration. As can be seen in **Figure 5.3**, the lower bound of parameter r_CN_2 was shifted from -0.1 to -0.01.

Table 5.1 The results for comparison of the simplified SMC-CUA method and GLUE method

Variable	Outlet	Behavioral simulation	P-factor	R-factor	R^2	NSE	P/R
1st iteration of SMC-CUA	Outlet 1	484(1000)	0.38	0.31	0.89	0.88	1.23
2nd iteration of SMC-CUA		976(1000)	0.38	0.3	0.91	0.91	1.23
GLUE		7660(10000)	0.38	0.53	0.91	0.90	0.72
1st iteration of SMC-CUA	Outlet 2	484(1000)	0.58	0.27	0.97	0.96	2.15
2nd iteration of SMC-CUA		976(1000)	0.58	0.27	0.98	0.97	2.15
GLUE		7660(10000)	0.63	0.47	0.97	0.96	1.34

*P-factor means the percentage of observations covered by the 95PPU; R-factor is measure of the relative width of 95% probability band.

To compare the results, the results of 10,000 simulations using the GLUE method are included in **Table 5.1**. **Table 5.1** also shows the results of the first iteration with original parameter ranges and the second iteration with the updated parameter range (only using updated parameter ranges of r_CN_2 as an example) by using the SMC-CUA method. The second iteration also improved the NSE and R^2 of the best simulation for both outlet 1 and outlet 2. Because the simulation performance is quite good, limited improvement can be found for the best simulation results in the second iteration. However, through the simplified SMC-CUA method, the behavioral simulations have dramatically increased by using updated parameter ranges. The percentages of behavioral parameter sets among the total parameter sets are larger than corresponding percentages in the GLUE method, which means the SMC-CUA method can more accurately capture the HPD region comparing to the random Monte Carlo sampling method of the GLUE method. The reasonable and acceptable results can be achieved at the circumstance of dramatically reducing parameter uncertainties indicating the advantages of the proposed SMC-CUA method.

In outlet 1, the best simulation of the SMC-CUA method and GLUE method can reach 0.91 and 0.90 for the value of NSE, respectively, and both methods achieve the same R^2 values as 0.91. The results show that the calibrated simulations from both methods are very close to the observed surface runoff due to the high NSE and R^2 values. The P-factor indicates the percentage of observation bracketed by 95 PPU, and R-factor can show the width of the uncertainty band (Wu and Chen, 2014a). The good uncertainty analysis is searching for the results that bracket most of the observed data with the smallest possible uncertainty band, which means the good uncertainty analysis results should have a relatively large P-factor with relatively small R-factor. Therefore, the greater the ratio of P-factor and

R-factor is, the better the simulation performance achieves. The increased ratio of P-factor and R-factor means the reduced uncertainty band still can cover reasonably good number of observations, indicating the desired uncertainty analysis results. The SMC-CUA method can provide a smaller R-factor value (R-factor = 0.3) than the GLUE method (R-factor = 0.53) (with the same P-factor value of 0.38). The ratio of P-factor and R-factor of the SMC-CUA method for outlet 1 is 1.23, which is much larger than the ratio value of 0.72 of the GLUE method. Although the results for outlet 1 barely show the improvement of the SMC-CUA method over the GLUE method for the best calibrated simulation, the ratio of P-factor and R-factor indicate that the SMC-CUA method can provide a better uncertainty analysis results than the GLUE method. In outlet 2, the best surface runoff simulation results from the second iteration also show the proposed SMC-CUA method has achieved a better performance than the results from the GLUE method with 10,000 simulation runs. The NSE of the SMC-CUA method and GLUE method are 0.97 and 0.96, and R^2 values of the two methods are 0.98 and 0.97, respectively, indicating the better calibration performance of the SMC-CUA method. The ratio of P-factor and R-factor for the SMC-CUA method (2.15) is much greater than the results for the GLUE method (1.34), indicating the better uncertainty analysis results.

From the above analysis, it is clearly showed that the SMC-CUA method could provide better calibration results and uncertainty analysis results than traditional GLUE method. At the same time, the SMC-CUA method is far more efficient comparing to the GLUE method. Only 2,000 simulation runs were conducted for the SMC-CUA method and achieved better calibration and uncertainty analysis results, but 10,000 simulation runs were required for the GLUE method. Another major advantage of the SMC-CUA method is that

the parameter uncertainty has been reduced by using updated parameter ranges. Therefore, the SMC-CUA method can help to effectively reduce the uncertainty. The uncertainty reduction is very meaningful, especially for uncertainty propagation problems under climate change condition. The uncertainty effects will be enlarged through the propagation, so the smaller uncertainty involved will have less effects to the total uncertainty.

5.4.2 **A real case study in Chongzhou**

In the real case study, the upstream of the Wenjing River watershed was selected as the study area. The information of study area has been provided in **Chapter 4**. As it is discussed above, the SMC-CUA method can be applied for calibration and uncertainty analysis of hydrological modeling. Therefore, the calibration and uncertainty analysis were conducted using the SMC-CUA method. Total 4 iterations with 1000 simulation runs per iteration were conducted. To get the reasonable uncertainty analysis, at least 35% of observed surface runoff should be included in 95PPU for each iteration. There are total 11 parameters involved in calibration and uncertainty analysis, and the definitions of the 11 parameters are shown in the **Table 4.1** in **Chapter 4**. The parameter ranges updated after each iteration according to the proposed algorithm. Since the improvement through the application of multiple iterations have been proofed in previous case, in order to investigate the performance of applying multiple iterations and criteria, two comparable experiments were conducted, including one set of simulation runs using one criterion and one set of simulation runs using two criteria.

5.4.2.1 **Simulations using one criterion**

Table 5.2 The statistic summary of the simulation results of each iteration using one criterion

Iteration	Threshold value	Behavioral parameter sets	P-factor	R-factor	R^2	NSE	P/R
First iteration	0.2	86	0.5	0.90	0.775	0.683	0.56
Second iteration	0.4	61	0.5	0.78	0.780	0.697	0.64
Third iteration	0.6	49	0.47	0.54	0.771	0.701	0.87
Fourth iteration	0.6	410	0.42	0.49	0.774	0.709	0.86

The statistical summary of simulation results using one criterion are shown in **Table 5.2**. As it is shown, the threshold values of the objective function for four iterations are set as different values (0.2, 0.4, 0.6 and 0.6). Because the HPD region is hard to determine for the first iterations, the relatively low threshold value of the objective function has been set for the preliminary estimate of HPD for different parameter ranges. The threshold value of the objective function can be adjusted for each iteration when approaching the HPD to obtain the smaller parameter ranges. Usually, the higher threshold value will lead to less behavioral parameter sets, so smaller parameter ranges will be estimated accordingly. In this study, the threshold value was set to 0.6 for the fourth iteration to guarantee the smaller parameter ranges for different parameters.

For the first iteration, the threshold value of objective function was set to 0.2 to get the preliminary estimate of optimal region. The original parameter ranges were used the same parameter ranges for SUFI-2 in the last chapter to make it comparable. The total of 86 behavioral parameters can be found with the original parameter ranges even though

relatively low threshold value was selected. The parameter sets generating 95PPU of surface runoff for the first iteration were used to update parameter ranges for the second iteration.

In the second iteration, the value of 0.4 was set for the threshold value of the objective function to screen the behavioral parameter sets due to the preliminary screening in the first iteration. The total of 61 behavioral parameter sets were selected for updating the parameter ranges for the third iteration.

In the third iteration, only 49 parameter sets can generate the behavioral simulations, because 0.6 was set for the threshold value of the objective function. Similarly, the parameter ranges for the fourth iteration can be estimated using parameter sets among the 49 parameter sets for calculating 95PPU of surface runoff. After this iteration, all the parameter ranges for four iterations have been decided. During each iteration, parameter ranges have been reduced and centered on the HPD region, and the parameter ranges for each iteration using one criterion were shown in **Table 5.3**.

In the fourth iteration, the updated parameter ranges were used for simulation, and the threshold value of the objective function was not changed (0.6). The number of behavioral parameter sets was dramatically increased to 410, indicating the parameter ranges around the HPD region for this case.

Table 5.3 Parameter range values of each iteration using one criterion

Parameters	First iteration		Second iteration		Third iteration		Fourth iteration	
	Lower bound	Upper bound	Lower bound	Upper bound	Lower bound	Upper bound	Lower bound	Upper bound
CN_2	-0.25	0.3	-0.22	0.29	-0.19	0.28	-0.19	0.13
ALPHA_BF	0.4	1	0.43	0.99	0.44	0.97	0.48	0.92
GW_DELAY	10	300	13.84	280.90	25.73	248.05	33.21	155.65
GWQMN	0	2000	13.75	1358.25	21.82	586.51	31.45	429.00
ESCO	0.8	1	0.81	0.99	0.83	0.99	0.84	0.99
CH_K	5	130	10.81	128.17	16.45	121.83	19.10	118.34
ALPHA_BNK	0	1	0.04	0.98	0.06	0.95	0.14	0.92
SOL_AWC	-0.2	0.4	-0.18	0.39	-0.13	0.38	-0.12	0.36
SFTMP	-5	5	-4.46	4.70	-4.07	4.38	-4.01	3.99
GW_REVAP	0.02	0.5	0.02	0.44	0.03	0.24	0.03	0.15
RCHRG_DP	0	1	0.01	0.64	0.01	0.37	0.01	0.19

To further investigate the performance of calibration and uncertainty analysis using the SMC-CUA method, the P-factor, R-factor, and R^2 and NSE values of the best simulation in each iteration were shown in **Table 5.2** as well. The smaller uncertainty bands could result in a smaller coverage of observed runoff data. Therefore, the larger value of P/R with an acceptable coverage is the desired results. Although the P-factor slightly decreased from 0.5 to 0.42 during different iterations, the R-factor was dramatically decreased from 0.90 to 0.54 at the same time. The ratio of P-factor and R-factor increased from 0.56 to 0.86 through four iterations, demonstrating the improvement of uncertainty analysis results. The R^2 values of four iterations are pretty constant with a high value (above 0.77) showing good correlation between simulated results and observed surface runoff. The NSE values for four iterations increased from 0.683 to 0.709, and a better calibrated simulation can be achieved. Through the application of the SMC-CUA method with one criterion, the ratio of P/R, R^2 and NSE all increased during the multiple iterations, indicating the improvement of calibration and uncertainty analysis using the SMC-CUA method.

5.4.2.2 **Simulations using two criteria**

From the above section, the calibration and uncertainty analysis results were improved during four iterations. To further test the proposed SMC-CUA method, two criteria were used to screen the behavioral parameter sets instead of one criterion. The R^2 was used as additional criterion to screen better parameter sets, which can be called "refined behavioral parameter sets", among the behavioral parameter sets. During each iteration, the results for behavioral parameter sets (screened by the objective function) and refined

behavioral parameter sets (screened by the objective function and R^2) in each iteration are shown in **Table 5.4**.

Table 5.4 The statistic summary of the simulation results of each iteration using two criteria

Iteration	No. of criteria	Threshold value	Behavioral parameter sets	P-factor	R-factor	R^2	NSE	P/R
First iteration	One	NSE = 0.2	86	0.50	0.90	0.775	0.683	0.56
	Two	NSE = 0.2 R^2 = 0.6	81	0.50	0.90	0.775	0.683	0.56
Second iteration	One	NSE =0.4	62	0.47	0.71	0.778	0.697	0.66
	Two	NSE =0.4 R^2 = 0.7	34	0.47	0.66	0.778	0.697	0.71
Third iteration	One	NSE = 0.6	74	0.44	0.52	0.779	0.725	0.85
	Two	NSE = 0.6 R^2 = 0.75	41	0.42	0.45	0.779	0.725	0.93
Fourth iteration	One	NSE = 0.6	605	0.39	0.39	0.787	0.743	1.00
	Two	NSE = 0.6 R^2 = 0.75	527	0.39	0.39	0.787	0.743	1.00

Table 5.4 also includes the results of P-factor, R-factor, R^2, NSE and P/R for each iteration. The threshold values of the objective function for four iterations were set as the same for the one criterion case (0.2, 0.4, 0.6, and 0.6). The R^2 were used as the additional criterion in each iteration, and the values were set as 0.6, 0.7, 0.75 and 0.75 for the four iterations due to the good correlation between simulated runoff results and observed surface runoff.

For the first iteration, the threshold value of the objective function was set to 0.2. Two situations were analyzed separately, including the results for behavioral parameters and the results for the refined behavioral parameter sets in each iteration. The threshold value of second criterion R^2 was set to 0.6 for screening the refined behavioral parameters among the

behavioral parameter sets. In the first iteration, there are total 81 refined behavioral parameter sets among 86 behavioral parameter sets. Because only 5 parameter sets were removed from behavioral parameter sets due to the lower R^2 values, P-factor and R-factor are the same for the two situations, which are 0.5 and 0.9, respectively. The values of R^2 and NSE for the best calibrated simulation are 0.775 and 0.683, indicating reasonably good simulation results. Because the best calibrated simulation usually will not be removed when using additional criteria, the R^2 and NSE of the best simulation will not change for two situations within an iteration. According to the 95PPU of the 81 parameter sets (screened by using two criteria), the updated parameter ranges for the second iteration were calculated.

For the second iteration, the threshold value of the objective function increased to 0.4. The 62 behavioral parameter sets can be found. The R^2 and NSE values of the best calibrated simulation increased to 0.778 and 0.697, respectively. When the R^2 was set to 0.7 for the second iteration, only 34 behavioral parameter sets were left as refined behavioral parameter sets. Therefore, the P-factor and R-factor are different for the two situations. The R-factor (0.66) of two criteria is smaller than R-factor (0.71) of one criterion, showing the effect of reducing the prediction uncertainty. The same P-factor value of 0.47 indicates that the reducing uncertainty does not affect the model prediction power and still covers the same number of observed data. The results with reduced uncertainty through two criteria are preferred results, and the 95PPU of the 34 refined behavioral parameter sets were used to calculate the parameter ranges for third iteration.

For the third iteration, the threshold value of NSE was set to 0.6. There are total 74 behavioral parameter sets after screening. The R^2 and NSE values of the best calibrated simulation are 0.779 and 0.725, respectively. The R^2 and NSE values are greater than results

in the second iteration, indicating the improvement of the calibrated results. The additional criterion R^2 was increased to 0.75 in this iteration for getting better refined behavioral parameter sets. Within 74 behavioral parameter sets, 41 parameter sets can achieve the value of R^2 greater than 0.75. The R-factor reduced from 0.52 to 0.45 when using two criteria. Even though the P-factor reduced a little (from 0.44 to 0.42), the ratio of P-factor and R-factor increased from 0.85 to 0.93, showing the improvement of uncertainty analysis results. The 95PPU of the 41 refined behavioral parameter sets were used to calculate the parameter ranges for fourth iteration. The exact values of each parameter range for four iterations are shown in **Table 5.7**.

For the last iteration, the threshold value of objective function and the additional criterion were set the same value as the third iteration. Due to the application of previous three iterations, the HPD region was estimated for each parameter. Therefore, the number of behavioral parameter sets was increased to 605, and the number of refined behavioral parameter sets was determined to 527. The R^2 and NSE of the best calibrated simulation are 0.787 and 0.743, respectively, which are the best calibrated simulation among the four iterations. The R-factor decreased to 0.39 with a P-factor of 0.39 for both situations. The ratio of P-factor and R-factor is 1.00, which is the largest value of four iterations. All those values of different indicators showed that the last iteration achieved the best calibrated simulation with the most balanced uncertainty analysis results.

Through four iterations, the SMC-CUA method can effectively calibrate the hydrological model and provide reasonably good uncertainty analysis results. In Each iteration the best calibrated simulation results were improved and a more balanced and reliable uncertainty analysis results were provided (larger ratio of P-factor and R-factor). The

prediction uncertainty decreased in each iteration represented by 95PPU of surface runoff. Through the multi-criteria screen process, the behavioral parameter sets in each iteration were reduced indicating the reduction of the phenomenon of equifinality, which demonstrates the advantages of the SMC-CUA method. **Figure 5.4** shows the 95PPU of surface runoff in each iteration. As it is shown, the 95PPU bands are decreasing during each iteration, and at same time the uncertainty bands move towards to the observed runoff and tend to cover more observed results. In order to evaluate the performance of propose method, the SUFI-2 method and GLUE method were applied to the same case for comparison.

Table 5.5 The statistic summary of the simulation results of each iteration using SUFI-2

Iteration	Threshold value	Behavioral parameter sets	P-factor	R-factor	R^2	NSE	P/R
First iteration	0.4	31	0.31	0.99	0.743	0.627	0.31
Second iteration	0.4	214	0.36	0.89	0.802	0.716	0.40
Third iteration	0.4	741	0.56	0.92	0.786	0.755	0.61
Fourth iteration	0.4	1000	0.42	0.45	0.782	0.753	0.93

The calibration and uncertainty analysis by using the SUFI-2 method were first conducted. The NSE was used as the likelihood function, and the threshold value of objective function was set to 0.4. Four iterations with 1,000 simulation runs each were conducted. The original parameter ranges were set as the same as the parameter ranges for the first iteration of the SMC-CUA method. The parameter range settings for each iteration were shown in **Table 5.8**. Due to the application of different updating algorithms for parameter range, the parameter ranges are converged in different ways. The algorithm for parameter updating in SMC-CUA can guarantee the reduction of parameter ranges after each iteration; On the other hand, according to evolution of parameter ranges in SUFI-2, the parameter ranges may not always decrease during different iterations, and parameter ranges

were always centered on the best estimates (Wu and Chen, 2014a). Some subjective adjustments are needed to make the parameter value within the practical range of the parameter. The detailed statistics for each iteration were shown in **Table 5.5**. The R^2 and NSE of best calibrated simulation are 0.782 and 0.753 in the fourth iteration, respectively, showing a very good calibration results. The best calibrated simulation results are slightly better than the calibrated results from the fourth iteration using the SMC-CUA method (due to the higher NSE value). The ratio of P-factor and R-factor is 0.93 in the fourth iteration, which is smaller than the ratio of P-factor and R-factor of 1.00 in the fourth iteration of the SMC-CUA method.

Therefore, the SUFI-2 method can provide slightly better calibrated simulation results, and the SMC-CUA method can give a more balanced uncertainty analysis results. To be noticed, if only three iterations have been conducted, the SMC-CUA method can still provide a reasonably good uncertainty analysis results (P/R = 0.93); at the same time, the SUFI-2 method can only provide relatively poor uncertainty analysis results (P/R = 0.61). The SMC-CUA method can more efficiently achieve a desired uncertainty analysis results with a reasonably good calibrated simulation results. When less computational resources are provided, the SMC-CUA method can make quick and reliable responses than the SUFI-2 method.

Table 5.6 The statistic summary of the simulation results of each iteration using GLUE

Iteration	Threshold value	Behavioral parameter sets	P-factor	R-factor	R^2	NSE	P/R
One iteration	0.6	28	0.39	0.51	0.791	0.699	0.76

For a better comparison, the GLUE method was also used for calibration and uncertainty analysis. The total of 10,000 simulation runs was conducted. The original parameter ranges for the SMC-CUA method were used as the parameter ranges for each parameter in the GLUE method. The NSE was used as the likelihood function to keep consistency with other two methods, and the threshold value was set to 0.6 because a large number of simulation runs was conducted. **Table 5.6** shows the calibration and uncertainty analysis results by using the GLUE method.

As it is shown in **Table 5.6**, there are only 28 behavioral parameter sets among the total 10,000 parameter sets, representing the low efficiency on searching the optimal results by using the GLUE method. The R^2 and NSE value are 0.791 and 0.699, respectively, which are smaller than the results from the fourth iteration of the SMC-CUA method (R^2 = 0.787 and NSE = 0.725). The ratio of P-factor and R-factor is 0.76, which is also much lower than the value of the SMC-CUA method (P/R = 1.00), indicating that the propose method can provide better calibrated simulation with better uncertainty analysis results. Meanwhile, only 4,000 simulation runs were conducted to achieve better calibration and uncertainty analysis for the SMC-CUA method comparing with the 10,000 simulation runs in the GLUE method, demonstrating the advantages of the propose method.

According to the results from three methods, it is clearly shown that the SMC-CUA method can reach similar good calibration results with SUFI-2 (which are better than the GLUE method) and provide the best uncertainty analysis results among three methods. The SMC-CUA method also showed the ability to efficiently search the HPD region and reduce the prediction uncertainty of surface runoff and parameter uncertainty at the same time, demonstrating its advantages over other methods.

Table 5.7 Parameter range values of each iteration using two criteria using SMC-CUA

Parameters	First iteration		Second iteration		Third iteration		Fourth iteration	
	Lower bound	Upper bound	Lower bound	Upper bound	Lower bound	Upper bound	Lower bound	Upper bound
CN_2	-0.25	0.3	-0.22	0.29	-0.18	0.25	-0.18	0.07
ALPHA_BF	0.4	1	0.43	0.99	0.47	0.96	0.52	0.95
GW_DELAY	10	300	13.63	281.30	22.83	169.09	38.56	102.33
GWQMN	0	2000	13.00	1375.00	54.03	505.09	81.32	446.23
ESCO	0.8	1	0.81	0.99	0.82	0.99	0.82	0.98
CH_K	5	130	10.31	128.31	14.89	120.62	16.84	117.72
ALPHA_BNK	0	1	0.04	0.98	0.09	0.88	0.12	0.83
SOL_AWC	-0.2	0.4	-0.17	0.39	-0.15	0.34	-0.12	0.32
SFTMP	-5	5	-4.25	4.71	-4.02	4.59	-3.89	4.01
GW_REVAP	0.02	0.5	0.02	0.44	0.04	0.26	0.04	0.12
RCHRG_DP	0	1	0.01	0.64	0.02	0.34	0.03	0.19

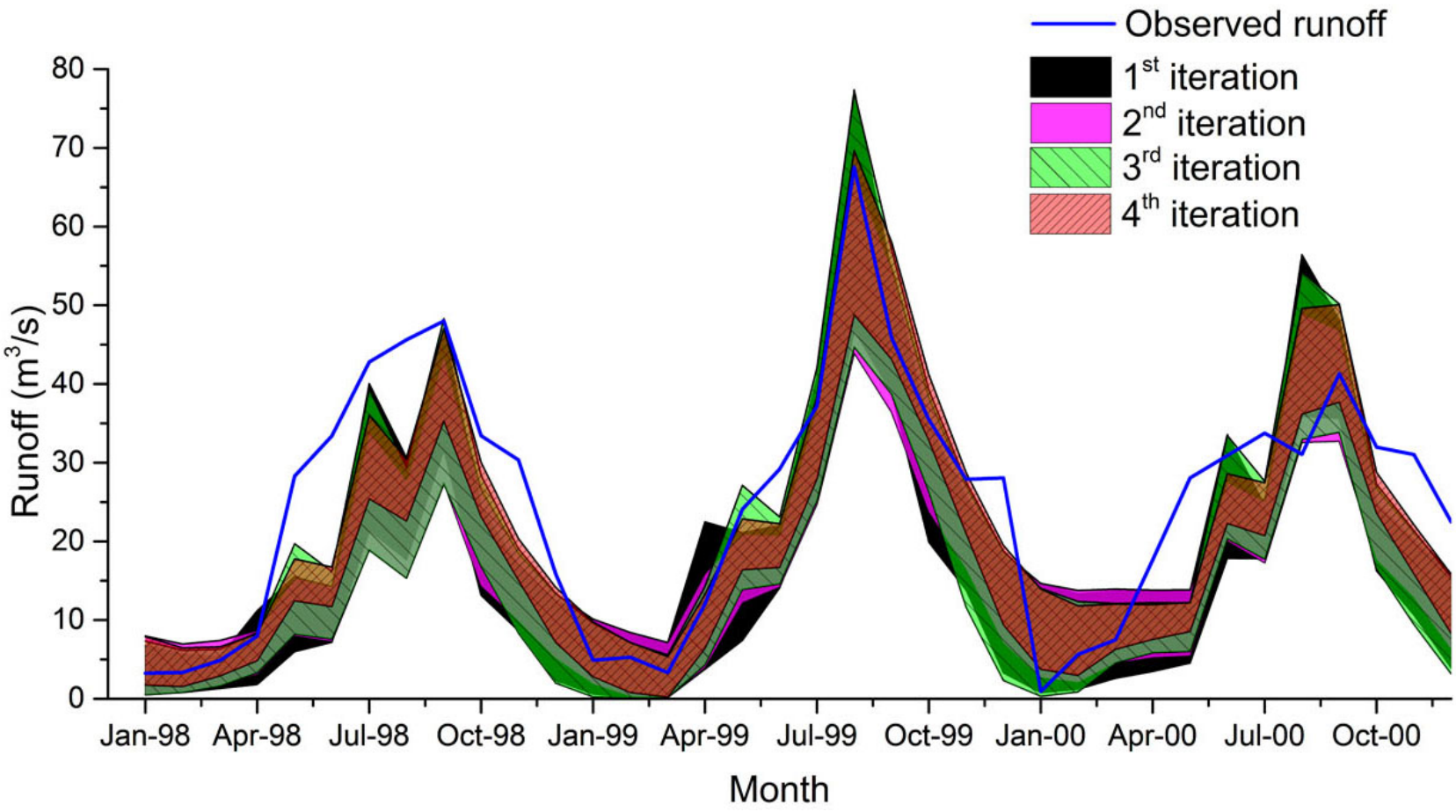

Figure 5.4 The 95PPU of surface runoff for four iterations using the SMC-CUA method

Table 5.8 Parameter range values of each iteration using SUFI-2

Parameters	First iteration		Second iteration		Third iteration		Fourth iteration	
	Lower bound	Upper bound	Lower bound	Upper bound	Lower bound	Upper bound	Lower bound	Upper bound
CN_2	-0.25	0.3	-0.4	0.1	-0.4	-0.02	-0.3	-0.1
ALPHA_BF	0.4	1	0.6	1	0.75	1	0.80	0.90
GW_DELAY	10	300	35	215	0	133	40	105
GWQMN	0	2000	0	1100	0	715	0	465
ESCO	0.8	1	0.87	1	0.91	1	0.94	1
CH_K	5	130	14	92	0	58	32	81
ALPHA_BNK	0	1	0.45	1	0.43	0.85	0.63	1
SOL_AWC	-0.2	0.4	-0.1	0.55	-0.12	0.33	-0.22	0.15
SFTMP	-5	5	-0.2	9	1	8.3	-0.3	5.9
GW_REVAP	0.02	0.5	0.01	0.3	0.01	0.16	0.02	0.12
RCHRG_DP	0	1	0	0.5	0	0.3	0	0.16

5.5 Summary

In this study, a new calibration and uncertainty analysis method was developed for hydrological modeling studies. Using the proposed framework, the SMC-CUA method aims to calibrate hydrological models and provide the balanced and reliable uncertainty analysis results in a high-efficient way. The feasibility and flexibility of SMC-CUA method were tested by two case studies using the SWAT model, including a hypothetical case using the demo data from SWAT-CUP and a real-world case in the upstream of the Wenjing River watershed.

From the first case study, only 2,000 simulation runs using the SMC-CUA method obtain the better values of R^2, NSE and P/R ratio than those from 10,000 simulation runs

using the GLUE method. The high efficiency of the SMC-CUA method and the ability for achieving more balanced uncertainty analysis results were proofed. In the real-world case study, the 4,000 simulation runs of the SMC-CUA method were used to compare to 4,000 simulation runs using the SUFI-2 method and 10,000 simulation runs using the GLUE method. The SMC-CUA method can provide better uncertainty analysis results than the SUFI-2 method with similarly good calibrated simulation, and also achieves the acceptable uncertainty analysis with less simulation runs. Comparing with the results of GLUE method, the SMC-CUA method is able to better calibration results and much better uncertainty analysis results with less simulation runs, indicating the high efficiency and the ability of searching optimal simulation and providing the balanced uncertainty analysis results.

Through the case studies, the results showed that the SMC-CUA method was able to fast locate the HPD regions of each parameter to improve the computational efficiency comparing to the SUFI-2 and GLUE method and reduce the parameter uncertainty without sacrificing the simulation performance for surface runoff prediction. Through the application of the addition criterion (R^2), behavioral parameter sets were further screened for refined behavioral parameter sets in each iterations, and the reduced number of behavioral parameter sets can control the phenomenon of equifinality showing the advantage of the SMC-CUA method. Due to the high computational efficiency, the SMC-CUA method could be applied to the high-dimensional parameter estimation problems and complex simulation models. The results also showed that the proposed SMC-CUA method provided the good calibrated simulation and more balanced uncertainty analysis comparing with the other two methods. In the SMC-CUA method, the parameter ranges are always centered on the best simulation results and narrowed down from the original ranges using the refined behavioral parameter

sets, thus the parameter uncertainty has been reduced after each iteration. The reduced parameter uncertainty is quite important when conducting the uncertainty analysis for propagation effects. The less uncertainty from the source would lead much smaller total uncertainty after propagation.

CHAPTER 6.
QUANTIFICATION OF UNCERTAINTY PROPAGATION EFFECTS DURING STATISTICAL DOWNSCALING OF PRECIPITATION AND TEMPERATURE TO HYDROLOGICAL MODELING USING A RESPONSE-BASED STATISTICAL EVALUATION METHOD (RESEM)

The contents in the chapter are based on the following publications:

1. **Wu, H.J.**, Chen, B., Snelgrove, K., and Lye, L.M. (2015). Quantification of uncertainty propagation effects during statistical downscaling of precipitation and temperature to hydrological modeling. *Journal of Environmental Informatics*, accepted (2015/08/29).
   Role: I developed the model, conducted case studies and drafted manuscript. Dr. Bing Chen is my PhD supervisor and provided advice in method development and manuscript drafting. Dr. Ken Snelgrove is my co-supervisor and provided assistance on manuscript editing. Dr. Leonard M. Lye is my PhD supervisory committee member and provided advice in manuscript drafting.

2. **Wu, H.J.,** and Chen, B. (2014). Uncertainty analysis for propagation effects from statistical downscaling to hydrological modeling. The International Conference on Marine and Freshwater Environments (iMFE) 2014 proceeding, St. John's, Newfoundland, CA, EMR #1330.
   Role: I developed the model, conducted case studies and drafted manuscript. Dr. Bing Chen is my PhD supervisor and provided advice in method development and manuscript drafting.

6.1 Background

The terms "persistent" and "irreducible" have been used to describe the uncertainty associated with the climate change, and the uncertainty extensively exists at the global and regional scale for different complex systems (Ficklin, 2010; Li *et al.*, 2013; Chen *et al.*, 2014). Normally, the major uncertainty in climate change studies comes from the selection of different GCMs, and the outputs of different GCMs and scenarios will lead to considerable differences in the downscaled results (Rowell, 2006; Kay *et al.*, 2009; Prudhomme and Davies, 2009; Ahmed *et al.*, 2013). However, the greatest interests have been given to the uncertainty that arise from GCMs, and the uncertainty during downscaling has been given much less attention (Graham *et al.*, 2007a; Chen *et al.*, 2011). Limited studies assessed the uncertainty related to the choice of downscaling methods, however, fewer studies have focused on estimating the uncertainty associated with a single downscaling method and the propagation effect on the uncertainty of hydrological responses. The purpose of this study is to quantify and evaluate the propagation uncertainty during downscaling to hydrological modeling through a single statistical downscaling framework using a response-based statistical evaluation method (RESEM). A case study in Sichuan province of China was conducted to demonstrate the feasibility and performance of the developed method. The soil and water assessment tool (SWAT) was used for hydrological modeling for the study area, and the statistical downscaling model (SDSM) was used to address the mismatch of data requirement between the GCM outputs and hydrological models.

6.2 Methodology

The framework in **Figure 6.1** shows the major steps of the proposed RESEM. Through the evaluation of the uncertainty in hydrologic responses (e.g., runoff), RESEM can quantify the uncertainty propagated from statistical downscaling to hydrological modeling. The first step is to decide which scenario and which GCM should be used for the case study. Secondly, after the selection of the GCM, SDSM will be applied to downscale precipitation and temperature from GCM predicator variables. And then, the downscaled precipitation and temperature can be directly applied as the input to the calibrated hydrological model (SWAT) for surface runoff simulation. The SWAT model is calibrated and validated by using observed data, and a reasonably good simulation performance needs (NSE > 0.65) to be achieved before the application of downscaled GCM outputs to ensure the reliability of simulation and prediction (Yen *et al.*, 2014). The quantitive analysis of uncertainty will be conducted after the application of downscaled data.

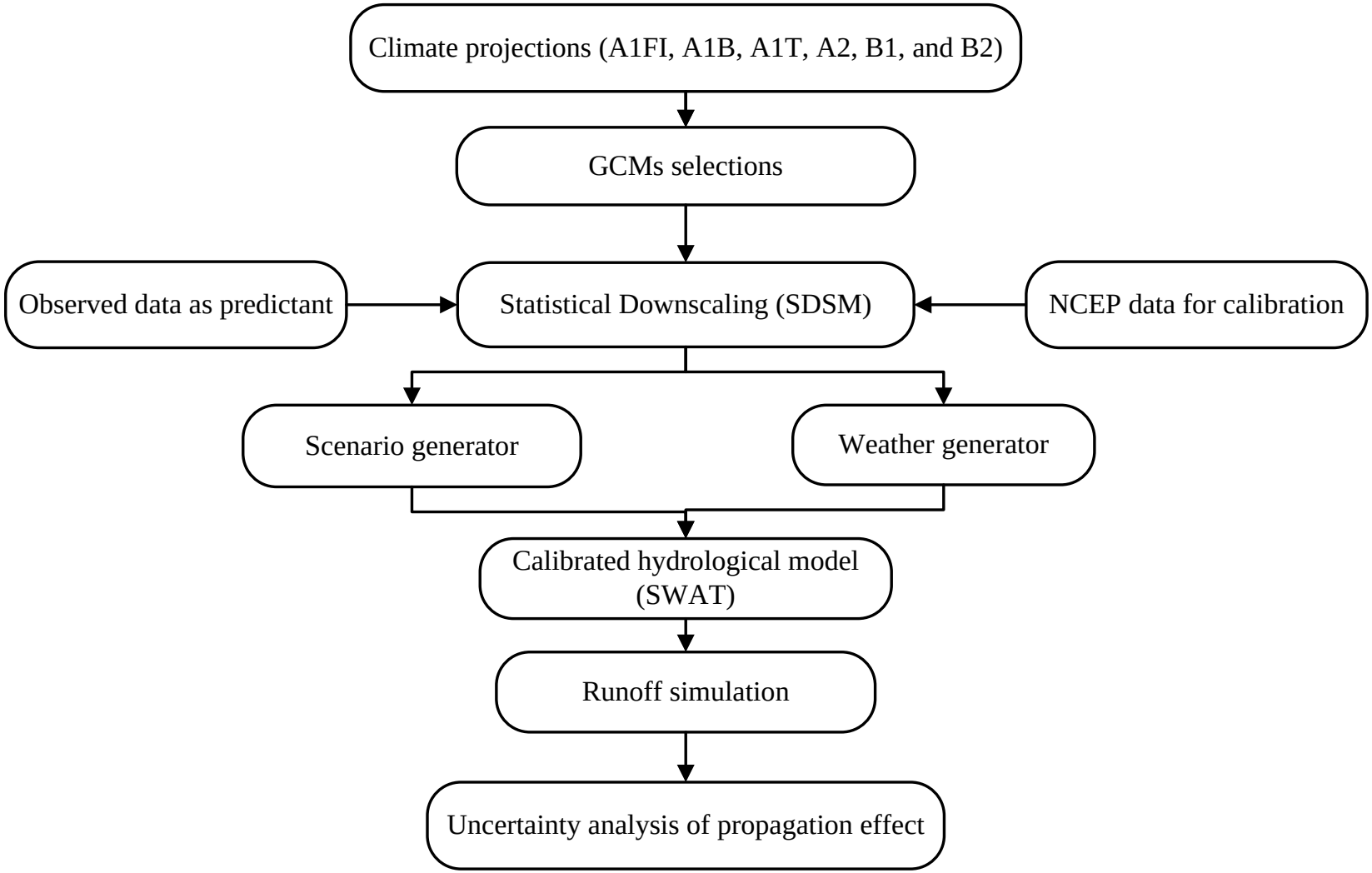

Figure 6.1 The framework of the proposed RESEM.

6.2.1 **Selection of climate change scenarios and GCMs**

There are six major types of emissions scenarios provided in the Special Report on Emissions Scenarios (SRES), including the A1FI, A1B, A1T, A2, B1, and B2 scenarios (IPCC, 2007). The A2 scenario predicts the greatest changes in precipitation and temperature by the end of this century, hence this scenario can be considered to represent the worst case scenario for hydrological studies (Gudmundsson, 2012; Samadi *et al.*, 2012). Therefore, the Hadley Centre Coupled Model 3 (HadCM3) for A2 scenario (which is named as H3A2a) was selected in this study for downscaling purposes. The National Center for Environmental Prediction (NCEP) reanalysis data was used to calibrate parameters for downscaling H3A2a in SDSM. The downscaled H3A2a outputs will be used as inputs to the SWAT model to make an assessment of the future projections of surface runoff. For hydrological studies, one constant and well performing GCM and a well calibrated hydrological model will be able to produce reasonably good prediction for the specific study area. Moreover, the uncertainty propagation effect from statistical downscaling to hydrological modeling is the key concern in this study. Therefore, only one GCM model was selected for this study, and the corresponding propagation effect of the uncertainty during statistical downscaling were quantified through the evaluation of the surface runoff simulation from the application of a hydrological modeling study.

6.2.2 **Statistical downscaling model (SDSM)**

The selected gridded GCM dataset has a resolution of 2.5°latitude by 3.75° longitude. Therefore, downscaling is necessary before the data can be used in the hydrology model. As a popular statistical downscaling method, SDSM was applied to downscale the H3A2a outputs in this study. SDSM, developed by Rob Wilby and Christian Dawson in the UK, is one of the most popular statistical downscaling tools, and can be best described as a hybrid of the stochastic weather generator and transfer function method (Wilby *et al.*, 2002; Hassan *et al.*, 2013). SDSM is able to construct climate change scenarios for small sites at daily time scale by using gird resolution of GCM outputs. Downscaling with SDSM involves a multiple regression-based model between some selected large scale GCM predictor variables and local scale predictants (such as precipitation and temperature). The NCEP reanalysis data were applied to screen the sensitive predictor variables and compute the parameters of regression equation. The parameters of the regression equation can be estimated by using the efficient dual simplex algorithm (Wilby and Dawson, 2007) or some other algorithms. Some bias may occur when using daily time-scale results with SDSM. However, the downscaled climate variables should be more reasonable for monthly time-scale water resource planning studies. Some studies suggested multiple downscaling methods could be applied for prediction purposes; however, a well-calibrated downscaling model should still be able to reflect the future situation to guide the long term strategy for water resource management.

6.2.3 **SWAT Hydrological Model**

SWAT is a physically based continuous distributed model developed by the United States Department of Agriculture (USDA) Agricultural Research Service (ARS). SWAT operates on a daily time step for an ungauged watershed, and is designed to predict the impacts of management practices on hydrology, sediment, and water quality in large complex watersheds over long periods of time (Arnold *et al.*, 1995; Arnold *et al.*, 1998; Xue *et al.*, 2014). The detailed descriptions of the SWAT model have been provided in **Section 2.1.3** of **Chapter 2**. Previously, SWAT has been shown to be a successful model of runoff and water quality simulation for different areas, demonstrating its feasibility and flexibility for various regions and environmental conditions (Yang *et al.*, 2008). From the data available and ungaged properties of the study area, SWAT is considered to be able to perform reasonably well for surface runoff in the study area. Therefore, SWAT was selected for this study.

6.2.4 **P-factor and R-factor**

The degree of all uncertainties considered is evaluated by using the P-factor, which is the percentage of observed data bracketed by the 95% prediction uncertainty (calculated at 2.5% and 97.5% levels of the cumulative distribution of output variables), or called 95PPU. The R-factor is another measure for quantifying the performance of uncertainty analysis, which is calculated by the average distance of uncertainty bands divided by the standard deviation of the observed data. Ideally, if the P-factor is 1 and the R-factor is 0, then the simulation results absolutely match the observed data (Abbaspour, 2011). However, due to

measurement errors and model uncertainties, a perfect simulation will generally not be achieved. The equations for calculating the P-factor and R-factor are shown in equations 4.3 and 4.2 on page 91 (Abbaspour *et al.*, 2007; Wu and Chen, 2014a; Xue *et al.*, 2014).

6.2.5 **Sequential uncertainty fitting version 2 (SUFI-2)**

Based on a Bayesian framework, SUFI-2 determines uncertainties through the sequential and fitting process, and it requires several iterations to achieve the final estimates. SUFI-2 starts by assuming a large parameter uncertainty to account for different possible sources (including model input, structure and parameter and measured data), so that the measured data will initially falls within 95PPU. And then, the uncertainty can be decreased by considering the following two rules: 1) 95PPU band brackets most of the observations (larger P-factor) and 2) the average distance of the upper (at 97.5%) and the lower level (at 2.5%) of 95PPU is small (smaller R-factor) (Abbaspour *et al.*, 2007). Therefore, a balanced P-factor and R-factor is the desired result for an acceptable uncertainty analysis (Wu and Chen, 2014a). In this study, three iterations were applied, and the ranges of each parameter were reduced after each iteration for seeking the optimal parameter set which can achieve the best simulation.

6.3 Case study

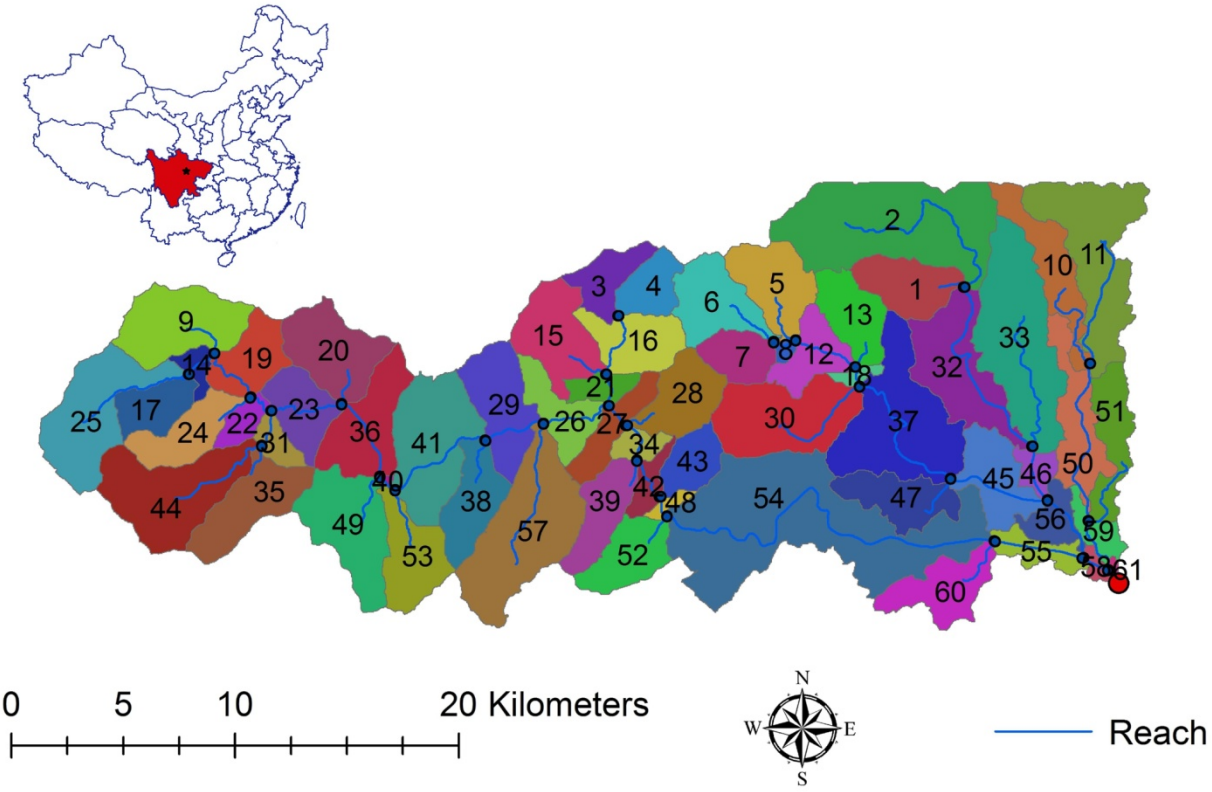

Figure 6.2 The location and 61 sub-basins of the study area.

The upper reaches of the Wenjing River watershed located in Sichuan province in western China is selected as the study area. The study area is about 25 km east to Chengdu, the capital city of Sichuan province, and the drainage area is about 653 km^2. **Figure 6.2** shows the location and 61 sub-basins of the study area. The annual mean temperature and sunshine duration are 15.9 °C and 1161.5 h, respectively, and the average annual precipitation is 1012.4 mm. The annual amount of precipitation is high in summer (588.0 mm) and can be as low as 29.9 mm in winter (IWHR, 2005). Since the main drinking water source for Chengdu and major water sources for irrigation activities in the downstream area

are from the upper reaches of the Wenjing River, this watershed urgently require efficient water resource management. For to this reason, this watershed was selected for the case study (Wu and Chen, 2014a). It is hoped that this study will provide scientific supports for the local water resources department and provide a good reference for long term water management based on future predictions.

6.4 Results and discussion

6.4.1 **Statistical downscaling**

The SWAT model requires a large number of meteorological data input (such as participation, temperature, solar radiation, relative humidity, wind speed). As it is known, precipitation is a key component of the hydrological cycle and is more important and sensitive to the surface runoff (Tofiq and Guven, 2014). Therefore, in this study, the assumption has been made that the biggest impacts to surface runoff are from precipitation. Due to the climate condition of the study area (no extremely cold days in winter), for this preliminary study, only the uncertainty related to precipitation is considered during statistical downscaling. Usually, precipitation data is inevitably more problematic during downscaling comparing to temperature. The reason is that the daily precipitation amounts at sites are normally poorly related to regional scale predictor variables, and precipitation is also a conditional process-- both the occurrence and amount processes must be specified when conducting downscaling (Wilby and Dawson, 2007). The downscaled temperature data were used as the input of the SWAT model as well, but the uncertainty of temperature was not considered in this study.

As the first step, the NCEP reanalysis data were applied first for calibrating the downscaling model. SDSM can screen the sensitive predictor variables to establish the empirical relationship between NCEP predictor variables and observed predictands. The calibration procedure can compute the parameters of multiple regression equations for NCEP predictor variables and observed predictands through optimization algorithms. And then, the parameters can be used for downscaling the H3A2a data. The 30 years (1981-2010) observed precipitation data were used as predictants for calibration. According to the coordinates of the study area, four H3A2a grid spots around study area (including 28X, 22Y; 28X, 23Y; 29X, 22Y and 29X, 23Y) were selected for screening the best NCEP predictor variables. After calibration, the 10 out of 26 screened NCEP predictor variables were applied to downscale the H3A2a outputs, including p_thas (wind direction at 1000 hPa height), p_zhas (divergence at 1000 hPa height), p5_fas (wind speed at 500 hPa height), p5_zas (vorticity at 500 hPa height), p5zhas (divergence at 500 hPa height), p8_fas (wind speed at 800 hPa height), p8_uas (zonal velocity component at 800 hPa height), p500as (geopotential at 500 hPa height), p850as (geopotential at 850 hPa height), and shumas (specific humidity at 1000 hPa height). The downscaling parameters were calculated by using above 10 sensitive predictor variables. Total 20, 30, 40, 50 and 60 downscaled precipitation ensembles were generated using SDSM for calculating 95PPU. When the number of ensembles is greater than 40, the 95PPU barely changed. Therefore, in order to improve the simulation efficiency, 40 downscaled precipitation ensembles have been used for calculating 95PPU. The temperature has been downscaled in the similar way. However, comparing to precipitation, the temperature has less contribution to the surface runoff. Therefore, only precipitation data have been downscaled to 40 ensembles to quantify the propagation uncertainty effects.

Both the precipitation and temperature data were downscaled and used as input of SWAT for the surface runoff simulation. Because the NSE was selected as the objective function for calibration using SUFI-2, the assumption has been made that the best simulation is the simulation which achieve the greatest NSE value. The mean precipitation of 40 NCEP ensembles (scenarios) generated by SDSM was used in the hydrological model for comparison purposes, because only the uncertainties from the GCM (H3A2a) to the hydrological model are the key concerns of this study. Therefore, all 40 H3A2a ensembles were reserved and used for uncertainty analysis.

6.4.2 **Hydrological modeling**

By using 30m resolution DEM, the study watershed was delineated into 61 sub-basins, and the outlet is located at sub-basin No. 61 in the southeast of the watershed (see **Figure 6.2**). The digital river channels were used for calibrating the water channel created by using DEM. Based on 10 groups of land uses, 16 types of soil and slope information, the study area was the watershed was divided into 270 HRUs for hydrological modeling. All observed meteorological data, including temperature, precipitation, wind speed, solar radiation, relative humidity data, were used as the input for the SWAT model.

If a hydrological model performs poorly, then it may continue to perform poorly in dealing with future climate scenarios (Hay *et al.*, 2014). Therefore, a model that performs well is a basic and essential requirement for conducting downscaling studies for hydrological modeling. Calibration and uncertainty analysis were conducted using SUFI-2 with three iterations (1000 runs each iteration) in this study. A three-year surface runoff data from 1998 to 2000 were used for calibration, and the remaining two years (2001-2002) data were used

for validation. The Nash-Sutcliffe coefficient (NSE) and coefficient of determination (R^2) were selected to evaluate the performance of simulation, and NSE was also selected as the objective function of SUFI-2. The definitions of NSE and R^2 are shown in equations 3.1 and 4.7 (Wu *et al.*, 2012; Wu and Chen, 2014a).

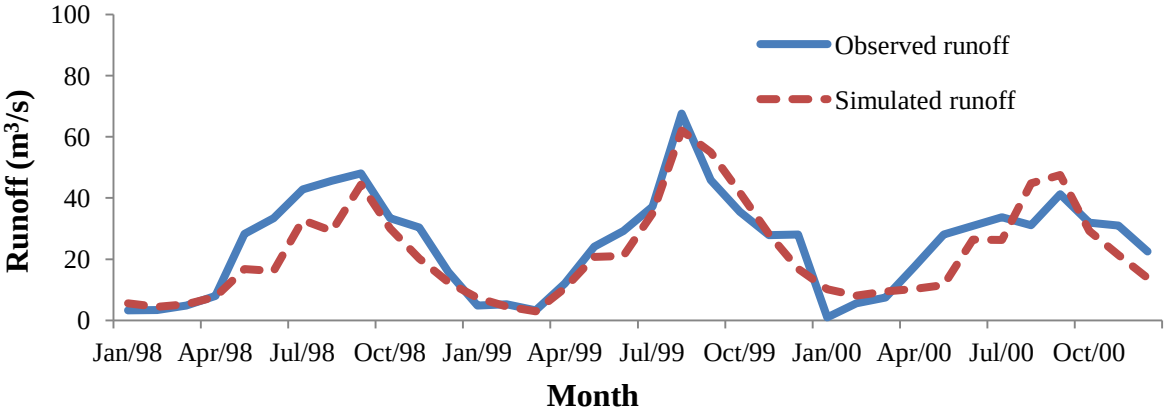

Figure 6.3 The average monthly simulated runoff and observed runoff in the calibration period of 1998-2000

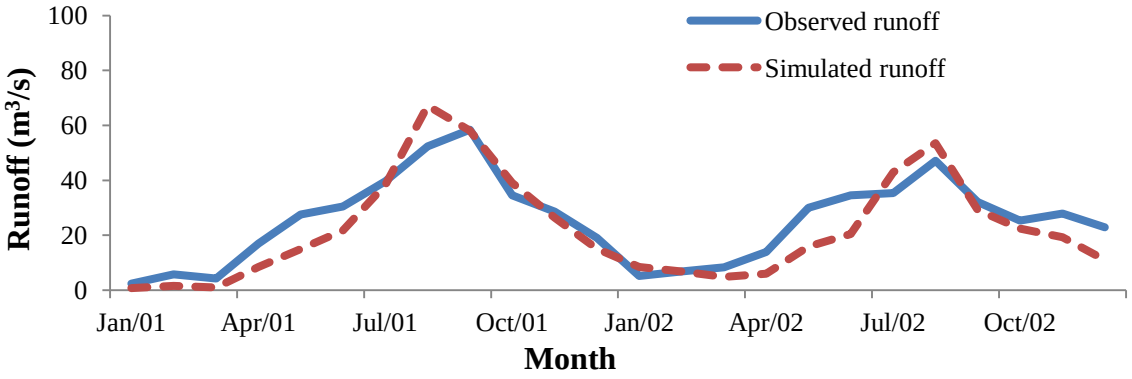

Figure 6.4. The average monthly simulated runoff and observed runoff in the validation period of 2001-2002

Based on the sensivity analysis results and recommendation in the user's manual, there is a total of 11 parameters selected for calibration. The parameter ranges are updated

after each iteration. After calibration, the NSE and R^2 of the best simulation were 0.77 and 0.80 for the calibration period (**Figure 6.3**), and 0.74 and 0.87 for the validation period (**Figure 6.4**), respectively. The good simulation performance indicates that the model can be applied to downscaling studies with some confidence. To evaluate the propagation effect of uncertainties from statistical downscaling to hydrological modeling, the parameter set which performs the best simulation was used as the default setting. Therefore, the uncertainties involved in hydrological modeling have been manually fixed and controlled, and the propagation effect of uncertainties reflected and evaluated using the simulated surface runoff is mainly from the application of statistical downscaling methods as well as the GCM outputs.

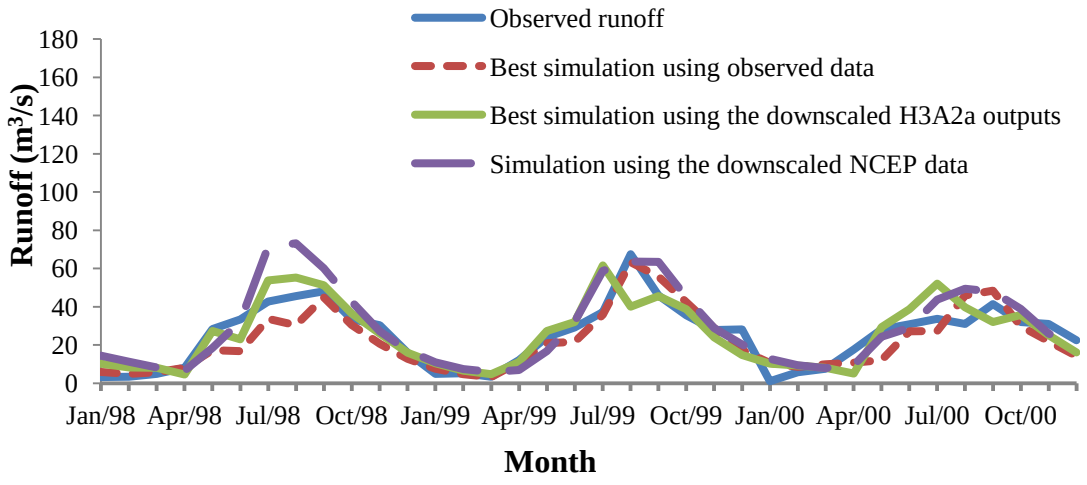

Figure 6.5 The hydrograph of observed, simulated runoff from SUFI-2, downscaled NCEP and H3A2a results for 1998-2000.

Figure 6.5 shows the hydrographs of observed runoff and three series of surface runoff simulations, which are simulated runoff by using observed precipitation, mean downscaled NCEP precipitation outputs, and downscaled precipitation outputs from H3A2a

with the best simulation. The overall simulation performance from the three different sources of precipitation input provided acceptable results. The surface runoff simulation produced by observed precipitation gave the highest NSE and R^2 values, which are 0.77 and 0.8 respectively. The surface runoff generated by using downscaled H3A2a precipitation (with NSE and R^2 values of 0.67 and 0.73, respectively) performed better than the simulations using the mean value of NCEP precipitation outputs (with NSE and R^2 values of 0.55 and 0.79, respectively). There are some underestimations during April to July each year when conducting simulation using observed precipitation data, but simulations generated by using precipitation data from two downscaled GCM models perform better in these three months. However, the simulations from two downscaled GCMs perform relatively poorly for capturing the time and magnitude of the peak flow. Therefore, the corresponding uncertainties cannot be ignored, and the 95PPU was calculated to improve the reliability of future predictions.

6.4.3 **Uncertainty analysis**

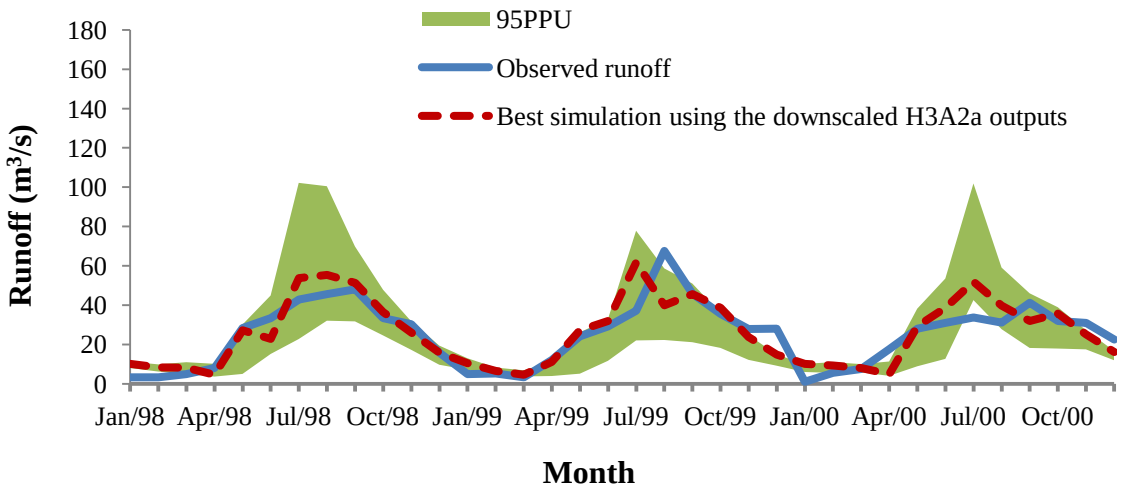

Figure 6.6 The hydrograph of the observed and best simulated runoff with 95PPU from downscaled H3A2a results for 1998-2000.

The 95PPU of the surface runoff simulation using downscaled H3A2a outputs is calculated at 2.5% and 97.5% levels of the cumulative distribution of surface runoff simulated by using downscaled precipitation for each month. A total of 40 ensembles were generated from the SDSM and used for uncertainty analysis. Because the uncertainty of surface runoff was caused by using different combinations of parameter sets, the uncertainty stemmed from hydrological modeling was mainly reflected by parameter uncertainty in this study. After calibration using SUFI-2, the best simulation (with the greatest NSE) was achieved, and the parameter set which leads the best simulation (NSE = 0.77 and R^2 = 0.8) was recorded as the optimum parameter set. When using the optimum parameter set for simulation, there are no other stochastic parameters in the SWAT model. Therefore, there is no extra uncertainty from the hydrological modeling. Different downscaled ensembles as the

input of the SWAT model were propagating the uncertainty from statistical downscaling to hydrological modeling. When using the optimum parameter set for simulation of downscaling studies, the uncertainty of surface runoff only arose from the application of different ensembles from the statistical downscaling. Therefore, the uncertainties evaluated using 95PPU are mainly from the application of the statistical downscaling method.

The 95PPU of surface runoff by using downscaled H3A2a results are shown in **Figure 6.6**. In **Figure 6.6**, the 95PPU can cover most of the observed runoff data and peak flows indicating a good coverage for extreme events. The statistical summaries are in **Table 6.1**. For a traditional uncertainty analysis using SUFI-2, the P-factor and R-factor results of the third iteration of SUFI-2 (using observed precipitation and temperature) are 0.56 and 0.48, respectively, indicating most of observed data are bracketed in a small band of 95PPU. For this downscaling study, although the width of the uncertainty band is relatively larger (R-factor of 1.34) comparing the R-factor for the third iteration results from SUFI-2, by considering the larger coverage (P-factor = 0.67), the uncertainties have been controlled well. The results have demonstrated that the downscaled H3A2a model results performed reasonably well for prediction purposes, and can provide a reliable scientific reference for local water resource management.

Table 6.1 Summary statistics of the best simulation and uncertainty analysis results for observed, downscaled NCEP and downscaled H3A2a data.

Data sources of the simulation	P-factor	R-factor	R^2	NSE
Observed data	0.56	0.48	0.8	0.77
Downscaled NCEP (mean)	N/A	N/A	0. 79	0.55
Downscaled H3A2a	0.67	1.34	0.73	0.67

Because the downscaled GCM model for SWAT simulation achieved reasonably good results, all the settings and calibrated parameter set were not changed for future prediction based on the assumption that the relationship between the local predictants and GCM predictor variables will remain the same in the future. The surface runoff prediction for the future five-year (2016-2020) period was conducted using the downscaled H3A2a data in this study. The precipitation and temperature from the H3A2a outputs for 2016-2020 were downscaled and used as the input for the SWAT model. The best surface runoff prediction was generated by applying the calibrated SWAT model and downscaled precipitation and temperature from the ensemble which achieved the best simulation for the year 1998-2000 (NSE = 0.67 and R^2 = 0.73).

The 95PPU for surface runoff simulation is calculated in a similar manner to the previous steps for uncertainty analysis. Because the uncertainty from hydrological modeling was fixed and controlled using the optimal parameter set, the 95PPU can be considered to be generated from the application of different ensembles of downscaled outputs only. The uncertainty from the statistical downscaling was propagated to the simulated surface runoff of hydrological modeling, and was revealed by using the 95PPU. As shown in **Figure 6.7**,

the 95PPU contains most data of the best prediction (93.3%) with a reasonably small uncertainty band for the year 2016-2020.

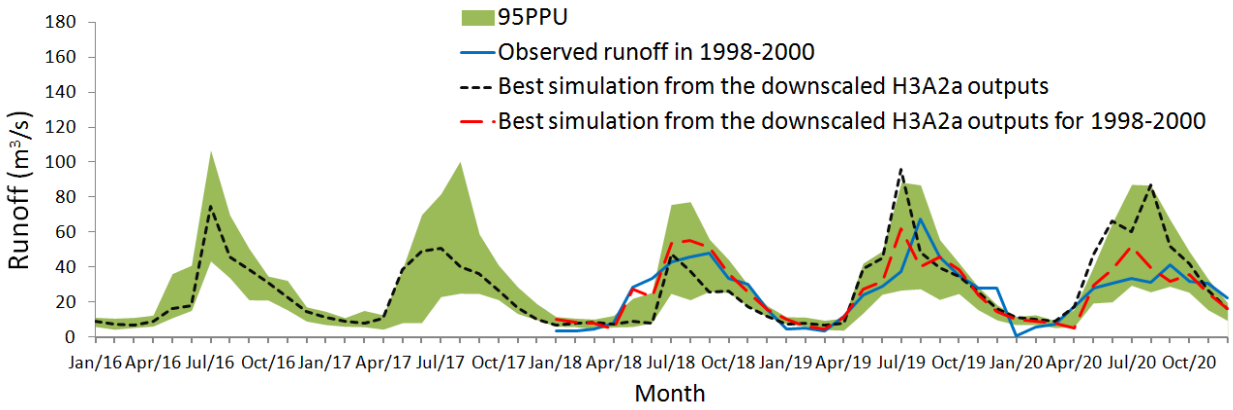

Figure 6.7 The best predicted surface runoff with 95PPU for 2016-2020.

The observed surface runoff and the best simulated runoff by using downscaled H3A2a outputs for 1998-2000 are also shown in **Figure 6.7** for the comparison of the runoff 20 years later (2016-2020). It generally shows an increasing trend for the surface runoff volume after 20 years. The simulated peak flow volume in 2019 could reach 95.68 m^3/s, which is more than 1.5 times of the peak flow (61.68 m^3/s) in 1999, and also more than 1.4 times of the observed runoff (67.56 m^3/s); the simulated peak flow in 2020 is 86.65 m^3/s, and it is more than 1.6 times of the peak flow (52.51 m^3/s) and also more than 2 times of the observed runoff (41.28 m^3/s) in 2000. The results indicate that the peak flow has a considerable increase in the summer time, especially for the year 2019-2020 under the A2 climate change scenario.

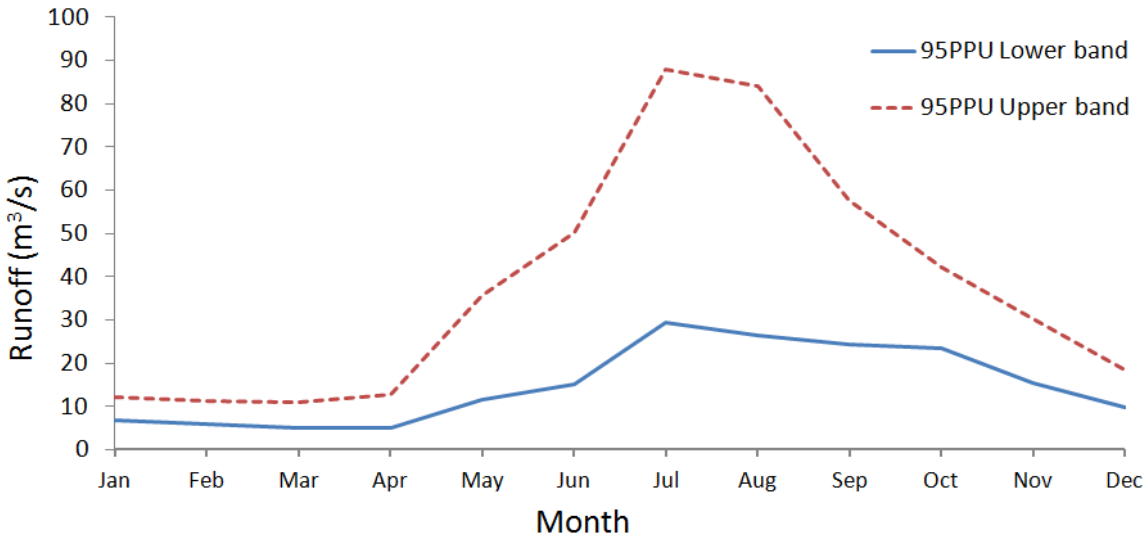

Figure 6.8 The annual 95PPU for surface runoff in the year 2016-2020.

Figure 6.8 shows the annual 95PPU of surface runoff in 2016-2020. The surface runoff uncertainty starts to increase from April to August and then begin to decrease till December. The variations of surface runoff are bigger in spring and summer and relatively smaller in fall and winter. The peak flow in summer could reach as high as 87.8 m^3/s in July, and the lowest flow could be as low as 5.05 m^3/s in March. Because the application of the calibrated parameter sets, the uncertainty evaluated in this study is mainly propagated from the application of statistical downscaling methods by using different ensembles of the downscaled H3A2a outputs.

This study innovatively made use of 95PPU, P-factor and R-factor to evaluate the uncertainty effects propagated from statistical downscaling to hydrological modeling. After sensitive predictor variables screening, calibration and downscaling using SDSM, the downscaled precipitation and temperature outputs were used for the surface runoff simulation. By fixing the uncertainty from hydrological modeling using the optimum

parameter set, the uncertainty quantified using 95PPU is the uncertainty propagated from the statistical downscaling to the hydrological modeling. The 95PPU is quite important for decision makers in the local water resource management department, because it provides the scientific reference for future surface runoff predictions in the watershed with reliable confidence intervals. The worst case scenario (A2 scenario) can also be evaluated and determined and precaution taken according to the future predictions to help local people reduce the risk of any property loss in the future.

6.5 Summary

In this study, hydrological modeling for the upstream of the Wenjing River watershed was successfully conducted. The NSE and R^2 of the calibrated SWAT model using the observed precipitation and temperature are 0.77 and 0.8, respectively, indicating reasonable performance of the calibrated model. SDSM was used to downscale the precipitation and temperature data from the H3A2a model to generate future climate data based on A2 scenarios. The NSE and R^2 of the best simulation using the downscaled H3A2a results are 0.67 and 0.73 in the year 1998-2000, respectively, demonstrating that the downscaled precipitation and temperature results can achieve a reasonably good match to the observed data.

The developed RESEM can effectively evaluate the propagation effect of uncertainty from statistical downscaling to hydrological modeling using 95PPU of the surface runoff, and a successful attempt has been made through the case study in this study. The different ensembles generated by statistical downscaling increased the input uncertainty of

hydrological modeling. When using the optimized parameter set for simulation, the increased uncertainty of surface runoff is mainly caused by statistical downscaling using SDSM. The P-factor and R-factor of uncertainty from downscaling are 0.67 and 1.34, respectively, also indicating an acceptable uncertainty analysis result for a downscaling study. Therefore, the downscaled H3A2a model is capable of future prediction with reasonable confidence. The 95PPU and R-factor also shows the uncertainty propagated from the statistical downscaling to hydrological modeling.

The continuous five-year future runoff prediction (from 2016 to 2020) along with the uncertainty estimation through 95PPU was conducted in this study. The simulation results in the year 2018-2020 indicate an increasing trend for the surface runoff volume comparing the simulated runoff and observed runoff data in the year 1998-2000. The prediction results and 95PPU can provide a scientific reference for long term evaluation and estimation of future water resource situation in the study area. The annual 95PPU can easily indicate that the uncertainty of surface runoff is greater in spring and summer (from April to October) and smaller in the rest of year.

The RESEM for quantifying the propagation uncertainty can be applied to other hydrological models as well showing its generality. In future studies, efforts should be concentrated on testing different hydrological models and collecting more observed runoff data to increase the lengths of calibration and validation period to further improve the reliability of hydrological simulation and confidence of prediction. More and up-to-date GCMs data can also be downscaled and applied to the calibrated SWAT model to compare the current results from the H3A2a model. These improvements would provide local

decision makers with more information based on different scenarios to improve the efficiency of water resource management.

CHAPTER 7.
ASSESSMENT OF UNCERTAINTY PROPAGATION FROM CLIMATE MODELING TO HYDROLOGIC FORECASTING UNDER CHANGING CLIMATIC CONDITIONS

The partial contents of the chapter were modified based on the following paper under preparation for journal publication:

1. **Wu, H.J.,** and Chen, B. (2014). Uncertainty analysis for propagation effects from statistical downscaling to hydrological modeling. The International Conference on Marine and Freshwater Environments (iMFE) 2014 proceeding, St. John's, Newfoundland, CA, EMR #1330.
   Role: I developed the model, conducted case studies and drafted manuscript. Dr. Bing Chen is my PhD supervisor and provided advice in method development and manuscript drafting.

2. **Wu, H.J.**, and Chen, B. Assessment of uncertainty propagation from climate modeling to hydrologic forecasting under changing climatic conditions. (to be submitted).
   Role: I developed the model, conducted case studies and drafted manuscript. Dr. Bing Chen is my PhD supervisor and provided advice in method development and manuscript drafting.

7.1 Background

The extensive human activities, mainly including the burning of fossil fuels and changes in land cover and use, are believed as the main contributors for increasing the greenhouse gas emissions (Dibike and Coulibaly, 2005). The increasing concentration of greenhouse gas emission was considered as the one of the main reasons for causing climate change. The IPCC claimed that climate change has considerable impacts on water basins and regions due to changes in air temperatures and precipitation (Minville *et al.*, 2010; Samadi *et al.*, 2012). Therefore, it is necessary to quantify the impacts of climate change on water resources under the future scenarios.

To estimate the impacts of future climate change resulting from the continuous increasing greenhouse gas concentration in the atmosphere, general circulation models (GCMs) were developed and applied (Dibike and Coulibaly, 2005). Nevertheless, due to the mismatch problem of the spatial resolution, the GCMs outputs cannot be directly used as the input of hydrological models. Downscaling methods were developed to solve the spatial and temporal resolution mismatch problems when using GCMs outputs for hydrological modeling studies. In order to provide the future hydrological predictions with high confidences, accurate and reliable hydrological simulations should be expected to achieve. However, different sources of uncertainties will be involved during downscaling the GCMs outputs, and there are also different types of uncertainty during hydrological modeling. Those different uncertainty sources are leading the total uncertainty hard to be quantified in a hydrological modeling study when applying downscaled GCMs results. Limited studies focus on breaking down the total uncertainty into different uncertainty components, and this

study attempts to investigate the effects and contributions of different uncertainty components to the total propagated uncertainty in hydrological modeling under changing climatic conditions.

7.2 Methodology

In this chapter, an integrated simulation-based evaluation system for uncertainty propagation analysis (ISES-UPA) has been proposed for evaluating the contributions of different uncertainty sources from statistical downscaling and hydrological modeling to the total propagated uncertainty. The uncertainty of statistical downscaling and hydrological modeling has been quantified separately at first. The two sources of uncertainty have been combined for new hydrological simulations, and the total uncertainty was evaluated. To understand the contributions of various uncertainty sources is highly interesting but quite difficult to implement. No reliable procedures yet exist for breaking down the total uncertainty into various components (Abbaspour, 2011). This study is trying to provide an attempt on this area. The case study in the upstream of the Wenjing River watershed, Sichuan of China, was used as the real case study. The results analysis and contributions of different uncertainty sources were discussed in this chapter. The framework of the proposed system is shown in **Figure 7.1**.

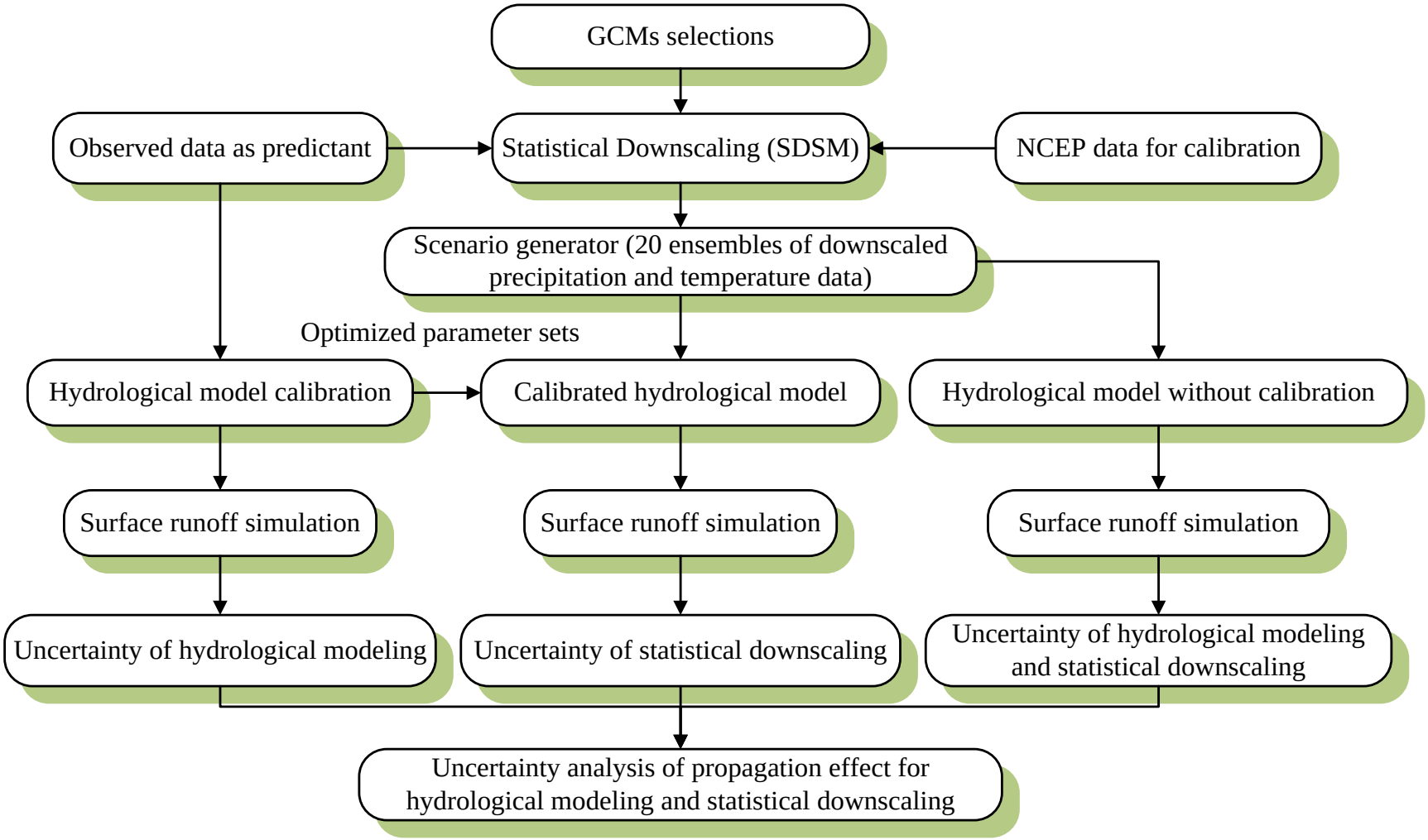

Figure 7.1 The framework of the ISES-UPA for evaluating the propagated uncertainty effects from hydrological modeling and statistical downscaling.

7.2.1 **GCM selection**

GCMs were developed and considered to be able to provide credible predictions and projections of climate changes into the next 100 years (Jiang *et al.*, 2007; Mpelasoka and Chiew, 2009; Wu and Chen, 2014b). Through downscaling processes, the large scale GCM outputs can be downscaled to local scale for the use of hydrological models for prediction purposes. There are many GCMs available nowadays. In the first step for real case studies, suitable GCMs should be considered for the study area. Due to accessibility or availability of data, only several GCMs can be found useful/suitable for certain area. According to different simulation purposes, different models can be selected as well. Because the A2 emission scenario stands for the predictions with biggest changes in precipitation and temperatures by end of this century and can be considered as the worst case scenario, the Hadley Centre Coupled Model 3 (HadCM3) for A2 scenario (H3A2a) was selected for downscaling in this case study (Gudmundsson, 2012; Samadi *et al.*, 2012).

7.2.2 **Statistical downscaling**

Different from dynamic downscaling, the statistical downscaling methods are based on statistical relationship between the large scale predictor variables and local scale predictants. The statistical downscaling methods mainly include three types of methods: weather generator, transfer function and weather typing (von Storch *et al.*, 1993; Wilby *et al.*, 1998; Zhang and Liu, 2005; J. Chen *et al.*, 2012). In this study, the SDSM was used for downscaling. SDSM, developed by Rob Wilby and Christian Dawson in the UK, is one of the most popular statistical downscaling tools, and can be best described as a hybrid of the

stochastic weather generator and transfer function method (Wilby *et al.*, 2002; Hassan *et al.*, 2013). The National Centers for Environmental Prediction (NCEP) reanalysis data was used to establish the statistical relationship between large scale predictors and local scale predictants and calibrate the downscaling parameters. The calibrated downscaling parameters can be used for scenario generator to produce different ensembles. The different ensembles generated from SDSM can be considered as the uncertainty from statistical downscaling. Usually, the precipitation has greater impacts to the surface runoff comparing temperature. Therefore, 20 ensembles of precipitation and one ensemble of temperature were generated from H3A2a outputs for uncertainty analysis of downscaling results in this case.

7.2.3 **Hydrological modeling**

In order to evaluate the propagated uncertainty effects, a well-behavioral hydrological modeling for the study area has to be achieved first. The soil and water assessment tool (SWAT) model (Arnold *et al.*, 1998), developed by the United States Department of Agriculture (USDA) Agricultural Research Service (ARS), was selected for surface runoff simulation in this study. SWAT requires specific information about weather, soil properties, topography, vegetation, and land management practices, and is a physically-based distributed model that operates on a daily time step for an ungauged watershed (Winchell *et al.*, 2009). After preparation of a number of required data inputs for SWAT and certain procedures for calibration and validation, the hydrological model for certain study areas can be established. The case study was conducted by using the previous hydrological modeling case for the upstream of the Wenjing River watershed. The sequential uncertainty fitting version 2 method (SUFI-2) was selected as the calibration method in this study.

7.2.4 **Uncertainty analysis**

7.2.4.1 **Indicators for uncertainty evaluation**

The 95% prediction uncertainty (95PPU) was used for quantifying and reflecting uncertainty of surface runoff. The degree of all uncertainties considered is evaluated by using the P-factor, which is the percentage of observed data bracketed by 95PPU. The R-factor is another measure for quantifying the performance of uncertainty analysis, which is calculated by the average distance of uncertainty bands divided by the standard deviation of the observed data. The formulas for P-factor and R-factor have been provided on page 91 in equation 4.3, 4.1 and 4.2. Usually, simulations with relatively large P-factor values along with small R-factor values at a same time are desired results.

7.2.4.2 **Uncertainty from statistical downscaling**

In the real case study, by using the statistical downscaled precipitation and temperature as the inputs of the SWAT model, a well calibrated hydrological model was used for quantifying the uncertainty propagated from statistical downscaling. Because the uncertainty from hydrological modeling was fixed by using the optimized parameter set which achieves the largest NSE value, the uncertainty generated from the application of different downscaled ensembles can be considered as the uncertainty during statistical downscaling. In this case, 20 downscaled precipitation ensembles can produce 20 simulations for surface runoff. After that, the NSE for the best simulation, 95PPU, P-factor, and R-factor can be calculated. The uncertainty evaluated in this step only comes from statistical downscaling.

7.2.4.3 **Uncertainty from hydrological modeling**

To avoid large sources of uncertainty from hydrological modeling, the hydrological model was first calibrated using SUFI-2 for two iterations. After two iterations from SUFI-2, all the parameter ranges has been reduced and adjusted towards to the optimal values. To reflect the uncertainty from hydrological modeling, the 1000 parameter sets sampled from parameter ranges in the third iteration of SUFI-2 using the Latin Hypercube Sampling (LHS) method were applied to simulate the surface runoff. Using observed meteorological data as input of the SWAT model, the 1000 parameter sets can produce 1000 surface runoff simulations, and the associated NSE for the best simulation, 95PPU, P-factor, and R-factor can be calculated and considered as uncertainty from hydrological modeling only.

7.2.4.4 **Total uncertainty for hydrological modeling and statistical downscaling**

To evaluate the propagated uncertainty effects of during statistical downscaling, the total uncertainty, which is defined to include the uncertainty from hydrological modeling and statistical downscaling in this study, was estimated. The assumption has been made that the precipitation has much greater impact on surface runoff comparing the temperature. Therefore, only precipitation data has been downscaled to different ensembles for uncertainty evaluation. The 20 ensembles of downscaled precipitation data along with the downscaled mean maximum and minimum daily temperature were used as input of the SWAT model. The surface runoff simulation was conducted using different downscaled ensembles input combined with the 1000 parameter sets generated from parameter ranges in the third iteration of SUFI-2 to evaluate the uncertainty propagation effects. There is a total of 20,000 simulations for surface runoff when combine uncertainty from two sources

together. The best simulation for surface runoff and associated uncertainty indictors can be estimated afterwards.

7.3 Case Study

In this chapter, the proposed ISES-UPA was applied to the case study in the upstream of the Wenjing River watershed. The detailed descriptions for study area and data acquisition were provided in **Section 4.3.1** of **Chapter 4**. The statistical downscaled results were used as the input of the hydrological model (SWAT) for uncertainty analysis. The results and discussion were provided in the next section.

7.4 Results and Discussion

7.4.1 **Statistical downscaling**

As one of the most popular statistical downscaling tool, the SDSM model was selected for downscaling the precipitation and temperature data for this study. The NCEP reanalysis data were first applied to screen the sensitive predictor variables, and H3A2a data were applied later for obtain the downscaled ensembles for the use of hydrological runoff simulation for quantifying the associated uncertainty. There are 26 daily predictor variables for NCEP and H3A2a. The definition of each predictor variables are shown in Table 7.1. After the screening process in SDSM, there are total ten important and sensitive predictor variables are selected in NCEP data and these predictor variables are used for calibration of precipitation. Similarly, the seven sensitive predictor variables of maximum daily temperature and five sensitive predictor variables of minimum temperature were screened, respectively. All the selected predictor variables for three different downscaling purposes are

listed in **Table 7.1**. These predictor variables are used to generate the parameters for the regression model between daily weather data and regional-scale atmospheric variables in SDSM.

Table 7.1 The full list of predictor variables and selected predictor variables for precipitation and temperature.

Predictor variable	Definition	Screened predictor variables		
		Precipitation	Daily maximum temperature	Daily minimum temperature
ncepmslpas	Mean sea level pressure			
ncepp__fas	Surface airflow strength			
ncepp__uas	Surface zonal velocity			
ncepp__vas	Surface meridional velocity			
ncepp__zas	Surface vorticity			
ncepp_thas	Surface wind direction	Selected		
ncepp_zhas	Surface divergence	Selected	Selected	
ncepp5_fas	500 hPa airflow strength	Selected		
ncepp5_uas	500 hPa zonal velocity		Selected	Selected
ncepp5_vas	500 hPa meridional velocity			
ncepp5_zas	500 hPa vorticity	Selected		
ncepp5thas	500 hPa wind direction			
ncepp5zhas	500 hPa divergence	Selected	Selected	
ncepp8_fas	850 hPa airflow strength	Selected		
ncepp8_uas	850 hPa zonal velocity	Selected		
ncepp8_vas	850 hPa meridional velocity			
ncepp8_zas	850 hPa vorticity			Selected

ncepp8thas	850 hPa wind direction			
ncepp8zhas	850 hPa divergence		Selected	
ncepp500as	500 hPa geopotential height	Selected	Selected	Selected
Ncepp850as	850 hPa geopotential height			
ncepr500as	Relative humidity at 500 hPa			
ncepr850as	Relative humidity at 850 hPa	Selected		
nceprhumas	Near surface relative humidity			
ncepshumas	Surface specific humidity	Selected	Selected	Selected
nceptempas	Mean temperature at 2m		Selected	Selected

The available observed precipitation and temperature data from 1980 to 2009 were obtained from local meteorological department of the study area. However, the available NCEP reanalysis data is from 1961 to 2001 when the experiment was conducted. Therefore, the total of 20 years from 1981 to 2000 were divided into the calibration (1981-1995) and (1996-2000) validation period during downscaling. **Figure 7.2** and **Figure 7.3** show the monthly mean downscaled precipitation using the NCEP reanalysis data and observed precipitation in calibration period (1981-1995) and validation period (1996-2000). Even though the overestimates for July and May in validation are noticeable, the R^2 value shows the acceptable results for the simulation. The R^2 value for downscaled monthly mean precipitation is 0.986 in the calibration period and 0.848 in the validation period, respectively. The seasonal precipitation results for the calibration and validation periods are shown in **Figure 7.4** and **Figure 7.5**. As it is shown, the simulation results for long-term perform better than monthly mean results. Although there are some overestimations in July for

monthly mean precipitation for both the calibration and validation periods, the seasonal precipitation results are more balanced and well simulated.

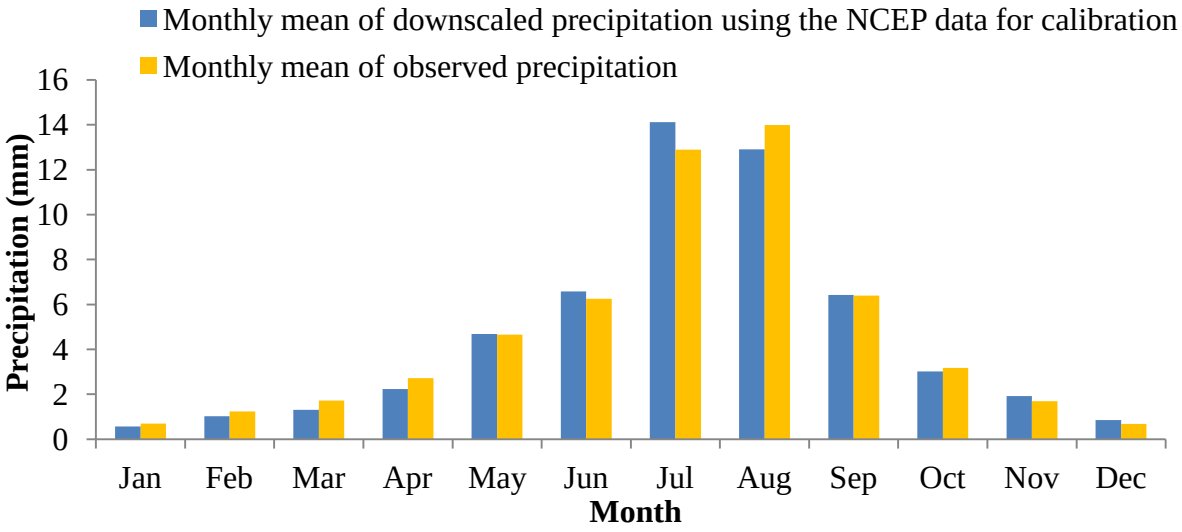

Figure 7.2 Observed and downscaled monthly mean precipitation using the NCEP reanalysis data in calibration period from 1981 to 1995

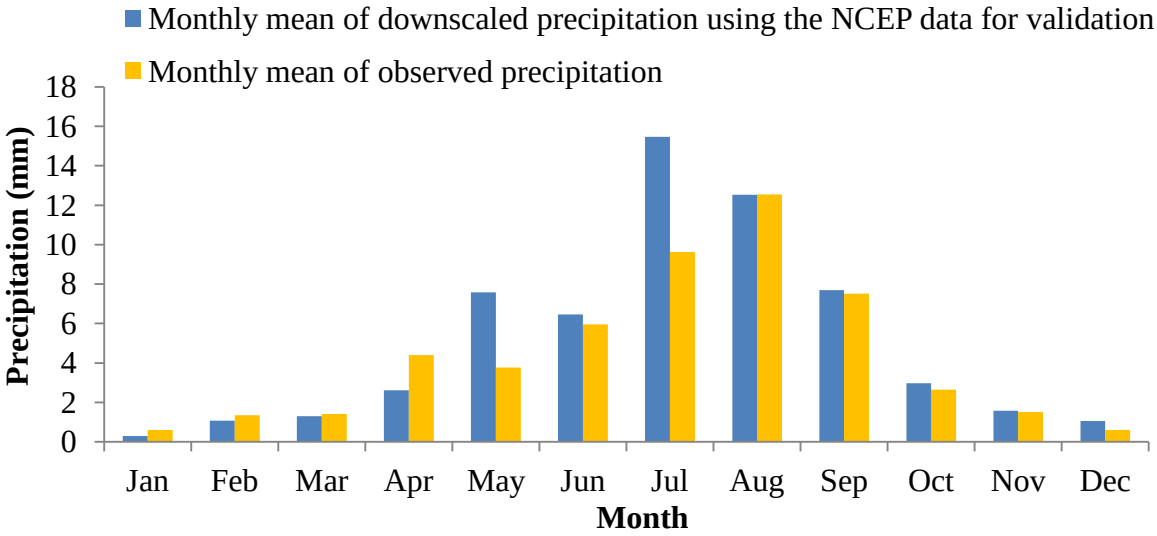

Figure 7.3 Observed and downscaled monthly mean precipitation using the NCEP reanalysis data in validation period from 1996 to 2000

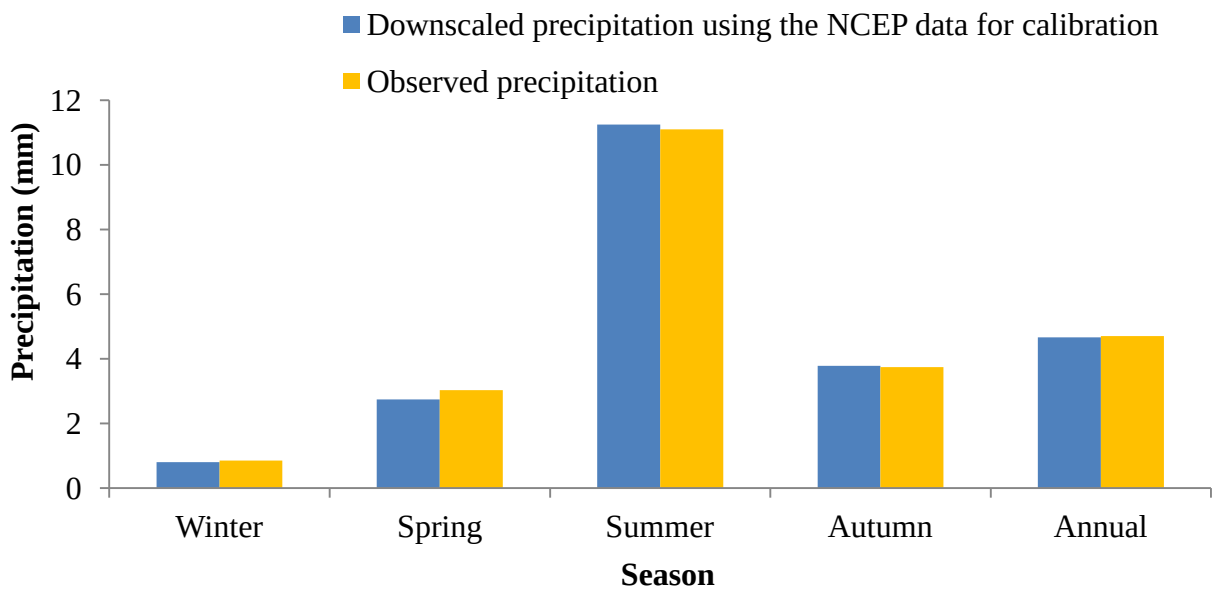

Figure 7.4 Observed and downscaled seasonal precipitation in calibration period from 1981 to 1995

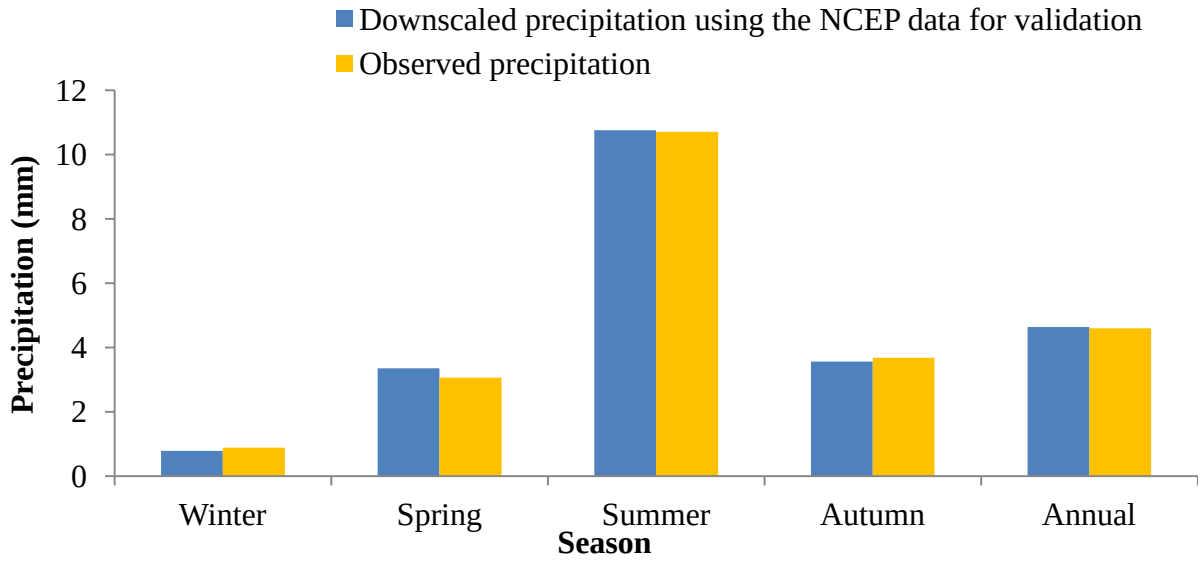

Figure 7.5 Observed and downscaled seasonal precipitation in validation period from 1996 to 2000

After the calibration and validation of downscaled precipitation using the NCEP reanalysis data, due to the good R^2 values, the H3A2a outputs can be downscaled using the regression parameters obtained from NCEP reanalysis data downscaling. In order to evaluate

the uncertainty of precipitation, total 20 synthetic ensembles were generated by using the H3A2a outputs in SDSM. The downscaled precipitation results were compared with observed data from 1981 to 1995 corresponding to the calibration period of the NCEP reanalysis data downscaling shown in **Figure 7.6**. The monthly mean of downscaled precipitation using the mean of 20 ensembles generated from H3A2a can achieve R^2 value of 0.760.

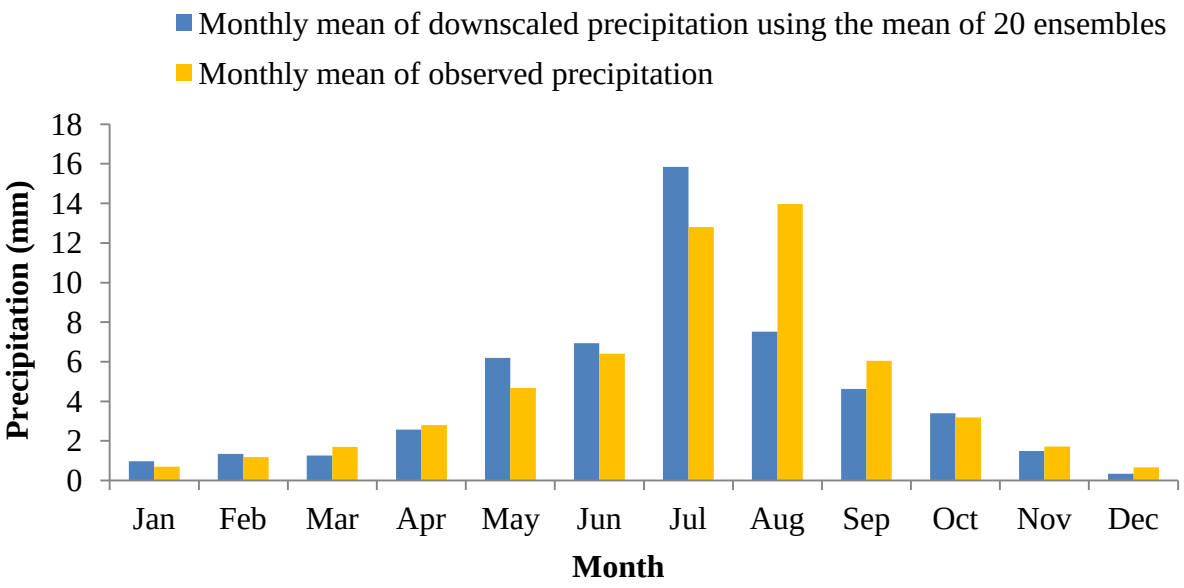

Figure 7.6 Observed and downscaled monthly mean precipitation using the H3A2a model from 1981 to1995

In order to investigate the uncertainty for the study period, the H3A2a outputs were downscaled for the same calibration and validation periods of the hydrological modeling study. According to available observed runoff data for hydrological simulation, five year (from 1998-2002) downscaled precipitation data are compared with observed data. The 20 ensembles of precipitation were subsequently used as input for the hydrological simulation

using optimized parameter sets (which achieved the greatest NSE using observed meteorological data). The ensemble which achieves the highest NSE value of 0.67 for surface runoff simulation in SWAT can be viewed as the best downscaled precipitation ensemble.

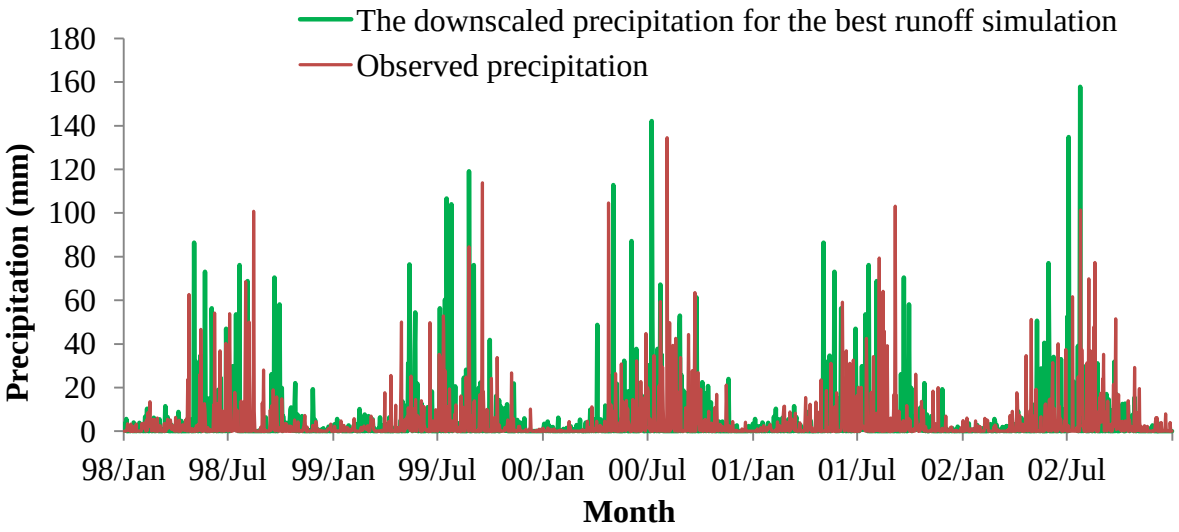

Figure 7.7 Observed and downscaled daily precipitation results using the H3A2a outputs from 1998 to 2002

Figure 7.7 shows the observed and downscaled daily precipitation using the best downscaled precipitation ensemble from H3A2a outputs. The precipitation downscaling is necessarily more problematic than temperature, especially for the downscaling for the daily step. The precipitation is relatively poorly related to regional-scale predictors, because the both occurrence and amount need to be specified which are not easy to be represented by constant relationships (Wilby *et al.*, 2002). Therefore, the downscaling precipitation normally cannot achieve very good results for most studies. Because the continuous surface runoff simulations are the desired results, the downscaled results which can match observed

data best for long term periods are expected. The downscaled monthly mean precipitation are calculated and summarized for further analysis.

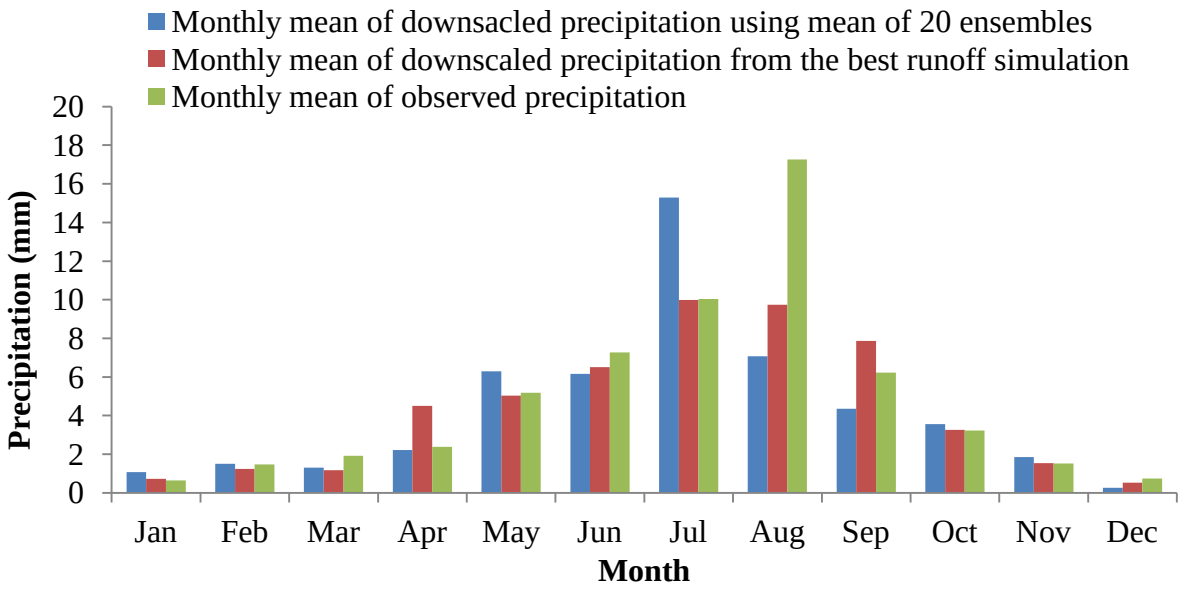

Figure 7.8 Observed, best downscaled precipitation, and mean of 20 downscaled ensembles results using the H3A2a outputs from 1998 to 2002

Figure 7.8 shows the downscaled precipitation using mean of 20 ensembles, best downscaled precipitation ensemble and observed precipitation. When using the mean of 20 ensembles and the best downscaled precipitation ensemble from the H3A2a outputs, the R^2 values for monthly mean precipitation are 0.508 and 0.794, respectively. The overestimation in July and underestimation in August are remained as the simulation from 1981 to 1995, leading to the relatively low R^2 value. Even though the downscaled precipitation in the July and August are not quite good, the downscaled results with the greatest R^2 value for long term (e.g., year 1998-2002) were selected as desired results. To be noticed, if event based hydrological models are used for hydrological simulations, seasonal or monthly downscaling and optimization may achieve better results for particular short term simulation. In this study,

although there are some overestimation in July and some underestimation in August for both the calibration and validation periods, the results still can be applied to hydrological modeling due to the reasonable R^2 values and simulation requirement for monthly runoff.

In a similar way, the maximum and minimum daily temperature data were downscaled using the same procedures. The NCEP reanalysis data were first used for screening parameters and calibration. The screened predictor variables for daily maximum and minimum temperature are shown in **Table 7.1**. To better match the time period of precipitation data as the input for the hydrological model, the temperature data was downscaled for the same period of downscaled precipitation. The assumption has been made that the temperature has less effects on surface runoff comparing precipitation since there are no extreme weather conditions and temperatures during a year in the study area, and uncertainty from temperature will not be evaluated in this study. Therefore, the mean of 20 temperature ensembles was used for the following analysis in this study.

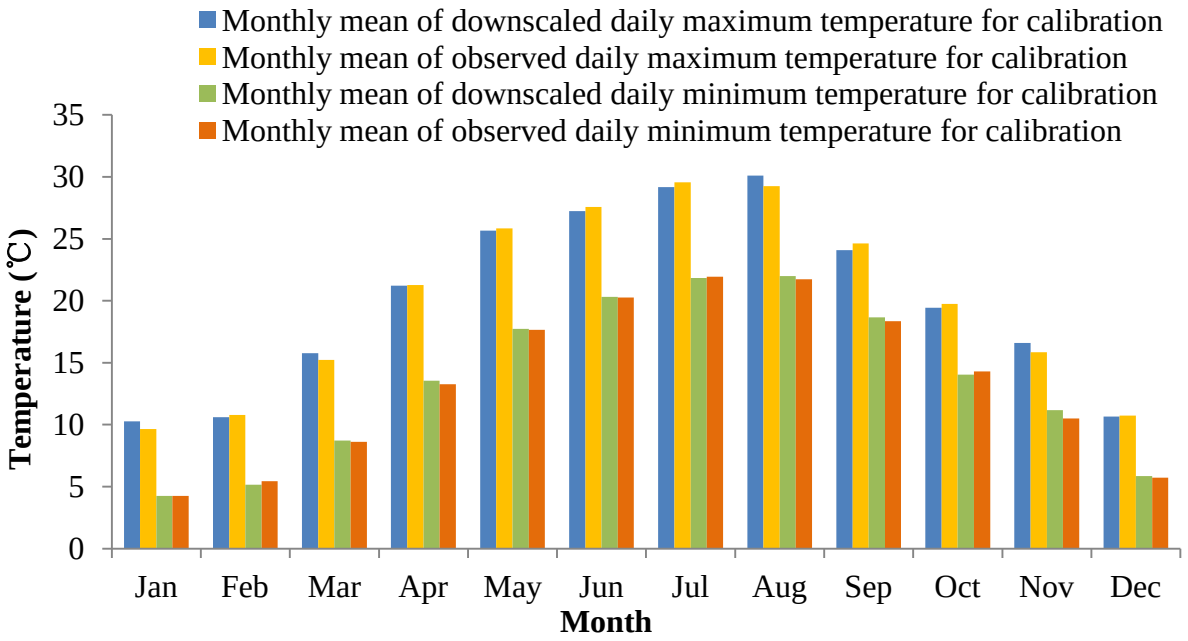

Figure 7.9 Monthly mean of observed and downscaled daily maximum and minimum temperature using the NCEP reanalysis data for the calibration period (1981-1995)

Figure 7.9 shows monthly mean of observed and downscaled daily maximum and minimum temperature using NCEP reanalysis data from 1981-1995. The R^2 values for monthly mean of daily maximum and minimum temperature are 0.996 and 0.998 in calibration period, respectively, showing extremely good downscaling performance for temperatures. For the validation period (from 1996-2000), the R^2 values of monthly mean of daily maximum and minimum temperature are 0.989 and 0.996, respectively, shown in **Figure 7.10**.

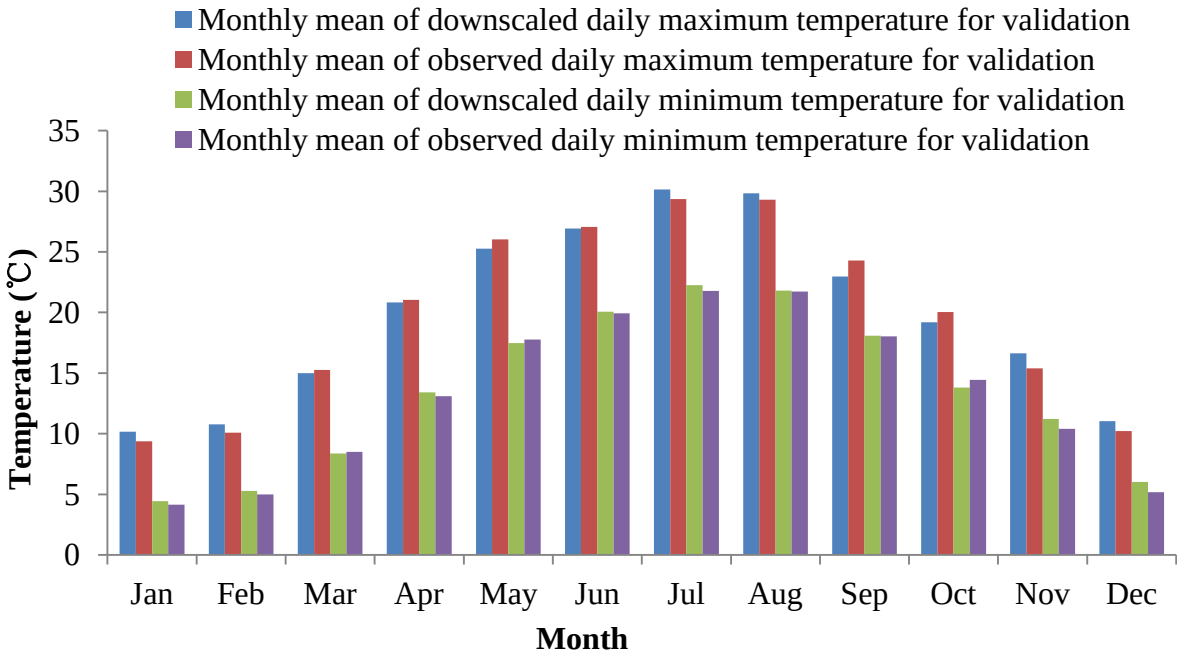

Figure 7.10 Monthly mean of observed and downscaled daily maximum and minimum temperature using the NCEP reanalysis data for the validation period (1996-2000)

As can be seen in **Figure 7.9** and **Figure 7.10**, the monthly mean downscaled maximum and minimum temperature match the observed results very well in both calibration and validation periods, indicating the good temperature downscaling performance by using SDSM. The H3A2a outputs were then applied to the calibrated regression parameters for downscaling.

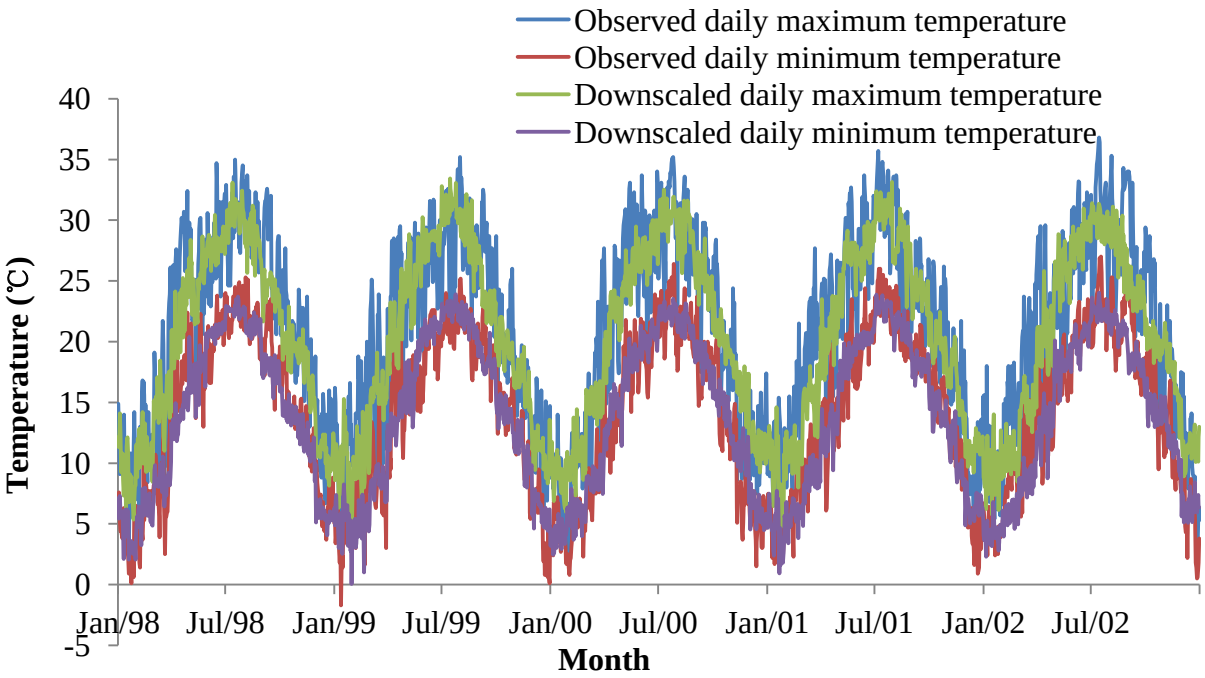

Figure 7.11 Observed and downscaled daily maximum and minimum temperature using the H3A2a outputs from 1998 to 2002

Figure 7.11 shows the observed and downscaled daily maximum and minimum temperature for the same calibration and validation period of hydrological modeling (1998-2002). The trends of observed and downscaled daily maximum and minimum temperature are close and similar although they cannot match well for the daily step. If performance of long term simulation is the main interest, the temperature downscaling simulation performs well for the study period.

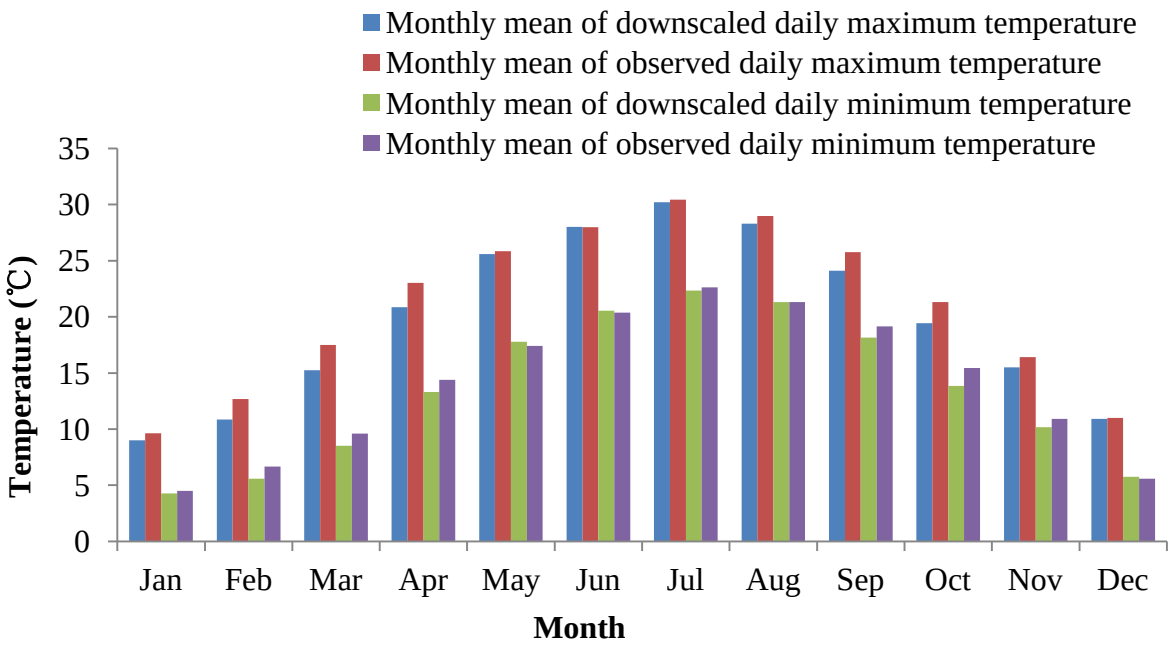

Figure 7.12 Monthly mean of observed and downscaled daily maximum and minimum temperature using the H3A2a outputs from 1998 to 2002

Figure 7.12 shows the monthly mean of the observed and downscaled daily maximum and minimum temperature using H3A2a. The R^2 values for monthly mean of daily maximum and minimum temperature are 0.987 and 0.991, respectively, indicating the good downscaling performance for temperatures in the period 1998-2002.

After downscaling the precipitation and temperature, two important meteorological inputs of the SWAT model were prepared for hydrological simulation. As the precipitation has the dominant effect on surface runoff, 20 downscaled ensembles for precipitation were applied to the SWAT model for uncertainty analysis through evaluating the surface runoff simulation. Because the uncertainty of the temperature is not considered in this study, the mean of 20 downscaled ensembles daily maximum and minimum temperature were used as the temperature input of the SWAT model.

7.4.2 **Hydrological modeling**

The study area is located at the upstream of the Wenjing River watershed, Sichuan, China. The information and detailed descriptions are provided in **Chapter 4**. The SWAT model was firstly calibrated and validated using observed meteorological data for the study area. The best simulation using observed meteorological data can achieve the NSE of 0.77 and R^2 of 0.80 for the calibration period, and NSE of 0.74 and R^2 of 0.87 for the validation period for surface runoff simulation after three iteration using SUFI-2. The parameter ranges (including original and updated ranges) for each iteration were shown in **Table 4.1**. The parameter set which generate the best simulation can be viewed as the optimized parameter set. The exact values for each optimized parameter have been shown in **Table 7.2**. By using the optimized parameter set, all uncertainty during hydrological modeling has been fixed. If uncertainty from different ensembles of meteorological data is involved, the uncertainty reflected by surface runoff should come from meteorological input data (which arise from statistical downscaling of the H3A2a outputs).

Table 7.2 The exact values of the optimized parameter set.

Parameters	Changing type	Optimized parameter values
CN_2	r	-0.25813
ALPHA_BF	v	0.815825
GW_DELAY	v	63.973
GWQMN	v	136.9425
ESCO	v	0.987075
CH_K	v	38.4025
ALPHA_BNK	v	0.943205
SOL_AWC	r	-0.16469
SFTMP	v	5.16915
GW_REVAP	v	0.022135
RCHRG_DP	v	0.0324

To make the simulation results comparable with the calibrated runoff simulation results, the calibration period for hydrological modeling was selected as the study period from 1998 - 2000 for uncertainty analysis. **Figure 7.13** shows the hydrograph of the observed surface runoff, best simulation after calibration using observed meteorological data, best simulation using downscaled H3A2a outputs with optimized parameter sets of the SWAT model. The best surface runoff simulation using observed meteorological data after calibration can achieve the NSE of 0.77 and R^2 of 0.8, and the simulation using best downscaled H3A2a outputs can reach the NSE of 0.67 and R^2 of 0.73.

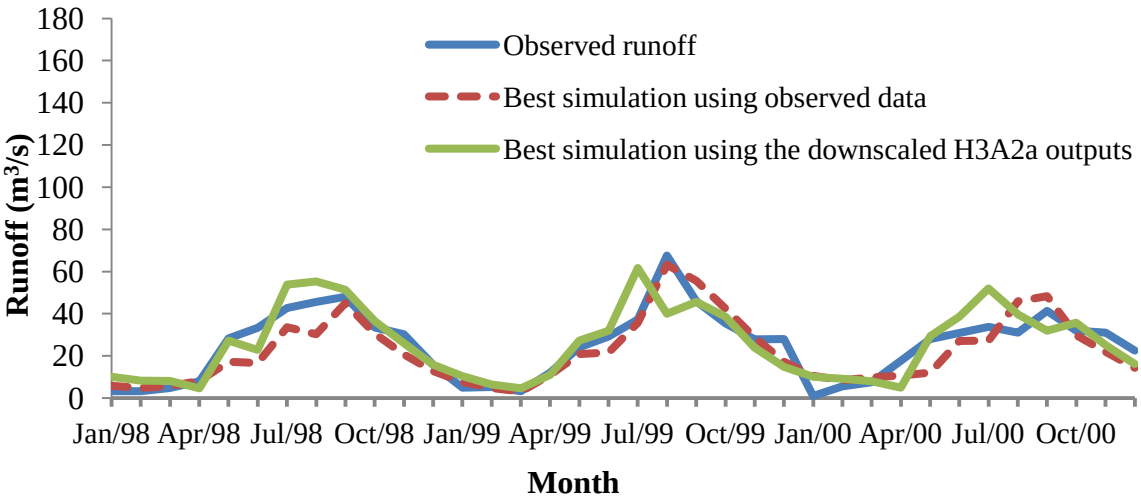

Figure 7.13 The hydrograph of the observed runoff, best simulation using observed meteorological and the downscaled H3A2a outputs.

7.4.3 **Uncertainty analysis**

Some uncertainty analysis results are shown in previous chapters. As mentioned before, each iteration includes 1000 parameter sets for 11 parameters when conducting calibration for hydrological modeling. The uncertainty of hydrological modeling considered in this study mainly comes from the application of different parameter sets. The uncertainty can be reflected by 95PPU of the surface runoff in Figure 4.11. When uncertainty from statistical downscaling is considered, the optimal parameter set of the hydrological model was used and the 95PPU of surface runoff is the propagated uncertainty from the application of different downscaled ensembles. **Figure 6.6** shows the uncertainty propagated from statistical downscaling by using 40 downscaled ensembles, and **Figure 7.14** shows the uncertainty propagated using 20 downscaled ensembles.

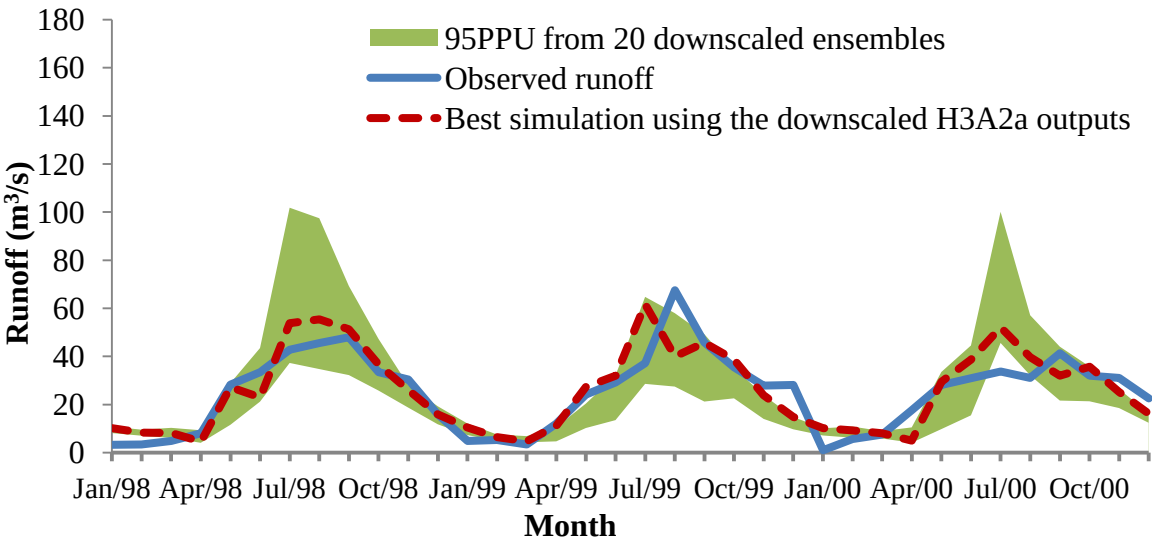

Figure 7.14 The hydrograph of the observed and best simulated runoff with 95PPU from downscaled H3A2a results for 1998-2000.

As can be seen in those plots, the uncertainty from statistical downscaling produced much larger uncertainty bands than the uncertainty band from hydrological modeling. The 95PPU using 40 downscaled ensembles produced a slightly larger uncertainty than 95PPU generated using 20 downscaled ensembles but required more calculation resources. Since limited changes can be found for generating the 95PPU for surface runoff by using different numbers of downscaled ensembles (see **Chapter 6**), 20 downscaled precipitation ensembles and mean of 20 downscaled daily maximum and minimum temperature ensembles were used for hydrological simulation for quantifying the uncertainty.

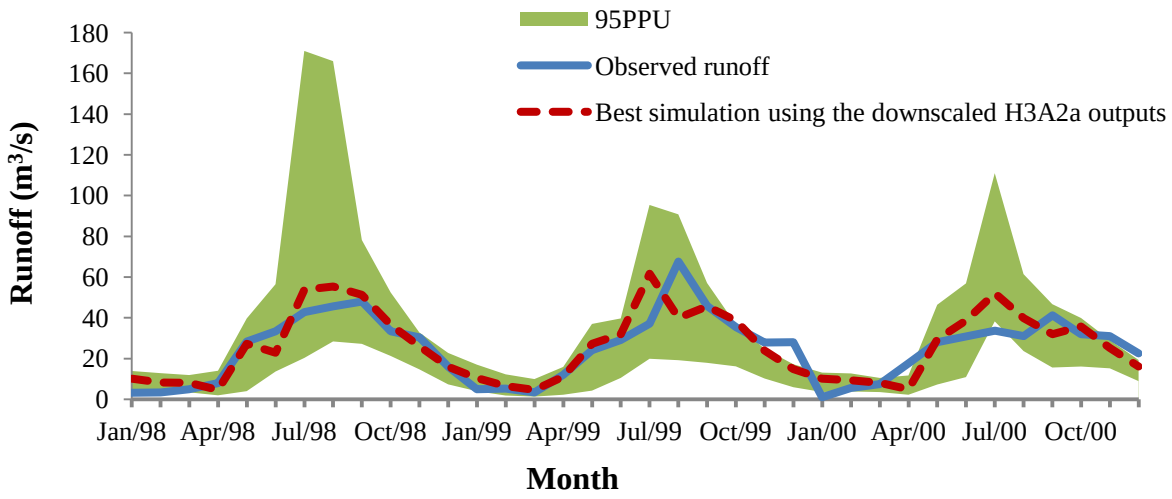

Figure 7.15 The hydrograph of the observed and best simulated runoff with 95PPU generated from hydrological modeling and downscaled H3A2a outputs for 1998-2000.

In this study, evaluating the total uncertainty which includes the uncertainty from hydrological modeling and statistical downscaling is the major task. According to the assumption made previously, the uncertainty from hydrological modeling was represented by using different parameter sets (1,000 parameter sets), and the uncertainty from statistical downscaling was evaluated using different downscaled ensembles (20 ensembles of precipitation). Therefore, a total of 20,000 simulations have been conducted to calculate the total uncertainty propagated from statistical downscaling to hydrological modeling (The SWAT hydrological simulations were conducted by using a Java programming developed by author. The programming codes were provided in APPENDIX. The uncertainty was reflected by using 95PPU of surface runoff. The 95PPU was calculated by using the lower level (at 2.5%) and upper level (at 97.5%) of cumulative distribution of predicted surface runoff. **Figure 7.15** shows the observed runoff, results of the best simulated surface runoff and 95PPU of total uncertainty using the downscaled H3A2A outputs. As it can be seen, the surface runoff during the peak flow period of the three years is much greater than the

uncertainty of runoff in other seasons. **Figure 7.15** also shows that the total uncertainty is obviously larger than the uncertainty from two other uncertainty sources due to the wider uncertainty bands.

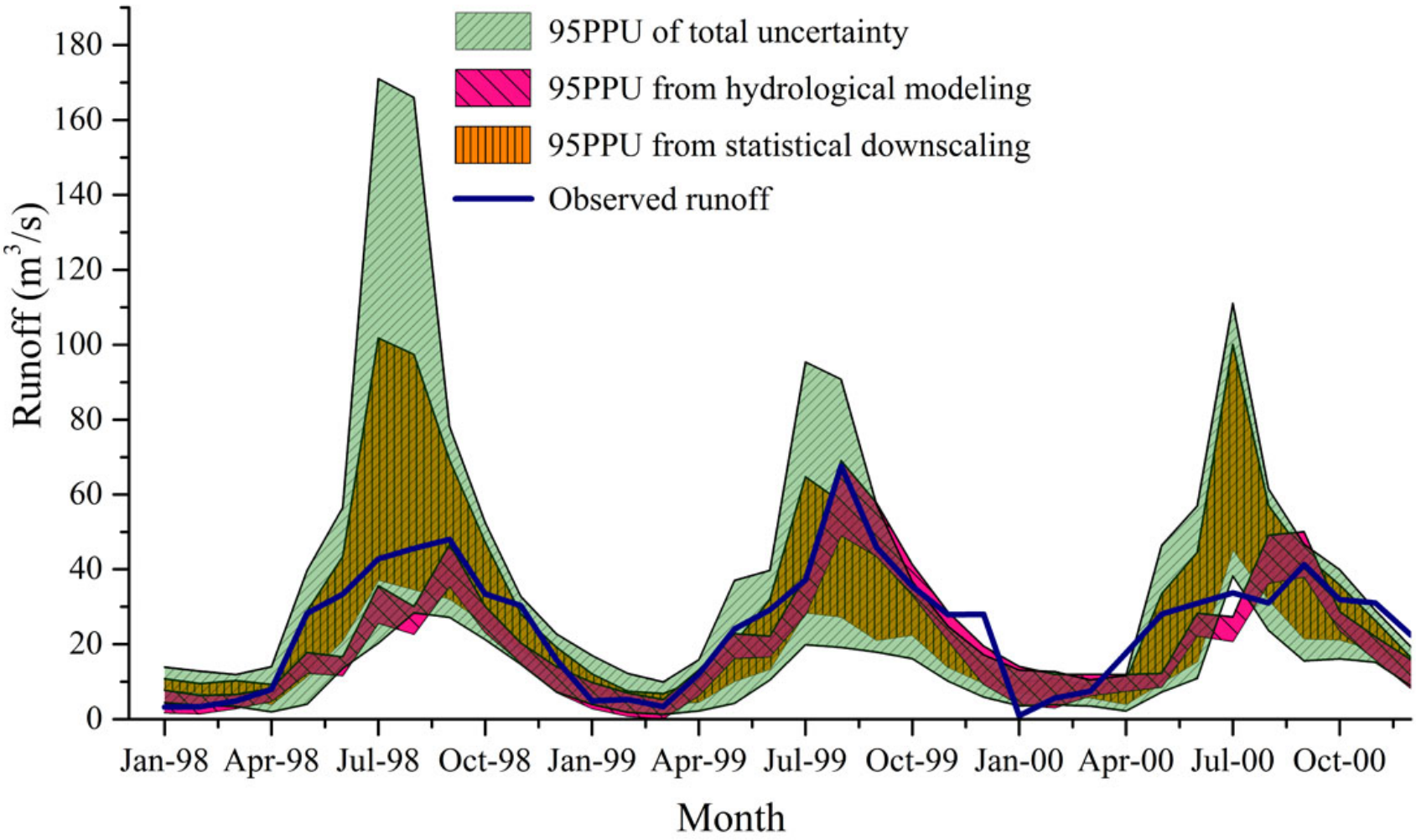

Figure 7.16 The observed runoff, 95PPU of total uncertainty, uncertainty from hydrological modeling, uncertainty from statistical downscaling

In order to show the propagation effects of the uncertainty clearly, the hydrograph (from 1998-2000) with uncertainty from different sources are shown in **Figure 7.16**. The green area is total uncertainty stemmed from hydrological modeling and statistical downscaling together. The brown area is the uncertainty arose from statistical downscaling only, and the pink area is the uncertainty from hydrological modeling only. In **Figure 7.16**, the pink area is much smaller than brown area, indicating that the uncertainty effects from hydrological modeling are much smaller than the uncertainty from statistical downscaling to the surface runoff. Moreover, both the brown area and pink area are smaller than the green area, demonstrating that the total uncertainty is larger than uncertainty of other two sources. However, the total uncertainty cannot be estimated by using simple addition of other two uncertainty sources, and the total uncertainty of surface runoff is obviously larger than the sum of two uncertainty sources. From the R-factor values, the uncertainty from different sources can be easily quantified and compared. The values of R-factor of 95PPU for total uncertainty, uncertainty from statistical downscaling, uncertainty from hydrological modeling are 2.03, 1.08 and 0.48, respectively. The larger R-factor values indicate the larger the uncertainty. When the relatively small uncertainty from statistical downscaling and hydrological modeling are combined together for new hydrological simulations, the propagated uncertainty is larger than the addition of other two uncertainty sources. If the average width of 95PPU was used to evaluate the uncertainty, the total uncertainty is about 2.15 times of 95PPU from statistical downscaling and about 4.44 times of 95PPU from hydrological modeling on monthly average. The extreme values of three 95PPU show the great difference of uncertainty effects. In 95PPU of total uncertainty band area, the largest

peak flow could reach 171 m^3/s in July of 1998; at the same month, the largest flow of 95PPU from statistical downscaling and from hydrological modeling are 101.8 m^3/s and 35.6 m^3/s which are much smaller than the peak flow from 95PPU of the total uncertainty. The values of P-factor of 95PPU for total uncertainty, uncertainty from statistical downscaling, uncertainty from hydrological modeling are 0.75, 0.47 and 0.44, respectively. The large uncertainty band still cannot cover all the observed surface runoff and it may be caused by some unexpected human activities in the study watershed, such as irrigation in the summer and some small dams for electricity generation.

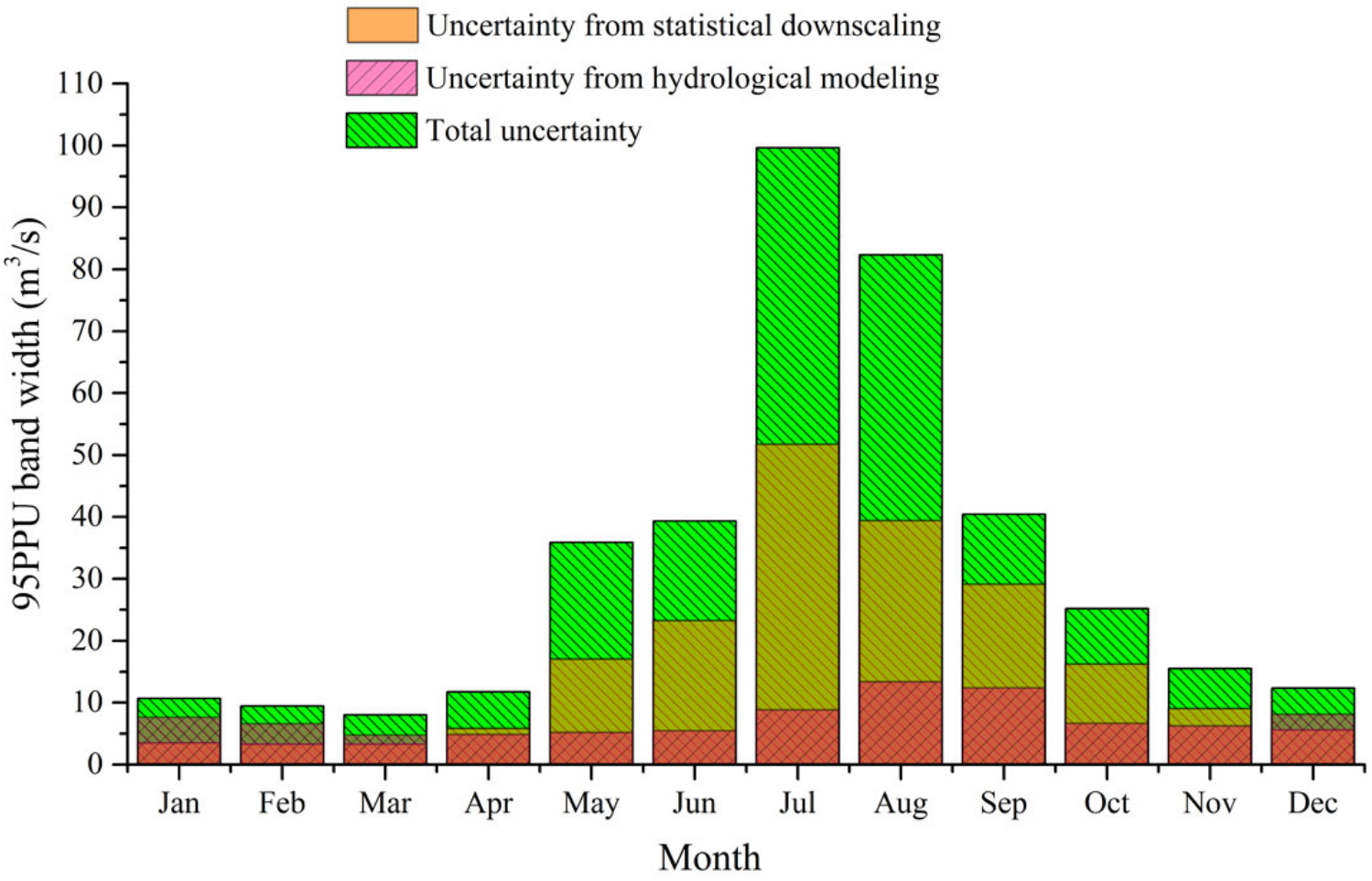

Figure 7.17 The uncertainty distribution of 95PPU of annual monthly surface runoff from different uncertainty sources for year 1998-2000.

Figure 7.17 shows the 95PPU of annual monthly surface runoff from different uncertainty sources during 1998-2000. As can be seen in the figure, the uncertainty from hydrological modeling only takes up a small portion of the total uncertainty, and the uncertainty from statistical downscaling contributes more to the total uncertainty. The total uncertainty propagated from uncertainty of statistical downscaling and hydrological modeling can be evaluated during the new simulations, and the results show that the total uncertainty is much greater than other two uncertainty sources. For example, in July, the 95PPU of total uncertainty is 1.92 times of uncertainty from statistical downscaling and 11.26 times of uncertainty from hydrological modeling; in August, the 95PPU of total uncertainty is 2.09 times of uncertainty from statistical downscaling and 6.17 times of uncertainty from hydrological modeling. These results can demonstrate that propagated uncertainty was dramatically increased in new simulations when combine two uncertainty sources together.

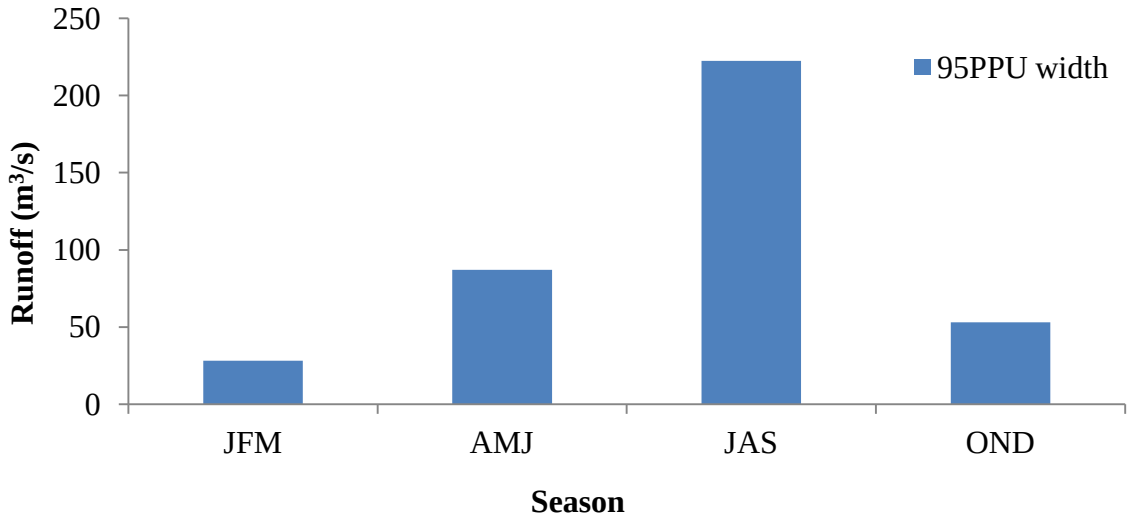

Figure 7.18 Annually seasonal mean width of 95PPU of the total uncertainty

Also, the uncertainty of three different sources during wet season (from May to Sep) is much larger than the uncertainty in dry season, which can be clearly shown in **Figure 7.17**. The 95PPU of total uncertainty in wet season (from May to September) is 5.39 times of total uncertainty in dry season (from Jan to Apr and from Oct to Dec) during the three years. If the seasonal results are concerned, the total uncertainty effects on four seasons are not evenly distributed. In **Figure 7.18**, the first season, including Jan, Feb, Mar (JFM) has the smallest 95PPU in all three years with average band width of 28.1 m^3/s; the second season, including Apr, May, and Jun (AMJ), has the second largest average uncertainty band width of 86.9 m^3/s in three years; the third season, including Jul, Aug, Sep (JAS), has the largest average uncertainty band in three years with value of 222.4 m^3/s; and the last season, including Oct, Nov, Dec (OND), has the third largest average uncertainty band width which is 53.6 m^3/s in all three years. As it can be clearly shown in **Figure 7.18**, the summer season (JAS) has greatest total uncertainty comparing with other three seasons. The dry season in each year shows less variation and uncertainty in study area. The reason of that could be concluded that the less uncertainty of surface runoff is mainly caused by less variation of downscaled GCM outputs (especially downscaled precipitation) during the dry season.

7.5 Summary

In this study, the ISES-UPA was proposed to quantify and evaluate the total propagated uncertainty effects from statistical downscaling and hydrological modeling. A case study in the Wenjing River watershed, Sichuan of China, was conducted to demonstrate the feasibility of the proposed method. At first, by using statistical methods (the SDSM model), the precipitation and temperature data were downscaled using the Hadley Centre

Coupled Model 3 (HadCM3) for A2 scenario (H3A2a). Due to the importance of precipitation, the uncertainty of precipitation was considered as uncertainty of statistical downscaling. The uncertainty of precipitation was reflected by using different downscaled precipitation ensembles as input of the hydrological model. The SWAT model was applied to hydrological modeling for the study area. The uncertainty arises from statistical downscaling and hydrological modeling were evaluated separately first, and then the total uncertainty are evaluated by using 95PPU of the surface runoff.

The results indicate that the total propagated uncertainty is much larger than the simple addition of other two uncertainty sources. From the **Figure 7.16** and **Figure 7.17**, the uncertainty from the three different sources has been clearly shown. The uncertainty effects from statistical downscaling alone and hydrological modeling alone are relatively small, but the propagated uncertainty was obviously enlarged when combining two uncertainty sources for new hydrological simulations. The results also show that the uncertainty of surface runoff during the wet season has larger uncertainty than the dry season.

By using the proposed ISES-UPA, the uncertainty propagation effects were evaluated. The uncertainty from statistical downscaling, uncertainty from hydrological modeling, and the total enlarged uncertainty from two uncertainty sources were compared and quantified in this study. If more uncertainty sources are involved, the uncertainty propagation effects can also be evaluated using the ISES-UPA, and the contributions of each uncertainty components could be shown in hydrographs for comparison. As the contributions of different uncertainty sources are investigated and quantified, the information can guide researchers/modelers to pay more efforts on controlling the uncertainty source which has greater impacts to the total uncertainty leading to more reliable and precise uncertainty analysis for prediction results.

The creditable and reliable quantification for the total uncertainty effects under future climate scenarios can reduce the potential risk of damages (e.g., flood, drought) and also reduce the potential resources waste/cost (e.g., overbuilding high quality infrastructure and dam) caused by extreme events. The uncertainty analysis results will provide more confidence to decision makers for efficient water resource management for the study area.

CHAPTER 8.
CONCLUSIONS AND RECOMMENDATIONS

8.1 Conclusions

The quality of sensitivity analysis, parameter calibration, and uncertainty analysis can affect the performance of hydrological studies. There are many limitations to different methods leading to difficulties in achieving acceptable hydrological modeling results, especially with different sources of uncertainty under climate change situations. For example, most traditional sensitivity analysis methods (e.g., OFAT) are unable to investigate the interactions between parameters and are incapable of finding the global optimized parameter set. The extensive computational requirement from traditional sensitivity analysis needs to be improved to enhance the efficiency of the parameter calibration process. For uncertainty analysis in hydrological modeling, different uncertainty analysis methods are available. However, using comprehensive multiple criteria to select the most suitable uncertainty analysis method under the same modeling framework has seldom been reported. Moreover, under changing climatic conditions, very limited studies have focused on evaluating the uncertainty propagated effects from statistical downscaling to hydrological modeling. Furthermore, no uncertainty analysis methods have been specifically developed for this type of propagation uncertainty.

Due to above limitations and needs, this thesis has presented several methods for supporting hydrological modeling under changing climatic conditions. The developed methods can be integrated into a system to achieve better performance for hydrological modeling studies through accurate sensitivity analysis, and efficient calibration for better simulation predictions with reliable uncertainty analysis. The thesis covers the improvement of sensitivity analysis, calibration, uncertainty analysis for hydrological modeling, and

uncertainty quantification for uncertainty propagation effects. A summary of each method follows:

1) The determination of significant parameters included in model calibration relies on the results of a sensitivity analysis. In **Chapter 3**, a DOE-aided sensitivity analysis and parameterization (DOE-SAP) method for hydrological modeling, which incorporates statistical design of experiment methods, linear/nonlinear optimization and verification process to improve the simulation performance of hydrological modeling, was proposed. A case study was conducted using the SLURP hydrological model. The original calibration was previously obtained by the auto calibration module built in the SLURP model. The proposed DOE-SAP method was applied to the calibrated parameter sets to identify if there are still some improvements that can be achieved. The results showed that further improvements can be made using the optimized parameter set suggested by the DOE model. The results also showed that the "precipitation factor" was involved in several interaction effects with other factors, which cannot be determined using traditional sensitivity analysis, the OFAT method. The study demonstrated the advantage of the DOE-SAP method to evaluate the effects of main parameters and interactions between parameters on the simulation responses. Furthermore, from the developed method, the key parameters can be identified to improve the optimization process.

2) Uncertainty analysis is an important procedure in hydrological modeling to demonstrate the reliability of simulation performance. In **Chapter 4**, three uncertainty analysis methods, the SUFI-2, GLUE and ParaSol methods, were compared using the a comprehensive uncertainty evaluation scheme (such as the R-factor, P-factor, the ratio of P-factor and R-factor, computational efficiency, and performance of best estimates, parameter

uncertainty, and prediction uncertainty). Two real-world hydrological case studies in the Wenjing River watershed and Huolin River watershed were used for testing the proposed method. From the results of both case studies, the SUFI-2 method has advantages over the other two uncertainty analysis methods based on accuracy of the calibration results (NSE of 0.77 and R^2 of 0.8 for the Wenjing case; NSE of 0.83 and R^2 of 0.85 values for the Huolin case) and more reliable uncertainty analysis. The SUFI-2 method also provided the best coverage of measurement (P-factor of 0.56 for the Wenjing case; and P-factor of 0.88 for the Huolin case) with reasonably small uncertainty bands (R-factor of 0.48 for the Wenjing case; and R-factor of 0.97 for the Huolin case). Compared to other methods, the SUFI-2 method can achieve reasonably good results with high computational efficiency (3,000 simulation runs), indicating the advantage for high dimensional and complex distributed hydrological models.

3) In Chapter 5, a sequential multi-criteria based calibration and uncertainty analysis (SMC-CUA) method for overcoming some drawbacks of traditional methods is proposed. Using the proposed framework, the method aims to calibrate hydrological models and provide balanced and reliable uncertainty analysis results in a highly efficient way. To achieve the goals, instead of using Monte Carlo random sampling for the prior distribution sampling of model parameters, Latin Hypercube Sampling method, a highly efficient method was used as the sampling method for parameter prior distributions. Moreover, the coefficient of determination was used as the additional criterion besides NSE to screen out the impractical behavioral simulations. The implementation of multiple iterations can improve the simulation and uncertainty analysis performance and control the phenomenon of equifinality during hydrological modeling. The feasibility and flexibility of the proposed

method were tested using a hypothetical and a real-world case study. Through the case studies, the results showed that the proposed method was able to quickly search the HPD regions of each parameter. This approach improved the computational efficiency compared to the SUFI-2 and GLUE methods and reduced the parameter uncertainty without sacrificing simulation performance for surface runoff prediction. The results also showed that the SMC-CUA method provided good calibrated simulations (NSE = 0743 and R^2 = 0.787) and more reliable uncertainty analysis (providing the highest P/R value of 1.00) compared with the other two methods (P/R of 0.93 for SUFI-2; and P/R of 0.76 for GLUE).

4) Uncertainty associated with climate change is always considered as irreducible and inevitable. Although the GCMs are the largest source uncertainty in climate change studies, the uncertainty related to downscaling also needs to be taken into account for better estimation and understanding of the impacts of climate change. To quantify the uncertainty propagation effects from statistical downscaling to hydrological modeling, an innovative response based statistical evaluation method (RESEM) was presented in Chapter 6 for estimating the propagated effects and providing long term prediction for hydrological responses. The proposed method was applied to a real case study. Statistical downscaling model (SDSM) was used to downscale the precipitation and temperature data from the H3A2a model to generate future climate data based on the A2 scenario. The RESEM successfully and effectively evaluated the propagation effect of uncertainty from statistical downscaling to hydrological modeling using 95PPU of the surface runoff, and also provided future predictions (2016-2020) for surface runoff using the selected climate scenario.

5) Limited studies focus on breaking down the total uncertainty into different uncertainty sources for hydrological modeling studies under climate change conditions.

Therefore, in Chapter 7 an integrated simulation-based evaluation system for uncertainty propagation analysis (ISES-UPA) was developed to investigate the effects and contributions of different uncertainty components on the total propagated uncertainty in hydrological modeling under changing climatic conditions. A case study was conducted to demonstrate the feasibility of the proposed method. Statistical downscaling for precipitation and temperature using SDSM were first conducted, and the downscaled results were used as the inputs for subsequent hydrological modeling. Through the used on the proposed ISES-UPA approach, the uncertainty from statistical downscaling, hydrological modeling, and combination of two uncertainty components were compared and quantified. The results indicated that the total propagated uncertainty is much larger than the simple addition of other two uncertainty sources, and also showed that the uncertainty of surface runoff during the wet season has larger uncertainty than the dry season.

In Chapter 8, an integrated hydrological modeling system under changing climatic conditions was further proposed based on the above developed methods, to include the DOE-SAP method, SMC-CUA method, and ISES-UPA. The framework of the integrated system is shown in **Figure 8.1**. These methods can support each other to achieve better hydrological modeling results. The DOE-SAP method provides the list of significant parameters and more reliable sensitivity analysis and calibration results, and the suggested significant parameters can be applied to the SMC-CUA method. If better calibration results can be obtained, the optimized parameter sets will be updated, and the updated parameter uncertainty ranges can return DOE-SAP method for further calibration if necessary. Both the DOE-SAP and SMC-CUA methods can better support the calibration of hydrological models. Reliable uncertainty analysis for hydrological modeling under changing climatic conditions requires well behaved

hydrological modeling results as the precondition. The ISES-UPA method for quantifying the uncertainty propagation effects during statistical downscaling can be applied to a calibrated hydrological model. Through the application of the developed methods, better calibrated results could be achieved and used for evaluating the uncertainty propagated effects from statistical downscaling to hydrological modeling.

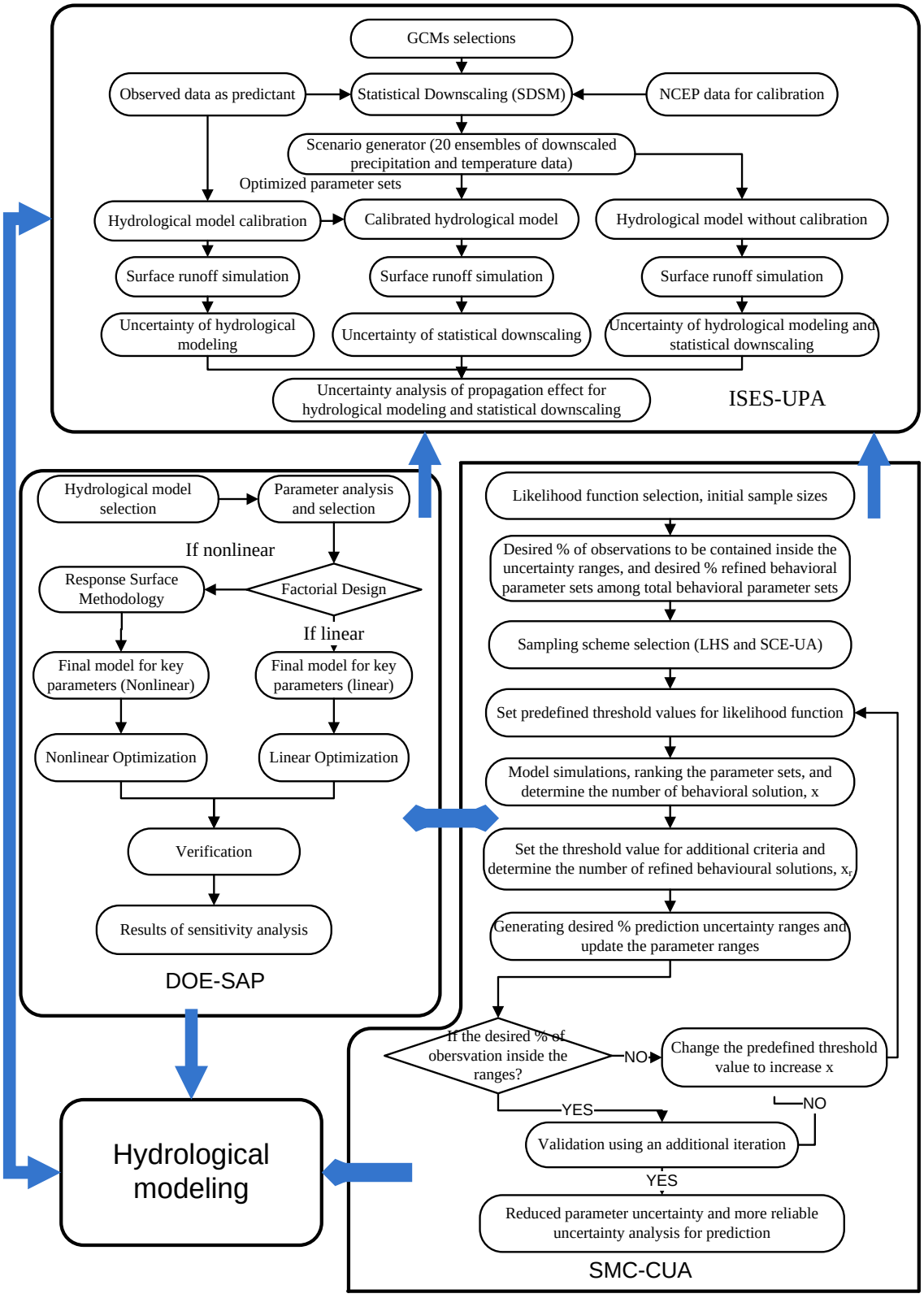

Figure 8.1 The integrated system of DOE-SAP, SMC-CUA, and ISES-UPA for hydrological modeling under changing climatic conditions

8.2 Publications

Refereed Journal Publications

1. **Wu, H.J.**, and Chen, B. (2015). Evaluating uncertainty estimates in distributed hydrological modeling for the Wenjing River watershed in China by GLUE, SUFI-2, and ParaSol methods. *Ecological Engineering,* 79, 110-121, 10.1016/j.ecoleng.2014.05.014/

2. Chen, B., Li P., **Wu, H.J.**, Husain, T., and Khan, F. (2015). MCFP: a Monte Carlo Simulation based Fuzzy Programming Approach for Municipal Solid Waste Management under Dual Uncertainties of Possibility and Continuous Probability. *Journal of Environmental Informatics*, doi:10.3808/jei.201500293.

3. **Wu, H.J.**, Chen, B., Snelgrove, K., and Lye, L.M. (2015). Quantification of uncertainty propagation effects during statistical downscaling of precipitation and temperature to hydrological modeling. *Journal of Environmental Informatics,* accepted (29/08/2015).

4. Zheng, J.S., Liu, B., Ping, J., Chen, B., **Wu, H.J.**, and Zhang, B.Y. (2015). Vortex and shaker assisted liquid-liquid micro extraction (VSA-LLME) coupled with gas chromatography and mass spectrometry (GC-MS) for analysis of 16 polycyclic aromatic hydrocarbons (PAHs) in offshore produced water. *Water, Air, and Soil Pollution*, 226(9): 318, DOI: 10.1007/s11270-015-2575-3

5. **Wu, H.J.**, and Chen, B. (2014). Using Statistical and Probabilistic Methods to Evaluate

Health Risk Assessment: A case study. *Toxics,* 2(2), 291-306; doi:10.3390/toxics2020291.

6. Xue, C., Chen, B., and **Wu, H.J.** (2014). Parameter uncertainty analysis of Surface flow and Sediment Yield in the Huolin Basin in China. *Journal of Hydrologic Engineering*, 19(6), 1224-1236, 10.1061/(ASCE)HE.1943-5584.0000909.

7. Li, P., Chen B., Li, Z.L., Zheng, X. **Wu, H.J.**, Jing L., and Lee K. (2014), "A Monte Carlo Simulation-based Two-Stage Adaptive Resonance Theory Mapping Model for Site Classification in Offshore Oil Spill Monitoring", Marine Pollution Bulletin, 86(1-2):434-442.

8. Li, P., **Wu, H.J.**, and Chen, B. (2013). RSW-MCFP: A Resource-oriented Solid Waste Management System for a Mixed Rural-Urban Area through Monte Carlo Simulation-Based Fuzzy programming. *Mathematical Problems in Engineering, 2013,* Article ID 780354, doi:10.1155/2013/780354.

9. **Wu, H.J.**, Lye, L. and Chen, B. (2012). A design of experiment aided sensitivity analysis and parameterization for hydrological modeling. *Canadian Journal of Civil Engineering*, 39, 460-472.

Other Refereed Publications

1. **Wu, H.J.,** and Chen, B. (2014). Uncertainty analysis for propagation effects from

statistical downscaling to hydrological modeling. The International Conference on Marine and Freshwater Environments (iMFE) 2014 proceeding, St. John's, Newfoundland, CA, EMR #1330.

2. **Wu, H.J.,** and Chen, B. (2014). Hydrological Modeling and Uncertainty Analysis for the up reach of the Wenjing Watershed, Sichuan, China. Poster presented at 2014 13th IWA Specialized Conference on Watershed and River Basin Management, San Francisco, USA.

3. Zheng, X., Chen, B., **Wu, H.J.** (2014) Interpolation method and uncertainty analysis in oil spilling trajectory model. The International Conference on Marine and Freshwater Environments (iMFE) 2014 proceeding, St. John's, Newfoundland, CA,

4. **Wu, H.J.**, Chen, B., and Li, P. (2013). Comparison of Sequential Uncertainty Fitting Algorithm (SUFI-2) and Parameter Solution (ParaSol) Method for Analyzing Uncertainties in Distributed Hydrological Modeling – A Case Study. CSCE 2013 General Conference proceeding, Montreal, Quebec, CA, Gen-309.

5. Jing, L., Chen, B., Zhang, B.Y., Li, P., and **Wu, H.J.** (2013). Modeling the Effects of Photon Flux, Salinity and Temperature on UVC Photolysis of Polycyclic Aromatic Hydrocarbons (PAHs) in Oily Seawater. Poster presented at the Arctic Oil & Gas North America Conference 2013, St. John’s, Canada.

6. **Wu, H.J.**, and Chen, B. (2011). Human Risk Assessment of Dermal Exposure to Water Pollutants: A Case Study. 64th Canadian Water Resources Association National Conference. St. John's, Newfoundland, CA.

7. Chen, B., Li, P., **Wu, H.J.** and Liu, B. (2011). "Integrated Environmental Planning for Municipal Solid Waste and Management of the City of Shuangcheng, China", Technical Report, United Nations Development Program (UNDP), 228pp.

8. **Wu, H.J.**, Lye, L., & Chen, B. (2010). Sensitivity Analysis of the Input Parameters of the SLURP Hydrological Model Using Design of Experiment (DOE) Methodology. CSCE 2010 General Conference proceeding, Winnipeg, Manitoba, CA, GC-059.

9. **Wu, H.J.**, Dadashzadeh, M., & Chen, Y. (2008). Pollution Investigation and Risk Assessment in the Nut Brook River and the Kelligrews River. Master thesis (project) of Memorial University of Newfoundland, St. John's, NL, CA.

10. Chen, B, and **Wu, H.J.** (2012). A Preliminary Study on Hydrological Characterization and Modeling of the Wenjingjiang River Watershed in the City of Chongzhou, Sichuan. Technical Report, *United Nations Development Program (UNDP).*

8.3 Recommendations for Future Work

Although all the proposed method has been successfully demonstrated and applied to real-case studies, there are still some improvements that can be made. The recommendations are listed as follows:

1. **Chapter 3** demonstrated the advantages of the DOE aided sensitivity analysis method over the traditional method, which mainly includes the evaluation of the effects of main parameters and interactions between parameters to simulation responses. It is recommended that uncertainties existing in the parameters should also be considered to further improve the performance of the simulation responses. Extensions of the developed system to other simulation modeling systems can be further explored to test the flexibility of the proposed DOE method.
2. For uncertainty comparison studies, the developed set of criteria, such as the best simulation estimation, coverage of observed data using 95PPU, width of the 95PPU bands, ratio of P-factor and R-factor, parameter uncertainty, prediction uncertainty, computational efficiency, and ease of implementation of three traditional uncertainty analysis methods (including SUFI-2, GLUE and ParaSol) was compared using two real-world cases. The results suggested that SUFI-2 provided better calibrated simulation results with reasonably good uncertainty analysis. The generality of findings still needs to be verified with more case studies. It is recommended that extended studies can be undertaken to further examine the capability of these three methods as well as other uncertainty analysis methods for different study regions.

3. The novel SMC-CUA method achieved better overall results than GLUE and SUFI-2 through a hypothetical and a real case. The reduced parameter uncertainty can significantly improve the performance of uncertainty control when conducting hydrological modeling studies under changing climatic conditions. It is recommended that the SMC-CUA method be applied to different hydrological modeling cases (such as using different hydrological models, hydrological responses, and study areas) to confirm the advantages of the proposed method over other method.
4. It is recommended that when conducting downscaling studies, the multiple and latest version of GCMs as well as different downscaling methods could be applied to compare the results using the RESEM and ISES-UPA. Also, the uncertainty from other input sources, such as temperature, humidity, wind speed, solar radiation, can be considered and their combined uncertainty effects be investigated for testing the flexibility of the proposed method. Moreover, GCMs have the limitations to reflect the extreme events. The source and propagation of uncertainty during extreme events would be enlarged than the normal event. Therefore, future studies can attempt to make use of statistical methods to quantify and evaluate the risk level of the extreme events.
5. In general, it is recommended that more real-world case studies in different areas could be applied to further test the feasibility and performance of all the developed methods. Moreover, case studies using the integrated system of the DOE-SAP, SMC-CUA, and ISES-UPA methods could be conducted to further evaluate the performance and demonstrate the feasibility of the integrated system.

REFERENCES

Abbaspour, K.C., Johnson, C.A., & Van Genuchten, M.T. (2004). Estimating uncertain flow and transport parameters using a sequential uncertainty fitting procedure. *Vadose Zone Journal, 3*(4), 1340-1352.

Abbaspour, K.C., Yang, J., Maximov, I., Siber, R., Bogner, K., Mieleitner, J., Zobrist, J., & Srinivasan, R. (2007). Modelling hydrology and water quality in the pre-alpine/alpine Thur watershed using SWAT. *Journal of Hydrology, 333*(2-4), 413-430.

Abbaspour, K.C. (2011). SWAT-CUP4: SWAT Calibration and Uncertainty Programs - A User Manual., Swiss Federal Institute of Aquatic Science and Technology, Switzerland.

Abbaspour, K.C. (2015). SWAT Calibration and Uncertainty Programs - A User Manual. Eawag: Swiss Federal Institute of Aquatic Science and Technology.

Abbott, M.B., Bathurst, J.C., Cunge, J.A., O'connell, P.E., & Rasmussen, J. (1986a). An introduction to the European Hydrological System—Systeme Hydrologique Europeen,“SHE”, 1: History and philosophy of a physically-based, distributed modelling system. *Journal of Hydrology, 87*(1), 45-59.

Abbott, M.B., Bathurst, J.C., Cunge, J.A., O'connell, P.E., & Rasmussen, J. (1986b). An introduction to the European Hydrological System—Systeme Hydrologique Europeen,“SHE”, 2: Structure of a physically-based, distributed modelling system. *Journal of Hydrology, 87*(1), 61-77.

Ahmed, K.F., Wang, G., Silander, J., Wilson, A.M., Allen, J.M., Horton, R., & Anyah, R. (2013). Statistical downscaling and bias correction of climate model outputs for climate change impact assessment in the U.S. northeast. *Global and Planetary*

Change, 100, 320-332.

Ajami, N.K., Duan, Q., & Sorooshian, S. (2007). An integrated hydrologic Bayesian multimodel combination framework: Confronting input, parameter, and model structural uncertainty in hydrologic prediction. *Water Resources Research, 43*(1).

Arbia, G., Griffith, D., & Haining, R. (1998). Error propagation modelling in raster GIS: overlay operations. *International Journal of Geographical Information Science, 12*(2), 145-167.

Archer, G., Saltelli, A., & Sobol, I. (1997). Sensitivity measures, ANOVA-like techniques and the use of bootstrap. *Journal of Statistical Computation and Simulation, 58*(2), 99-120.

Armstrong, R.N., & Martz, L.W. (2008). Effects of reduced land cover detail on hydrological model. *Hydrol. Process, 22*, 2395-2409.

Arnold, J.G., Williams, J.R., & Maidment, D.R. (1995). Continuous-Time Water and Sediment-Routing Model for Large Basins. *Journal of Hydraulic Engineering, 121*(2), 171-183.

Arnold, J.G., Srinivasan, R., Muttiah, R.S., & Williams, J.R. (1998). Large area hydrologic modeling and assessment Part I: Model development. *Journal of the American Water Resources Association, 34*(1), 17.

Aronica, G., Bates, P., & Horritt, M. (2002). Assessing the uncertainty in distributed model predictions using observed binary pattern information within GLUE. *Hydrological Processes, 16*(10), 2001-2016.

ASCE Task Committee. (1993). Criteria for evaluation of watershed models. *Journal of Irrigation and Drainage Engineering, 119*(3), 429-442.

Aslan, N. (2007). Application of response surface methodology and central composite rotatable design for modeling the influence of some operating variables of a Multi-Gravity Separator for coal cleaning. *Fuel, 86*(5), 769-776.

Bae, D.-H., Jung, I.-W., & Lettenmaier, D.P. (2011). Hydrologic uncertainties in climate change from IPCC AR4 GCM simulations of the Chungju Basin, Korea. *Journal of Hydrology, 401*(1-2), 90-105.

Bajsic, I., & Kunsek, I. (2003). Factorial design of drying phenomena. *Instrumentation Science & Technology, 31*(2), 141-153.

Ballio, F., & Guadagnini, A. (2004). Convergence assessment of numerical Monte Carlo simulations in groundwater hydrology. *Water Resources Research, 40*(4).

Baroni, G., & Tarantola, S. (2014). A General Probabilistic Framework for uncertainty and global sensitivity analysis of deterministic models: A hydrological case study. *Environmental Modelling & Software, 51*, 26-34.

Barr, A.G., Kite, G., Granger, R., & Smith, C. (1997). Evaluating three evapotranspiration methods in the SLURP macroscale hydrological model. *Hydrological Processes, 11*(13), 1685-1705.

Bastola, S., Murphy, C., & Sweeney, J. (2011). The role of hydrological modelling uncertainties in climate change impact assessments of Irish river catchments. *Advances in Water Resources, 34*(5), 562-576.

Beck, M.B. (1987). Water quality modeling: a review of the analysis of uncertainty. *Water Resources Research, 23*(8), 1393-1442.

Bedient, P.B., Huber, W.C., & Vieux, R.E. (2012). *Hydrology and floodplain analysis* (5th Edition ed.). Upper Saddle River, NJ: Prentice Hall.

Benke, K.K., Lowell, K.E., & Hamilton, A.J. (2008). Parameter uncertainty, sensitivity analysis and prediction error in a water-balance hydrological model. *Mathematical and Computer Modelling, 47*(11–12), 1134-1149.

Beven, K., & Kirkby, M. (1979). A physically based, variable contributing area model of basin hydrology. *Hydrological Sciences Journal, 24*(1), 43-69.

Beven, K., & Binley, A. (1992). The future of distributed models: Model calibration and uncertainty prediction. *Hydrological Processes, 6*(3), 279-298.

Beven, K., & Freer, J. (2001). Equifinality, data assimilation, and uncertainty estimation in mechanistic modelling of complex environmental systems using the GLUE methodology. *Journal of Hydrology, 249*(1), 11-29.

Bian, J.M., Tang, J., Lin, N.F., Li, Z.Y., & Zhang, F. (2006). Research on Water Resource Carrying Capacity in Semiarid Area-A Case Study in Huolin River Basin, Southwestern Songnen Plain. *Journal of Jilin University (Earth Science Edition), 36*(1), 73-77.

Blasone, R.-S. (2007). Parameter estimation and uncertainty assessment in hydrological modelling: Kgs. Lyngby.

Blasone, R.-S., Madsen, H., & Rosbjerg, D. (2008a). Uncertainty assessment of integrated distributed hydrological models using GLUE with Markov chain Monte Carlo sampling. *Journal of Hydrology, 353*(1), 18-32.

Blasone, R.-S., Vrugt, J.A., Madsen, H., Rosbjerg, D., Robinson, B.A., & Zyvoloski, G.A. (2008b). Generalized likelihood uncertainty estimation (GLUE) using adaptive Markov Chain Monte Carlo sampling. *Advances in Water Resources, 31*(4), 630-648.

Brazier, R.E., Beven, K.J., Anthony, S.G., & Rowan, J.S. (2001). Implications of model

uncertainty for the mapping of hillslope-scale soil erosion predictions. *Earth Surface Processes and Landforms, 26*(12), 1333-1352.

Brown, J.D., & Heuvelink, G. (2005). Assessing uncertainty propagation through physically based models of soil water flow and solute transport. *Encyclopedia of hydrological sciences*.

Brown, J.D., & Heuvelink, G.B.M. (2006). Assessing Uncertainty Propagation Through Physically based Models of Soil Water Flow and Solute Transport. *Encyclopedia of hydrological sciences, 6*(79), 1181-1195.

Carpenter, T.M., & Georgakakos, K.P. (2006). Intercomparison of lumped versus distributed hydrologic model ensemble simulations on operational forecast scales. *Journal of Hydrology, 329*(1-2), 174-185.

Caya, D., & Laprise, R. (1999). A semi-implicit semi-Lagrangian regional climate model: The Canadian RCM. *Monthly Weather Review, 127*(3), 341-362.

Chadwick, R., Coppola, E., & Giorgi, F. (2011). An artificial neural network technique for downscaling GCM outputs to RCM spatial scale. *Nonlinear Processes in Geophysics, 18*(6), 1013-1028.

Chen, B., Li, P., Wu, H.J., Husain, T., & Khan, F. (2014). MCFP a Monte Carlo simulation-based fuzzy programming approach for optimization under dual uncertainties of possibility and continuous probability. *Journal of Environmental Informatics*, JEI (13JM073001).

Chen, H., Xu, C.-Y., & Guo, S. (2012). Comparison and evaluation of multiple GCMs, statistical downscaling and hydrological models in the study of climate change impacts on runoff. *Journal of Hydrology, 434-435*, 36-45.

Chen, J., Brissette, F.P., & Leconte, R. (2011). Uncertainty of downscaling method in quantifying the impact of climate change on hydrology. *Journal of Hydrology, 401*(3), 190-202.

Chen, J., Brissette, F.P., & Leconte, R. (2012). Coupling statistical and dynamical methods for spatial downscaling of precipitation. *Climatic Change, 114*(3-4), 509-526.

Chen, J., Brissette, F.P., Chaumont, D., & Braun, M. (2013). Performance and uncertainty evaluation of empirical downscaling methods in quantifying the climate change impacts on hydrology over two North American river basins. *Journal of Hydrology, 479*, 200-214.

Christiaens, K., & Feyen, J. (2002). Constraining soil hydraulic parameter and output uncertainty of the distributed hydrological MIKE SHE model using the GLUE framework. *Hydrological Processes, 16*(2), 373-391.

Cooke, R. (1991). *Experts in uncertainty : opinion and subjective probability in science*. New York: New York : Oxford University Press.

Crawford, N.H., & Linsley, R.K. (1966). Digital Simulation in Hydrology. *Stanford Watershed Model IV*, Stanford University, Stanford, CA, the United States.

Cryer, S., & Havens, P. (1999). Regional sensitivity analysis using a fractional factorial method for the USDA model GLEAMS. *Environmental Modelling & Software, 14*(6), 613-624.

Cukier, R.I., Fortuin, C.M., Shuler, K.E., Petschek, A.G., & Schaibly, J.H. (1973). Study of the sensitivity of coupled reaction systems to uncertainties in rate coefficients. I Theory. *The Journal of Chemical Physics, 59*(8), 3873-3878.

Czitrom, V. (1999). One-factor-at-a-time versus designed experiments. *The American*

Statistician, 53(2), 126-131.

Daniel, C. (1958). On varying one factor at a time. *Biometrics, 14*(3), 430-431.

Daniel, E.B., Camp, J.V., LeBoeuf, E.J., Penrod, J.R., Dobbins, J.P., & Abkowitz, M.D. (2011). Watershed modeling and its applications: A state-of-the-art review. *Open Hydrology Journal, 5*(2).

Deng, L.Y., & Tang, B. (1999). Generalized resolution and minimum aberration criteria for Plackett-Burman and other nonregular factorial designs. *Statistica Sinica, 9*(4), 1071-1082.

Di Luzio, M., Srinivasan, R., & Arnold, J.G. (2004). Technical Note A GIS-Coupled Hydrological Model System for the Watershed Assessment of Agricultural Nonpoint and Point Sources of Pollution. *Transactions in GIS, 8*(1), 113-136.

Diaz-Nieto, J., & Wilby, R.L. (2005). A comparison of statistical downscaling and climate change factor methods: impacts on low flows in the River Thames, United Kingdom. *Climatic Change, 69*(2-3), 245-268.

Dibike, Y., Gachon, P., St-Hilaire, A., Ouarda, T.B.M.J., & Nguyen, V.T.V. (2008). Uncertainty analysis of statistically downscaled temperature and precipitation regimes in Northern Canada. *Theoretical and Applied Climatology, 91*(1-4), 149-170.

Dibike, Y.B., & Coulibaly, P. (2005). Hydrologic impact of climate change in the Saguenay watershed: comparison of downscaling methods and hydrologic models. *Journal of Hydrology, 307*(1-4), 145-163.

Duan, Q.y., Sorooshian, S., & Gupta, V. (1992). Effective and efficient global optimization for conceptual rainfall-runoff models. *Water Resour. Res, 28*(4), 1015-1031.

Duan, Q.y., Sorooshian, S., & Gupta, V.K. (1994). Optimal use of the SCE-UA global

optimization method for calibrating watershed models. *Journal of Hydrology, 158*(3), 265-284.

Duan, Q.y. (2003). Global optimization for watershed model calibration. *Calibration of watershed models*, 89-104.

Feyen, L., Beven, K.J., De Smedt, F., & Freer, J. (2001). Stochastic capture zone delineation within the generalized likelihood uncertainty estimation methodology: conditioning on head observations. *Water Resources Research, 37*(3), 625-638.

Ficklin, D.L. (2010). *Modeling the Impacts of Climate Change on Hydrology and Agricultural Pollutant Runoff in California's Central Valley.* (Dissertation/Thesis), University of California, the United States.

Ficklin, D.L., & Barnhart, B.L. (2014). SWAT hydrologic model parameter uncertainty and its implications for hydroclimatic projections in snowmelt-dependent watersheds. *Journal of Hydrology, 519*, 2081-2090.

Foglia, L., Hill, M.C., Mehl, S.W., & Burlando, P. (2009). Sensitivity analysis, calibration, and testing of a distributed hydrological model using error‐based weighting and one objective function. *Water Resources Research, 45*(6).

Freer, J., Beven, K., & Ambroise, B. (1996). Bayesian Estimation of Uncertainty in Runoff Prediction and the Value of Data: An Application of the GLUE Approach. *Water Resources Research, 32*(7), 2161-2173.

Gallagher, M., & Doherty, J. (2007). Parameter estimation and uncertainty analysis for a watershed model. *Environmental Modelling & Software, 22*(7), 1000-1020.

Gassman, P.W., Reyes, M.R., Green, C.H., & Arnold, J.G. (2007). The soil and water assessment tool: historical development, applications, and future research directions.

American Society of Agricultural and Biological Engineers, 50(4), 1211-1250.

Georgakakos, K.P., & Carpenter, T.M. (2003). A methodology for assessing the utility of distributed model forecast applications in an operational environment. *Weather Radar Information and Distributed Hydrological Modelling*(282), 85-92.

Ghoraba, S.M. (2015). Hydrological modeling of the Simly Dam watershed (Pakistan) using GIS and SWAT model. *Alexandria Engineering Journal, 54*(3), 583-594.

Gilks, W.R. (2005). *Markov chain monte carlo*: Wiley Online Library.

Golmohammadi, G., Prasher, S., Madani, A., & Rudra, R. (2014). Evaluating Three Hydrological Distributed Watershed Models: MIKE-SHE, APEX, SWAT. *Hydrology, 1*(1), 20-39.

Gong, Y., Shen, Z., Hong, Q., Liu, R., & Liao, Q. (2011). Parameter uncertainty analysis in watershed total phosphorus modeling using the GLUE methodology. *Agriculture, Ecosystems & Environment, 142*(3-4), 246-255.

Gooseff, M.N., Bencala, K.E., Scott, D.T., Runkel, R.L., & McKnight, D.M. (2005). Sensitivity analysis of conservative and reactive stream transient storage models applied to field data from multiple-reach experiments. *Advances in Water Resources, 28*(5), 479-492.

Graham, L.P., Andréasson, J., & Carlsson, B. (2007a). Assessing climate change impacts on hydrology from an ensemble of regional climate models, model scales and linking methods – a case study on the Lule River basin. *Climatic Change, 81*(S1), 293-307.

Graham, L.P., Hagemann, S., Jaun, S., & Beniston, M. (2007b). On interpreting hydrological change from regional climate models. *Climatic Change, 81*(S1), 97-122.

Gudmundsson, L. (2012). Assessing the suitability of weather generators based on

Generalised Linear Models for downscaling climate projections. Norwegian Meteorological Institute, Norway.

Haario, H., Laine, M., Mira, A., & Saksman, E. (2006). DRAM: efficient adaptive MCMC. *Statistics and Computing, 16*(4), 339-354.

Hamlet, A.F., & Lettenmaier, D.P. (1999). Effects of climate change on hydrology and water resources in the Columbia River Basin1. *JAWRA Journal of the American Water Resources Association, 35*(6), 1597-1623.

Hao, F.H., Chen, L.Q., & Liu, C.M. (2003). Model output uncertainty due to spatial variability of rainfall. *Progress in Geography, 22*(5), 446-453.

Hassan, Z., Shamsudin, S., & Harun, S. (2013). Application of SDSM and LARS-WG for simulating and downscaling of rainfall and temperature. *Theoretical and Applied Climatology, 116*(1-2), 243-257.

Hasselmann, K., Latif, M., Hooss, G., Azar, C., Edenhofer, O., Jaeger, C.C., Johannessen, O.M., Kemfert, C., *et al.* (2003). The challenge of long-term climate change. *Science, 302*(5652), 1923-1925.

Hay, L.E., LaFontaine, J., & Markstrom, S.L. (2014). Evaluation of Statistically Downscaled GCM Output as Input for Hydrological and Stream Temperature Simulation in the Apalachicola–Chattahoochee–Flint River Basin (1961 – 99). *Earth Interactions, 18*(9), 1-32.

Helton, J.C., & Davis, F.J. (2003). Latin hypercube sampling and the propagation of uncertainty in analyses of complex systems. *Reliability Engineering & System Safety, 81*(1), 23-69.

Herman, J.D., Kollat, J.B., Reed, P.M., & Wagener, T. (2013). Technical note: Method of

Morris effectively reduces the computational demands of global sensitivity analysis for distributed watershed models. *Hydrology and Earth System Sciences, 17*(7), 2893-2903.

Heuvelink, G.B. (1998). *Error propagation in environmental modelling with GIS*: CRC Press.

Hobson, A.N. (2005). *Use of a stochastic weather generator in a watershed model for streamflow simulation.* (Master thesis), University of Colorado, Denver, CO, U.S.A.

Hoeting, J.A., Madigan, D., Raftery, A.E., & Volinsky, C.T. (1999). Bayesian model averaging: a tutorial. *Statistical science*, 382-401.

Hornberger, G.M., & Spear, R. (1981). Approach to the preliminary analysis of environmental systems. *J. Environ. Manage.;(United States), 12*(1).

Iman, R.L., Davenport, J.M., & Zeigler, D.K. (1980). Latin Hypercube Sampling (Program User's Guide). Sandia National Laboratories: Albuquerque, NM.

IPCC. (2007). Fourth Assessment Report, Climate Change. Cambridge: Cambridge University Press.

IPCC. (2014). The Fifth Assessment Synthesis Report of the Climate Change 2014. Geneva, Switzerland.

Iskra, I., & Droste, R. (2008). Parameter uncertainty of a watershed model. *Canadian Water Resources Journal, 33*(1), 5-22.

IWHR. (2005). Investigation on Current Drinking Water Supply Mechanism in Chongzhou. Report of China Institute of Water Resources and Hydropower Research, Beijing, China.

Jain, S.K., Kumar, N., Ahmad, T., & Kite, G. (1998). SLURP model and GIS for estimation of runoff in a part of Satluj catchment, India. *Hydrological Sciences Journal, 43*(6),

875-884.

Janssen, P., Heuberger, P., & Sanders, R. (1992). UNCSAM 1.1: A Software Package for Sensitivity and Uncertainty Analysis. Manual. *RIVM Rapport 959101004*.

Jiang, T., Chen, Y.D., Xu, C.-y., Chen, X., Chen, X., & Singh, V.P. (2007). Comparison of hydrological impacts of climate change simulated by six hydrological models in the Dongjiang Basin, South China. *Journal of Hydrology, 336*(3-4), 316-333.

Jin, X., Xu, C.-Y., Zhang, Q., & Singh, V. (2010). Parameter and modeling uncertainty simulated by GLUE and a formal Bayesian method for a conceptual hydrological model. *Journal of Hydrology, 383*(3), 147-155.

Jing, L. (2009). *Field investigation and hydrological modelling of a sub-arctic wetland system by SLURP and WATFLOOD.* (M.Eng. Thesis), Faculty of Engineering and Applied Science, Memorial University of Newfoundland, St. John's, NL, Canada.

Jing, L., & Chen, B. (2011a). Hydrological modeling of subartic wetlands: comparison between SLURP and WATFLOOD. *Environmental Engineering Science, 28*(7), 521-533.

Jing, L., & Chen, B. (2011b). Field investigation and hydrological modelling of a subarctic wetland-the Deer River watershed. *Journal of Environmental Informatics, 17*(1), 36-45.

Johanson, R.C., & Davis, H.H. (1980). *Users manual for hydrological simulation program-Fortran (HSPF)* (Vol. 80): Environmental Research Laboratory, Office of Research and Development, US Environmental Protection Agency.

Kannan, N., Rajakumar, A., & Rengasamy, G. (2004). Optimisation of process parameters for adsorption of metal ions on straw carbon by using response surface methodology.

Environmental technology, 25(5), 513-522.

Karimi, P., Abdollahi, H., Aslan, N., Noaparast, M., & Shafaei, S. (2010). Application of response surface method and central composite design for modeling and optimization of gold and silver recovery in cyanidation process. *Mineral Processing & Extractive Metallurgy Review, 32*(1), 1-16.

Kavetski, D., Franks, S.W., & Kuczera, G. (2002). Confronting input uncertainty in environmental modelling. *Calibration of watershed models*, 49-68.

Kavetski, D., Kuczera, G., & Franks, S.W. (2006). Bayesian analysis of input uncertainty in hydrological modeling: 2. Application. *Water Resources Research, 42*(3).

Kay, A.L., Davies, H.N., Bell, V.A., & Jones, R.G. (2009). Comparison of uncertainty sources for climate change impacts: flood frequency in England. *Climatic Change, 92*(1), 41-63.

Khan, M.S., Coulibaly, P., & Dibike, Y. (2006a). Uncertainty analysis of statistical downscaling methods. *Journal of Hydrology, 319*(1-4), 357-382.

Khan, M.S., Coulibaly, P., & Dibike, Y. (2006b). Uncertainty analysis of statistical downscaling methods using Canadian Global Climate Model predictors. *Hydrological Processes, 20*(14), 3085-3104.

Khawas, A., Banerjee, A., & Mukhopadhyay, S. (2011). A response surface method for design space exploration and optimization of analog circuits. Conference proceedings, 2011 IEEE Computer Society Annual Symposium on VLSI. .

King, D.M., & Perera, B.J.C. (2013). Morris method of sensitivity analysis applied to assess the importance of input variables on urban water supply yield–a case study. *Journal of Hydrology, 477*, 17-32.

Kite, G. (1975). Performance of two deterministic hydrological models. *IASH-AISH Publication, 115*, 136-142.

Kite, G. (1998). Manual for the SLURP hydrological model. *NHRI, saskatoon, Canada*.

Kite, G.W. (1997). Manual for the SLURP hydrological model, V.11. National Hydrology Research Institute, saskatoon, Canada.

Kouwen, N. (1998). WATFLOOD users manual. *Water Resources Group, University of Waterloo.(Available at the University of Waterloo, Waterloo, Canada, Department of Civil Engineering.)*.

Kuczera, G., & Parent, E. (1998). Monte Carlo assessment of parameter uncertainty in conceptual catchment models: the Metropolis algorithm. *Journal of Hydrology, 211*(1), 69-85.

Kuczera, G., Kavetski, D., Renard, B., & Thyer, M. (2007). Bayesian total error analysis for hydrologic models: Markov Chain Monte Carlo methods to evaluate the posterior distribution. *Mod. and Simul. Soc. of Aust. and NZ, Christchurch, NZ.*

Kwak, J.-S. (2005). Application of Taguchi and response surface methodologies for geometric error in surface grinding process. *International journal of machine tools and manufacture, 45*(3), 327-334.

Legates, D.R., & McCabe Jr, G.J. (1999). Evaluating the use of "goodness-of-fit" measures in hydrologic and hydroclimatic model validation. *Water Resources Research, 35*(1), 233-241.

Li, L., Xia, J., Xu, C.-Y., & Singh, V.P. (2010). Evaluation of the subjective factors of the GLUE method and comparison with the formal Bayesian method in uncertainty assessment of hydrological models. *Journal of Hydrology, 390*(3-4), 210-221.

Li, P., Wu, H.J., & Chen, B. (2013). RSW-MCFP: A Resource-Oriented Solid Waste Management System for a Mixed Rural-Urban Area through Monte Carlo Simulation-Based Fuzzy Programming. *Mathematical Problems in Engineering, 2013*, 1-15.

Li, Y.M., Li, Y.L., & Yu, S.M. (2008). Design optimization of a current mirror amplifier integrated circuit using a computational statistics technique. *Mathematics and Computers in Simulation, 79*(4), 1165-1177.

Li, Z.L., Chen, B., Wu, H.J., & Ye, X.D. (2015a). A hybrid Stochastic-Design of Experiment aided parameterization method for modeling aquifer NAPL contaminations. . *Environmental Modeling and Assessment, submitted*.

Li, Z.L., Chen, B., Wu, H.J., & Ye, X.D. (2015b). Modeling bio-surfactant enhanced aquifer remediation based on a hybrid Stochastic-Design of Experiment aided parameterization method. . *Journal of Environmental Engineering, submitted*.

Liebscher, H.J. (1993). Hydrology for the water management of large river basins. *Hydrological Sciences Journal, 38*(1), 1-13.

Liu, Y., Chen, J., & Du, P. (2002). [Parameters identification and uncertainty analysis for environmental model]. *Huan jing ke xue= Huanjing kexue/[bian ji, Zhongguo ke xue yuan huan jing ke xue wei yuan hui" Huan jing ke xue" bian ji wei yuan hui.], 23*(6), 6-10.

Liu, Z.J., & Weller, D.E. (2008). A stream network model for integrated watershed modeling. *Environmental Modeling & Assessment, 13*(2), 291-303.

Lopes, V.L. (1996). On the effect of uncertainty in spatial distribution of rainfall on catchment modelling. *Catena, 28*(1), 107-119.

MacLean, A. (2005). Statistical evaluation of WATFLOOD. Department of Civil and Environmental Engineering, University of Waterloo, On, Canada.

Maidment, D. (1993). Handbook of applied hydrology. *McGrawHill Book Company, New York.*

Makowski, D., Wallach, D., & Tremblay, M. (2002). Using a Bayesian approach to parameter estimation; comparison of the GLUE and MCMC methods. *Agronomie, 22*(2), 191-203.

Manetsch, T.J. (1990). Toward efficient global optimization in large dynamic systems-The adaptive complex method. *Systems, Man and Cybernetics, IEEE Transactions on, 20*(1), 257-261.

Manson, H.R. (2003). *Uncertainty and sensitivity analysis of GIS based continuous hydrological modeling.* (Ph.D Thesis), Ryerson University, Ontario, Canada.

Mantovan, P., & Todini, E. (2006). Hydrological forecasting uncertainty assessment: Incoherence of the GLUE methodology. *Journal of Hydrology, 330*(1-2), 368-381.

McCuen, R.H. (1974). A sensitivity and error analysis cf procedures used for estimating evaporation1: Wiley Online Library.

McKay, M.D., Beckman, R.J., & Conover, W.J. (1979). Comparison of three methods for selecting values of input variables in the analysis of output from a computer code. *Technometrics, 21*(2), 239-245.

McMichael, C.E., Hope, A.S., & Loaiciga, H.A. (2006). Distributed hydrological modelling in California semi-arid shrublands: MIKE SHE model calibration and uncertainty estimation. *Journal of Hydrology, 317*(3-4), 307-324.

Melching, C.S. (1995). Reliability Estimation. In V. P. Singh (Ed.), *Computer Models of*

Watershed Hydrology (pp. 69-118). USA: Water Resources Publications: Colorado.

Minville, M., Brissette, F., & Leconte, R. (2008a). Uncertainty of the impact of climate change on the hydrology of a nordic watershed. *Journal of Hydrology, 358*(1-2), 70-83.

Minville, M., Brissette, F., & Leconte, R. (2008b). Uncertainty of the impact of climate change on the hydrology of a nordic watershed. *Journal of Hydrology, 358*(1), 70-83.

Minville, M., Brissette, F., & Leconte, R. (2010). Impacts and uncertainty of climate change on water resource management of the Peribonka river system. *Journal of Water Resources Planning and Management, 136*(3), 376.

Montanari, A. (2005). Large sample behaviors of the generalized likelihood uncertainty estimation (GLUE) in assessing the uncertainty of rainfall-runoff simulations. *Water Resources Research, 41*(8), n/a-n/a.

Montgomery, D.C. (2008). *Design and analysis of experiments*: John Wiley & Sons.

Moradkhani, H., & Sorooshian, S. (2008). General review of rainfall-runoff modeling: model calibration, data assimilation, and uncertainty analysis *Hydrological modelling and the water cycle* (pp. 1-24): Springer.

Moreda, F., Koren, V., Zhang, Z., Reed, S., & Smith, M. (2006). Parameterization of distributed hydrological models: learning from the experiences of lumped modeling. *Journal of Hydrology, 320*(1-2), 218-237.

Morris, M.D. (1991). Factorial sampling plans for preliminary computational experiments. *Technometrics, 33*(2), 161-174.

Mpelasoka, F.S., & Chiew, F.H.S. (2009). Influence of Rainfall Scenario Construction Methods on Runoff Projections. *Journal of Hydrometeorology, 10*(5), 1168-1183.

Mugunthan, P., & Shoemaker, C.A. (2006). Assessing the impacts of parameter uncertainty for computationally expensive groundwater models. *Water Resources Research, 42*(10).

Muleta, M.K., & Nicklow, J.W. (2005). Sensitivity and uncertainty analysis coupled with automatic calibration for a distributed watershed model. *Journal of Hydrology, 306*(1), 127-145.

Nash, J.E., & Sutcliffe, J.V. (1970). River flow forecasting through conceptual models part I—A discussion of principles. *Journal of Hydrology, 10*(3), 282-290.

Neitsch, S.L., Arnold, J.G., Kiniry, J.R., & Williams, J.R. (2011). Soil and Water Assessment Tool Theoretical Documentation, Version 2009. Grassland, soil and water research service, Texas, the United States.

Nelder, J.A., & Mead, R. (1965). A simplex method for function minimization. *The computer journal, 7*(4), 308-313.

Oubeidillah, A.A., Kao, S.-C., Ashfaq, M., Naz, B.S., & Tootle, G. (2014). A large-scale, high-resolution hydrological model parameter data set for climate change impact assessment for the conterminous US. *Hydrology and Earth System Sciences, 18*(1), 67-84.

Pappenberger, F., Beven, K., Horritt, M., & Blazkova, S. (2005). Uncertainty in the calibration of effective roughness parameters in HEC-RAS using inundation and downstream level observations. *Journal of Hydrology, 302*(1-4), 46-69.

Paturel, J.E., Servat, E., & Vassiliadis, A. (1995). Sensitivity of conceptual rainfall-runoff algorithms to errors in input data—case of the GR2M model. *Journal of Hydrology, 168*(1), 111-125.

Piper, B. (1989). Sensitivity of Penman estimates of evaporation to errors in input data. *Agricultural Water Management, 15*(3), 279-300.

Plesu, N., Grozav, I., Iliescu, S., & Ilia, G. (2009). Acrylic blends based on polyaniline. Factorial design. *Synthetic Metals, 159*(5), 501-507.

Poulin, A., Brissette, F., Leconte, R., Arsenault, R., & Malo, J.-S. (2011). Uncertainty of hydrological modelling in climate change impact studies in a Canadian, snow-dominated river basin. *Journal of Hydrology, 409*(3-4), 626-636.

Prudhomme, C., & Davies, H. (2009). Assessing uncertainties in climate change impact analyses on the river flow regimes in the UK. Part 2: future climate. *Climatic Change, 93*(1), 197-222.

Qian, B., Gameda, S., de Jong, R., Falloon, P., & Gornall, J. (2010). Comparing scenarios of Canadian daily climate extremes derived using a weather generator. *Climate research (Open Access for articles 4 years old and older), 41*(2), 131.

Refsgaard, J.C. (1997). Parameterisation, calibration and validation of distributed hydrological models. *Journal of Hydrology, 198*(1-4), 69-97.

Rossman, L.A. (2010). *Storm water management model user's manual, version 5.0*: National Risk Management Research Laboratory, Office of Research and Development, US Environmental Protection Agency Cincinnati.

Rostamian, R., Jaleh, A., Afyuni, M., Mousavi, S.F., Heidarpour, M., Jalalian, A., & Abbaspour, K.C. (2008). Application of a SWAT model for estimating runoff and sediment in two mountainous basins in central Iran. *Hydrological Sciences Journal, 53*(5), 977-988.

Rowell, D.P. (2006). A Demonstration of the Uncertainty in Projections of UK Climate

Change Resulting from Regional Model Formulation. *Climatic Change, 79*(3), 243-257.

Salathé, E.P. (2003). Comparison of various precipitation downscaling methods for the simulation of streamflow in a rainshadow river basin. *International Journal of Climatology, 23*(8), 887-901.

Saltelli, A., Tarantola, S., & Chan, K.-S. (1999). A quantitative model-independent method for global sensitivity analysis of model output. *Technometrics, 41*(1), 39-56.

Saltelli, A., Chan, K., & Scott, E. (2000). *Sensitivity Analysis*. NY, the United States: John Wiley and Sons.

Samadi, S., Carbone, G.J., Mahdavi, M., Sharifi, F., & Bihamta, M.R. (2012). Statistical downscaling of climate data to estimate streamflow in a semi-arid catchment. *Hydrology and Earth System Sciences Discussions, 9*(4), 4869-4918.

Schoof, J.T., & Pryor, S. (2001). Downscaling temperature and precipitation: A comparison of regression ‐ based methods and artificial neural networks. *International Journal of Climatology, 21*(7), 773-790.

Scott, D.T., Gooseff, M.N., Bencala, K.E., & Runkel, R.L. (2003). Automated calibration of a stream solute transport model: implications for interpretation of biogeochemical parameters. *Journal of the North American Benthological Society, 22*(4), 492-510.

Sennikovs, J., & Bethers, U. (2009). Statistical downscaling method of regional climate model results for hydrological modelling. Conference proceedings, Proc. 18 th World IMACS/MODSIM Congress, Cairns, Australia.

Seo, D.J., Perica, S., Welles, E., & Schaake, J.C. (2000). Simulation of precipitation fields from probabilistic quantitative precipitation forecast. *Journal of Hydrology, 239*(1),

203-229.

Setegn, S.G., Srinivasan, R., Melesse, A.M., & Dargahi, B. (2010). SWAT model application and prediction uncertainty analysis in the Lake Tana Basin, Ethiopia. *Hydrological Processes, 24*(3), 357-367.

Shen, Z.Y., Hong, Q., Yu, H., & Liu, R. (2008). Parameter uncertainty analysis of the non-point source pollution in the Daning River watershed of the Three Gorges Reservoir Region, China. *Science of the total environment, 405*(1), 195-205.

Shen, Z.Y., Hong, Q., Yu, H., & Niu, J.F. (2010). Parameter uncertainty analysis of non-point source pollution from different land use types. *Science of the total environment, 408*(8), 1971-1978.

Shen, Z.Y., Chen, L., & Chen, T. (2012). Analysis of parameter uncertainty in hydrological and sediment modeling using GLUE method: a case study of SWAT model applied to Three Gorges Reservoir Region, China. *Hydrology and Earth System Sciences, 16*(1), 121-132.

Shrestha, D.L., Kayastha, N., & Solomatine, D.P. (2009). A novel approach to parameter uncertainty analysis of hydrological models using neural networks. *Hydrology and Earth System Sciences, 13*(7), 1235-1248.

Simate, G.S., Ndlovu, S., & Gericke, M. (2009). Bacterial leaching of nickel laterites using chemolithotrophic microorganisms: process optimisation using response surface methodology and central composite rotatable design. *Hydrometallurgy, 98*(3), 241-246.

Singh, V.P., & Woolhiser, D.A. (1976). Sensitivity of linear and nonlinear surface runoff models to input errors. *Journal of Hydrology, 29*(3), 243-249.

Singh, V.P. (1977). Sensitivity of some runoff models to errors in rainfall excess. *Journal of Hydrology, 33*(3), 301-318.

Singh, V.P. (1995). Watershed Modeling. *Computer models of watershed hydrology*: Water Resources Publications.

Singh, V.P., & Frevert, D.K. (2003). Watershed Modeling. Conference proceedings, World Water & Environmental Resources Congress 2003.

Smithson, M. (2012). *Ignorance and uncertainty: emerging paradigms*: Springer Science & Business Media.

Sobol's, I.M. (1993). Sensitivity analysis for nonlinear mathematical models. *Mathematical Modeling and Computational Experiment, 1*(4), 407-414.

Solman, S.A., & Nuñez, M.N. (1999). Local estimates of global climate change: a statistical downscaling approach. *International Journal of Climatology, 19*(8), 835-861.

Song, X., Zhang, J., Zhan, C., Xuan, Y., Ye, M., & Xu, C. (2015). Global sensitivity analysis in hydrological modeling: Review of concepts, methods, theoretical framework, and applications. *Journal of Hydrology, 523*, 739-757.

Sorooshian, S., Duan, Q., & Gupta, V.K. (1993). Calibration of rainfall‐runoff models: Application of global optimization to the Sacramento Soil Moisture Accounting Model. *Water Resources Research, 29*(4), 1185-1194.

Srikanthan, R., & McMahon, T. (2001). Stochastic generation of annual, monthly and daily climate data: A review. *Hydrology and Earth System Sciences Discussions, 5*(4), 653-670.

St. Laurent, M.E., & Valeo, C. (2007). Large-scale distributed watershed modelling for reservoir operations in cold boreal regions. *Canadian Journal of Civil Engineering,*

34(4), 525-538.

Stedinger, J.R., Vogel, R.M., Lee, S.U., & Batchelder, R. (2008). Appraisal of the generalized likelihood uncertainty estimation (GLUE) method. *Water Resources Research, 44*(12).

Su, M., Stolte, W.J., & Van der Kamp, G. (2000). Modelling Canadian prairie wetland hydrology using a semi - distributed streamflow model. *Hydrological Processes, 14*(14), 2405-2422.

Tadesse, A., & Anagnostou, E.N. (2005). A statistical approach to ground radar-rainfall estimation. *Journal of Atmospheric and Oceanic Technology, 22*(11), 1720-1732.

Teutschbein, C., Wetterhall, F., & Seibert, J. (2011). Evaluation of different downscaling techniques for hydrological climate-change impact studies at the catchment scale. *Climate Dynamics, 37*(9), 2087-2105.

Thiemann, M., Trosset, M., Gupta, H., & Sorooshian, S. (2001). Bayesian recursive parameter estimation for hydrologic models. *Water Resources Research, 37*(10), 2521-2535.

Thorne, R., & Woo, M.K. (2006). Efficacy of a hydrologic model in simulating discharge from a large mountainous catchment. *Journal of Hydrology, 330*(1), 301-312.

Thyer, M., Renard, B., Kavetski, D., Kuczera, G., Franks, S.W., & Srikanthan, S. (2009). Critical evaluation of parameter consistency and predictive uncertainty in hydrological modeling: A case study using Bayesian total error analysis. *Water Resources Research, 45*(12).

Tofiq, F.A., & Guven, A. (2014). Prediction of design flood discharge by statistical downscaling and General Circulation Models. *Journal of Hydrology, 517*, 1145-1153.

Tripp, D.R., & Niemann, J.D. (2008). Evaluating the parameter identifiability and structural

validity of a probability-distributed model for soil moisture. *Journal of Hydrology, 353*(1), 93-108.

USDA Soil Conservation Service. (1972). *SCS national engineering handbook, section 4: hydrology*. USDA, SCS, Washington, USA.

Van Griensven, A., & Meixner, T. (2006). Methods to quantify and identify the sources of uncertainty for river basin water quality models. *Water Science & Technology, 53*(1), 51-59.

Van Griensven, A., Meixner, T., Grunwald, S., Bishop, T., Diluzio, M., & Srinivasan, R. (2006). A global sensitivity analysis tool for the parameters of multi-variable catchment models. *Journal of Hydrology, 324*(1), 10-23.

Van Griensven, A., & Meixner, T. (2007). A global and efficient multi-objective auto-calibration and uncertainty estimation method for water quality catchment models. *Journal of Hydroinformatics, 9*(4), 277-291.

Vázquez, R., Beven, K., & Feyen, J. (2009). GLUE based assessment on the overall predictions of a MIKE SHE application. *Water Resources Management, 23*(7), 1325-1349.

Verma, A.K., Jha, M.K., & Mahana, R.K. (2010). Evaluation of HEC-HMS and WEPP for simulating watershed runoff using remote sensing and geographical information system. *Paddy and Water Environment, 8*(2), 131-144.

von Storch, H., Zorita, E., & Cubasch, U. (1993). Downscaling of Global Climate Change Estimates to Regional Scales: An Application to Iberian Rainfall in Wintertime. *Journal of Climate, 6*(6), 1161-1171.

Vrugt, J.A., Gupta, H.V., Bouten, W., & Sorooshian, S. (2003). A Shuffled Complex

Evolution Metropolis algorithm for optimization and uncertainty assessment of hydrologic model parameters. *Water Resources Research, 39*(8), n/a-n/a.

Vrugt, J.A., & Robinson, B.A. (2007). Treatment of uncertainty using ensemble methods: Comparison of sequential data assimilation and Bayesian model averaging. *Water Resources Research, 43*(1).

Vrugt, J.A., Diks, C.G.H., & Clark, M.P. (2008). Ensemble Bayesian model averaging using Markov Chain Monte Carlo sampling. *Environmental Fluid Mechanics, 8*(5-6), 579-595.

Vrugt, J.A., Ter Braak, C.J., Gupta, H.V., & Robinson, B.A. (2009). Equifinality of formal (DREAM) and informal (GLUE) Bayesian approaches in hydrologic modeling? *Stochastic Environmental Research and Risk Assessment, 23*(7), 1011-1026.

Wang, Q.J. (1991). The genetic algorithm and its application to calibrating conceptual rainfall‐runoff models. *Water Resources Research, 27*(9), 2467-2471.

Wilby, R., Charles, S., Zorita, E., Timbal, B., Whetton, P., & Mearns, L. (2004). Guidelines for use of climate scenarios developed from statistical downscaling methods.

Wilby, R.L., & Wigley, T.M.L. (1997). Downscaling general circulation model output: a review of methods and limitations. *Progress in Physical Geography, 21*(4), 530-548.

Wilby, R.L., Hassan, H., & Hanaki, K. (1998). Statistical downscaling of hydrometeorological variables using general circulation model output. *Journal of Hydrology, 205*(1), 1-19.

Wilby, R.L., Dawson, C.W., & Barrow, E.M. (2002). sdsm — a decision support tool for the assessment of regional climate change impacts. *Environmental Modelling and Software, 17*(2), 145-157.

Wilby, R.L., & Harris, I. (2006). A framework for assessing uncertainties in climate change impacts: Low‐flow scenarios for the River Thames, UK. *Water Resources Research, 42*(2).

Wilby, R.L., & Dawson, C.W. (2007). SDSM 4.2 -- A decision support tool for the assessment of regional climate change impacts. Loughborough Unuiversity, UK.

Wilks, D.S. (2010). Use of stochastic weathergenerators for precipitation downscaling. *Wiley Interdisciplinary Reviews: Climate Change, 1*(6), 898-907.

Winchell, M., Srinivasan, R., Luzio, M.D., & Arnold., J. (2009). *ARCSWAT 2.3.4 interface for SWAT2005*. Grassland, soil and water research service, Texas, the United States.

Wood, A.W., Leung, L.R., Sridhar, V., & Lettenmaier, D.P. (2004). Hydrologic Implications of Dynamical and Statistical Approaches to Downscaling Climate Model Outputs. *Climatic Change, 62*(1), 189-216.

Wu, H., Lye, L.M., & Chen, B. (2012). A design of experiment aided sensitivity analysis and parameterization for hydrological modeling. *Canadian Journal of Civil Engineering, 39*(4), 460-472.

Wu, H., & Chen, B. (2014a). Evaluating uncertainty estimates in distributed hydrological modeling for the Wenjing River watershed in China by GLUE, SUFI-2, and ParaSol methods. *Ecological Engineering*.

Wu, H., & Chen, B. (2014b). Uncertainty analysis for propagation effects from statistical downscaling to hydrological modeling. Conference proceedings, International Conference on Marine and Freshwater Environments (iMFE), St. John's, Newfoundland, CA.

Wu, H.J., Chen, B., & Li, P. (2013). Comparison of Sequential Uncertainty Fitting Algorithm

(SUFI-2) and Parameter Solution (ParaSol) Method for Analyzing Uncertainties in Distributed Hydrological Modeling - A Case Study. Conference proceedings, SCE 2013 General Conference proceeding, Montreal, Quebec, CA.

Xu, C.y. (1999). From GCMs to river flow: a review of downscaling methods and hydrologic modelling approaches. *Progress in Physical Geography, 23*(2), 229-249.

Xu, C.Y., & Singh, V.P. (2004). Review on regional water resources assessment models under stationary and changing climate. *Water Resources Management, 18*(6), 591-612.

Xu, H. (2009). Algorithmic construction of efficient fractional factorial designs with large run sizes. *Technometrics, 51*(3), 262-277.

Xue, C. (2011). *SWAT-aided surface runoff and sediment yield modeling and parameter uncertainty analysis.* (Master Thesis), North China Electric Power University, Beijing, China.

Xue, C., Chen, B., & Wu, H. (2014). Parameter Uncertainty Analysis of Surface Flow and Sediment Yield in the Huolin Basin, China. *Journal of Hydrologic Engineering, 19*, 1124-1236.

Yang, J., Reichert, P., & Abbaspour, K.C. (2007a). Bayesian uncertainty analysis in distributed hydrologic modeling: a case study in the Thur River basin (Switzerland). *Water Resources Research, 43*(10), doi:10.1029/2006WR005497.

Yang, J., Reichert, P., Abbaspour, K.C., & Yang, H. (2007b). Hydrological modelling of the Chaohe Basin in China: Statistical model formulation and Bayesian inference. *Journal of Hydrology, 340*(3), 167-182.

Yang, J., Reichert, P., Abbaspour, K.C., Xia, J., & Yang, H. (2008). Comparing uncertainty

analysis techniques for a SWAT application to the Chaohe Basin in China. *Journal of Hydrology, 358*(1), 1-23.

Yen, H., Wang, X., Fontane, D.G., Harmel, R.D., & Arabi, M. (2014). A framework for propagation of uncertainty contributed by parameterization, input data, model structure, and calibration/validation data in watershed modeling. *Environmental Modelling & Software, 54*, 211-221.

Zak, S.K., & Beven, K.J. (1999). Equifinality, sensitivity and predictive uncertainty in the estimation of critical loads. *Science of the total environment, 236*(1), 191-214.

Zhan, C.S., Song, X.M., Xia, J., & Tong, C. (2013). An efficient integrated approach for global sensitivity analysis of hydrological model parameters. *Environmental Modelling & Software, 41*, 39-52.

Zhang, X., Srinivasan, R., & Bosch, D. (2009). Calibration and uncertainty analysis of the SWAT model using Genetic Algorithms and Bayesian Model Averaging. *Journal of Hydrology, 374*(3-4), 307-317.

Zhang, X.C. (2005). Spatial downscaling of global climate model output for site-specific assessment of crop production and soil erosion. *Agricultural and Forest Meteorology, 135*(1), 215-229.

Zhang, X.C., & Liu, W.Z. (2005). Simulating potential response of hydrology, soil erosion, and crop productivity to climate change in Changwu tableland region on the Loess Plateau of China. *Agricultural and Forest Meteorology, 131*(3), 127-142.

Zhang, Y.J., & Chen, B. (2008). Modeling of non-point source pollution in wetland systems—A case study in the HuoLin River watershed. *Journal of North China Electric Power University*, Beijing, China.

APPENDIX

THE JAVA CODE FOR DOWNSCALING STUDIES IN THE UPSTREAM OF THE WENJING WATERSHED CASE

```
/**
 * @(#)MySwat.java
 * * MySwat application
 * * @author Hongjing Wu
 * @version 1.00 2013/3/27
 * * @file description:
 *
 *        This is the program entrance, contains the main method
 *        Internally gathering all required parameters
 *        Change each properties' value in all the files according to the input parameters.
 *        Recalculate the SWAT program by input times , and gather the new results.
 *
 */
import java.io.*;
import javax.swing.JOptionPane;

public class MySwat {
   private static String currentLine;
   private static String[] currentParas;

   // main() method, to start the program.
   // Welcome !!!
   public static void main(String[] args) {
         System.out.println("Welcome to MySWAT!");
         String singlePara = null;
         String[] paras = null;

                  // Make sure input contains 5 parameters then let go
         do {
                  singlePara = JOptionPane.showInputDialog(null,
               "Parameter row number\n" +
               "Parameter file directory and name \n" +
               "Swat2009 folder directory \n" +
               "Directory of replaced files \n" +
               "Times of replace",
               "Input parameter", JOptionPane.QUESTION_MESSAGE);
         paras = singlePara.split(" ");
         } while (paras == null || paras.length != 5);

      String comparableFilePath = JOptionPane.showInputDialog(null,
            "Please input comparable result file path: ",
            "Comparable File", JOptionPane.QUESTION_MESSAGE);

      FileChange fc = new FileChange();
         ChangeProperties cp = new ChangeProperties(fc);
         ExecuteSwat es = new ExecuteSwat();
```

```
// paras[0] row number
// paras[1] input file path with file name
// paras[2] mgt, hru, sol...folder path
// paras[3] Replaced source files path
// paras[4] Replaced source folder number
System.out.println("Parameter 1 : " + paras[0]);
System.out.println("Parameter 2 : " + paras[1]);
System.out.println("Parameter 3 : " + paras[2]);
System.out.println("Parameter 4 : " + paras[3]);
System.out.println("Parameter 5 : " + paras[4]);

if(comparableFilePath.endsWith("txt")) {
	System.out.println("Comparable File : " + comparableFilePath);
	es.readComparableFile(comparableFilePath);
}

ChangeProperties cp2 = new ChangeProperties(fc, paras[2]);
int rowNo = Integer.parseInt(paras[0]);
try {
	System.out.println(paras[1]);
	RandomAccessFile raf = new RandomAccessFile(paras[1], "rw");
	String titleLine = raf.readLine();
	String[] titleParas = titleLine.split("\\s+");
	char[] titleChars = new char[11];
	for(int i = 0; i < 11; i++) {
		titleChars[i] = titleParas[i].charAt(0);
		System.out.println(titleChars[i]);
	}

	currentLine = null;
	currentParas = null;


	for(int i = 0; i < rowNo; i++) {

		String sourceFolderPath = paras[3];
		if(sourceFolderPath != null && !sourceFolderPath.isEmpty()
&& !sourceFolderPath.endsWith("\\")) {
		sourceFolderPath = sourceFolderPath + "\\\\";
	}

		fc.copyDirectory(paras[3], "C:\\MySwatTest");
		currentLine = raf.readLine();
```

```
                                for(int fileCopyNo = 0; fileCopyNo <
Integer.parseInt(paras[4]); fileCopyNo++) {

                                fc.copyOverrideFiles("C:\\MySwatTest", paras[2]);

                                currentParas = currentLine.split("\\s+");
                                float[] values = new float[11];
                                for(int j = 0; j < 11; j++) {
                                        values[j] = Float.parseFloat(currentParas[j]);
                                        System.out.println(values[j]);
                                }
                                cp2.changeValue(titleChars, values);
                                es.executeSwat2009(paras[2]);
                                        es.gatherOutput(paras[2]);
                                        System.out.println("<<<<<<<<<<<<<  " + (i+1) + "
parameter, " + (fileCopyNo + 1) + " folder is done  >>>>>>>>>>>>>");
                        }
                        }
                } catch (Exception e) {
                        e.printStackTrace();
                }
        }
}
```

```
/**
 * @(#)FileChange.java
 *
 *
 * @author Hongjing Wu
 * @version 1.00 2013/3/27
 *
 * @file description:
 *
 *        This class contains file operation functions
 *  1. Functions to do file and directory copy, move and deletion.
 *        2. Function for updating the values of each property.
 */
import java.io.*;
import java.util.ArrayList;
import java.util.Iterator;
import java.util.Calendar;
import java.util.Date;
import java.util.List;
import java.util.TimeZone;
import java.nio.channels.FileChannel;

public class FileChange {

        public FileChange(){}

        // Update the files base on the directory of the folder, extention name, parameter
name and the new value
   public void updateFiles(String path, String ext, float newValue, String para) {
        ArrayList<File> files = getExtFiles(path, ext);
        for(File file : files) {
                updateValue(newValue, para, file.getName());
        }
   }

   // Get all the files with the same extension name in the path directory
   public ArrayList<File> getExtFiles(String path, String ext){
      // get file list where the path has
      File fileInDir = new File(path);
      if(!fileInDir.exists()) {
         return null;
      }
      // get the folder list
      File[] fileArray = fileInDir.listFiles();
      ArrayList<File> extFiles = new ArrayList<File>();
      for(int i=0;i<fileArray.length;i++){
```

```
            if(fileArray[i].isFile()){
               // only take file name
               // System.out.println("^^^^^" + array[i].getName());
               // take file path and name
               // System.out.println("#####" + array[i]);
               // take file path and name
               // System.out.println("*****" + array[i].getPath());
                     if(fileArray[i].getName().endsWith(ext)
&& !fileArray[i].getName().equals("output.hru")
&& !fileArray[i].getName().equals("outputb.hru")) {
                              extFiles.add(fileArray[i]);
                     }
            }else if(fileArray[i].isDirectory()){
               //getFile(array[i].getPath());
            }
         }
         return extFiles;
      }

      // update the value of 1 parameter in 1 file, except the sol file. (SOL file change is in the
next function: updateSolValue)
      public void updateValue(float newValue, String para, String fileName) {

            if(fileName.endsWith("sol")) {
                     updateSolValue(newValue, "SOL_AWC_1", fileName);
                     return;
            }

            // check if the file exist
            File file = new File(fileName);
            if(!file.exists()) {
                     System.out.println("File does not exist: " + fileName);
                     return;
            }
            try {
                     RandomAccessFile raf = new RandomAccessFile(fileName, "rw");
                     String str = null;
                     do{
                              try{
                                       str = raf.readLine();
                              } catch(IOException ioe){
                                       ioe.printStackTrace();
                              }

                     } while(str.indexOf(para) == -1);
                     if (str == null) {
```

```
                        return;
                } else {
                        String newValueStr = String.valueOf(newValue);
                        StringBuffer newStr = new StringBuffer(str);
                        int numLen = newValueStr.length();
                        int strLen = str.length();
                        int linePos = str.indexOf("|");
                        int whiteLen = str.trim().indexOf("|") - str.trim().indexOf("  ");
                        int i = numLen;
                        int pos = linePos - whiteLen;
                        for(; i>0; i--, pos--) {
                                newStr.replace(pos-1, pos,
String.valueOf(newValueStr.charAt(i-1)));
                        }
                        while(pos > 0) {
                                newStr.replace(pos-1, pos, String.valueOf(" "));
                                pos--;
                        }
                        raf.seek(raf.getFilePointer() - str.length());
                        raf.writeBytes(newStr.substring(2).toString());
                }
                raf.close();
        } catch(FileNotFoundException ffe){
                ffe.printStackTrace();
        } catch(IOException ioe) {
                ioe.printStackTrace();
        }
    }
    // update the value in sol file
    public void updateSolValue(float newValue, String para, String fileName) {
        // check if the file exist
        File file = new File(fileName);
        if(!file.exists()) {
                System.out.println("File does not exist: " + fileName);
                return;
        }
        if(para.equals("SOL_AWC_1")) {
                try {
                        RandomAccessFile raf = new RandomAccessFile(fileName,
"rw");
                        String str = null;
                        do{
                                try{
                                        str = raf.readLine();
                                } catch(IOException ioe){
                                        ioe.printStackTrace();
```

```
                        }

                    } while(str.indexOf("Ave. AW Incl. Rock Frag") == -1);
                    if (str == null || str.length() < 27) {
                        return;
                    } else {
                    String newValueStr = String.valueOf(newValue);
                    if(newValueStr.length() > 10) {
                        newValueStr = newValueStr.substring(0, 10);
                    }
                    if(newValueStr.contains("E")) {
                        newValueStr = newValueStr.substring(0,
newValueStr.indexOf("E"));
                    }

                    String valueOneTwo[] = str.substring(27).trim().split("\\s+");
                    String valueTwo = "";
                        if(valueOneTwo == null || valueOneTwo.length != 2) {
                            return;
                        }
                        valueTwo = valueOneTwo[1];

                        String spaceStr = "";
                        for(int len = 0; len < str.length() - 35 -
newValueStr.length() - valueTwo.length(); len++) {
                            spaceStr = spaceStr + " ";
                        }

                        raf.seek(raf.getFilePointer() - str.length() - 2);
                    raf.writeBytes(" Ave. AW Incl. Rock Frag  :       " +
newValueStr + spaceStr + valueTwo);
                    }
                    raf.close();
                } catch(FileNotFoundException ffe){
                    ffe.printStackTrace();
                } catch(IOException ioe) {
                    ioe.printStackTrace();
                }
        }
    }

    public void backupSourceFiles(String sourceFolderPath) {
        if(sourceFolderPath != null && !sourceFolderPath.isEmpty()
&& !sourceFolderPath.endsWith("\\")) {
            sourceFolderPath = sourceFolderPath + "\\\\";
        }
```

```
        String backupPath = sourceFolderPath + "temp" + "\\\\";

        File sourceDir = new File(sourceFolderPath);
        File[] sourceDirList = sourceDir.listFiles();

        if(sourceDirList != null) {
                for(File file : sourceDirList) {
                        FileChannel inputChannel = null;
                        FileChannel outputChannel = null;
                        try {
                                inputChannel = new FileInputStream(file).getChannel();
                                File outputFile = new File(backupPath + file.getName());
                                outputChannel = new
FileOutputStream(outputFile).getChannel();

                                outputChannel.transferFrom(inputChannel, 0,
inputChannel.size());
                                System.out.println("Done copy " + file.getAbsolutePath() + ",
deleting!");
                        } catch(Exception e) {
                                e.printStackTrace();
                        } finally {
                                try {
                                        inputChannel.close();
                                        outputChannel.close();
                                } catch(Exception e) {
                                        e.printStackTrace();
                                }
                        }
                }
        }
   }

   public void copyOverrideFiles(String sourceFolderPath, String targetFolderPath) {
        System.out.println("Copy start!");
        System.out.println("~~~~~~~~~~~~~~~~~~~~~~");

        if(sourceFolderPath != null && !sourceFolderPath.isEmpty()
&& !sourceFolderPath.endsWith("\\")) {
                sourceFolderPath = sourceFolderPath + "\\\\";
        }

        if(targetFolderPath != null && !targetFolderPath.isEmpty()
&& !targetFolderPath.endsWith("\\")) {
                targetFolderPath = targetFolderPath + "\\\\";
```

```
        }

        File sourceDir = new File(sourceFolderPath);
        File[] sourceDirList = sourceDir.listFiles();

        if(sourceDirList != null) {
                for(File folder : sourceDirList) {
                        if(folder.listFiles() != null || folder.listFiles().length == 0) {
                                File[] batchFiles = folder.listFiles();
                                for(File file : batchFiles) {
                                        FileChannel inputChannel = null;
                                        FileChannel outputChannel = null;
                                        try {
                                                inputChannel = new
FileInputStream(file).getChannel();
                                                File outputFile = new File(targetFolderPath +
file.getName());
                                                outputChannel = new
FileOutputStream(outputFile).getChannel();

                                                outputChannel.transferFrom(inputChannel, 0,
inputChannel.size());
                                                System.out.println("Done copy " +
file.getAbsolutePath() + ", deleting!");
                                        } catch(Exception e) {
                                                e.printStackTrace();
                                        } finally {
                                                try {
                                                        inputChannel.close();
                                                outputChannel.close();
                                                boolean fileDeleteStatus = file.delete();
                                               System.out.println("Delete " + fileDeleteStatus);
                                                System.out.println("--------------------");
                                                } catch (Exception e) {
                                                        e.printStackTrace();
                                                }
                                        }
                                }

                                // delete the folder after copy
                                if(folder.listFiles() == null || folder.listFiles().length == 0) {
                                        System.out.println("Folder copy completed, " +
folder.getAbsolutePath() + " is getting deleted!");
                                        folder.delete();
                                } else {
```

```
                                        System.out.println("Folder is not empty! " +
folder.getAbsolutePath());
                                    }
                                    break;
                                } else {
                                    System.out.println("Folder is empty, " +
folder.getAbsolutePath() + " is getting deleted!");
                                    folder.delete();
                                }
                            }
                        }
                    }

    public static void copyDirectory(String srcDirPath, String destDirPath) throws
IOException {
            File srcDir = new File(srcDirPath);
            File destDir = new File(destDirPath);
        copyDirectory(srcDir, destDir, true);
    }

    private static void copyDirectory(File srcDir, File destDir, boolean preserveFileDate)
throws IOException {
        if (srcDir == null) {
            throw new NullPointerException("Source must not be null");
        }
        if (destDir == null) {
            throw new NullPointerException("Destination must not be null");
        }
        if (srcDir.exists() == false) {
            throw new FileNotFoundException("Source '" + srcDir + "' does not exist");
        }
        if (srcDir.isDirectory() == false) {
            throw new IOException("Source '" + srcDir + "' exists but is not a directory");
        }
        if (srcDir.getCanonicalPath().equals(destDir.getCanonicalPath())) {
            throw new IOException("Source '" + srcDir + "' and destination '" + destDir + "' are
the same");
        }
        doCopyDirectory(srcDir, destDir, preserveFileDate);
    }

            private static void doCopyDirectory(File srcDir, File destDir, boolean
preserveFileDate) throws IOException {
                if (destDir.exists()) {
                    if (destDir.isDirectory() == false) {
```

```
                    throw new IOException("Destination '" + destDir + "' exists but is not a
directory");
                }
            } else {
                if (destDir.mkdirs() == false) {
                    throw new IOException("Destination '" + destDir + "' directory cannot be
created");
                }
                if (preserveFileDate) {
                    destDir.setLastModified(srcDir.lastModified());
                }
            }
            if (destDir.canWrite() == false) {
                throw new IOException("Destination '" + destDir + "' cannot be written to");
            }
            // recurse
            File[] files = srcDir.listFiles();
            if (files == null) {  // null if security restricted
                throw new IOException("Failed to list contents of " + srcDir);
            }
            for (int i = 0; i < files.length; i++) {
                File copiedFile = new File(destDir, files[i].getName());
                if (files[i].isDirectory()) {
                    doCopyDirectory(files[i], copiedFile, preserveFileDate);
                } else {
                    doCopyFile(files[i], copiedFile, preserveFileDate);
                }
            }
        }

        private static void doCopyFile(File srcFile, File destFile, boolean preserveFileDate)
throws IOException {
    if (destFile.exists() && destFile.isDirectory()) {
        throw new IOException("Destination '" + destFile + "' exists but is a directory");
    }

    FileInputStream input = new FileInputStream(srcFile);

    FileOutputStream output = new FileOutputStream(destFile);
    try {
        copy(input, output);
    } finally {
        closeQuietly(output);
    }

    if (srcFile.length() != destFile.length()) {
```

```
            throw new IOException("Failed to copy full contents from '" +
                    srcFile + "' to '" + destFile + "'");
        }
        if (preserveFileDate) {
                        destFile.setLastModified(srcFile.lastModified());
        }
            }

            private static int copy(InputStream input, OutputStream output) throws IOException
{
        byte[] buffer = new byte[1000];
        int count = 0;
        int n = 0;
        while (-1 != (n = input.read(buffer))) {
            output.write(buffer, 0, n);
            count += n;
        }
        return count;
    }

            private static void closeQuietly(OutputStream output) {
                try {
                    if (output != null) {
                        output.close();
                    }
                } catch (IOException ioe) {
                    // ignore
                    ioe.printStackTrace();
                }
            }
}
```

```
/**
 * @(#)ChangeProperties.java
 *
 *
 * @author HongjingWu
 * @version 1.00 2013/3/27
 *
 * @file description:
 *
 *        This class contains value calculation logic
 *
 */
import java.io.*;
import java.util.*;

public class ChangeProperties {

        private ArrayList<File> mgtFiles;
        private ArrayList<File> gwFiles;
        private ArrayList<File> hruFiles;
        private ArrayList<File> rteFiles;
        private ArrayList<File> solFiles;
        private ArrayList<File> bsnFiles;

        private HashMap<File, Float> mgt_CN2;
        private HashMap<File, Float> gw_ALPHA_BF;
        private HashMap<File, Float> gw_GW_DELAY;
        private HashMap<File, Float> gw_GWQMN;
        private HashMap<File, Float> hru_ESCO;
        private HashMap<File, Float> rte_CH_K2;
        private HashMap<File, Float> rte_ALPHA_BNK;
        private HashMap<File, Float> sol_SOL_AWC_1;
        private HashMap<File, Float> bsn_SFTMP;
        private HashMap<File, Float> gw_GW_REVAP;
        private HashMap<File, Float> gw_RCHRG_DP;


    public ChangeProperties() {
    }
    public ChangeProperties(FileChange fc) {
        this.fc = fc;
    }
    public ChangeProperties(FileChange fc, String path) {
        this.fc = fc;
        loadOldValues(path);
    }
```

```
    /*
    private final String[] solPara = {"SOL_AWC_1", "SOL_K", "SOL_BD", "SOL_Z"};
    private final String[] mgtPara = {"CN2"};
    private final String[] gwPara = {"ALPHA_BF", "GW_DELAY", "GWQMN",
"REVAPMN", "GW_REVAP"};
    private final String[] hruPara = {"ESCO", "CANMX"};
    private final String[] rtePara = {"CH_N2", "CH_K2", "ALPHA_BNK"};
    private final String[] bsnPara = {"SFTMP"};
    */
    private static FileChange fc = null;
    private float newValue;
    private float oldValue;

    public void setFileChange(FileChange fc) {
        this.fc = fc;
    }
    public FileChange getFileChange() {
        return this.fc;
    }

        // function to load all the old values from files.
    public void loadOldValues(String path) {
        mgtFiles = fc.getExtFiles(path, "mgt");
        gwFiles = fc.getExtFiles(path, "gw");
        hruFiles = fc.getExtFiles(path, "hru");
        rteFiles = fc.getExtFiles(path, "rte");
        solFiles = fc.getExtFiles(path, "sol");
        bsnFiles = fc.getExtFiles(path, "bsn");

        mgt_CN2 = new HashMap();
        gw_ALPHA_BF = new HashMap();
        gw_GW_DELAY = new HashMap();
        gw_GWQMN = new HashMap();
        hru_ESCO = new HashMap();
        rte_CH_K2 = new HashMap();
        rte_ALPHA_BNK = new HashMap();
        sol_SOL_AWC_1 = new HashMap();
        bsn_SFTMP = new HashMap();
        gw_GW_REVAP = new HashMap();
        gw_RCHRG_DP = new HashMap();

        for(File fileT : mgtFiles) {
            float old_value_CN2 = getOldValueForPara(fileT, "CN2");
            if(old_value_CN2 != -100000.0f) {
                mgt_CN2.put(fileT, old_value_CN2);
```

```
		}
	}

	for(File fileT : hruFiles) {
		float old_value_ESCO = getOldValueForPara(fileT, "ESCO");
		if(old_value_ESCO != -100000.0f) {
			hru_ESCO.put(fileT, old_value_ESCO);
		}
	}

	for(File fileT : rteFiles) {
		float old_value_CH_K2 = getOldValueForPara(fileT, "CH_K2");
		float old_value_ALPHA_BNK = getOldValueForPara(fileT,
"ALPHA_BNK");
		if(old_value_CH_K2 != -100000.0f) {
			rte_CH_K2.put(fileT, old_value_CH_K2);
		}
		if(old_value_ALPHA_BNK != -100000.0f) {
			rte_ALPHA_BNK.put(fileT, old_value_ALPHA_BNK);
		}
	}

	for(File fileT : solFiles) {
		float old_value_SOL_AWC_1 = getOldValueForPara(fileT, "SOL_AWC_1");
		if(old_value_SOL_AWC_1 != -100000.0f) {
			sol_SOL_AWC_1.put(fileT, old_value_SOL_AWC_1);
		}
	}

	for(File fileT : bsnFiles) {
		float old_value_SFTMP = getOldValueForPara(fileT, "SFTMP");
		if(old_value_SFTMP != -100000.0f) {
			bsn_SFTMP.put(fileT, old_value_SFTMP);
		}
	}

	for(File fileT : gwFiles) {
		float old_value_ALPHA_BF = getOldValueForPara(fileT, "ALPHA_BF");
		float old_value_GW_DELAY = getOldValueForPara(fileT, "GW_DELAY");
		float old_value_GWQMN = getOldValueForPara(fileT, "GWQMN");
		float old_value_GW_REVAP = getOldValueForPara(fileT, "GW_REVAP");
		float old_value_RCHRG_DP = getOldValueForPara(fileT, "RCHRG_DP");

		if(old_value_ALPHA_BF != -100000.0f) {
			gw_ALPHA_BF.put(fileT, old_value_ALPHA_BF);
		}
```

```
                if(old_value_GW_DELAY != -100000.0f) {
                        gw_GW_DELAY.put(fileT, old_value_GW_DELAY);
                }

                if(old_value_GWQMN != -100000.0f) {
                        gw_GWQMN.put(fileT, old_value_GWQMN);
                }

                if(old_value_GW_REVAP != -100000.0f) {
                        gw_GW_REVAP.put(fileT, old_value_GW_REVAP);
                }

                if(old_value_RCHRG_DP != -100000.0f) {
                        gw_RCHRG_DP.put(fileT, old_value_RCHRG_DP);
                }
        }
    }

        // function to change the values in files
    public void changeValue(char[] types, float[] values){
        //make sure the input are 11 parameters
        if(types == null || types.length < 11
                        || values == null || values.length < 11) {
                System.out.println("At least one of the parameters input are not 11 values!");
                return;
        }

        //CN2.mgt
        //mgtFiles, mgt_CN2<File, float>
        //types[0], values[0]
        if(mgt_CN2 != null) {
                Iterator mgtCN2It = mgt_CN2.entrySet().iterator();
                        while(mgtCN2It.hasNext()) {
                                Map.Entry pair = (Map.Entry<File, Float>)mgtCN2It.next();
                                float newValue = 0.0f;
                                if(types[0] == 'r') {
                                        newValue = cellingFloorFloat_5((Float)pair.getValue()
* (1.0f + values[0]));
                                } else if (types[0] == 'a') {
                                        newValue = cellingFloorFloat_5((Float)pair.getValue()
+ values[0]);
                                } else if (types[0] == 'v') {
                                        newValue = cellingFloorFloat_5(values[0]);
                                }
                                /*
```

```
                                System.out.println("New: " + newValue);
                                System.out.println("Old: " + (Float)pair.getValue());
                                System.out.println("Value: " + values[0]);
                                System.out.println("Filename: " +
((File)pair.getKey()).getName());
                                System.out.println("Path: " + ((File)pair.getKey()).getPath());
                                System.out.println("--------------------");
                                */
                                fc.updateValue(newValue, "CN2",
((File)pair.getKey()).getPath());
                        }
        }


        //ALPHA_BF.gw
        //gwFiles, gw_ALPHA_BF<File, float>
        //type[1], values[1]
        if(gw_ALPHA_BF != null) {
                Iterator gwALPHA_BFIt = gw_ALPHA_BF.entrySet().iterator();
                        while(gwALPHA_BFIt.hasNext()) {
                                Map.Entry pair = (Map.Entry<File,
Float>)gwALPHA_BFIt.next();
                                float newValue = 0.0f;
                                if(types[1] == 'r') {
                                        newValue = (Float)pair.getValue() * (1.0f + values[1]);
                                } else if (types[1] == 'a') {
                                        newValue = (Float)pair.getValue() + values[1];
                                } else if (types[1] == 'v') {
                                        newValue = values[1];
                                }
                                fc.updateValue(newValue, "ALPHA_BF",
((File)pair.getKey()).getPath());
                        }
        }


        //GW_DELAY.gw
        //gwFiles, gw_GW_DELAY<File, float>
        //type[2], values[2]
        if(gw_GW_DELAY != null) {
                Iterator gwGW_DELAYIt = gw_GW_DELAY.entrySet().iterator();
                        while(gwGW_DELAYIt.hasNext()) {
                                Map.Entry pair = (Map.Entry<File,
Float>)gwGW_DELAYIt.next();
                                float newValue = 0.0f;
                                if(types[2] == 'r') {
```

```
                                        newValue = (Float)pair.getValue() * (1.0f + values[2]);
                                } else if (types[2] == 'a') {
                                        newValue = (Float)pair.getValue() + values[2];
                                } else if (types[2] == 'v') {
                                        newValue = values[2];
                                }
                                fc.updateValue(newValue, "GW_DELAY",
((File)pair.getKey()).getPath());
                        }
        }


        //GWQMN.gw
        //gwFiles, gw_GWQMN<File, float>
        //type[3], values[3]
        if(gw_GWQMN != null) {
                Iterator gwGWQMNIt = gw_GWQMN.entrySet().iterator();
                        while(gwGWQMNIt.hasNext()) {
                                Map.Entry pair = (Map.Entry<File,
Float>)gwGWQMNIt.next();
                                float newValue = 0.0f;
                                if(types[3] == 'r') {
                                        newValue = (Float)pair.getValue() * (1.0f + values[3]);
                                } else if (types[3] == 'a') {
                                        newValue = (Float)pair.getValue() + values[3];
                                } else if (types[3] == 'v') {
                                        newValue = values[3];
                                }
                                fc.updateValue(newValue, "GWQMN",
((File)pair.getKey()).getPath());
                        }
        }

        //ESCO.hru
        //hru, hru_ESCO<File, float>
        //type[4], values[4]
        if(hru_ESCO != null) {
                Iterator hruESCOIt = hru_ESCO.entrySet().iterator();
                        while(hruESCOIt.hasNext()) {
                                Map.Entry pair = (Map.Entry<File, Float>)hruESCOIt.next();
                                float newValue = 0.0f;
                                if(types[4] == 'r') {
                                        newValue = (Float)pair.getValue() * (1.0f + values[4]);
                                } else if (types[4] == 'a') {
                                        newValue = (Float)pair.getValue() + values[4];
                                } else if (types[4] == 'v') {
```

```
                                        newValue = values[4];
                                }
                                fc.updateValue(newValue, "ESCO",
((File)pair.getKey()).getPath());
                        }
        }


        //CH_K2.rte
        //rte, rte_CH_K2<File, float>
        //type[5], values[5]
        if(rte_CH_K2 != null) {
                Iterator rteCH_K2It = rte_CH_K2.entrySet().iterator();
                        while(rteCH_K2It.hasNext()) {
                                Map.Entry pair = (Map.Entry<File, Float>)rteCH_K2It.next();
                                float newValue = 0.0f;
                                if(types[5] == 'r') {
                                        newValue = (Float)pair.getValue() * (1.0f + values[5]);
                                } else if (types[5] == 'a') {
                                        newValue = (Float)pair.getValue() + values[5];
                                } else if (types[5] == 'v') {
                                        newValue = values[5];
                                }
                                fc.updateValue(newValue, "CH_K2",
((File)pair.getKey()).getPath());
                        }
        }


                //ALPHA_BNK.rte
        //rte, rte_ALPHA_BNK<File, float>
        //type[6], values[6]
        if(rte_ALPHA_BNK != null) {
                Iterator rteALPHA_BNKIt = rte_ALPHA_BNK.entrySet().iterator();
                        while(rteALPHA_BNKIt.hasNext()) {
                                Map.Entry pair = (Map.Entry<File,
Float>)rteALPHA_BNKIt.next();
                                float newValue = 0.0f;
                                if(types[6] == 'r') {
                                        newValue = (Float)pair.getValue() * (1.0f + values[6]);
                                } else if (types[6] == 'a') {
                                        newValue = (Float)pair.getValue() + values[6];
                                } else if (types[6] == 'v') {
                                        newValue = values[6];
                                }
```

```
                                fc.updateValue(newValue, "ALPHA_BNK",
((File)pair.getKey()).getPath());
                        }
        }


                //SOL_AWC_1.sol
        //sol, sol_SOL_AWC_1<File, float>
        //type[7], values[7]
        if(sol_SOL_AWC_1 != null) {
                Iterator solSOL_AWC_1It = sol_SOL_AWC_1.entrySet().iterator();
                        while(solSOL_AWC_1It.hasNext()) {
                                Map.Entry pair = (Map.Entry<File,
Float>)solSOL_AWC_1It.next();
                                float newValue = 0.0f;
                                if(types[7] == 'r') {
                                        newValue = cellingFloorFloat_2((Float)pair.getValue()
* (1.0f + values[7]));
                                } else if (types[7] == 'a') {
                                        newValue = cellingFloorFloat_2((Float)pair.getValue()
+ values[7]);
                                } else if (types[7] == 'v') {
                                        newValue = cellingFloorFloat_2(values[7]);
                                }
                                fc.updateSolValue(newValue, "SOL_AWC_1",
((File)pair.getKey()).getPath());
                        }
        }


                //SFTMP.bsn
        //bsn, bsn_SFTMP<File, float>
        //type[8], values[8]
        if(bsn_SFTMP != null) {
                Iterator bsnSFTMPIt = bsn_SFTMP.entrySet().iterator();
                        while(bsnSFTMPIt.hasNext()) {
                                Map.Entry pair = (Map.Entry<File, Float>)bsnSFTMPIt.next();
                                float newValue = 0.0f;
                                if(types[8] == 'r') {
                                        newValue = (Float)pair.getValue() * (1.0f + values[8]);
                                } else if (types[8] == 'a') {
                                        newValue = (Float)pair.getValue() + values[8];
                                } else if (types[8] == 'v') {
                                        newValue = values[8];
                                }
```

```
                        fc.updateValue(newValue, "SFTMP",
((File)pair.getKey()).getPath());
                    }
        }


                //GW_REVAP.gw
        //gw, gw_GW_REVAP<File, float>
        //type[9], values[9]
        if(gw_GW_REVAP != null) {
                Iterator gwGW_REVAPIt = gw_GW_REVAP.entrySet().iterator();
                    while(gwGW_REVAPIt.hasNext()) {
                        Map.Entry pair = (Map.Entry<File,
Float>)gwGW_REVAPIt.next();
                        float newValue = 0.0f;
                        if(types[9] == 'r') {
                            newValue = (Float)pair.getValue() * (1.0f + values[9]);
                        } else if (types[9] == 'a') {
                            newValue = (Float)pair.getValue() + values[9];
                        } else if (types[9] == 'v') {
                            newValue = values[9];
                        }
                        fc.updateValue(newValue, "GW_REVAP",
((File)pair.getKey()).getPath());
                    }
        }


                //RCHRG_DP.gw
        //gw, gw_RCHRG_DP<File, float>
        //type[10], values[10]
        if(gw_RCHRG_DP != null) {
                Iterator gwRCHRG_DPIt = gw_RCHRG_DP.entrySet().iterator();
                    while(gwRCHRG_DPIt.hasNext()) {
                        Map.Entry pair = (Map.Entry<File,
Float>)gwRCHRG_DPIt.next();
                        float newValue = 0.0f;
                        if(types[10] == 'r') {
                            newValue = (Float)pair.getValue() * (1.0f +
values[10]);
                        } else if (types[10] == 'a') {
                            newValue = (Float)pair.getValue() + values[10];
                        } else if (types[10] == 'v') {
                            newValue = values[10];

                        }
```

```
                                fc.updateValue(newValue, "RCHRG_DP",
((File)pair.getKey()).getPath());
                        }
                }
        }

   public void changeValue(char changeType, String para, String ext, float underQue, float
onQue, String path){
                ArrayList<File> files = fc.getExtFiles(path, ext);
        RandomAccessFile raf;
        String str = null;
        for(File file : files) {
                try{
                        raf = new RandomAccessFile(file, "rw");
                        do{
                                try{
                                        str = raf.readLine();
                                } catch(IOException ioe){
                                        ioe.printStackTrace();
                                }

                        } while(str.indexOf(para) == -1);
                        if (str == null) {
                                return;
                        } else {
                                String[] strParts = str.split("  ");
                                for(int i = 0; i < strParts.length; i++) {
                                        if(strParts[i].trim().length() >= 1) {
                                                oldValue = Float.parseFloat(strParts[i].trim());
                                                break;
                                        }
                                }
                        }
                        raf.close();
                } catch (IOException ioe) {
                        ioe.printStackTrace();
                }
                        if (changeType == 'r') {
                        //r, old value multiply the input
                                newValue = oldValue * (float)(Math.random()*(onQue -
underQue) + 1 + underQue);
                } else if (changeType == 'a') {
                        //a, old value add the input
                        newValue = oldValue + underQue + (float)(Math.random()*(onQue -
underQue));
                } else if (changeType == 'v'){
```

```
                        //v, old value replaced by the input
                        newValue = underQue + (float)(Math.random()*(onQue - underQue));
                } else {
                        return;
                }
                System.out.println(file.getName() + " : " + para + ", change from: "  +
oldValue + ", to: " + newValue + "!");

                fc.updateValue(newValue, para, file.getName());
        }
    }

    private float getOldValueForPara(File file, String para) {
        RandomAccessFile raf;
        String str = null;
        float old_value = 0.0f;
        try{
                raf = new RandomAccessFile(file, "rw");
                if(para.equals("SOL_AWC_1")) {
                        do{
                                try{
                                        str = raf.readLine();
                                } catch(IOException ioe){
                                        ioe.printStackTrace();
                                }
                        } while(str.indexOf("Ave. AW Incl. Rock Frag") == -1);
                } else {
                        do{
                                try{
                                        str = raf.readLine();
                                } catch(IOException ioe){
                                        ioe.printStackTrace();
                                }
                        } while(str.indexOf(para) == -1);
                }


                if (str == null) {
                        return -100000.0f;
                } else if (para.equals("SOL_AWC_1")) {
                        String[] strParts = str.substring(str.indexOf(":")+1).trim().split("\\s+");
                        if(strParts[0].trim().length() >= 1) {
                                        old_value = Float.parseFloat(strParts[0].trim());
                                }
                } else {
                        /*
```

```
                        String[] strParts = str.split("  ");
                        for(int i = 0; i < strParts.length; i++) {
                                if(strParts[i].trim().length() >= 1) {
                                        old_value = Float.parseFloat(strParts[i].trim());
                                        break;
                                }
                        }
                        */
                        String[] strParts = str.trim().split("\\s+");
                                if(strParts[0].trim().length() >= 1) {
                                        old_value = Float.parseFloat(strParts[0].trim());
                                }
                }
                raf.close();
                } catch (IOException ioe) {
                        ioe.printStackTrace();
                }
                return old_value;
}

private Float cellingFloorFloat_2(Float input) {
        Float output = 0.0f;
        Float temp = input * 100;
        Integer tempInt = temp.intValue();

        if(temp - tempInt >= 0.5f) {
                tempInt = tempInt + 1;
        }

        temp = tempInt.floatValue();

        output = temp / 100;

        return output;
}

private Float cellingFloorFloat_5(Float input) {
        Float output = 0.0f;
        Float temp = input * 100000;
        Integer tempInt = temp.intValue();

        if(temp - tempInt >= 0.5f) {
                tempInt = tempInt + 1;
        }

        temp = tempInt.floatValue();
```

```
        output = temp / 100000;

        return output;
    }
}
```

```
/**
 * @(#)ExecuteSwat.java
 *
 *
 * @author Hongjing Wu
 * @version 1.00 2013/4/4
 *
 * @file description:
 *
 *        This class contains SWAT program execution and result gathering functions.
 *
 */
import java.io.*;
import java.util.ArrayList;
import java.util.HashMap;
import java.util.Map;

public class ExecuteSwat{

        // output file name: output.rch
        private final String OUTPUT_RCH = "output.rch";
   public ExecuteSwat() {
   }

   private String currentLine;
   private String[] currentLineStrs;
        private ArrayList<String> currentLineStrsAL;
        private Map<Integer, Float> comparableMap = new HashMap();

   public void executeSwat2009(String path) {
        //System.out.println(path);
        try{
                String pathNew = path.replace("\\\\", "/");
                System.out.println(pathNew);
                //Process proc = Runtime.getRuntime().exec("cmd.exe /c start " + pathNew +
"\\swat2009.exe");
                Process proc = Runtime.getRuntime().exec("cmd.exe /c start " + path +
"/swat2009.exe");
                try{
                        proc.waitFor();
                        Thread.currentThread().sleep(5000);
                                //Thread.currentThread().yield();
                                System.out.println("Exit Value: " + proc.exitValue());
                        } catch(Exception e){
                                e.printStackTrace();
                        }
```

```
        } catch (Exception e) {
                e.printStackTrace();
        }
    }

    public void gatherOutput(String path) {
        ArrayList<String> FLOW_OUTcms = new ArrayList<String>();
        try {
                RandomAccessFile raf = new RandomAccessFile(path + "\\" +
OUTPUT_RCH, "rw");
                for(int r = 0; r<9 ; r++) {
                        raf.readLine();
                }
                while(raf.getFilePointer() < raf.length()) {
                        currentLine = null;
                        currentLineStrs = null;
                        currentLineStrsAL = new ArrayList<String>();
                        currentLine = raf.readLine();
                        currentLineStrs = currentLine.split(" ");
                        if(currentLineStrs.length < 2) {
                                continue;
                        }
                        for(int i=0; i<currentLineStrs.length; i++) {
                                if(currentLineStrs[i].length() >= 1) {
                                        currentLineStrsAL.add(currentLineStrs[i]);
                                }
                        }
                        if(currentLineStrsAL.get(1).equals("61")) {
                                FLOW_OUTcms.add(currentLineStrsAL.get(6));
                        }
                }
                //write result into a output file
                writeResult(path, FLOW_OUTcms);
                raf.close();
                System.out.println("gatherOutput() Complete!");
        } catch (Exception e) {
                e.printStackTrace();
        }
    }

    private void writeResult(String path, ArrayList<String> FLOW_OUTcms) {
        String resultFileName = path + "\\MySwatResult.txt";
        File resultFile = new File(resultFileName);
        if(!resultFile.exists()) {
                try{
                        resultFile.createNewFile();
```

```
                } catch(Exception e) {
                        e.printStackTrace();
                }
        }
        try{
                BufferedWriter bw = new BufferedWriter(new FileWriter(resultFile, true));

                ArrayList<String> replaced_FLOW_OUTcms = new ArrayList();

                for(int i=0; i<FLOW_OUTcms.size(); i++) {
                        if(i != 12 && i != 25 && i != 38 && i != 39) {
                                replaced_FLOW_OUTcms.add(FLOW_OUTcms.get(i));
                        }
                }

                for(int i=0; i<replaced_FLOW_OUTcms.size(); i++) {
                        bw.append(replaced_FLOW_OUTcms.get(i) + "\r\n");
                }

                if(!comparableMap.isEmpty() && comparableMap.size() == 36) {
                        String NSEResult = "";
                        String RResult = "";
                        String[] results =
calculateComparableResults(replaced_FLOW_OUTcms);
                        NSEResult = results[0];
                        RResult = results[1];
                        bw.append(NSEResult + "\r\n");
                        bw.append(RResult + "\r\n");
                }
                bw.append("----------\r\n");
                bw.close();
        } catch(Exception e) {
                e.printStackTrace();
        }
   }

   public void readComparableFile(String path) {

        try {
                RandomAccessFile raf = new RandomAccessFile(path, "rw");
                for(int i = 0; i < 36; i++) {
                        String currentLine = "";
                        currentLine = raf.readLine();
                        Float currentNumber = Float.parseFloat(currentLine);
                        comparableMap.put(i, currentNumber);
                }
```

```
        } catch (Exception e) {
                e.printStackTrace();
        }

    }

    //comparableMap
    private String[] calculateComparableResults(ArrayList<String> FLOW_OUTcms) {
        String NSEResult = "";
        String RResult = "";
        String[] results = new String[2];
        Map<Integer, Float> flowMap = new HashMap();

        int times = FLOW_OUTcms.size();

        for(int i=0; i < times; i++) {
                        flowMap.put(i, Float.parseFloat(FLOW_OUTcms.get(i)));
                }

        float oi_all = 0.0f;
        float oi_star = 0.0f;
        float si_all = 0.0f;
        float si_star = 0.0f;

        for(int i = 0; i < times; i++) {
                oi_all += comparableMap.get(i);
                si_all += flowMap.get(i);
        }

        oi_star = oi_all / times;
        si_star = si_all / times;

        float RFractions = 0.0f;
        float RNumerator = 0.0f;
        float RNumeratorLeft = 0.0f;
        float RNumeratorRight = 0.0f;

        float fractions = 0.0f;
        float numerator = 0.0f;

        for(int i = 0; i < times; i++) {
                //NSE
                fractions = (flowMap.get(i) - comparableMap.get(i)) * (flowMap.get(i) -
comparableMap.get(i)) + fractions;
                numerator = (comparableMap.get(i) - oi_star) * (comparableMap.get(i) -
oi_star) + numerator;
```

```
                //R
                RFractions = (comparableMap.get(i) - oi_star) * (flowMap.get(i) - si_star) +
RFractions;
                RNumeratorLeft = (comparableMap.get(i) - oi_star) * (comparableMap.get(i)
- oi_star) + RNumeratorLeft;
                RNumeratorRight = (flowMap.get(i) - si_star) * (flowMap.get(i) - si_star) +
RNumeratorRight;
        }

        //NSE
        if(numerator != 0) {
                Float NSEFloat = 1 - (fractions / numerator);
                NSEResult = NSEFloat.toString();
        } else {
                NSEResult = "Error: NSE Denominator is 0!";
        }

        //R
        RFractions = RFractions * RFractions;
        RNumerator = RNumeratorLeft * RNumeratorRight;

        if(RNumerator != 0) {
                Float RFloat = RFractions / RNumerator;
                RResult = RFloat.toString();
        } else {
                RResult = "Error: R Denominator is 0!";
        }

        results[0] = NSEResult;
        results[1] = RResult;
        return results;
   }
}
```